UNIVERSITÉ DU QUÉBEC À MONTRÉAL

RÉACTIONS (PHOTO)CATALYTIQUES POUR L'INDUSTRIE PHARMACEUTIQUE : MÉTHODES NOVATRICES GUIDÉES PAR LA THÉORIE ET L'ÉTUDE DE MÉCANISMES

THÈSE

PRESENTÉE

COMME EXIGENCE PARTIELLE

DU DOCTORAT EN CHIMIE

PAR

TAYLOR HOPE

MAI 2023

UNIVERSITÉ DU QUÉBEC À MONTRÉAL

(PHOTO)CATALYTIC REACTIONS FOR THE PHARMACEUTICAL INDUSTRY: NOVEL METHODS GUIDED BY THEORY, SPECTROSCOPY AND MECHANISTIC STUDIES

THESIS

PRESENTED

AS A PARTIAL FULFILLMENT

OF THE DOCTORATE IN CHEMISTRY

BY

TAYLOR HOPE

MAY 2023

UNIVERSITÉ DU QUÉBEC À MONTRÉAL
Service des bibliothèques

Avertissement

ACKNOWLEDGEMENTS

First and foremost, I would like to thank my supervisor Mathieu Frenette for his expertise and invaluable advice throughout my graduate degree. Thank you for allowing me grow as a chemist and for creating a welcoming research environment. Thank you for encouraging me out of my comfort zone *just* before every presentation. I'm proud of what has been accomplished over the last 5 years.

Thank you, Joshua Byers, Erin Dodd, and Alexandre Gagnon, for being on my evaluation committee over the years. Your willingness to help me grow and ask constructive questions led me to become a more balanced researcher. Thank you, Charles Yeung, for agreeing to read this thesis.

I would like to extend my gratitude to the staff at UQAM, especially Luc Arseneault, Pascale Beauchemin, Gwénaël Chamoulaud, Charlotte De La Chevrotière, Julie Desgroseilliers, Jacqueline Hue Tieu, Mylène Lacharité, and Galyna Shul for the assistance they provid to myself and other students.

Thank you to the Frenette group past and present for their support over the years: Antoine Juneau, Yohann Gagné, Steven Mauries, Jason Malenfant, Lucille Kuster, Iannick Lepage, Meghan Heer, Nicole Removski, Jacinthe Maisonneuve, and Emma Guillet. I will always cherish our time both inside and outside the lab.

Finally, I would like to thank Debra, Jordan, and Priscilla who unconditionally support me. You have always there to encourage me and believe in me. There are no words to describe the importance you have had and will continue to have on my life. I would not have been able to do this without you.

TABLE OF CONTENT

LIST OF FIGURES

LIST OF TABLES

LIST OF ABBREVIATIONS AND ACRONYMS

$^1O_2$ Singlet oxygen

2SS   Dithioimide

2OS   Thioimide

2OO   Imide

A   Absorption or acceptor

B3LYP   Becke's 3-parameter exchange and Lee-Yang-Parr's correlation function hybrid density functional

BHT   Butylated hydroxytoluene

BSA   Bovine Serum Albumin

bpy   2,2'- bipyridine

c   Concentration

CPCM   Conductor-like polarization model

CV   Cyclic voltammetry

D   Donor

DPA   9,10-diphenylanthracene

DFT   Density Functional Theory

E*$_{1/2}$	Excited state redox potential
GC-MS	Gas Chromatography Mass Spectrometry
HOMO	Highest Occupied Molecular Orbital
IC	Internal Conversion
IRF	Instrument Response Function
ISC	Intersystem Crossing
KIE	Kinetic Isotope Effect
LanL2DZ	Double -ζ functional from the Los Alamos laboratory
l	Pathlength
LFP	Laser Flash Photolysis
LUMO	Lowest Unoccupied Molecular Orbital
M06-2X	Minnesota hybrid density functional, 2006
MB	Methylene Blue
MesArc	9-mesityl-10-methyl acridinium
Nd:YAG	Neodymium-doped yttrium aluminum garnet
OPO	Optical Parametric Oscillator
Oxi	Oxidation

PBS   Phosphate Buffered Saline

PC   Photocatalyst

PIFA   [bis(trifluoroacetoxy)iodo]benzene

Q   Quencher

RDS   Rate Determining Step

Red   Reduction

RFT   Riboflavin tetraacetate

SET   Singlet Electron Transfer

^{t}Bu   t*ert*-butyl

TS   Transition State

THF   Tetrahydrofuran

UV-Visible   Ultraviolet-Visible

LIST OF SYMBOLS AND UNITS

ΔG Change in Free energy

$\Delta G^{\ddagger}$ Free energy of activation

ΔH Change in enthalpy

$\Delta H^{\ddagger}$ Enthalpy of activation

ΔS Change in entropy

ε Molar absorption coefficient

τ Excited state lifetime

λ Wavelength

Φ_r Quantum yield of a reaction

Φ_f Quantum yield of fluorescence

Φ_0 Quantum yield without quencher

Φ_Q Quantum yield with quencher

a.u.   Arbitrary units or absorption units

$^{\circ}C$ Degrees in Celsius

cal   Calorie

F   Faradays constant (96 485.33 s•A/mol)

g	Gram
K	Kelvin
k_d	Rate of decay
k_{DPA}	Rate constants for the reaction between $^1O_2$ and DPA
k_{nr}	Rate of non-radiative pathways
k_r	Rate of reaction of $^1O_2$ with phenols
k_q	Rate of quenching
kcal	Kilocalorie
L	Litre
mmol	Millimole
M	Molar or mol/L
mL	Millilitre
mM	Millimolar (10^{-3} M)
ppm	Parts per million
μm	Micromolar (10^{-6} M)
Sec	Seconds
V	Volts

RÉSUMÉ

Mes contributions à la recherche sont une interface entre la chimie appliquée et fondamentale. En général, je m'efforce à obtenir une compréhension approfondie des réactions dans le but de résoudre les problèmes du monde qui nous entoure. Dans ce travail hautement collaboratif, mon rôle est d'obtenir un aperçu mécanistique précis des réactions chimiques développées par les leaders de l'industrie. J'ai eu le privilège de collaborer et de publier avec des chimistes de Pfizer et de Merck sur des problèmes de recherche percutants et difficiles.

La compréhension d'un processus chimique peut être extrêmement avantageux. Si nous pouvons mesurer la thermodynamique et la cinétique d'une réaction, nous pouvons prédire les conditions qui devraient fonctionner et écarter celles qui sont susceptibles d'échouer. L'identification des intermédiaires de réaction ouvre également de nouvelles voies cachées du schéma réactionnel global. Notre approche de la chimie « d'investigations de mécanismes et solutions innovantes » repose sur la spectroscopie indépendante en temps, ou temporellement résolue, la chimie analytique classique et la chimie computationnelle. Le but de mon doctorat est de combiner deux mondes de la chimie : la chimie synthétique et la chimie physique de pointe.

L'expérience unique de notre groupe en chimie organique physique combinée à une passion pour la compréhension d'énigmes mécanistiques complexes a abouti à plusieurs publications à haut impact avec nos collaborateurs. Dans mon cas, les collaborateurs sont à la fois industriels (Pfizer et Merck) et académiques (Thomas Poisson, U. Rouen et Kenneth Maly, U. Wilfrid-Laurier). Ils ont cultivé des questions de recherche passionnantes pour lesquelles je m'applique à offrir des explications détaillées aux résultats expérimentaux. Nous accomplissons cette compréhension mécanistique en fournissant une analyse computationnelle, telle que la théorie fonctionnelle de la densité (DFT), et des résultats expérimentaux via des méthodes telles que l'extinction de Stern-Volmer, le rendement quantique de fluorescence et de phosphorescence, l'analyse cinétique et la voltamétrie cyclique pour souligner les étapes spécifiques d'un mécanisme proposé.

En combinant des techniques spectroscopiques avec des méthodes de calcul de pointe, nous sommes en mesure de soutenir ou de réfuter certaines voies mécanistiques. Cette approche altère directement la manière dont les chimistes développent des réactions. En comprenant chaque étape d'un mécanisme, nous pouvons mieux développer des réactions plus efficaces.

Mots clés : Photochimie, catalyse, spectroscopie, intermédiaires réactifs, études mécanistes, cinétique de réaction, réaction de Minisci, thione, fer-oxo, recombinaison radicalaire-radicalaire, photoredox, calculs DFT, couplage phénol-phénol.

ABSTRACT

My research contributions overlap with the frontiers of applied and fundamental chemistry. Generally, I strive to obtain a deep understanding of reactions that solve real-world problems. In this highly collaborative work, my role is to obtain precise mechanistic insight into chemical reactions developed by industry leaders. I have been privileged to collaborate and publish with chemists at Pfizer and Merck on these impactful and challenging research problems.

The rewards of understanding a chemical process, can be extremely beneficial. If we can measure the thermodynamics and kinetics of a reaction, we can predict conditions that should be successful from those that are likely to fail. The identification of reaction intermediates also opens novel routes hidden from the overall reaction scheme. Our "mechanistic insight and innovative solutions" approach to chemistry is informed by steady-state and time-resolved spectroscopy, classical analytical chemistry and computational chemistry. The goal of my doctorate is to combine two worlds of chemistry: synthetic chemistry and state-of-the-art physical chemistry.

Our group's unique background in physical organic chemistry combined with a passion to understand complex mechanistic puzzles has resulted in several high-impact publications with our collaborates. In my case, the collaborators are both industrial (Pfizer and Merck) and academic (Thomas Poisson, U. Rouen and Kenneth Maly, U. Wilfrid-Laurier). They have cultivated exciting research questions where I strive to offer detailed explanations to experimental results. We accomplish this mechanistic understanding by providing computational analysis, such as Density Functional Theory, and experimental results via methods such as Stern-Volmer quenching, quantum yields, kinetic analysis and cyclic voltammetry to emphasize specific steps of a proposed mechanism.

By combining spectroscopic techniques with state-of-the-art computational methods, we are able to support or refute certain mechanistic pathways. This approach directly alters the way in which chemists develop reactions. By understanding each step in a reaction mechanism, we can better develop more efficient reactions.

Keywords : Photochemistry, catalysis, spectroscopy, reactive intermediates, mechanistic studies, reaction kinetics, Minisci reaction, thione, iron-oxo, radical-radical recombination, photoredox, DFT calculations, phenol-phenol coupling.

CHAPITRE 1

INTRODUCTION

1.1   Why Study Reaction Mechanisms

To understand a chemical reaction, it would be ideal to see the specific bond-breaking and bond forming steps of participating molecules – *the reaction mechanism*. Since it isn't possible to observe every elementary step between starting material and product, we infer from mechanistic precedence and other factors such as reactions kinetics, thermodynamics, and spectroscopic characteristics. Traditionally, synthetic chemists publish a novel reaction and subsequently, physical chemists gather evidence to uncover the reaction's mechanism. Several opportunities are missed with this poor overlap between the development of a reaction and the determination of its mechanism. For one, assumed mechanisms may misguide further innovation. And for the other, mechanistic corrections may be ignored or cloaked in complex graphs and data tables. By investigating the underlying machinery that makes a reaction work while simultaneously optimizing reaction conditions, we can identify the bottlenecks that need improvement and make those adjustments in real time. In addition, the identification of a key reaction intermediate can give insight about alternative, productive routes that could be taken with different reagents.

The detailed process by which a reaction takes place is important information because it influences the way reactions are developed. Oftentimes, chemists can propose two or more mechanisms consistent with the data they have at hand, such as the mechanisms explored in Chapter 3, Chapter 5, and Chapter 6. Many reactions can proceed by more than one competing pathway and by understanding how the product is formed, reaction conditions can be modified to favour one pathway over all the others. A mechanistically informed reaction development can force the desired product to also be the major product, while minimizing the amount of off cycle side-product formation.

Chemical reactions can proceed via several intermediate products, from reactive radicals to persistent and long-lived excited states. Knowledge of these reactive intermediates can be translated into novel reactions. For example, Litwinienko *et al.* (2011) describes how free radicals exhibit different reactivities based on their solvent.

Theories to explain reaction mechanisms have been driven by the discovery of novel chemical changes. My research aims to demonstrate the importance of mechanistic studies in directing the discovery and development of synthetically valuable (photo)catalytic reactions.

1.1.1   Photoredox Mechanisms

The field of photoredox catalysis is expanding into novel territory. This largely has to do with the development of inexpensive and high intensity visible LEDs. Traditionally, photochemical synthetic procedures used high energy ultraviolet lights resulting in uncontrollable excitation of the molecules and photodecomposition, severely limiting the scope of the reactions. By switching to visible LEDs, which not only are brighter and cost less, but have a narrow wavelength band of irradiation, meaning their energy is more selectively converted into useful chemistry than broadband light sources.

Due to its inherent potential for synthetic chemists, photocatalysis has over the last decade undergone an extraordinary expansion (Figure 1.1). In a relatively short amount of time, a staggering number of photochemical methodologies have been introduced. Using light to initiate a chemical reaction has revealed novel reaction pathways that were previously very difficult to access via polar and/or thermal chemistry. Photocatalysis enables excited state molecules and radical species to react in non-traditional routes and at various redox states. Furthermore, photoredox reactions occur under more mild conditions, and can be selectively activated allowing for spatiotemporal control.
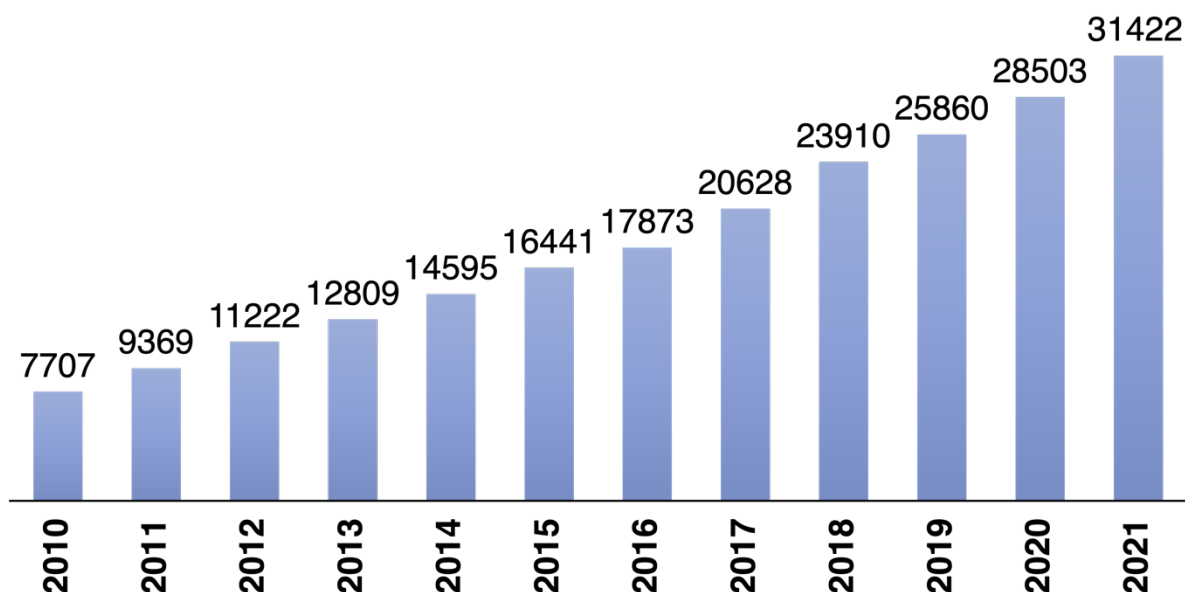
Figure 1.1. Number of publications that contain the term "photocatalysis" between 2010 and 2021. From scifinder.cas.org, June 2022.

The start of modern photoredox catalysis were initiated by the groups of David MacMillian at Princeton University, Tehshik Yoon at the University of Wisconsin-Madison, and Corey Stephenson at the University of Michigan. The three groups independently published visible light initiated photochemical reactions in 2008 and 2009 (Nicewicz and MacMillan, 2008; Ischay et al., 2008; Narayanam et al., 2009) (Figure 1.2). The reactions were photocatalyzed by $Ru(bpy)_3Cl_2$ where bpy is 2,2'- bipyridine.

a)

HOTf

Ru   2,6-lutidine, DMF
hv, 23°C, 6hrs

93% yield, 90% ee

Nicewicz and MacMillan, **2008**

b)

Ph ... Ph

Ru   i-Pr$_2$NEt, LiBF$_4$
MeCN, hv
50 min

Ph

89% yield

Ischay *et al.*, **2008**

c)

Ru   i-Pr$_2$NEt
formic acid, DMF
hv, 4 hrs

Boc

90% yield

Narayanam *et al.*, **2009**
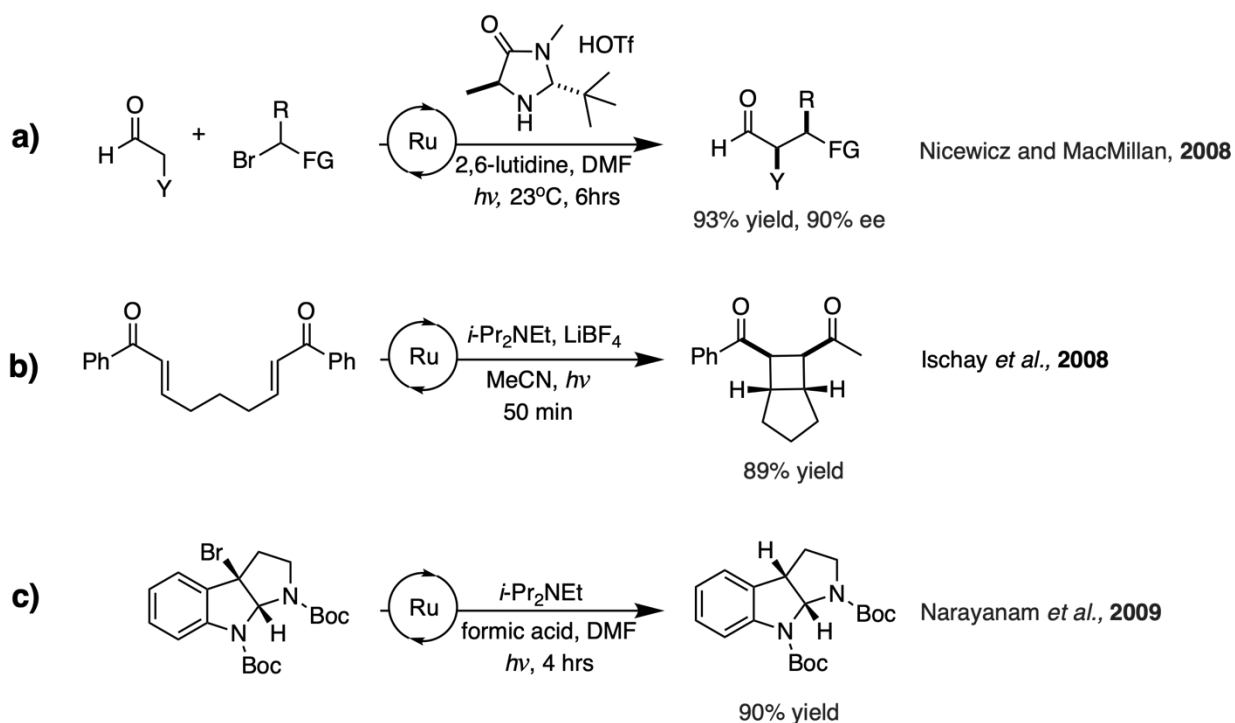
Figure 1.2. Applications of photoredox catalysis: a) Asymmetric alkylation of aldehydes photocatalyzed by Ru(bpy)$_3$Cl$_2$ using a fluorescent bulb from the MacMillian group (Nicewicz and MacMillan, 2008) b) [2+2] cycloaddition of enones photocatalyzed by Ru(bpy)$_3$Cl$_2$ using visible light from the Yoon group (Ischay *et al.,* 2008) and c) Oxidative dehalogenation of bromopyrroloindoline photocatalyzed with Ru(bpy)$_3$Cl$_2$ using a fluorescent bulb from the Stephenson group (Narayanam *et al.,* 2009).

These publications from 2008 and 2009 overlapped with synthetic chemists renewed interest in free radical chemistry. Many photoredox reactions often involve radical intermediates and these species were previously thought to give complex product mixtures. However, using carefully optimized conditions, highly selective and efficient reactions can lead to clean and high yielding products.

When using heat to promote chemical reactions, there is a balance of needing enough heat (energy) for the reaction to proceed, but not so much as to destabilize the products or promote side-reactions. That delicate balance can be achieved in photoredox catalysis by selecting a certain wavelength of light to selectively promote the photocatalyst into an excited state leaving the starting material or products unaffected. Visible light in this case has a clear advantage as most organic molecules do not absorb in the visible region. However, it is possible to selectively excite the photocatalyst (PC)

with ultraviolet light if there is no absorption overlap with the products. (Brimioulle and Bach, 2013; McTiernan *et al.,* 2016; Revol *et al.,* 2013). A variety of PCs are readily available by simply matching their spectral and electrochemical properties to the reaction conditions.

As the field of photochemistry continues to grow and evolve (Figure 1.3), the need for detailed mechanistic studies has become more and more essential. The impact of these studies on day-to-day uses for chemists will lead to more ambitious synthetic methods that can be rationally optimized over time.
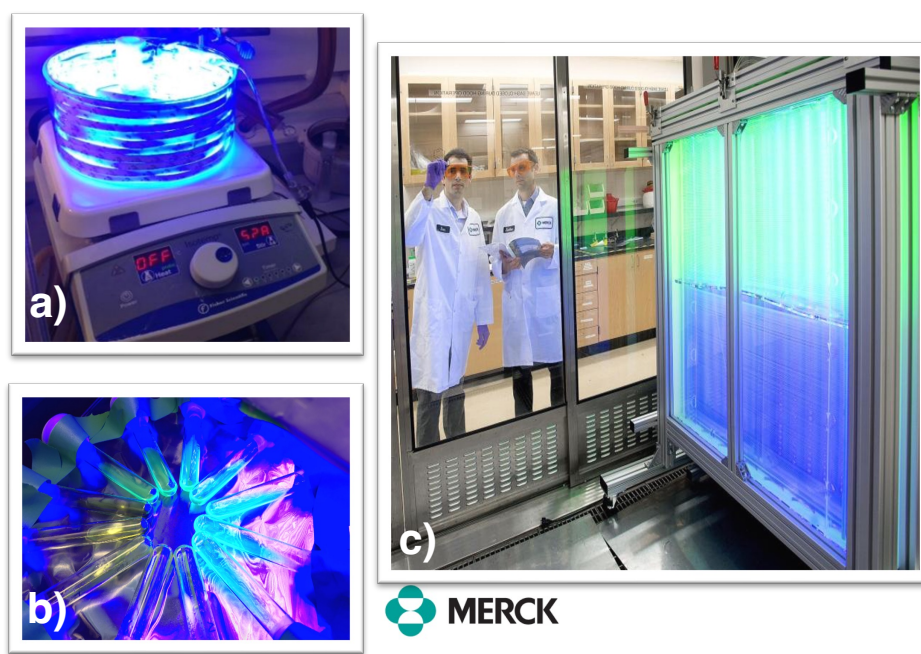
Figure 1.3. Evolution of photoredox a) Sample wrapped around a LED strip b) fluorescent photocatalysts excited using LEDs and c) industrial-scale flow reactor at Merck using LEDs (Merck Media Group, 2018).

1.2   Deducing Reaction Mechanisms

Free radicals and PC require similar conditions for their reactivity. The reaction between a molecule and the PC and/or free radical must be done in a fairly short time frame because although they are very reactive, they can have short lifetimes.

There are several literature sources that have been helpful in elucidating reaction mechanisms, such as the work from Focsaneanu and Scaiano (2006), that are helpful in understanding the reactivity of radicals. The overall methodology of determining photochemical reaction mechanisms is nicely described in the chapter "Photochemistry and Radical Generation: Approaches in Mechanism Elucidation" by Yoon from the textbook "Free radicals: Fundamentals and applications in organic synthesis" by Fensterbank, and Ollivier (2021) and the article by Buzzetti *et al.* (2019) which outlines mechanistic studies to consider when developing novel photochemical reactions.

A paper from the Scaiano group (Pitre *et al.,* 2013) outlines how a detailed understanding of the excited state kinetics that govern photochemical reactions is essential to the design and optimization of a reaction. They developed a more cost effective and metal free alternative for the photocatalytic oxidative hydroxylation of aryl boronic acids proposed by Zou *et al.,* (2012) by switching the PC from Ru(bpy)$_3$Cl$_2$ to methylene blue (MB). Figure 1.4 describes the conditions for the ruthenium-based reaction which required 16 to 72 hours of irradiation whereas using MB under similar conditions required just 7 hours of irradiation.
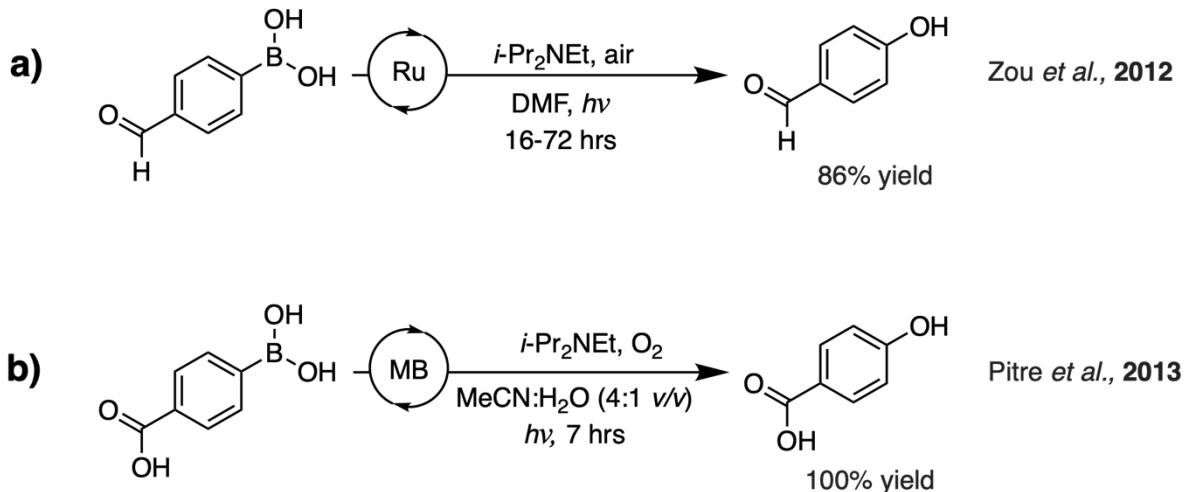
Figure 1.4. Conditions for the oxidative hydroxylation of phenylboronic acid using the photocatalyst a) Ru(bpy)$_3$Cl$_2$ and b) methylene blue (MB).

Characterization of a reaction mechanism can be done based on many different fundamental concepts. While understanding the thermodynamics of a reaction dictates if a product *can* favourably form, the kinetics of a reaction dictates if the reaction *will* take place at all. The balance

of these two properties is essential in designing a successful reaction, and both must be carefully considered. Tandem reaction design and mechanism discovery is not only feasible, but also invaluable to the advancement of novel chemical reactions.

1.3 Examining the Thermodynamics of an Excited States with Redox Properties

A common power struggle in catalytic reactions is the strength of the oxidant and reductant. If one is too strong or weak, the product will be inefficiently formed. An advantage of photochemical reactions is the ability to manipulate a relatively inert PC and produce an oxidizing and reducing agent *in situ* by selectively exciting the catalyst. A large part of what makes photoredox chemistry so enticing is this improved control.

When a PC absorbs a photon, it is promoted to the singlet excited state. The excited state singlet can be transformed to a triplet state through intersystem crossing (ISC). The spin flip process is favoured by the heavy atom effect, for organic PC the additional of halogens are typically sufficient. Once in the triplet state, the electron is spin forbidden to directly relax back to the ground state, resulting in a longer lifetime. A photocatalysts excited state mimics that of an "electron hole pair" where it can react as both an oxidant (Figure 1.5A) and a reductant (Figure 1.5B).

a) Oxidation of a photocatalyst (PC) by an acceptor (A)

A ^{3}[PC]*   A$^{-\bullet}$ PC$^{+\bullet}$
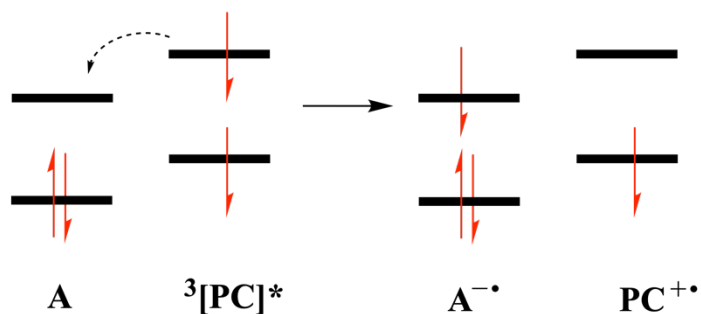
b) Reduction of a photocatalyst (PC) by a donor (D)

D ^{3}[PC]*   D$^{+\bullet}$ PC$^{-\bullet}$
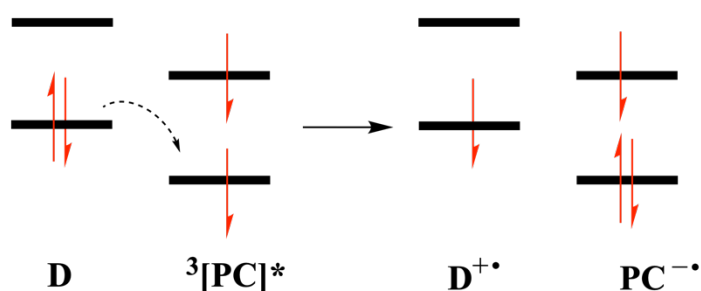
Figure 1.5. Typical a) oxidation and b) reduction pathways between a photocatalysts (PC) and an acceptor (A) or donor (D) molecule.

Reactive intermediates each have unique reactivity patterns that can be used to create synthetically useful products. If we examine the thermodynamics of these redox processes, we see that for the PC to be a good oxidant, the removal of an electron from the half-filled HOMO of the ^{3}[PC]* to the LUMO of the ground state molecule must be exothermic. While for the PC to be a good reductant, the addition of an electron from the half-filled HOMO of ^{3}[PC]* must again be exothermic. If the inverse were to happen, these processes would become endothermic. Using this reasoning, PC in the excited state are both better reducing and oxidizing agents.

When designing a reaction, the redox potentials of the PC and other molecules in the reaction are crucial. The general rule is to select reducing/oxidizing pairs with favourable thermodynamic electron transfers. For the single-electron-transfer (SET) step to have positive free energy, the total potential must be negative:

$$\Delta G = -nFE \qquad\qquad \text{eq 1.1}$$

Where ΔG is the free energy of the electron transfer (kJ), n the number of electrons involved (1 electron in photoredox), F the Faraday constant (96 485.33 s•A/mol) and E the global potential (V). The latter can be obtained from the redox potentials of the species involved.

In 2014, DiRocco published the "Electrochemical Series of Photocatalysts and Common Organic Compounds" (Figure 1.6) which shows both ground state and excited state redox potentials of common photocatalysts along with the ground state redox potentials of various organic compounds.
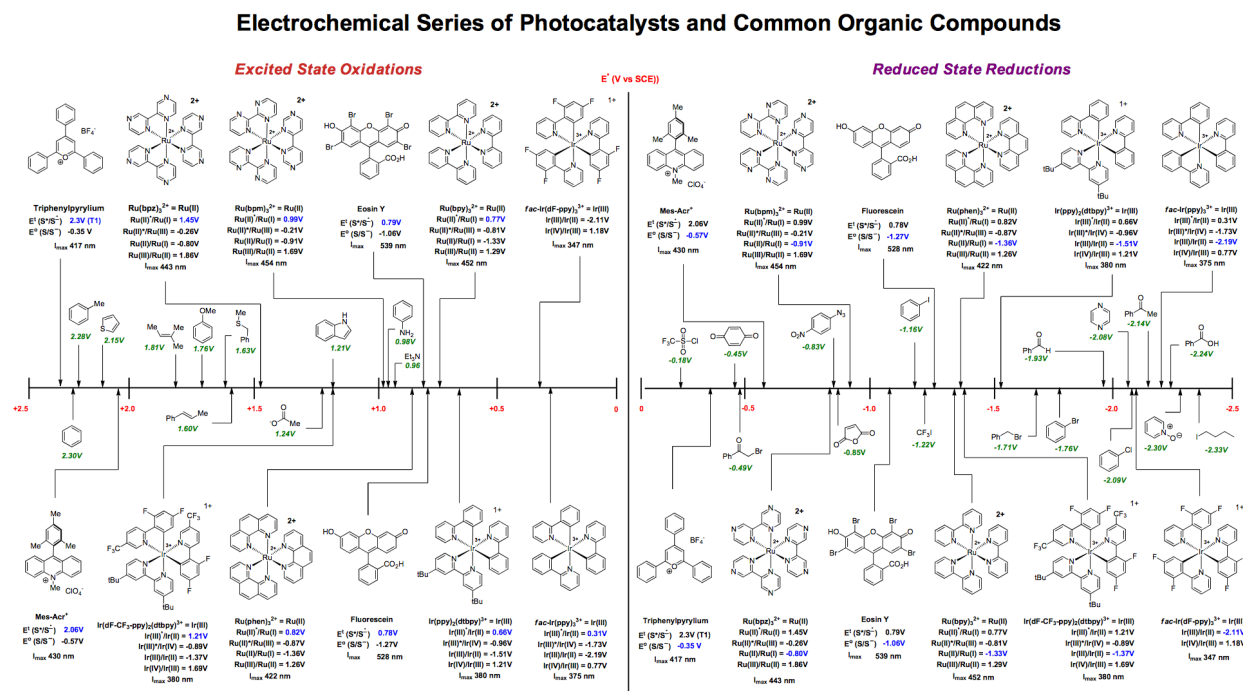
Figure 1.6. Electrochemical Series of Photocatalysts and Common Organic Compounds, from DiRocco (2014).

This series is a simplified overview that helps guide synthetic chemists to decipher if a photoredox reaction will be thermodynamically favourable or not. It is crucial to understand whether the initial electron transfer to or from the excited state photocatalyst is thermodynamically possible given it is the first step of the catalytic cycle. If the first step is thermodynamically unfavourable, it can be predicted based on this chart. For example, a PC that is a strong oxidizing agent is characterized

by having a larger positive potential (left-hand side of Figure 1.6) and will oxidize (remove an electron from) the molecule with a smaller potential. Whereas a PC will act as a reducing agent if it has a larger negative potential (right-hand side of Figure 1.6) and will reduce a molecule with a smaller potential (value closer to the middle of the chart in Figure 1.6).

By understanding the thermodynamics of each step in the mechanism, the reaction can be more efficiently optimized. One of the fundamental ideas behind photoredox catalysis is the utilisation of PC to achieve high-energy reactions using low-energy photons.

1.4   Kinetics of Reactive Intermediates

Reduction and oxidation properties are often used as a guide for developing photocatalytic reactions, as their potentials are helpful guides in determining whether a reaction is thermodynamically feasible. However, kinetic factors also affect a reaction feasibility. Even if the initial redox reaction is thermodynamically favourable, it does not mean that the reaction will happen. To determine exactly what pathways are involved in a chemical transformation, we must individually examine the kinetics of each pathway.

The important of kinetics is especially true for photochemical reactions where its synthetic abilities depend on making highly reactive intermediate species. The characterization and detection of these intermediates is key for an in-depth mechanistic study of these photochemical reaction. However, these reactive intermediates and excited-state molecules are short-lived, limiting their ability to efficiently engage in bimolecular processes.

For two reactive intermediates to successfully recombine in appreciable yields, their lifetime must be sufficiently long and effective concentration sufficiently large. Their yield would be governed by the first order rate law of a bimolecular reaction, in which the rate is proportional to the concentration of the two species that are reacting:

$$\text{Rate} = k\,[A][B] \hspace{4cm} \text{eq 1.2}$$

This means that for reactive intermediates, as their concentration in solution of a photochemical reaction is usually very low, it is unlikely that it will recombine with another reactive intermediate in a synthetically useful rate.

In the case of radical recombination, it would require the radicals to be generated at more or less equal rates, one radical to be longer lived and not self-terminate (the persistent radical, P•, eq 1.3) while the other be shorter lived (the transient radical, T•, eq 1.4), known as the "Fisher-Ingold Persistent Radical Effect" (Bravo *et al.,* 1997; Fischer, 1986; Fischer, 2001; Studer, 2001;). Another less likely condition is for the radicals be generated in very close proximity to each other. The first description of Persistent Radical Effect occurred many years before the term was coined by Fischer in 1986, by Bachmann and Wiselogle, (1936) where pentaphenylethane was heated and the main product was the starting material and not tetraphenylethane as expected. Bachmann and Wiselogle reasoned that the dissociation of the starting material was reversible, and that the triphenylmethyl radical is a persistent radical that did not self-terminate while the diphenylmethyl radical did. Years later Perkins, (1964) reacted phenylazotriphenylmethane in benzene. Much as Bachmann and Wiselogle found the persistent radical dimer of phenylcyclohexydienyl did not form.

Typical examples of the Fisher-Ingold Persistent Radical Effect are found in radical recombination reactions. The reason that the cross coupled product is favoured over the dimers are due to the nature of both the persistent and transient radicals. The persistent radical cannot self-terminate, resulting in its build up, whereas the transient radical can self-terminate (eq 1.6) or couple with the persistent radical (eq 1.5). The self-termination of T• results in a build-up of P• increasing it concentration and therefore accelerating and favouring the cross-coupled product (Fischer, 2001).

$$\text{X-P} \rightarrow \text{P•} + \text{X•} \qquad\qquad \text{eq 1.3}$$

$$\text{X-T} \rightarrow \text{T•} + \text{X•} \qquad\qquad \text{eq 1.4}$$

$$\text{P•} + \text{T•} \rightarrow \text{T-P} \qquad\qquad \text{eq 1.5}$$

$$\text{T•} + \text{T•} \rightarrow \text{T-T} \qquad\qquad \text{eq 1.6}$$

A photochemical example of the Fisher-Ingold Persistent Radical Effect is from Kothe *et al.* (1998) where they examined the spectroscopic and kinetic properties for a reaction between a decatungstate species ($W_{10}O_{32}^{4-}$) and an organic hydrogen donor (R-H). In the simplified mechanism depicted in Figure 1.7, they determined that during irradiation of the sample there was a large build-up of the decatungstate intermediate ($H-W_{10}O_{32}^{4-}\bullet$, the persistent radical) in the presence of various organic hydrogen atom donors. When examining the system using a pulsed laser, they noted that the transient radical (R•) quickly decayed, whereas the decatungstate intermediate was much longer lived. They rationalized the selectivity of the product using the Persistent Radical Effect.
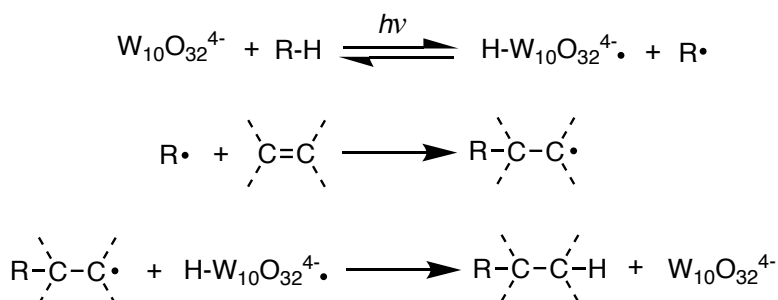
Figure 1.7. Photochemical reaction of polyoxymetalate anions between a decatungstate species and a transient radical (Kothe *et al.,* 1998).

While it is likely that many reactions in the literature could benefit from re-optimization based on the Fischer–Ingold Persistent Radical Effect, it is not a "one size fits all" description of radical-radical cross-coupling reactions. Focsaneanu *et al.* (2005) published a synthetic method to form 2,2,3-triphenylproprionitrile using one technique to form the persistent radicals and another for the transient radical (Figure 1.8).
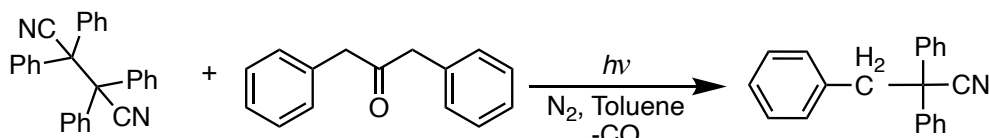
Figure 1.8. Synthesis of 2,2,3-Triphenylproprionitrile (Focsaneanu *et al.,* 2005).

The persistent radical was formed thermally, and the transient radical was generated photochemically. While the reaction was inspired by the Fischer–Ingold Persistent Radical Effect, it was later noted that the system was actually a radical trapping mechanism, and not an example of the Fischer–Ingold Persistent Radical Effect (Focsaneanu and Scaiano, 2006) (Figure 1.9).
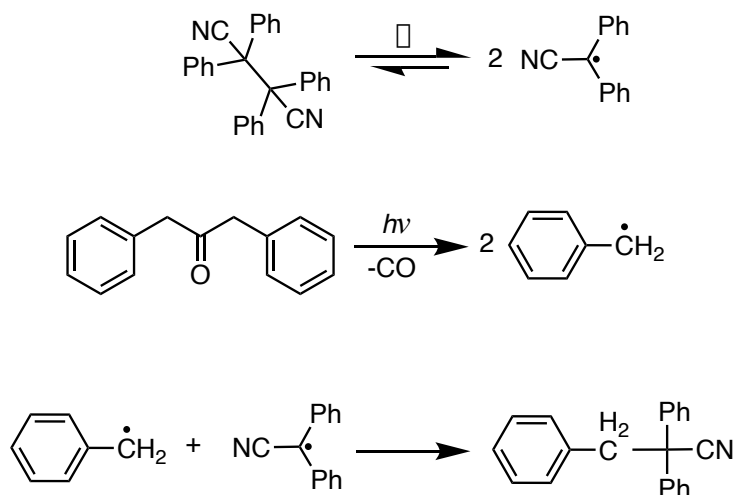
Figure 1.9. C-C bond forming mechanism through independent control of persistent and transient radicals. (Focsaneanu *et al.,* 2005).

Radicals are only one of many reactive intermediates that photochemical reactions are known to make. Excited state kinetics can be an effective tool in understanding photochemical mechanisms.

In the previous section we discussed that a PC acts as both a better oxidizing and reducing agent in the excited state. Therefore measuring the rate that the PC reacts with various species in the system will help determine the most likely reaction mechanism. Through both steady-state and time-resolved spectroscopy, we can examine the kinetics of the PC in its singlet and/or triplet state. The lifetime of a PC in its triplet excited state is longer lived than that of the singlet excited state (10^{-12} - 10^{-9} seconds vs 10^{-6} - 10^{-3} seconds, respectively). However, what will determine if the PC favourably reacts from the singlet, or the triplet is the rate at which it reacts with other species in solution, known as being "quenched".

If the PC is fluorescent, it is relatively easy to measure its singlet excited state lifetime. By monitoring the change in fluorescence as a function of quencher (Q) concentration, something

known as a Stern-Volmer plot, with various quenchers will determine the bimolecular quenching rate constant for each quencher. A more detailed discussion on Stern-Volmer plots will be in Section 2.6. If the PC favours reacting from the triplet, is it possible to measure the change in phosphorescence using the same techniques as above. Weakly emissive excited states or fast reactions create more challenges for kinetic analysis, however there are techniques such as laser flash photolysis (LFP) that can measure ultra-fast changes in absorption. More on Stern-Volmer and LFP are discussed in Chapter 2.

The excited state of a PC is a reactive intermediate, and as such is unlikely to react with other reactive intermediates in solution in synthetically useful rates. Using the rate constant of a reaction gives us an idea of how efficient each quencher can react with the PC, but it does not consider what the concentration of the quencher in the reaction is. Although one pathway may be the fastest, if the concentration of the quencher is not sufficient in solution it is unlikely to be the dominant reaction pathway. Nevertheless, kinetics data can be used to optimize a reaction mechanism by adjusting quencher concentrations to favour certain reaction pathways.

A thorough investigation into the thermodynamics and kinetics of a reaction will dictate the optimal reaction conditions. By revealing mechanistic insights into the complex working of the overall reaction, intelligent reaction design will follow. Understanding individual steps in a reaction mechanism leads to more efficiently optimized reactions, and all reactions can benefit from simultaneous reaction development and mechanistic investigation.

1.5   Objectives

The goal of my doctorate is to combine two worlds of chemistry: synthetic chemistry and state-of-the-art physical chemistry. Our "mechanistic insight and innovative solutions" approach to chemistry has, up until this point, been informed by steady-state and time-resolved spectroscopy, classical analytical chemistry, and computational chemistry. This tactic has resulted in several high-impact publications with researchers from Pfizer and Merck. The mechanisms we have studied are interestingly complicated and they open novel modes of reactivity with a surprisingly broad scope. We have shown that our "mechanistic insight and innovative solutions" approach has helped several synthetic chemists explain reactions.

My first mechanistic collaboration was with Pfizer in Chapter 2. We investigated the mechanisms of a photochemical reactions that successfully formed C_{aryl}-C_{alkyl} bonds without the aid of a transition metal photocatalyst. It is worth noting that the mechanism determined in this work is significantly different from the initially proposed mechanism.

In Chapter 3 we sought to identify the mechanism in a photoconversion of a dithioimide liquid crystal to its parent imide. In the presence of molecular oxygen, thione to ketone photoconversions are well understood. For our dithioimide, however, the photoconversion still proceeds in the absence of molecular oxygen and in anhydrous ether solvents (tetrahydrofuran and diethyl ether). Strangely, the thione to ketone photoconversion fails in dichloromethane and chloroform, which points to ethers as an unprecedented source of oxygen for this reaction.

My first collaboration was with Merck in Chapter 4. We set out to examine a catalytic reaction mechanism using an iron complex that can transform alkyl amines to amides; importantly, the reaction is similar to that of cytochrome P450 in the liver, where this reaction will help active pharmaceutical agents to make drug metabolites of unknown toxicity. The reaction investigated is an α-C-H oxidation. A potential structure of the iron centred catalyst was determined with high level DFT calculations and an in-depth computational look at the mechanism was performed. In this collaboration, we examined several potential mechanisms, along with numerous spin states.

In my final and most recent collaboration, we explore how the field of photoredox catalysis is expanding into novel territory. Chapter 5 details a new collaboration with Merck Exploratory Science Center in Cambridge Mass., where we are investigating a method to tag proteins using a naturally occurring photocatalyst: riboflavin. This blue light absorbing dye can oxidize phenols into the triplet excited state leading to persistent radicals that terminate via dimerization. This surprisingly efficient process has been used to tag proteins in vitro and in vivo with the spatial and temporal control afforded by light-activated processes.

TECHNIQUES TO INVESTIGATE A (PHOTO)CHEMICAL REACTION MECHANISM (THEORETICAL AND EXPERIMENTAL METHODS)

2.1 Photocatalytic Initiation

The first step of all photocatalytic reactions is excitation with light. Using a light source with sufficient energy will excite an electron from an atom or molecule from the highest occupied molecular orbital (e.g., HOMO, HOMO-1, etc) to the lowest unoccupied molecular orbital (e.g., LUMO, LUMO+1, etc) to create an excited state. If the overall spin of the molecule is zero, the ground state is called S_0, and subsequent singlet excited states follow the S_n nomenclature, where n is the order in overall energy. Therefore, the absorption of a photon will lead to a $S_0 \rightarrow S_n$ transition. Most excited state transitions can be depicted using a Jablonski diagram in Figure 2.1.
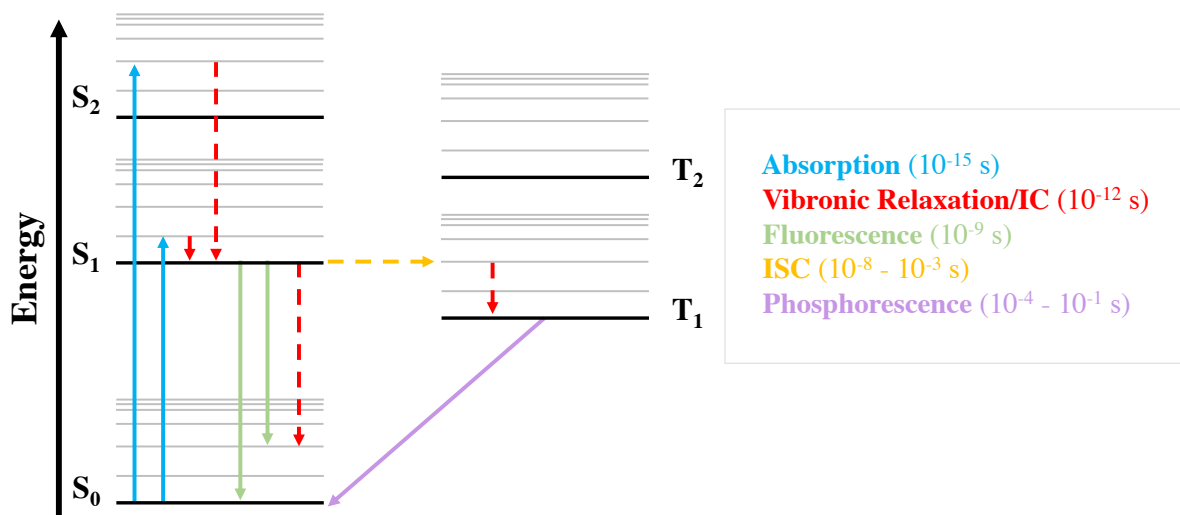
Figure 2.1. Jablonski diagram showing radiative and non-radiative transitions.

After the initially formed excited state, the molecule will relax to the lowest singlet exited state (S_1) where it can undergo radiative or non-radiative transitions according to Kasha's rule which states that: photon emission occurs from the lowest excited state of a given multiplicity (Kasha, 1950). It can either transition via, **1)** a non-radiative relaxation to the ground state ($S_1 \rightarrow S_0$ + *heat*), **2)** a radiative relaxation to the ground state via fluorescence ($S_1 \rightarrow S_0$ + *light*) or **3)** it can undergo intersystem crossing (ISC) to the triplet state ($S_1 \rightarrow T_n$). For an electron to ISC it must undergo a

spin flip. It can then relax to the first triplet excited state (T_1). To return to the ground state it can either undergo a non-radiative relaxation to the ground state ($T_1 \rightarrow S_0 + $ *heat*) or radiative relaxation to the ground state via phosphorescence ($T_1 \rightarrow S_0 + $ *light*).

Usually, molecules will undergo non-radiative relaxation to the ground state and release its extra energy as heat. However, some molecules have properties that favour releasing its extra energy through emission of a photon, via fluorescence or phosphorescence. In principle, the amount of energy absorbed should be equal to the energy emitted, but from Kasha's rule we can see that that is not always the case and will vary with the excitation wavelength of light used. Depending on the type of transition you want to monitor, there are several different spectroscopic techniques available to observe these different transitions.

2.2   Absorption Spectroscopy

Determining the photo-physical properties of a PC and starting material is typically the initial step in investigating a photochemical reaction mechanism. Absorption of a molecule is presented in the Jablonski diagram in Figure 2.1 using a blue upward arrow. The absorption of the photocatalyst will determine what wavelengths of light should be used to excite the photocatalyst without exciting the starting material.

Absorption spectroscopy is typically obtained using an Ultraviolet-Visible (UV-visible) spectrophotometer. It is a widely used technique due to its fast and precise ability to measure absorption spectra. A spectrum is obtained by passing light through a cuvette containing a solution of the molecule of interest and measuring the intensity of the light that passes through the sample (I) and correcting it by comparing the intensity of the light that passes through a blank sample, typically solvent (I_0) as shown in Figure 2.2. This is done for wavelengths in the ultraviolet and visible region, usually between 200 – 700 nm. The resulting spectrum is then shown as the absorption (A) vs wavelength, based on the equation:

$$A = - \log \frac{I}{I_0}$$

eq. 2.1

UV-visible spectroscopy can be used as quantitative analysis of both organic molecules, and transition metals ions. The Beer-Lambert law (eq. 2.2) is a way of measuring the concentration (c) of a solution with relation to its absorption (A), pathlength (l) and molar absorption coefficient (ε).

$$A = \varepsilon * c * l \qquad\qquad \text{eq. 2.2}$$
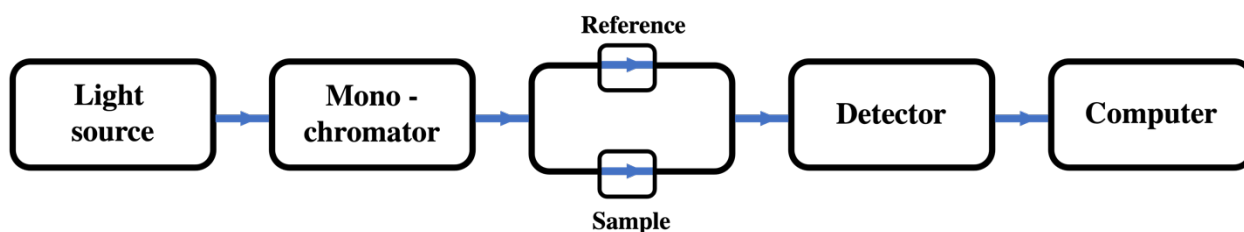
Figure 2.2. Ultraviolet-visible spectrophotometer with dual beam.

The solvent has an important impact on the excited state and will therefore change the absorption spectrum, known as the solvatochromatic effect. The data obtained from this technique is solvent dependant and should not be generalized for a molecule in different solvents.

2.3   Emission Spectroscopy

Absorption spectroscopy is considered complementary to emission spectroscopy. Emission details transitions from the excited state to the ground state (Figure 2.1, green and purple downward arrows), while absorption measures transitions from the ground state to the excited state. Emission spectra are often more selective to one analyte than absorption spectroscopy since relatively few molecules are emissive.

Fluorescence is the luminescence from the singlet excited state when a molecule relaxes back down to the ground state and releases a photon ($S_1 \rightarrow S_0 + light$). Instead of direct relaxation back to the ground state, the singlet excited state can ISC to the triplet excited state. The triplet is a chemically different species with different properties then the singlet. The likelihood of a photocatalyst to ISC will depend on its structure, and the probably increases if there is a heavy atom on the molecule. The influence of the heavy atom effect can explain why transition metals such as ruthenium and iridium are so dominant in photoredox catalysis, as the likelihood for ISC is high. Molecules without a heavy atom can still perform ISC but via other mechanisms.

18

The triplet can relax back to the ground state via a thermal pathway ($T_1 \rightarrow S_0 + heat$) or with the release of a photon ($T_1 \rightarrow S_0 + light$), known as phosphorescence. As the relaxation of a triplet to the ground state is a spin-forbidden process, the lifetime of a triplet is much longer than that of singlet, however the emission can be much lower.

Emission spectroscopy can be measured using a fluorimeter. To do this a specific wavelength of light must pass through a sample, and the light emitted from the sample is measured by the detector. Both the emission and excitation spectrum can be measured. The general setup of a fluorimeter is as follows: the light source emits many wavelengths of light that passes through a slit and is filtered through a diffraction grating where only certain wavelengths of light are permitted to pass through the sample. The sample will then emit a longer wavelength which then goes through a second set of windows and diffraction grating to filter out unwanted wavelengths of light before passing through to the detector (Figure 2.3A). Employment of pulsed light allows for time-resolved spectroscopy when paired with the appropriate detector to measure the fluorescence lifetime (Figure 2.3B).
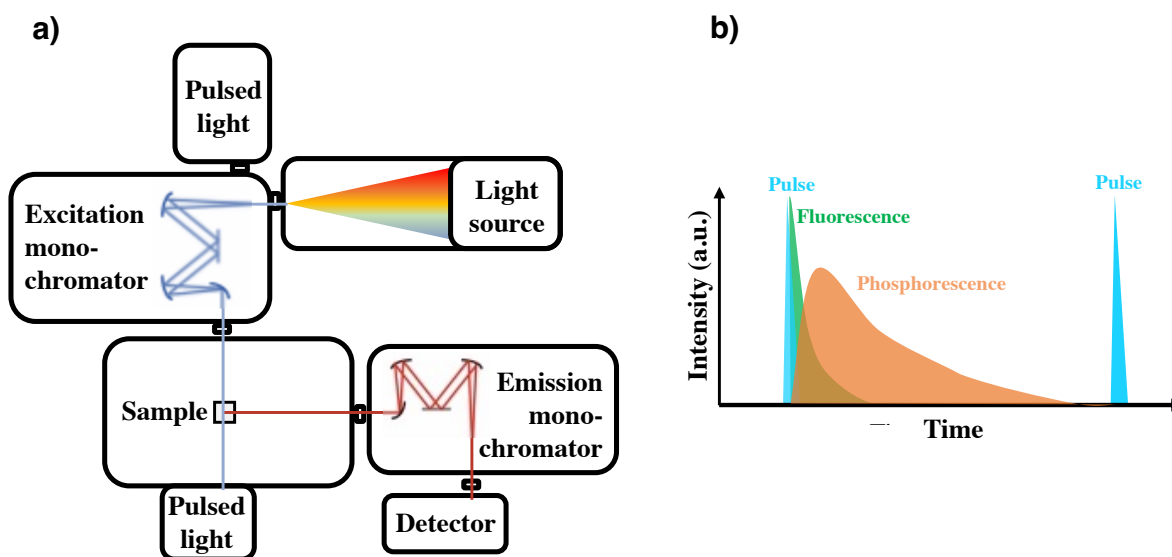
Figure 2.3. a) Fluorometer equipped with pulsed light sources and a gated detector for phosphorescence (Horiba Scientific, 2022) b) Time resolved luminescence (Bünzli, 2013).

2.4 Electrochemistry

Electrochemistry, in the context of photoredox catalysis, is useful to determine reduction potentials of reagents/catalysts, which can help predict the transfer of electrons between species in a reaction. Often, the redox steps occur in a series of single electron transfers (SET). A common photocatalytic cycle is depicted in Figure 2.4 and begins when the PC is irradiated into the excited state, [PC]*. The excited state, in this example, is a good oxidizing agent and will accept an electron from a quencher resulting in a reduced photocatalyst (PC$^{\bullet-}$). An acceptor molecule can then donate an electron to PC$^{\bullet-}$ where the PC will return to the ground state for the cycle to continue.
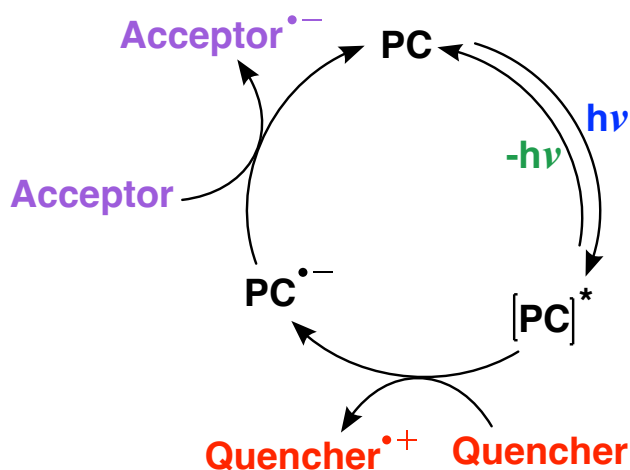
Figure 2.4. General photoredox cycle with [PC]* acting as an oxidizing agent.

The reduction and oxidation potential of a molecule can be determined using cyclic voltammetry (CV), by measuring the change in the potential of the working and reference electrode. The current of the working electrode is then plotted as a function of applied voltage to give a cyclic voltammogram, an example CV of ferrocene is presented in Figure 2.5. The redox potential of a molecule is considered reversible when we can see both an oxidation and reduction peak. In an ideal 1-electron transfer voltammogram, the difference in between the two peaks positions is 59 mV.
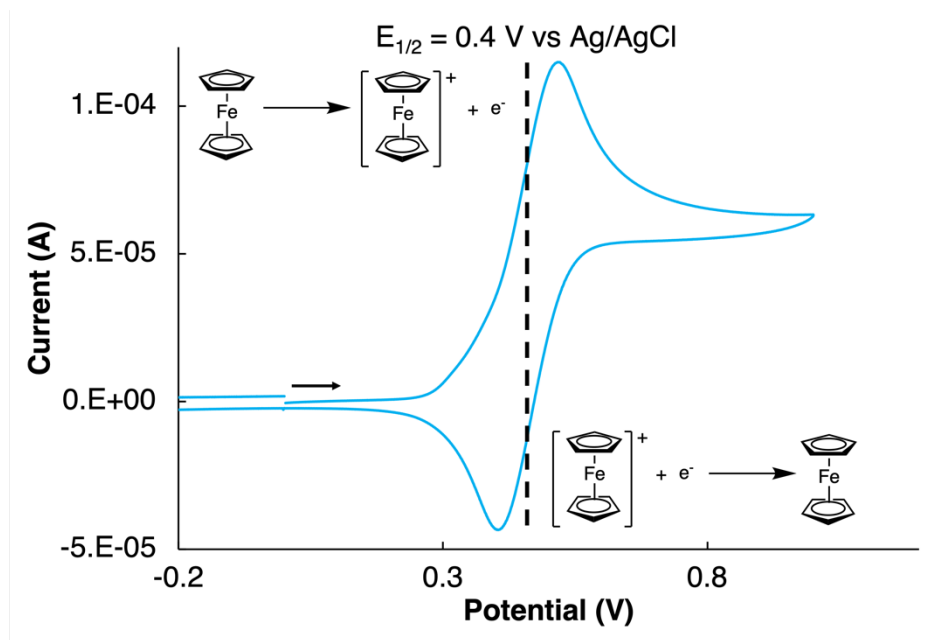
Figure 2.5. Cyclic voltammogram of ferrocene in acetonitrile.

The redox potential of a PC and quencher is pivotal in a reaction design. For a reaction to take place the reduction or oxidation potential must be thermodynamically favourable, with the overall potential being negative resulting in a positive free energy (ΔG) as shown in eq. 1.1.

2.4.1 Calculating Excited State Redox Potentials

For a PC in the excited state, it is important to use its excited state redox potential in determining its ΔG. To measure the excited state redox potential (E*$_{1/2}$), the ground state redox potential is combined with the absorption and emission spectra of a molecule. The Rehm and Weller equation (Rehm and Weller, 1970) is commonly used to evaluate the excited state redox potentials:

$$E^*_{1/2}{}^{red} = E_{1/2}{}^{red} + E_{00} \qquad \text{eq. 2.3}$$

$$E^*_{1/2}{}^{oxi} = E_{1/2}{}^{oxi} - E_{00} \qquad \text{eq. 2.4}$$

Where E*$_{1/2}$ is the excited state reduction (red) or oxidation (oxi) potential. E$_{1/2}$ is the oxidation or reduction potentials of the ground state, measured with cyclic voltammetry. E$_{00}$ refers to the transition from the lowest vibronic state. This is estimated to be the intersection between the

21

absorption and emission spectra by converting wavelength to electron volts. The Rehm-Weller equation can be used for both singlet and triplet excited state, using the intersection between the absorption and fluorescence spectrum for the singlet excited state and absorption and phosphorescence for the triplet excited state. The singlet will produce a stronger excited state oxidant or reductant because it is higher in energy. However, the lifetime of the triplet is longer increasing the probability of a bimolecular reaction.

2.5 Laser Flash Photolysis

Time-resolved absorption spectroscopy is a powerful tool to study the reaction kinetics of photochemical reactions. To initiate the reaction an ultra-fast intense laser pulse (nano- to femtosecond pulse) passes through the sample using a laser flash photolysis (LFP) setup (Figure 2.6). This fast laser pulse "instantaneously" forms reactive intermediates, such as triplets, singlets, radicals, carbenes, etc, that can be followed on short timescales. Immediately after the pulsed laser hits the sample, the change in absorption can be measured, as either a function of time or wavelength. A blank is taken for correction by measuring the absorption of the sample before the laser is pulsed. The decay in the absorption of the excited state can be used to measure the lifetime of the excited state with and without quencher.

To measure a sample, a very short laser pulse on the order of 1-10 nanoseconds of a Nd:YAG (neodymium-doped yttrium aluminum garnet) laser is pulsed. The direct emission of a Nd:YAG laser of 1064 nm is rarely used. To convert 1064 nm into more useful wavelengths, crystals are used to emit photons at higher frequencies. It is excited by 2 or more photons to create an imaginary excited state which can then emit a photon that is 2 or more times higher in frequency upon relaxation. The laser can now access wavelengths of 532, 355 and 266 nm from the splitting of the original 1064 nm wavelength. It is possible to use an optical parametric oscillator (OPO) to access the entire range of wavelengths in the UV-Visible-IR (300-3000 nm) or use short OPO pulses.
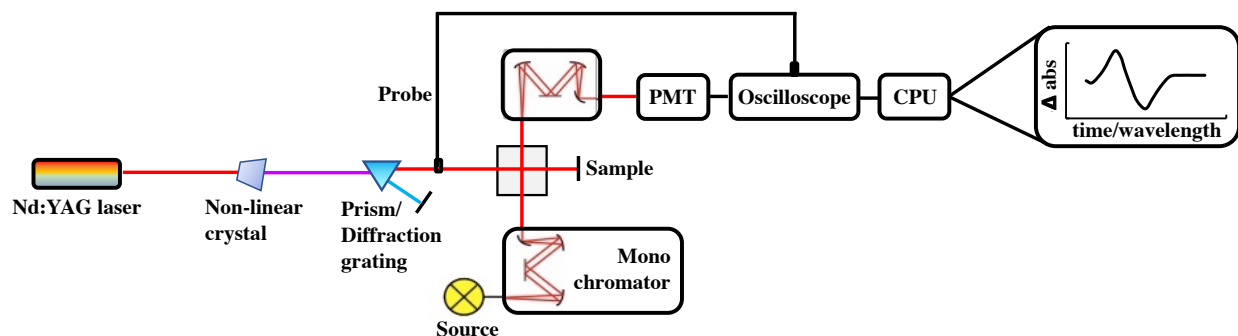
Figure 2.6. Laser Flash Photolysis setup.

With this technique, we can determine the reactivity of reactive intermediates with a multitude of reagents. In contrast to a fluorimeter that only detects when molecules emit a photon, LFP can directly detect excited states or reaction intermediates using their absorption spectra on nano- to milli-second timescales (10^{-9} to 10^{-3} s, respectively).

2.6   Rection Kinetics Using Stern-Volmer Quenching

Steady state quenching studies are another method to analyze the kinetics of a photochemical reaction. Processes such as fluorescence and phosphorescence are examples of *intra*molecular deactivation, or quenching. *Inter*molecular quenching is another possible pathway for the PC to return to the ground state when in the presence of other chemical species, or quenchers (Q). The general scheme can be represented as:

$$\text{PC} + hv \xrightarrow{k_{abs}} \text{[PC]*}$$

$$\text{[PC]*} \xrightarrow{k_{nr}} \text{PC} + heat$$

$$\text{[PC]*} \xrightarrow{k_{rad}} \text{PC} + hv'$$

$$\text{[PC]*} + \text{Q} \xrightarrow{k_q} \text{quenching reaction}$$
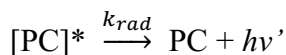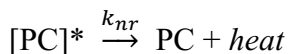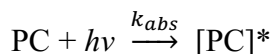
To determine if the molecule will favour returning to the ground state via a non-radiative pathway (release a photon via fluorescence) or be quenched depends on the rate of each individual reaction. The rate of emission (k_{rad}) is in competition with other deactivation pathways such as non-radiative

23

pathways (k_{nr}) and quenching (k_q). In the absence of quencher, the excited state lifetime is equal to $(k_{nr} + k_{rad})^{-1}$. The emission quantum yield with and without quencher, Φ_0 and Φ_Q, can be defined using these rate constants:

$$\Phi_0 = \frac{\text{photons emited}}{\text{photons absorbed}} = \frac{k_{rad}}{k_{rad} + k_{nr}} = k_{rad}\tau_0 \qquad \text{eq. 2.5}$$

and

$$\Phi_Q = \frac{k_{rad}}{k_{rad} + k_{nr} + k_Q[Q]} \qquad \text{eq. 2.6}$$

When comparing the quantum yield of emission without quencher and in the presence of quencher (Φ_0/Φ_Q) you can derive the Stern-Volmer relationship:

$$\frac{\Phi_0}{\Phi_Q} = 1 + k_q\tau_0[Q] \qquad \text{eq. 2.7}$$

This relationship allows for us to measure the effect that a quencher has on the intensity of the photocatalytic emission spectra and relate it to k_q. By increasing the concentration of quencher in solution the emission intensity should decrease, the amount by which is related to the rate at which the photocatalyst reacts with the quencher. The species in solution that quench's the photocatalyst the fastest can then be identified. Since the ratio of quantum yield is equal to the ratio of emission intensity and excited state lifetime, the Stern-Volmer equation can also be written as:

$$\frac{\Phi_0}{\Phi_Q} = \frac{I_0}{I_Q} = \frac{\tau_0}{\tau_Q} = 1 + k_q\tau_0[Q] \qquad \text{eq. 2.8}$$

The nature of quenching however cannot be distinguished by solely looking at change in emission intensity as a function of quencher concentration. Dynamic quenching can be distinguished from static quenching by monitoring the excited state lifetime of the photocatalyst (time resolved)

instead of the emission spectrum (steady state) as the concentration of quencher increases (Figure 2.7 and 2.8). This is because static quenching inhibits the formation of the excited state and would therefore show no change in the fluorescence lifetime. Whereas dynamic quenching is a process that takes place through diffusional collision.
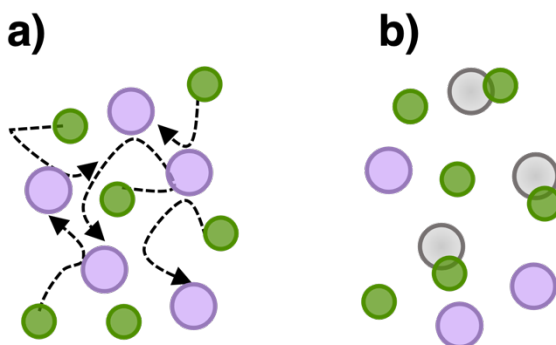
Figure 2.7. Quenching in solution by a) dynamic or b) static mechanisms.

The Stern-Volmer relationship can be applied for both time-resolved and steady state analysis. Importantly, it cannot distinguish between chemical quenching (electron transfer) and physical quenching (energy transfer).
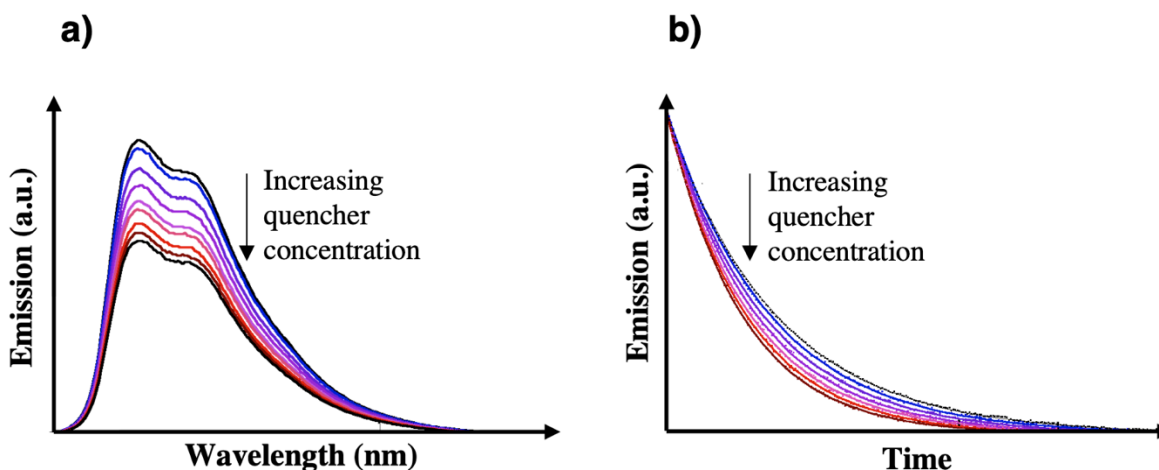
Figure 2.8. Spectra of a) steady-state emission quenching and b) time-resolved emission quenching.

The graph of emission intensity with and without quencher (or quantum yield or excited state lifetime, from eq. 2.8, vs quencher concentration gives a Stern-Volmer plot where the slope is equal to $k_q\tau_0$. By knowing τ_0, k_q can be determined between a PC and various quenchers (Figure 2.9).
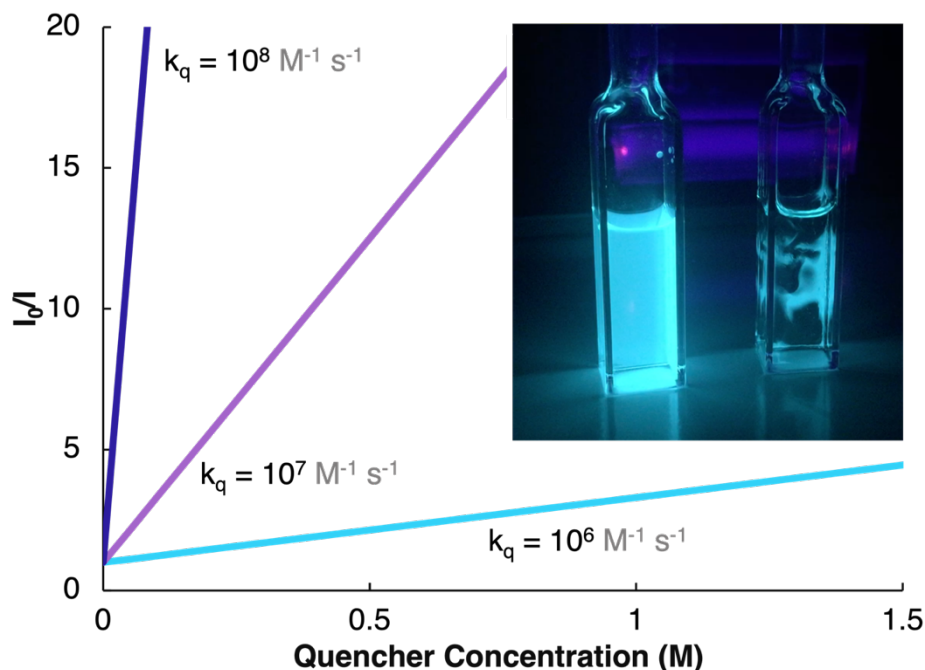
Figure 2.9. Idealized Stern-Volmer plot with fast (dark blue), medium (purple) and slow (pale blue) quenchers. Inset: $Ir^{III}Ln$ in degassed acetonitrile under UV-light excitation before (left) and immediately following (right) addition of an amine quencher (DABCO was used for this picture) to illustrate the emission quenching by the electron transfer reaction.

2.7 Quantum Yield

When examining a photochemical reaction, an important question is to address how photon efficient the reaction is. The quantum yield of a reaction (Φ_r) is a measure of the number of molecules produced per photon absorbed (eq. 2.9). If Φ_r is greater than one, this is direct evidence that a chain propagation reaction takes place, which is most common for radical photoredox based reactions mechanisms. If Φ_r is less than one, it does not indicate a closed cycle mechanism, but rather could also point to inefficient chain propagation. The quantum yield is an important characteristic in a photochemical reaction mechanism because the optimization of a chain reaction can significantly differ from a non-chain reaction.

$$\Phi_r = \frac{\text{mol of produced formed}}{\text{mol of photons absorbed}} \qquad \text{eq. 2.9}$$

The number of molecules produced can be determined by a multitude of analytical methods such as UV-Visible or mass spectrometry. However, measuring the number of photons absorbed by a sample is not trivial, therefore we use a reference system based on ruthenium-diphenylanthracene-O_2 system with a known yield as described by Pitre *et al.* (2015), illustrated in Figure 2.10
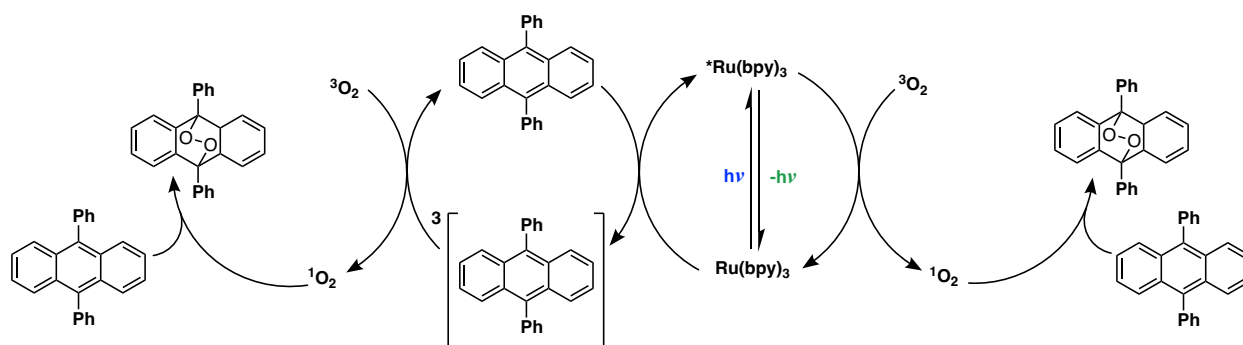
Figure 2.10. Reaction mechanism based on ruthenium-diphenylanthracene-O_2 actinometry (Pitre *et al.,* 2015).

The experimental conditions of the reference system (actinometry) must be strictly respected for the results to yield exact data. The intensity of the light, the absorption and emission, and the sample geometry must be carefully matched between the sample and the reference.

The quantum yield of the ruthenium-diphenylanthracene-O_2 actinometry system is 0.019. The reaction between singlet oxygen ($^1O_2$) and 9,10-diphenylanthracene (DPA) is monitored using UV-visible spectroscopy. The absorption decrease is caused by the loss of DPA's π conjugation as it reacts with $^1O_2$ via a [4+2] cycloaddition at a known rate constant (Figure 2.11).
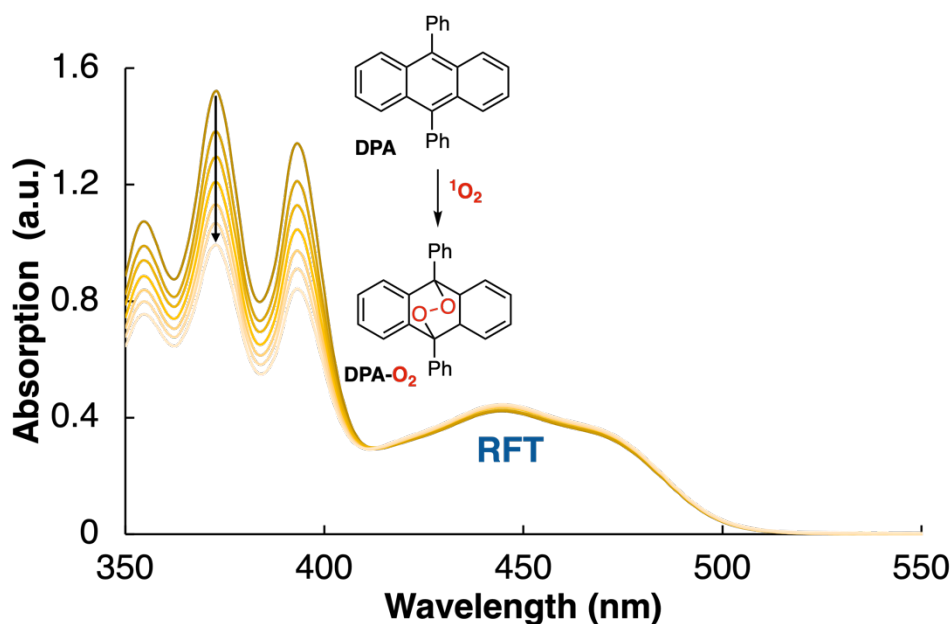
Figure 2.11. Absorption spectra of **DPA** and **RFT** during blue-light irradiation—the absorption decrease is caused by the loss of **DPA's** π conjugation as it reacts with $^1O_2$, via a [4+2] cycloaddition at a known rate constant ($k_q = 2.0 \times 10^6$ M^{-1} s^{-1}).

2.8 Determining The Theoretical Thermodynamics of a Reaction Mechanisms Using Density Functional Theory

Experimentally determining the energy of excited state molecules can be challenging. The emission of many organic molecules is low, resulting in difficulties when trying to determine their energies from spectroscopy alone. A useful solution to this is density functional theory (DFT) calculations. DFT is a computational method that derives characteristics of molecules based on a physical property that is common to all molecules, their electron density. DFT methods have evolved from its predecessor, Hartree-Fock, to incorporate exchange interactions increasing its overall utility.

There are many different approaches to structural determination using computational chemistry. However, there is no one ideal computational method that encompasses reliable and accurate information of all systems. The ideal method will vary depending on the objective of the project and the computational cost one is willing to spend. The projects detailed herein are investigated using methods based on DFT, which is a subset of the quantum chemical method. The major disadvantage of DFT is has a limited consideration for dispersion interaction and solvent modelization, and it usefulness is limited to relatively small molecules.

Semi empirical methods are one way to overcome the atom size limitation that DFT calculations can impose. These calculations are also based on quantum chemical methods but rely on different approximations. Semi-empirical methods are often less accurate, but the trade-off is its utility on larger systems. Another method to simulate chemical systems is based on molecular mechanics, where unlike quantum mechanics electrons are not explicitly accounted. Molecular mechanics is most used for systems that have thousands of atoms such as proteins.

DFT calculations have aided in mechanistic studies through the calculation of transition state energies, radicals, ions, triplet excited states and determination of the lowest energy confirmation among other possibilities. These reactive and often short-lived intermediates can be challenging to directly observe, and therefore difficult to know their exact pathway in a reaction mechanism. By calculating the thermodynamics of individual steps in a reaction mechanism, it is possible to evaluate several different reaction mechanisms in a relatively short period of time. DFT can also predict with good accuracy reduction and oxidation potentials of organic and inorganic molecules leading to unexpected photoredox pairs.

To run a DFT computation several aspects need to be specified: the molecule and its geometry, the spin multiplicity, the functional, and the basis set. The most common density functional is B3LYP, which was developed by Becke, Lee, Yang and Parr (Becke, 1992; Becke 1993; Lee *et al.,* 1998) in the late 90's. The choice of functional is dependent on the system under investigation and the atoms present on the molecule under investigation. Other common functionals include M06-2X which work well for amine group atoms but are not suitable for transition metals, and ωB97xD which includes empirical dispersion. The choice of basis set influences the accuracy and time involved for the calculation. However, not all basis sets can be used for all atoms and the choice of basis set will depend on the atoms under investigation. For example if the molecule contains only H, C, N, and O atoms then 6-311G might be most suitable, but for molecules with transition metals and other heavy atoms other basis sets may be more suitable such as LanL2DZ.

The trade-off often made in computational chemistry is between finding the most accurate calculation system while remaining computationally reasonable with respect to how long each calculation will take. The limitations in DFT such as dispersion corrections and solvent

modelization can be managed with the option to add additional dispersion correction or solvent modelization without sacrificing much computational cost.

Density functional theory is a valuable technique used to support and validate experimental results. DFT can be used model difficult or impossible to isolate reactive intermediates that provide valuable insight into a reactions mechanism, predict the favourability of individual reaction steps along with many other characteristics that support the powerful insight that comes with combining experimental and computational chemistry in mechanistic elucidation.

2.8.1   Solvent Modelization

The solvent chosen for a reaction influences the stability of the molecules. When computationally calculating solvent there are two options, explicit and implicit solvent modeling. Explicit models consider molecular details of each solvent molecule as a separate optimization and is computationally very demanding while also slightly ambiguous. Whereas the implicit model treats solvent as a continuous polarizable medium on the accessible surface of the molecule. The surface of the molecule represents the part accessible by the solvent and allows for the Van der Waals radius to be considered. The decision to model solvent explicitly or implicitly will vary depending on the computational power available and the system under investigation.

Conductor-like polarizable conductor model (CPCM) is one of the most common methods used to model implicit solvent as it has a good relationship with experimental values while maintaining a relatively low computational cost.

CHAPITRE 3

METAL-FREE VISIBLE LIGHT C-H ALKYLATION OF HETEROAROMATICS VIA HYPERVALENT IODINE-PROMOTED DECARBOXYLATION

3.1   Résumé

Genovino, J., Lian, Y., Zhang, Y., **Hope, T.O**., Juneau, A., Gagné, Y., Ingle, G., Frenette, M. (2018). Metal-Free-Visible Light C–H Alkylation of Heteroaromatics via Hypervalent Iodine-Promoted Decarboxylation. Organic Letters, 20(11), 3229-3232. doi: 10.1021/acs.orglett.8b01085

Une alkylation C-H d'hétéroaromatiques à l'aide d'un photocatalyseur organique sans métal, d'acides carboxyliques et d'iode hypervalent sous irradiation à la lumière bleue est rapportée. La réaction est applicable à la fonctionnalisation à un stade avancé de produits pharmaceutiques et de composés de type médicament, et tolère une large gamme de groupes fonctionnels. En plus des calculs DFT, des expériences de contrôle et des expériences photophysiques ont été utilisées pour examiner le mécanisme de la réaction.
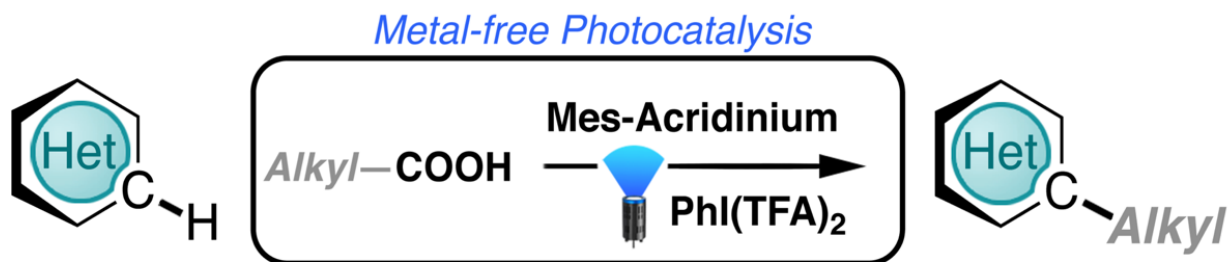
Figure 3.1. Alkylation d'un hétéroarène catalysée par un photocatalyseur mésityl-acridium à partir d'acides carboxyliques aliphatiques et d'oxydant à base d'iode hypervalent. (Alkylation of a heteroarene catalyzed by a mesityl-acridium photocatalyst starting from alkyl carboxylic acids and hypervalent iodine as an oxidant).

Supplemental information is available in Annexe A and includes a description of quantum yield experiments, reference system spectra and kinetic traces, time-resolved Stern-Volmer quenching results, additional cyclic voltammograms, and DFT energies and atomic coordinates.

3.2   Foreword

The work presented in this chapter is the result of a collaboration with researchers at Pfizer Worldwide Medicinal Chemistry in Groton, Connecticut. The original concept, the optimization of the reaction and its conditions, the control experiments, compounds characterization and in general the organic chemistry aspect was completed by our collaborators at Pfizer: Julien Genovino, Yajing Lian, Yuan Zhang and Gajendra Ingle.

Chemical actinometry, quenching rate constants, and cyclic voltammetry experiments were performed by Antoine Juneau and me. The DFT studies were performed by Antoine Juneau, Yohann Gagné, Mathieu Frenette and me.

As a lead author from my research group on this study, our objective in this collaboration was to complement the reaction developed by Julien Genovino and his colleagues with an in-depth mechanistic understanding backed by computational and experimental results.

3.3   Abstract

C-H alkylation of heteroaromatics using a metal free organic photocatalyst, carboxylic acids and hypervalent iodine under blue light irradiation is reported. The reaction is applicable to the late-stage functionalization of pharmaceuticals and drug like compounds and is tolerant of a wide range of functional groups. In addition to DFT calculations, control experiments and photophysical experiments were used to examine the reaction mechanism.

3.4   Introduction

The C-H alkylation of heteroaromatics is a synthetically desirable and useful reaction in the pharmaceutical industry for rapid late-stage functionalization of potential pharmaceutical products. A well-known way to functionalize electron-deficient heteroarenes is via the addition of carbon-centered radicals under oxidative conditions, a method known as the Minisci reaction (Minisci *et al.,* 1971). Minisci used simple and inexpensive carboxylic acids to generate alkyl radicals however, the use of silver nitrate, ammonium persulfate, and sulfuric acid at elevated temperatures, are quite harsh conditions that present many practical limitations.

Nevertheless, this reaction served as inspiration for many C-H alkylation reactions using photoredox catalysis. Using photons to help synthesize alkyl centre radicals means that harsh conditions such as high temperatures are no longer necessary. An advantage of using photoredox catalysis is that it allows for more mild and efficient reaction conditions at room temperature. DiRocco *et al,* (2014) proposed the first photoredox-mediated Minisci alkylation reaction of N-heteroarenes. They used iridium as the photocatalyst and peroxides as the alkylating reagent. However, this method requires 10 equivalents of the coupling partner, uses an expensive metal catalyst, and has a limited alkyl scope. This method was later improved by Chen *et al.* (2016) who proposed a Minisci type reaction that could tolerate a broader range of functional groups and alkyl radicals but required the use of a ruthenium photocatalyst. In that same year, McCallum and Barriault, (2016) developed a cross coupling Minisci reaction using unactivated bromoalkanes. Again, this method required the use of expensive and rare gold as the photocatalyst and high energy UVA lights. In 2017 the Frenette group collaborated with researchers at Pfizer on a visible-light-driven Minisci reaction with the goal of enhancing reaction conditions by replacing the often-exploited and expensive transition metal photocatalyst with a more earth abundant metal. Using $Mn_2(CO_2)_{10}$ as the photocatalyst is more cost-effective, however it will be problematic to remove from the eventual pharmaceutical product. The reaction also required expensive alkyl iodides as the starting material (Nuhant *et al.,* 2017).

Each method developed exhibits some inherent limitations. In light of these advances, the present collaboration sought to develope a more efficient Minisci type reaction without the use of a metal photocatalyst or expensive starting material. The result is this collaboration between Pfizer and the Frenette group (Genovino *et al.,* 2018), where the first metal-free and visible light promoted C-H alkylation of heteroaromatics using hypervalent iodine decarboxylates at room temperature is investigated.

This Minisci type reaction was proposed as an alternative for C_{aryl}-C_{alkyl} coupling with more attractive reaction conditions. Our synthetic method used an organic photocatalyst instead of a transition metal photocatalysts to limit the contamination of the eventual pharmaceutical produced. In addition, the reaction used carboxylic acids as starting material due to their inexpensive and abundant nature. Our method tolerates a broad range of carboxylic acids (Figure 3.2A), and

heteroarenes (Figure 3.2B), to give products in moderate to excellent yields, including three drugs which were selected to test the protocol as a late-stage C-H functionalization method.
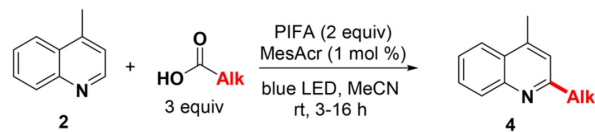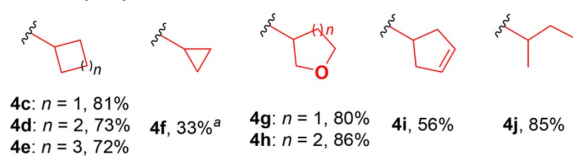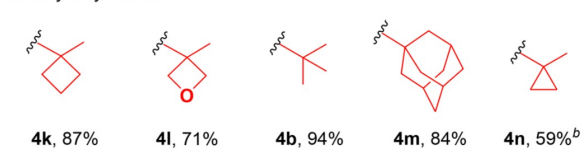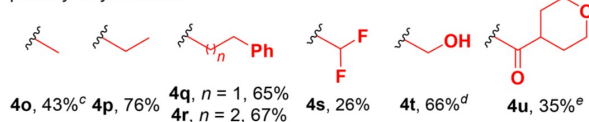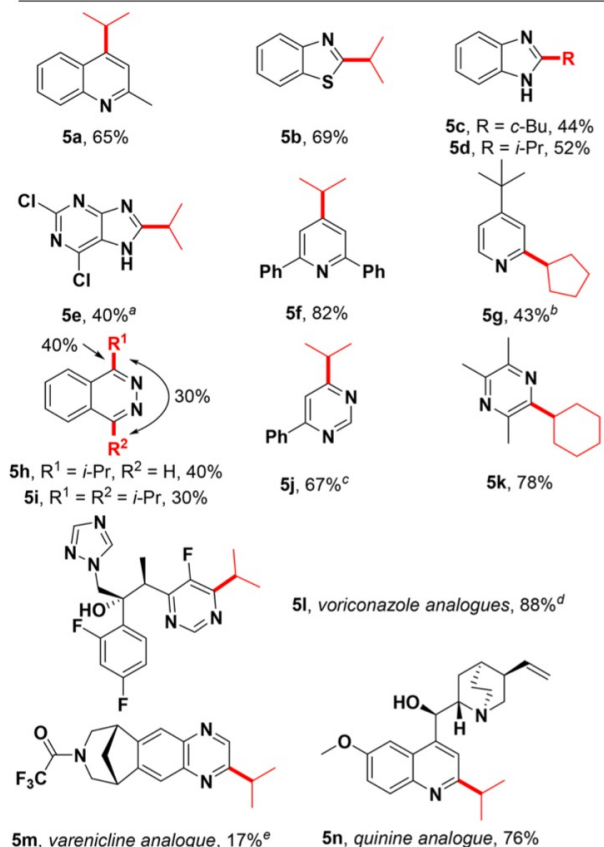
Figure 3.2. Reaction scope for a) carboxylic acid b) heteroaromatics and drugs.

Initially, our collaborators proposed the reaction mechanism shown in Figure 3.3. The alkyl radical initiator adds to the protonated heteroarene to form a radical cation. The latter allows the redox 9-mesityl-10-methyl acridinium (MesAcr) catalytic cycle to get started: MesAcr in its excited state oxidizes the radical cation heteroarene and yields the desired alkylated product and reduced MesAcr. The reduced PC can reduce the bulk of hypervalent iodine-carboxylic acid adduct to continue generating the alkyl radicals while the photooxidant in its ground state is regenerated (pathway B).

This mechanism is supported by the evidence of a slow background reaction, and low conversion of the product without the presence of photocatalyst in solution. However, we believe that this mechanism is unlikely to be the primary reaction mechanism due to the low concentration of both the PC in excited state and radical cation heteroarene in solution. These are two reactive species that would favourably react, however their effective concentration in solution would not be enough to generate the yields described in Figure 3.2 in 3-16 hours.
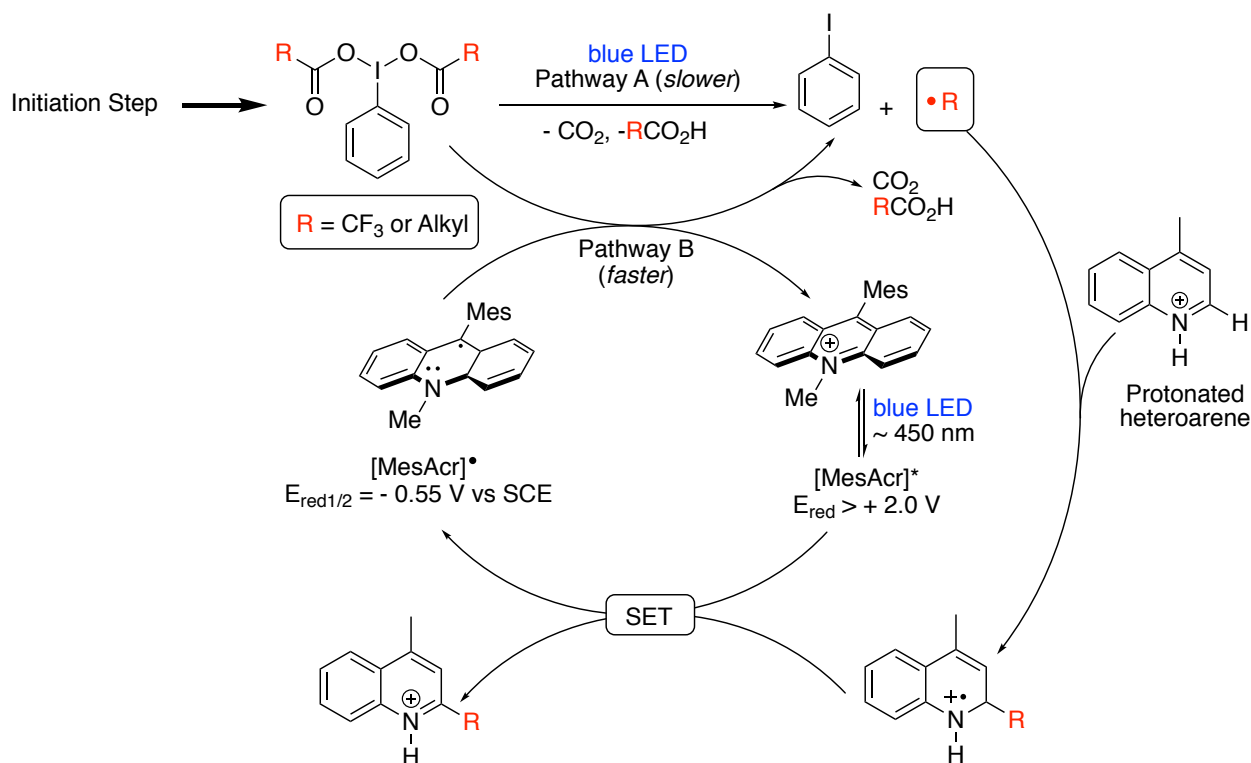
Figure 3.3. Alternative reaction mechanism.

Our counter proposed reaction mechanism is outlined in Figure 3.4 as a chain mechanism initiated with excitation of the organic PC, MesAcr, with blue light. MesAcr then enters the exited state [MesAcr$^+$]* where it undergoes a reduction from an electron donor. Once reduced, it transfers an electron to an acceptor, the hypervalent iodine, to initiate the chain reaction. The hypervalent iodine radical anion will then rapidly collapse leading to the formation of the alkyl radical. The alkyl radical will then combine with the protonated heteroarene in the alpha position resulting in a radical cation. This radical cation will then undergo deprotonation to give an α-amino radical. This α-amino radical will undergo a single electron transfer (SET) with another hypervalent iodine to

produce a radical anion hypervalent iodine and the product. The hypervalent iodine radical anion then continues in the catalytic cycle.
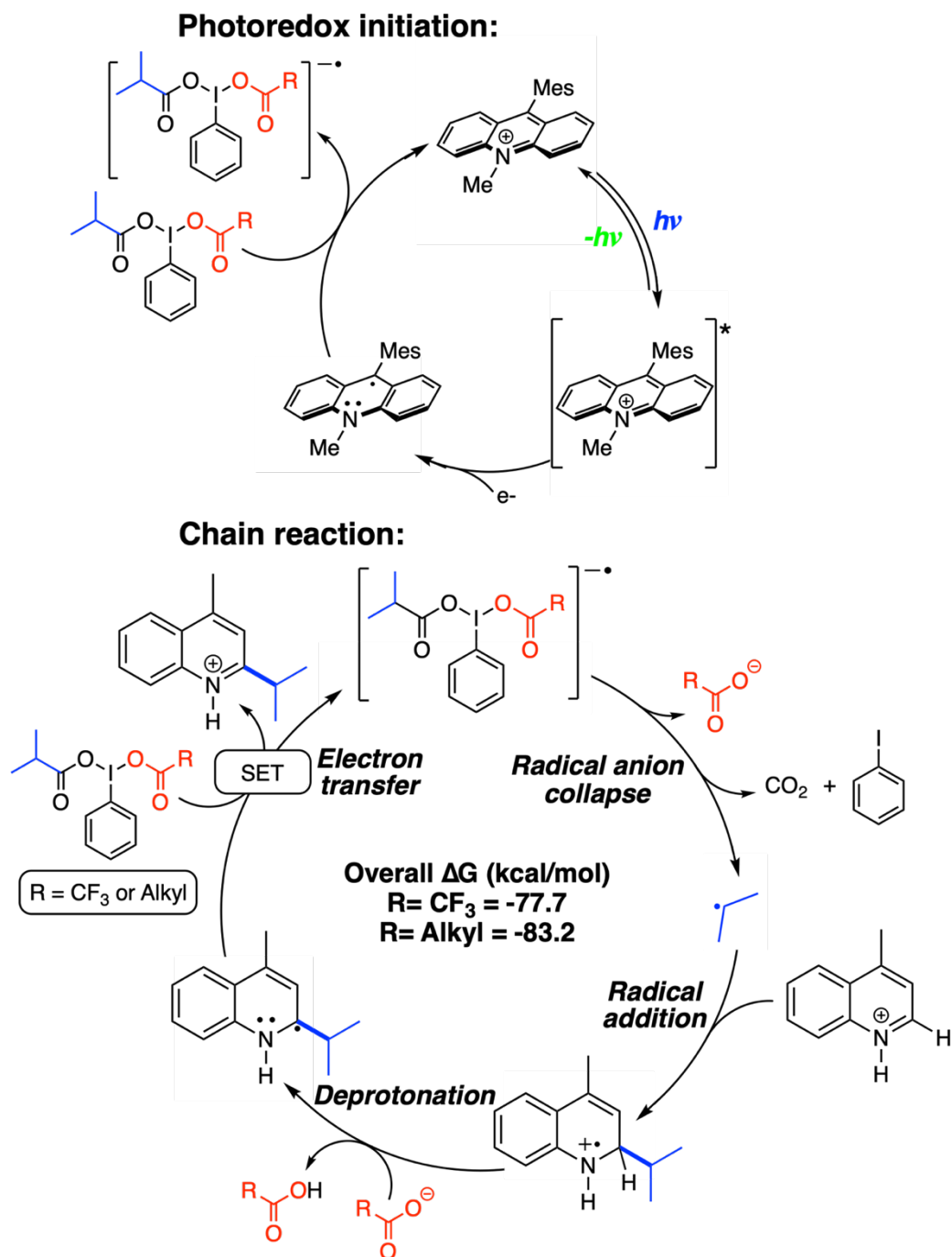
Figure 3.4. Proposed reaction mechanism for the C_{sp2}-C_{sp3} Minisci reaction.

These results show that this mild catalytic system tolerates a wide variety of functional groups. While the proposed chain reaction mechanism is more photon efficient when compared to a closed catalytic cycle, although an inefficient chain reaction is likely.

3.5   Experimental Methods

3.5.1   Quantum Yield

3.5.1.1   Chemical Actinometry of the Reference System

The quantum yield of the reaction was obtained from a Ru(bpy)$_3$ (where bpy is 2,2'- bipyridine) and 9,10-diphenylanthracene (DPA) chemical actinometer according to the protocol described by Pitre *et al.* (2015). Ru(bpy)$_3$(PF$_6$)$_2$ was used as opposed to Ru(bpy)$_3$Cl$_2$ and the quantum yield was assumed to stay unchanged. Experiments were performed using 16 W blue outdoor LED by Feit Electricity. Quartz cuvettes were held by an in-house built support secured to a platform shaker set at 600 rpm, air-cooled using a fan (For in-house LED setup see Annexe A Figure A.1). Light intensity on the sample was measured to be ~ 84 µmol•s^{-1}•m^{-2} using a LI-COR Quanta Photometer for the low intensity quantum yield, and ~ 700 µmol•s^{-1}•m^{-2} for the high intensity quantum yield.

A 3 mL solution of DPA and Ru(bpy)$_3$(PF$_6$)$_2$ was prepared according to the conditions used by Pitre *et al.* (2015) and added to a 1 x 1 quartz cuvette under air. Aliquots were taken during irradiation to monitor the decay of DPA at 372 nm over 12 minutes (for plots see Annexe A Figure A.2).

3.5.1.2   Chemical Actinometry of our System

To a quartz cuvette under N$_2$, MesAcr$^+$ BF$_4^-$ (0.01 eq, 0.03 mmol, 1 mM) was mixed with lepidine (1 eq, 0.3 mmol, 0.1 M), [bis(trifluoroacetoxy)iodo]benzene (PIFA) (2 eq, 0.0006 mmol, 0.4 M) and cyclohexane carboxylic acid (3 eq, 0.9 mmol, 0.3 M) in acetonitrile to a total volume of 3 mL. The cuvette was deoxygenated and sealed with a rubber septum under a positive pressure of N$_2$ using a balloon. The cuvette was placed in the in-house LED setup and aliquots were taken over 225 minutes (See Annexe A Figure A.4 for plots). The expected product was analyzed using GC-MS (225.1 m/z) with benzaldehyde as internal standard, and the pure product was isolated by flash chromatography. The Ru(bpy)$_3$(PF$_6$)$_2$ concentration of the actinometer experiment was adjusted to

match the absorption of the MesAcr in the experimental conditions (Shown in Figure A.3 where $A_{450\ nm} = 0.2$ for MesAcr and $Ru(bpy)_3(PF_6)_2$). Lepidine, cyclohexane carboxylic acid and PIFA all have a very weak absorbance in the visible region and were not considered as a significative source of error on amount of light absorbed by MesAcr.

3.5.2   Quenching Rate Constant – Stern-Volmer

Steady state and time-resolved quenching rate constant measurements were carried out on a PTI QuantaMaster 40 (Horiba). Samples were excited at 430 nm for steady state, and time-resolved experiments were measured at 403 nm due to the limited selection of pulsed LEDs available. In a 1 x 1 cm quartz cuvette a solution of $MesAcr^+$ BF_4^- (25 µM) in acetonitrile was added and deoxygenated with N_2.

Time-resolved measurements were obtained using a deoxygenated solution of pivalic acid (6.56 M) and lepidine (2.26 M) in acetonitrile that were added via a gas-tight syringe. To the decay trace, a mono-exponential decay was fitted and corrected for the instrument response factor (IRF). Based on the Stern-Volmer equation described in section 2.6, a quenching rate constant was determined.

Steady-state measurements were performed with each quencher (lepidine, lepidine protonated with pivalic acid, lepidine protonated with trifluoroacetic acid, lepidine PF_6^-, and pivalic acid) following the same protocol as above, using an excited-state lifetime $\tau_0 = 8.48$ ns, as determined from the time-resolved experiment.

3.5.3   Cyclic Voltammetry

PIFA ((Bis(trifluoroacetoxy)iodo)benzene)

A solution of PIFA (5 mM) and tetraethylammonium tetrafluoroborate (0.1 M) was prepared in HPLC-grade acetonitrile and deoxygenated with N_2. Cyclic voltammograms were measured using a carbon working electrode, platinum counter electrode and Ag/AgCl reference electrode (3 M NaCl) from -1.0 to + 1.0 V. An internal standard of ferrocene (5 mM) was added to reference the value against Fc/Fc^+.

Lepidine

A solution of lepidine (0.01 M), tetraethylammonium tetrafluoroborate (0.1 M) and ferrocene (0.05 M) was prepared in anhydrous acetonitrile and deoxygenated using N_2. Cyclic voltammograms were measured using a carbon working electrode, platinum counter electrode and Ag/AgCl reference electrode (3 M NaCl) from -2.0 to + 1.5 V (for plot see Annexe A Figure A.5). Protonated lepidine was obtained by adding trifluoracetic acid (0.03 M) to the solution and the cyclic voltammogram was measured between -2.5 to + 1.5 V.

3.5.4   Theoretical Potentials

The reduction potentials of the half reactions ($E_{1/2}$) of PIFA, lepidine and protonated lepidine were obtained according to the calculations detailed by Nicewicz *et al*. (2015). Light atoms (H, C, O, N and F) were calculated using B3LYP/6-311++G(2d,2p) while iodine was calculated using LanL2DZ with added diffuse and polarization functions. Values were referenced from V vs SCE to V vs Fc/Fc$^+$ using a ferrocene potential of 400 mV vs SCE.

$$E_{1/2}^{0,calc} = -\frac{\Delta G_{\frac{1}{2}}^0}{n_e F} - E_{\frac{1}{2}}^{0,SHE} + E_{\frac{1}{2}}^{0,SCE} - E_{1/2}^{0,Fc/Fc+} \qquad \text{eq. 3.1}$$

3.5.5   Computational Methods

Density Functional Theory (DFT) calculations were performed using the Gaussian 09, (2016) suite at the B3LYP level of theory which uses Becke's 3-parameter exchange and Lee, Yang and Parr's correlation function (Becke, 1992; Becke 1993; Lee *et al.,* 1998). All geometry optimization and frequency calculation used the conductor-like polarizable continuum model (CPCM) to simulate the acetonitrile solvent (Barone and Cossi, 1998).

All atoms except iodine were calculated at B3LYP/6-311++G(2d,2p) level of theory. Iodine was calculated at LanL2DZ with diffuse and polarization functions (Check *et al.,* 2001).

Resulting outputs were verified for imaginary frequencies to ensure the optimized structures were local minima for ground states (no imaginary frequency) or saddle points for transition states (one imaginary frequency). The free energies (ΔG) were calculated using the zero-point energy corrected Gibbs free energy at 298.15 K (Sum of Thermal and Free Energies in Gaussian Output), and free enthalpies (ΔH) were calculated using the zero-point energy corrected enthalpy at 298.15K (Sum of electronic and thermal Enthalpies in Gaussian Output). A scheme of individual steps in the reaction can be found in Annexe A in the section "Computational methods".

3.6   Results And Discussion

3.6.1   Quantum Yield of The Reaction: Chemical Actinometry

When examining a photochemical reaction, the natural first question is: how light efficient is this reaction? In other words, how many photons absorbed are required to form one molecule of product? To answer this question actinometry experiments were performed. A chain reaction mechanism was proposed which would suggest the quantum yield value be above one. However, when the experiment was preformed, we measured the quantum yield to be 0.18. This does not mean that it is not a chain reaction but rather that it is an inefficient chain reaction. The inefficient nature of the photocatalyst oxidation step could potentially be explained by the low quantum efficiency of this process.

The quantum yield at maximum efficiency is 0.08 for the low light intensity reaction using 90–150-minute data points and a quantum yield at overall efficiency of 0.05, for the total timescale of the kinetics of 0-210 minutes when product formation plateaued. Using high intensity lights for the experiment afforded an increase in quantum yield to 0.18 for data points between 20-40 minutes, and an overall quantum yield of 0.07 for the total reaction time of 0-90 minutes.

3.6.2   Quenching Rate Constant – Stern-Volmer

The PC is unable to reduce the hypervalent iodine due to its high redox potential ($E^*_{red} > +2.0$ V), resulting in an unknown electron donor in the photoredox initiation step. To better understand the reactivity of [MesAcr$^+$]* a series of steady-state (Figure 3.5) and time-resolved (Figure 3.6) Stern−Volmer quenching experiments were performed.
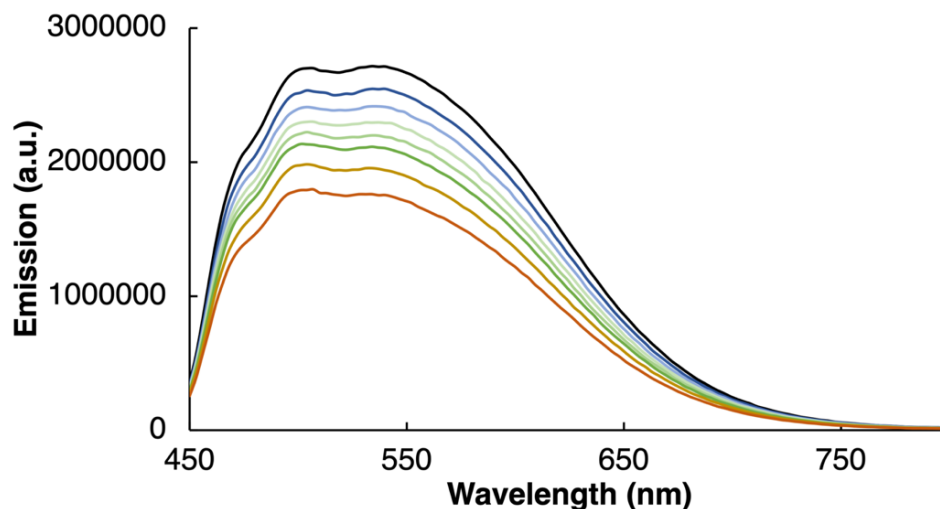
Figure 3.5. Steady state emission quenching of MesAcr$^+$ BF$_4^-$ with increasing concentration of lepidine and pivalic acid: (−) 0 mM, (−) 1.5 mM, (−) 3.0 mM, (−) 4.6 mM, (−) 6.1 mM, (−) 7.5 mM, (−) 10.5 mM, and (−) 14.8 mM.
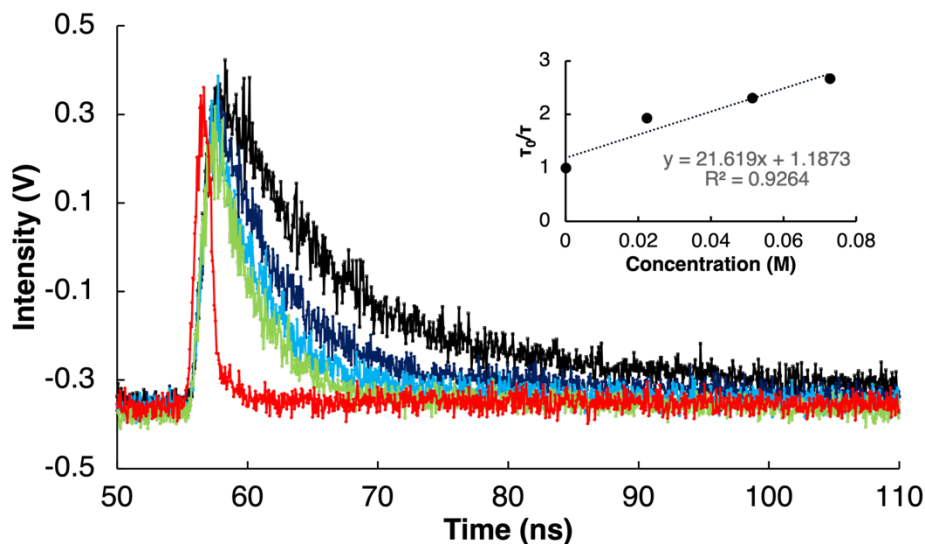
Figure 3.6. Time-resolved emission quenching of MesAcr$^+$ BF$_4^-$ with increasing concentration of protonated lepidine: (−) 0 mM, (−) 22.3 mM, (−) 51.4 mM, (−) 72.7 mM, (−) IRF. Inset: Stern-Volmer graph.

The Stern-Volmer quenching experiments are summarized in Figure 3.7 and corresponding rate constants in Table 3.1. These results shows that lepidine (black line), reacts quickly (k_q = 4.42 x 10^9 M^{-1}s^{-1}), while the protonated version (blue line) reacts relatively slowly (k_q = 2.24 x 10^8 M^{-1}s^{-1}). The addition of pivalic acid and trifluoroacetic acid to the lepidine solution (red and orange line,

respectively) is not sufficient to fully protonate the lepidine, leading to high quenching constants (k_q = 4.02 x 10^9 M^{-1}s^{-1} and k_q = 7.26 x 10^8 M^{-1}s^{-1}, respectively). The oxidation of [MesAcr$^+$]* by pivalic acid was measured and found that it does not sufficiently oxidize [MesAcr$^+$]*, despite being precedented in the literature (Griffin *et al.,* 2015).
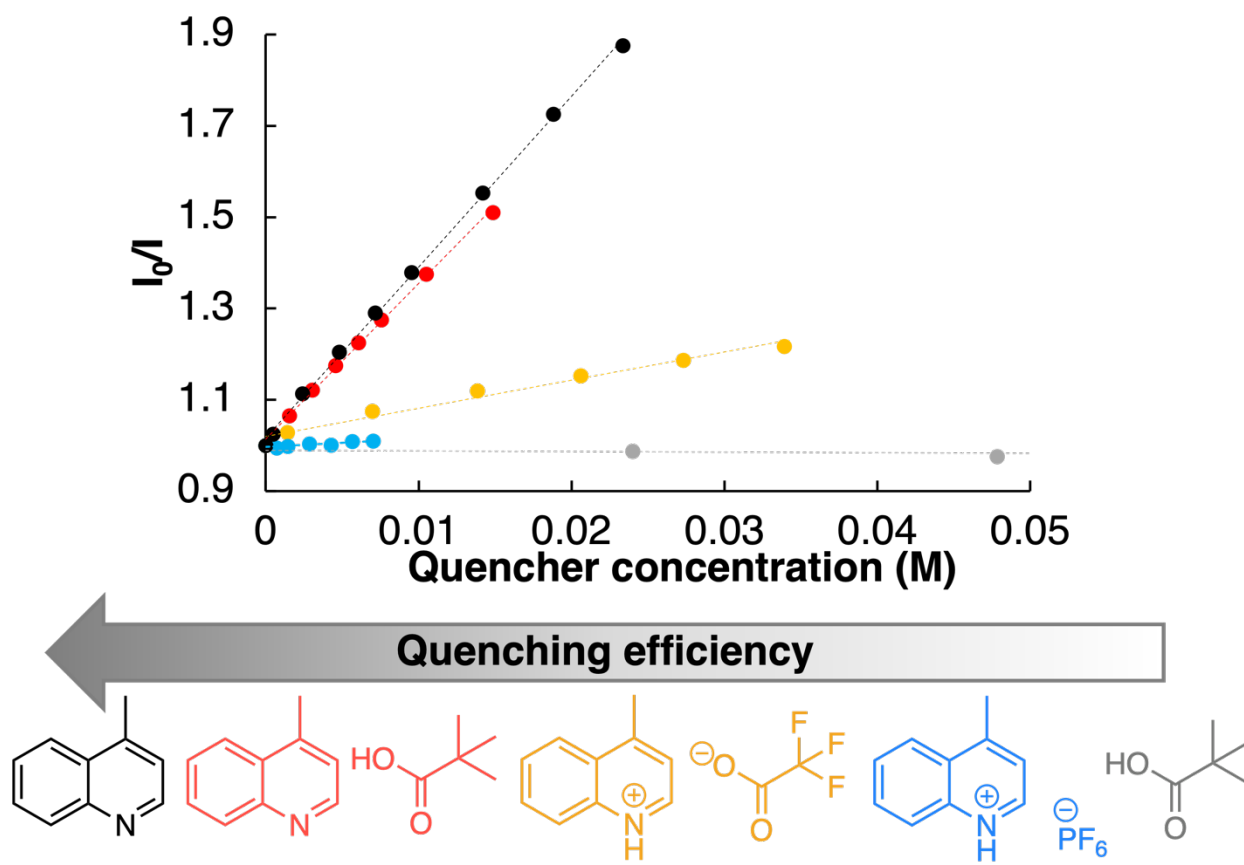
Figure 3.7. Emission quenching of MesAcr by lepidine (black), lepidine and pivalic acid (red), lepidine and trifluoroacetic acid (yellow), lepidine PF$_6^-$ (blue) and pivalic acid (grey) with increasing quenching efficiencies.

Table 3.1. Steady-state and time resolved quenching rate constants for the oxidation of [MesAcr$^+$]*.

	$k_q^{\text{Steady-state}}$ (M^{-1} s^{-1})	$k_q^{\text{Time-resolved}}$ (M^{-1} s^{-1})
Lepidine and pivalic acid	4.02 x 10^9	2.55 x 10^9
Lepidine and trifluoroacetic acid	7.26 x 10^8	
Lepidine PF$_6^-$	2.24 x 10^8	
Lepidine	4.42 x 10^9	

The species responsible for the reduction of [MesAcr⁺]* thus far remains unclear. We believe inefficient oxidation of trace carboxylate or neutral heteroaromatic may be sufficient to generate small amounts of reduced MesAcr as part of the initiation step.

3.6.3 Computational Methods

The mechanism was calculated using lepidine to represent the heteroarene, an isopropyl radical as the alkyl radical, and isopropyl carboxylic acid and trifluoro carboxylic acid as the carboxylic acid. Ligand exchange between the alkyl carboxylic acid and -CF_3 group on PIFA is possible resulting in calculations of different side groups for the hypervalent iodine and the carboxylic acid. A thermodynamic energy profile of the reaction is shown in Figure 3.8.

We have considered the zero-point energy of the mechanism to be the energy of the protonated lepidine and isopropyl radical. The radical addition of lepidine and isopropyl radical was found to be endergonic at 7.73 kcal/mol with a transition state (*TS1*) barrier of 18.1 kcal/mol resulting in the formation of a lepidine radical cation. Although the radical addition step was found to be sightly endergonic, it is still thermodynamically feasible. The lepidine radical cation then undergoes deprotonation with either isopropyl or trifluoro carboxylate as possible base sources. It was calculated that the deprotonation was much more favourable with isopropyl carboxylate as opposed to the trifluoro carboxylate, -24.5 kcal/mol vs -6.7 kcal/mol, respectively, with a transition state barrier (*TS2*) of 4.2 kcal/mol and 10.7 kcal/mol respectively, although both are likely to occur. The transition state was calculated by simultaneously distancing the proton from the carboxylate and while moving it closer to the lepidine radical cation.

The resulting α-amino radical will undergo a SET with the hyper valent iodine adduct to form the product and a hypervalent iodine radical anion favourably. The free energy of the SET is -24.3 kcal/mol for R = alkyl and -37.6 kcal/mol for R = CF_3. No transition state was determined for this step. The hypervalent iodine radical anion collapses with no significant barrier found leading to the formation of the carboxylate, carbon dioxide, iodobenzene and an isopropyl radical. This step is exergonic with a free energy of -42.1 kcal/mol for R = alkyl and -40.3 kcal/mol for R = CF_3.

The overall reaction is thermodynamically favourable with a free energy of -83.2 kcal/mol for and -77.7 kcal/mol for R = alkyl and R = CF₃, respectively (See Annexe A Figure A.6 for the proposed ΔG^o for the overall catalytic cycle).
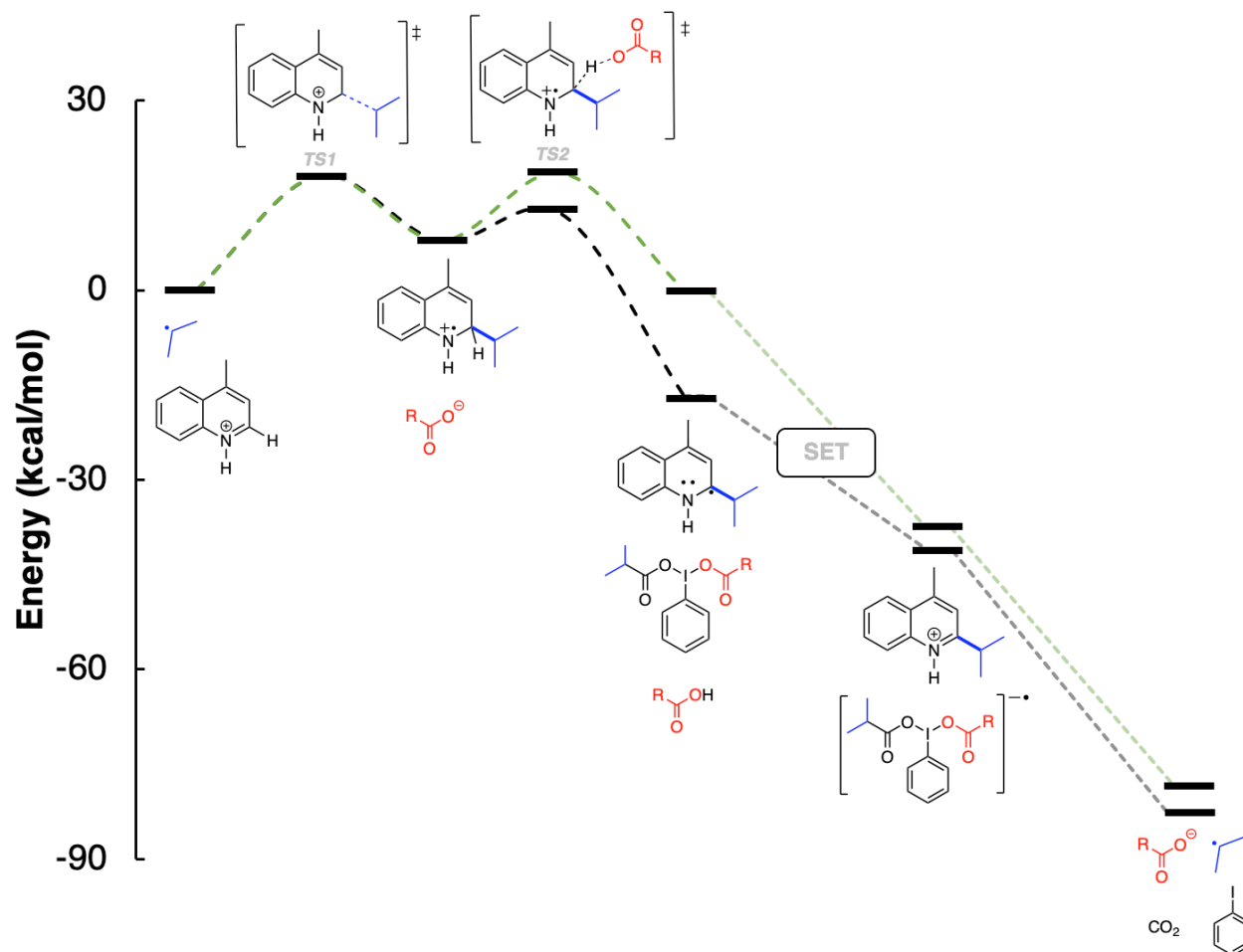
Figure 3.8. Thermodynamic energy profile for each step in the catalytic cycle. Obtained using B3LYP/6-311++G(2d,2p)//CPCM:ACN for all atoms except for iodine, which was calculated using LanL2DZ with added diffuse and polarization functions. R = CF₃ (green) and R = alkyl (black).

3.6.4   Single Electron Transfer Step

The proposed (SET) step between lepidine's α-amino radical and PIFA was experimentally validated using cyclic voltammetry. This step is the major differentiating factor between our mechanism and previously published mechanisms under similar conditions. In acetonitrile, the reduction potential of protonated lepidine and PIFA were −1.34 V and −0.527 V vs Fc/Fc⁺,

respectively (Figure 3.9). Both half reactions therefore predict a favorable SET reaction with a +0.814 V driving force.
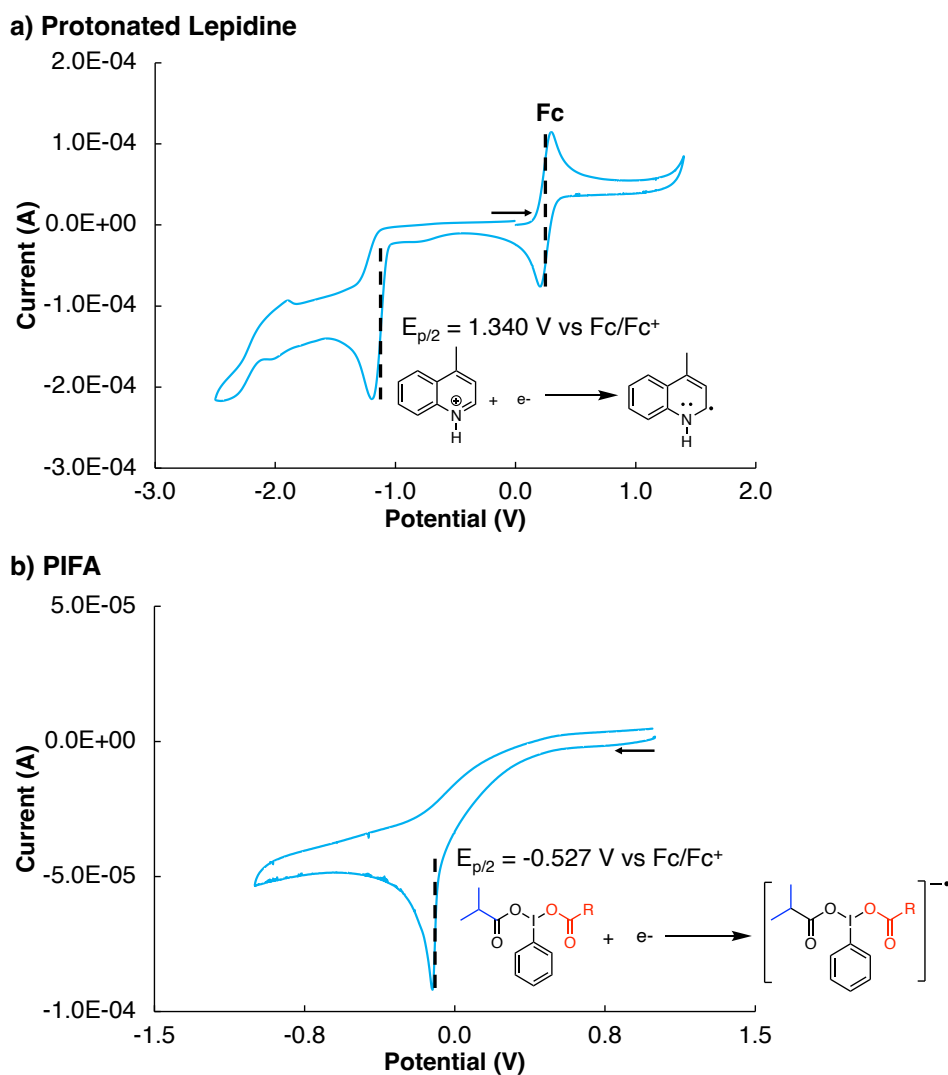
Figure 3.9. Cyclic voltammetry of a) lepidine protonated with trifluoroacetic acid and b) PIFA in acetonitrile.

The cyclic voltammogram for PIFA (Figure 3.9B) suggests that it undergoes an irreversible reduction. What may be occurring is that once PIFA receives an electron it undergoes rapid decomposition. This is supported by DFT calculations where the radical anion of PIFA was found to breakdowns with no significant barrier (for DFT $\Delta G^{\ddagger}$ calculation see Annexe A, computational

methods section, Energies obtained from DFT calculations and basis set used for each atom for step **H ➔ A + D + J + K**).

The SET step was theoretically calculated for lepidine within good agreement of experimental results. The theoretical reduction potential of protonated lepidine was found to be -1.297 V vs Fc/Fc$^+$. While the theoretical reduction potential of neutral lepidine was found to be -2.574 V vs Fc/Fc$^+$ (See Annexe A, Figure A.5 for schemes and calculations).

Overall the redox potentials shows that the reduction of PIFA by protonated lepidine is thermodynamically favorable both experimentally and theoretically.

3.7   Conclusion

This collaboration reported on a metal-free photoredox C−H functionalization of heteroarenes using an acridinium photocatalyst and hypervalent iodine reagents under blue LEDs. Given the wide array of inexpensive and commercially available carboxylic acid, and its characteristic ability to from alkyl radicals from carboxylates (Zuo *et al.,* 2014; Griffin *et al.,* 2015), this approach provides a valuable contribution to the Minisci-type alkylation reaction.

The protocol shows convincing generality for various alkyl radicals and heteroaromatics. Mechanistic studies are supported with electrochemistry, actinometry, DFT, steady-state and time-resolved photochemical methods that provide evidence for each individual steps in the proposed mechanism. We were able to correct a key previously incorrect intermediate for this photoredox-catalysed Minisci reactions, and show that we formed a highly reducing species, the α-amino radical, that can turn-over a catalytic chain reaction with various oxidants (Huff *et al.,* 2016; Matsui *et al.,* 2017; Garza-Sanchez *et al.,* 2017; Cheng *et al.,* 2017). However the low quantum yield can be due to an inefficient initiation step (e.g., inefficient oxidation of a carboxylate) and/or inefficient chain propagation.

CHAPITRE 4

EFFICIENT PHOTOCONVERSION OF THIONES TO KETONES: EXPLORING ETHERS AS A SOURSE OF OXYGEN

4.1 Résumé

Nous rapportons la photoconversion d'un dithioimide et d'un thioimide en leurs imides correspondants dans des solvants éthérés. Contrairement à la photooxydation des thioimides rapportée jusqu'à présent, qui a lieu en présence d'agents oxydants tels que l'oxygène, cette transformation a lieu en l'absence d'agent oxydant stœchiométrique, indiquant une implication directe du solvant éthéré comme source d'oxygène.
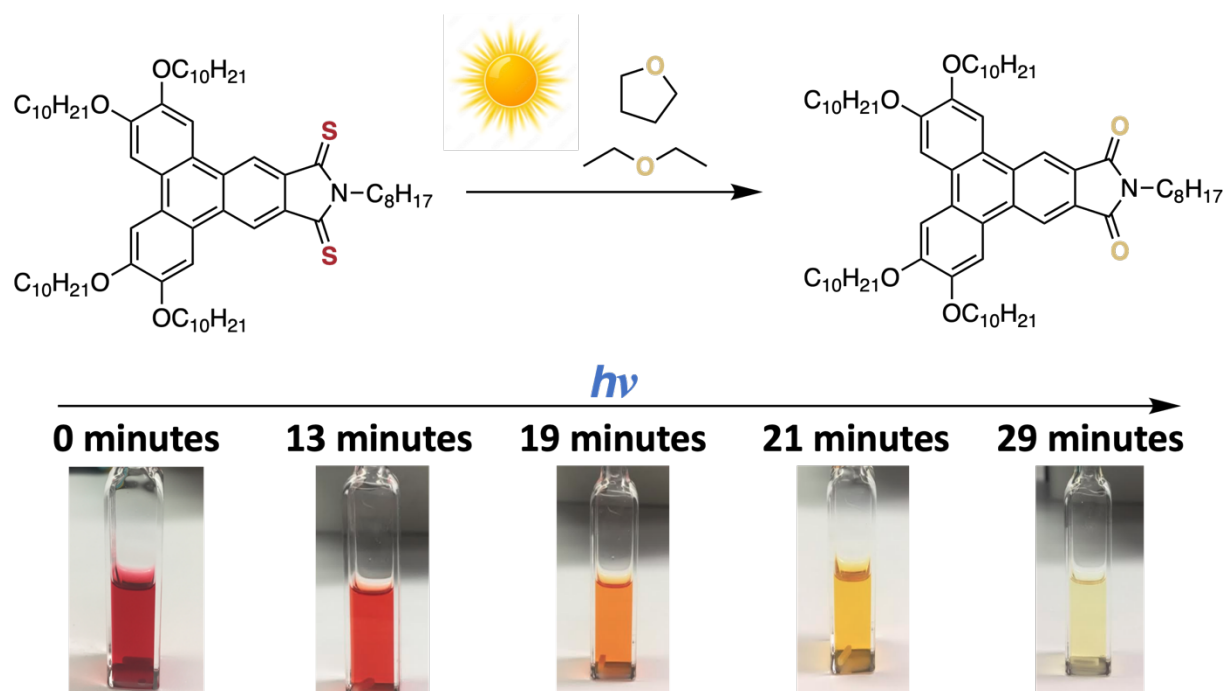
Figure 4.1. Photoconversion du dithioimide en imide correspondant dans un solvant éthéré. (Photoconversion of dithioimide to the corresponding imide in ethereal solvent).

Supplemental information is available in Annexe B and includes results on quantum yield, solvent scope, GC-MS data, and DFT energies and atomic coordinates.

4.2 Foreword

The work presented in this chapter is a result of a collaboration with Kenneth Maly, professor in the Department of Chemistry & Biochemistry at the University of Wilfrid Laurier in Waterloo, Ontario. The synthesis of the products under investigation was completed by Katie M. Psutka, Kevin J. A. Bozek, and Kenneth Maly.

Quantum yield, reaction kinetics, quantum yield of fluorescence, DFT studies, and laser flash photolysis experiments were performed by Meghan Heer, Mathieu Frenette, and me. GC-MS and absorption experiments were performed by Emma Guillet, Mathieu Frenette, and me.

The objective of this collaboration is to determine the source of oxygen in the photoconversion of a dithioimide liquid crystal species to its parent imide and elucidate the mechanism for this reaction.

4.3 Abstract

We report the photoconversion of a dithioimide and thioimide to the corresponding imides in ethereal solvents. Unlike previously reported photooxidation of thioimides, which take place in the presence of oxidizing agents such as oxygen, this transformation takes place in the absence of stoichiometric oxidizing agent, pointing to the direct involvement of the ethereal solvent as the oxygen source.

4.4 Introduction

There has been a considerable increase in the development of organic electronics for new materials. The design and synthesis of novel electron-accepting materials, which can be used in organic semiconducting devices, photovoltaics, and light emitting diodes, is one field in particular that is drawing attention. Imides, such as naphthalene and perylene diimides, have been widely studied and show low LUMO energies, which make them great candidates for electron accepting materials (Würthner *et al.,* 2016; Zhan *et al.,* 2011).

A benefit of using organic materials is the ability to enhance their properties through structural modifications. Imides for example when thionated with Lawesson's reagent, a thiation compound used in the conversion of carbonyls into its thionated analogue, have been shown to have tunable

LUMO energies for a variety of materials, such as small molecule electron accepting materials (Ie *et al.,* 2013; Etheridge *et al.,* 2015), conjugated polymers (Lévesque *et al.,* 2014; Liu et *al.,* 2018), and liquid crystalline compounds (Psutka *et al.,* 2016; Psutka *et al.,* 2019). Imides produced from this process have lower LUMO energies and overall lower HOMO-LUMO gaps, which produce materials with enhanced electron mobilities and electron affinities (Tilley *et al.,* 2015; Kozycz *et al.,* 2015; Yang *et al.,* 2015; Welford *et al.,* 2018).

During an investigation into the phase behaviour of liquid crystal imides and thioimides (Psutka *et al.,* 2014; Psutka *et al.,* 2016; Psutka *et al.,* 2019) there was a colour change from red to yellow under ambient light in just 2 hours. It's important to note that this conversion was only observed to take place when the solvent was ethereal (tetrahydrofuran or diethyl ether). Oddly, using chloroform and dichloromethane as solvent did not produce the same colour changing results or occurred on a much longer timescale. Our colleagues discovered that the red dithioimide (**2SS**) or orange thioimide (**2OS**) starting material photo-converted to a yellow imide (**2OO**) through NMR analysis of the products. The molecules used in the investigation are depicted in Figure 4.2.
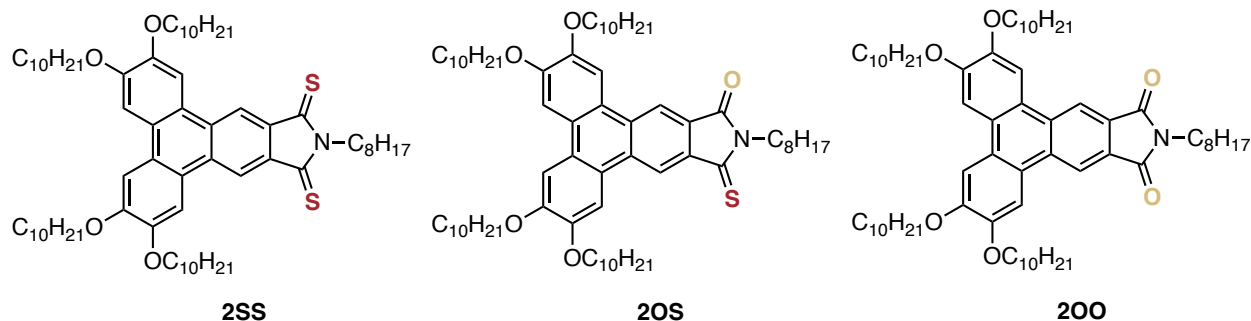
Figure 4.2. Triphenylenes series: (**2SS**) dithioimide, (**2OS**) thioimide and (**2OO**) imide.

In the presence of molecular oxygen, this photochemical reaction is well understood (Ramnath *et al.,* 1983). However, rigorous testing was done on tetrahydrofuran (THF) to ensure that the potential oxygen source did not come from the solvent. The solvent was deoxygenated via distillation, purging with inert gas, and freeze-pump-thawing the solvent. The amount of water in THF was determined via a Karl-Fischer titrator to contain 3.02 ppm of water. Peroxide test strips, which have a limit of detection of 1 mg of peroxides/L, did not detect any peroxides in THF. The photodegradation was observed in concentrated stock solutions of 1 mM, so the oxygen or peroxide

content necessary would need to be much larger than the trace water or peroxides found in THF. These results suggest that the oxygen is incorporated from the THF or diethyl ether which is an unprecedented source of oxygen for this reaction

Kinetics experiments with the addition of typical oxidants were performed, and no appreciable change was observed in the yield or rate of reaction. Spectroscopic analysis of the dithioimide indicates that although a relatively photon efficient process in THF, it selectively reacts with only certain ethereal solvents. Analysis of the side products suggests a potential first step of the reaction mechanism.

To confirm the ether solvent as the ultimate source of oxygen, we propose the synthesis of isotopically enriched THF from ^{18}O water, depicted in Figure 4.3. However, attempts to synthesize this have so far been unsuccessful.
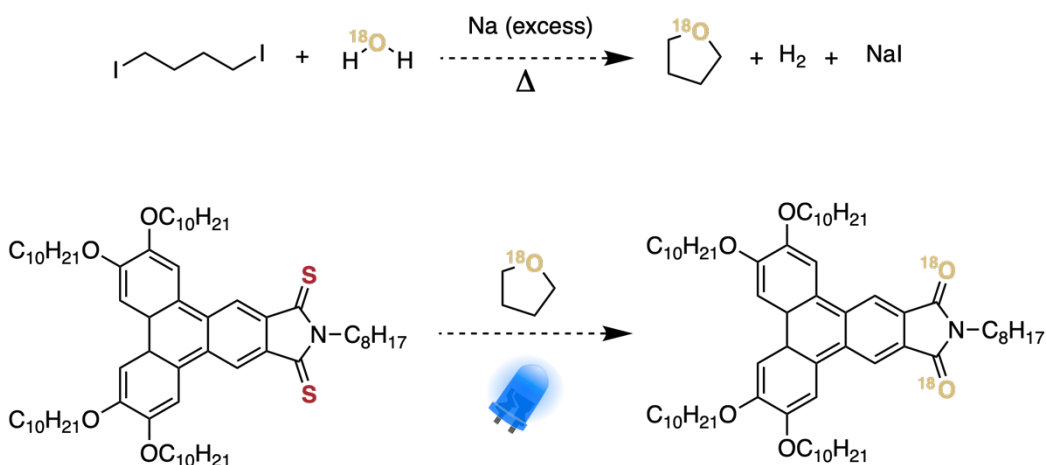
Figure 4.3. Proposed reaction conditions to synthesize O-18 THF and incorporation into 2OO.

The photodegradation of these compounds has significant consequences for their application in devices since thioimides have the potential to be useful as electron-accepting materials. Additionally, the cleavage of two C-O bonds in ethers at room temperature without strong acids or bases is quite surprising and deserves an in-depth investigation. Herein we investigated the photodegradation of thioimides and its mechanism.

4.5   Experimental Methods

4.5.1   Quantum Yield of The Reaction: Visible Light Actinometry

4.5.1.1   Chemical Actinometry of The Reference System

The quantum yield of the reaction was obtained from a Ru(bpy)$_3$ and DPA chemical actinometer by comparing the consumption of DPA in a reference solution to that of our reaction from a protocol by Pitre *et al.* (2015). Ru(bpy)$_3$(PF$_6$)$_2$ was used as opposed to Ru(bpy)$_3$Cl$_2$ and the quantum yield was assumed to stay unchanged. Experiments were performed using a PTI QuantaMaster 40 (Horiba). Samples were irradiated at 450 nm in a 1 x 1 cm quartz cuvettes. Stirring was achieved by placing the cuvettes on a shaking platform.

A solution of DPA (0.1 mM) and Ru(bpy)$_3$(PF$_6$)$_2$ (0.19 mM) was added to a quartz cuvette under air. UV-Visible spectra were taken during irradiation to monitor the decay of DPA at 372 nm due to $^1O_2$ over time (See Annexe B, Figure B.1 for spectra).

4.5.1.2   Chemical Actinometry of Our System

To a 1 x 1 cm quartz cuvette the molecules of interest (**2SS** or **2OS**, 0.545 mM) was added to deoxygenated solvents (THF, diethyl ether, chloroform, or dichloromethane) to a total volume of 2 mL (See Annexe B Table B.1 for a summary of the quantum yield in the different solvents). The cuvette was deoxygenated and sealed with a rubber septum under a positive pressure of N$_2$. The cuvette was placed in the PTI QuantaMaster 40 (Horiba) fluorimeter for irradiation at 450 nm and UV-Visible spectra was taken over 5 minutes to monitor the change in absorption.

To ensure equal photon absorption, the actinometry standard and the sample absorb >95% of light at the excitation wavelength and both solutions were irradiated under identical conditions (Spectra in Annexe B Figure B.1, B.2, B.3 and B.4 show A$_{450\ nm}$ = 2.5 for the reference system and our systems).

4.5.2   Reaction Kinetics

A 2 mL solution of **2SS** (0.2 mM) was added to a quartz cuvette with degassed THF from a solvent purification system and various oxidants were added to cuvette. The deoxygenated cuvette was

placed in the PTI QuantaMaster 40 (Horiba) fluorimeter for irradiation at 450 nm and UV-Visible spectra was taken at different time intervals to monitor the change in absorption over time.

The kinetics of the reaction were measured against THF from a solvent purification system, distilled THF, THF with 2.7 M water, THF with the cuvette open to air, and 20 mM AIBN in THF that was heated to 37 °C and shaken overnight to produce peroxides.

4.5.3 Laser Flash Photolysis

The transient absorption spectrum of **2SS** was measured after pulsed laser irradiation at 532 nm (~20 mJ/pulse) from the second harmonic of a Surelite II Nd:YAG laser (Continuum). The time-resolved emission following the laser excitation was measured at 600 nm using a fiber-optic based laser-flash photolysis system (miniLFP from Luzchem Research, Ottawa, Canada).

To a quartz cuvette under N_2, **2SS** (A_{532} = 0.5, 0.058 mM) was added to 2.5 mL degassed chloroform. The cuvette was deoxygenated with argon and sealed with a rubber septum. Pre-degassed THF quencher was added neat via syringe in 0.1 mL increments. The transient absorption decay monitored at 600 nm was fit to mono-exponential decay kinetics.

4.5.4 Gas Chromatography Mass Spectrometry (GC-MS)

4.5.4.1 GC-MS Quantification of Butylated Hydroxytoluene in THF and Diethyl Ether

The amount of butylated hydroxytoluene (BHT) in THF and diethyl ether was determined using GC-MS analysis (220.35 m/z) and a calibration curve with benzaldehyde as internal standard in acetonitrile. The concentration of BHT in THF and diethyl ether was determined to be 245 ppm and 13 ppm, respectively.

4.5.4.2 GC-MS Quantification of Reaction Side Products

The photodegradation reaction of **2SS** in the presence of 2,3-dihydrobenzofuran (0.1 M) in chloroform was also studied to attempt to identify ether cleavage photoproducts. The concentration of benzofuran was determined using GC-MS analysis (118.13 m/z) in chloroform via a calibration curve.

4.6   Results and Discussion

4.6.1   Quantum Yield of The Reaction: Visible Light Actinometry

Actinometry experiments revealed that **2SS** in THF and diethyl ether gave quantum yields of 0.36 and 0.07, respectively (Figure 4.4 and 4.5) while dichloromethane and chloroform gave yields of < 0.001. The quantum yields are summarized in Table 4.1. An excitation wavelength of 450 nm was used with a monitoring wavelength of 600 nm. The monitoring wavelength of 600 nm was chosen because the absorption at 600 nm is less likely to be influenced by photoproducts.
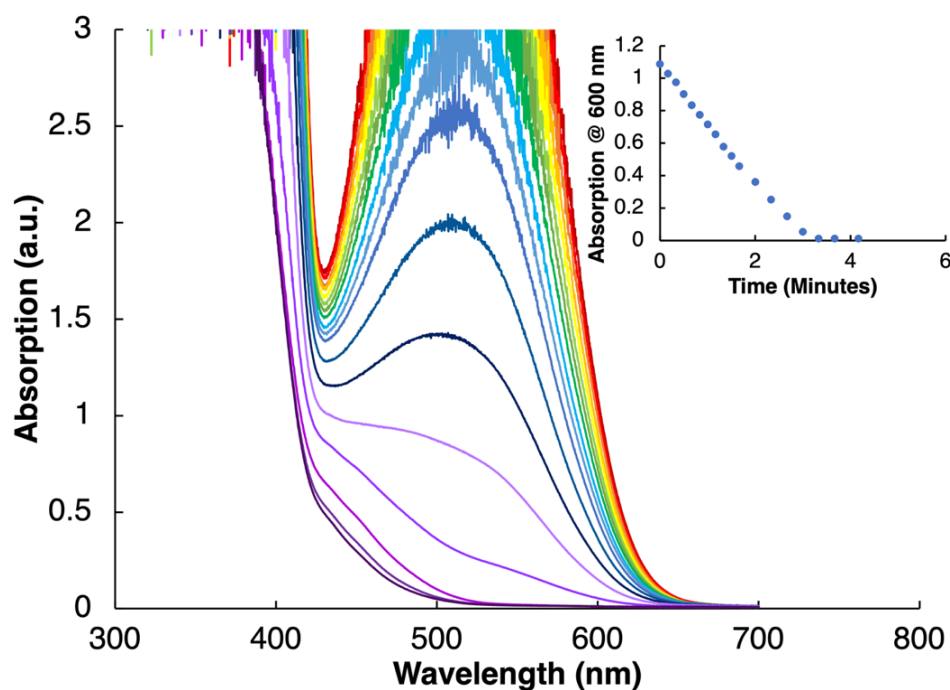
Figure 4.4. Absorption spectra of the actinometry experiment performed with **2SS** (0.545 mM) in THF and irradiated at 450 nm. Inset: Absorption at 600 nm vs. irradiation time.
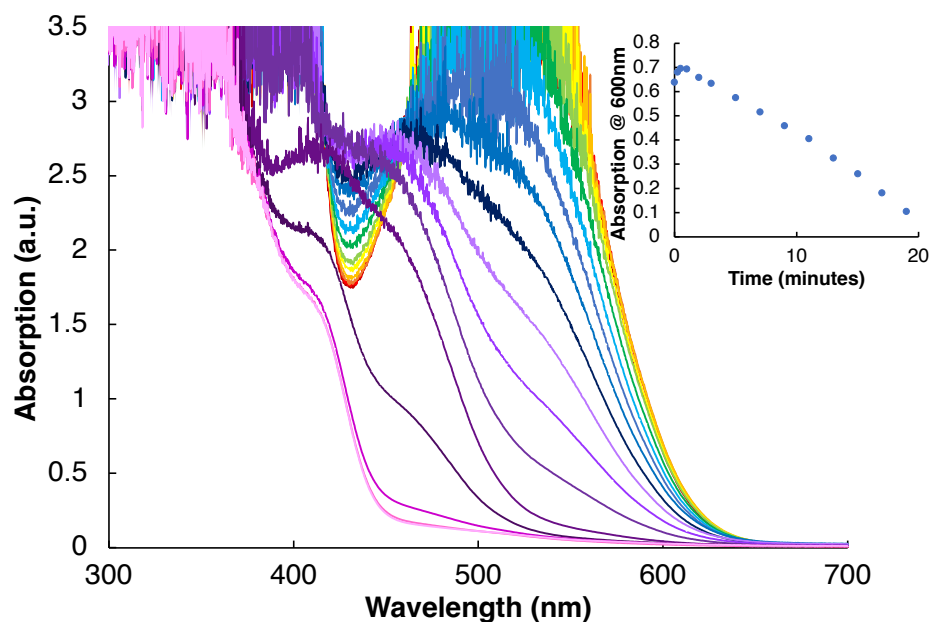
Figure 4.5. Absorption spectra of the actinometry experiment performed with 2SS (0.545 mM) in diethyl ether and irradiated at 450 nm. Inset: Absorption at 600 nm vs. irradiation time.

Table 4.1. Quantum yield for the decrease in absorption of **2SS** in various solvents under N_2.

Solvent	Reaction Quantum Yield (ϕ)
THF	0.36
Diethyl ether	0.07
Chloroform	< 0.001
Dichloromethane	< 0.001

Additional actinometry spectra of **2SS** and **2OS** in various solvents can be found in Annexe B Figure B.1. – B.4 and Table B.1. The results from quantum yield experiments are summarized in Table 4.1 and indicate that the photoconversion most efficiently takes place ethereal solvents with quantum yield values of 0.36 and 0.07 for THF and diethyl ether, respectively. While little or no photoconversion takes place in non-etheral solvents with a quantum yield of <0.001 for both dichloromethane and chloroform. See Annexe B Figure B.2 and Figure B.3 for **2SS** actinometry spectra in dichloromethane and chloroform and Figure B.4. for for **2OS** actinometry in THF. The results are summarized in Annexe B Table B.1.

4.6.2 Reaction Kinetics

To further investigate if the source of oxygen in the photochemical reactions is from the solvent itself and not from impurities, e.g., water, oxygen or peroxides, these impurities were explicitly added to the reaction medium in control experiments. If the oxygen source were indeed from the impurities, their addition should increase the rate of this chemical transformation. None of the explicitly added oxygen sources appreciably increased the reaction yield nor the rate of reaction (Table 4.2 and Figure 4.6).
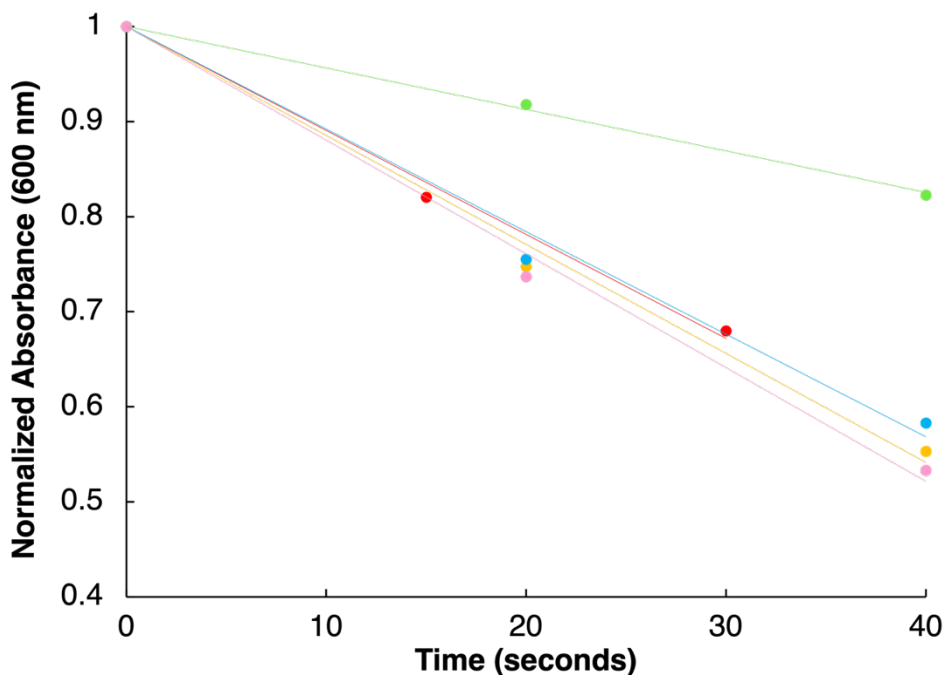
Figure 4.6. Rate of reaction of **2SS** upon the addition of various potential oxidants. Distilled THF (red), THF from a solvent-purification system (orange), THF + 2.7 M H_2O (green), THF + O_2 (blue), and THF + 20 mM AIBN (pink).

The addition of water (green trace in Figure 4.6) shows the largest deviation in rate from the other potential oxygen sources, and that may be a result of small amount of precipitate that formed when the water was added to the cuvette.

THF may react with oxygen to form the explosive compound 2-hydroperoxytetrahydrofuran, to avoid these commercial suppliers often stabilized THF with butylated hydroxytoluene (BHT). To see if BHT was a reactant in these transformations, it was removed by purifying THF via distillation

(red trace in Figure 4.6). The rate of reaction did not appreciably change between THF directly from a solvent purification system (orange trace in Figure 4.6) and distilled THF.

Table 4.2. Rates of reaction between **2SS** and possible oxygen sources.

Potential Impurity	Slope[a]
None (Distilled THF)	-0.0109
BHT (Solvent system)	-0.0115
H_2O	-0.0044
O_2	-0.0108
Peroxides (AIBN)	-0.012

[a]The kinetic fitting was anchored at time zero to the normalized absorption.

4.6.3   Laser Flash Photolysis

Laser-flash photolysis studies were carried out to probe the initial steps of this surprising photochemical transformation. A transient differential absorption spectrum was taken in chloroform after a 532 nm laser pulse. There is an increase in absorption at 600 nm 0.5 µs after the laser pulse indicating a triplet formation of **2SS** (Figure 4.7).
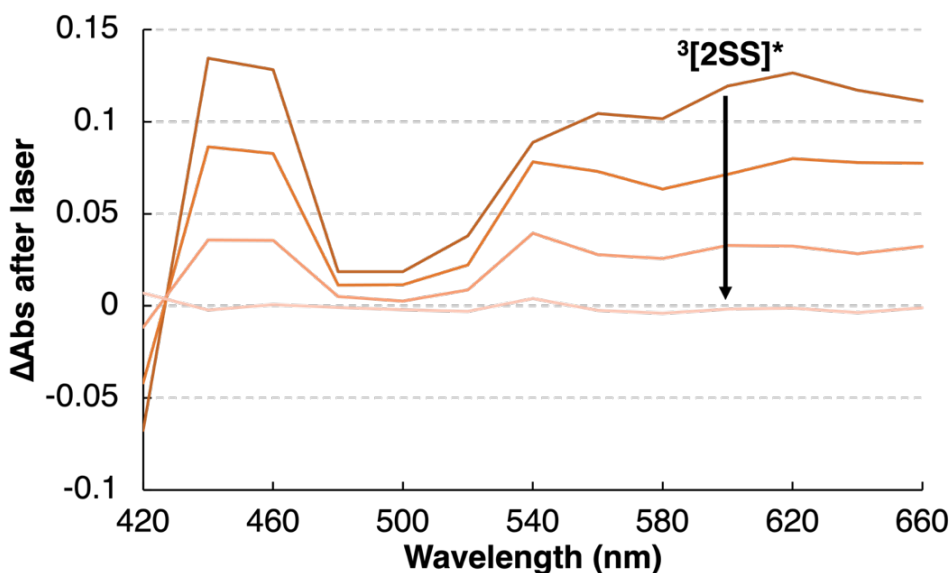
Figure 4.7. Transient absorption spectrum of the **2SS** in chloroform at (–) 0.5 µs, (–) 3 µs, (–) 8 µs (–) 35 µs after laser pulse irradiation (532 nm).

Increasing amounts of THF were added to a solution of **2SS** in chloroform to monitor the change in absorption at 600 nm associated to the triplet excited state ^{3}[**2SS**]* (Figure 4.8). The addition of THF lowers the initial absorption at 600 nm, meaning less triplet is formed (Figure 4.9). However, when we probed the decay rate constant of this triplet, it seemed unaffected by the addition of THF (Figure 4.10). Overall, increasing the concentration of THF lowers the initial yield of ^{3}[**2SS**]*, but does not shorten its lifetime. This strongly indicates that **2SS** is reacting with THF from the singlet excited state, ^{1}[**2SS**]*, rather than ^{3}[**2SS**]*.
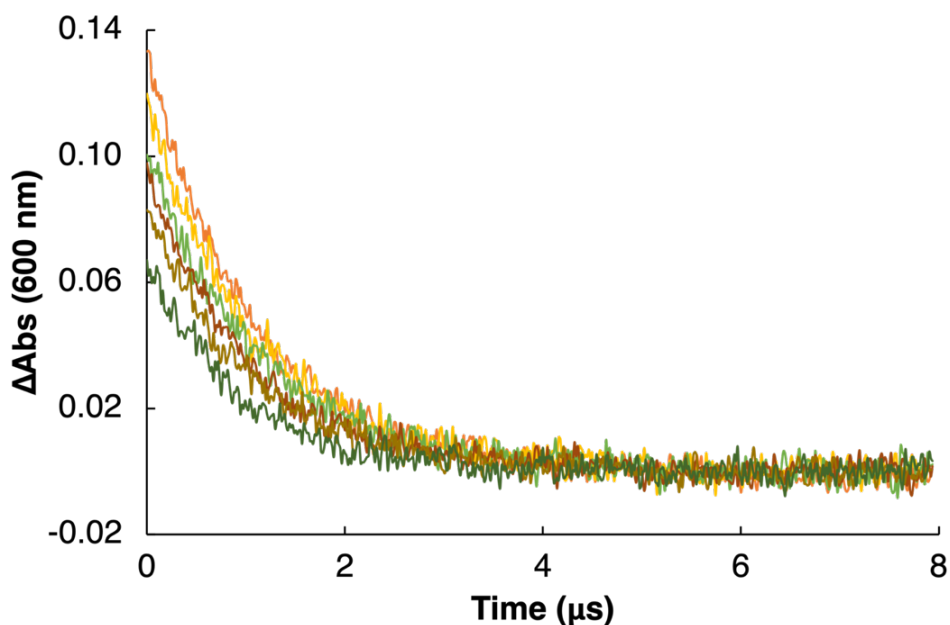
Figure 4.8. Change in absorption at 600 nm following laser excitation of **2SS** in deoxygenated chloroform to follow signal associated to triplet excited state ^{3}[**2SS**]* with increasing amounts of THF (top trace = 0 M THF, bottom trace = 2.05 M THF).
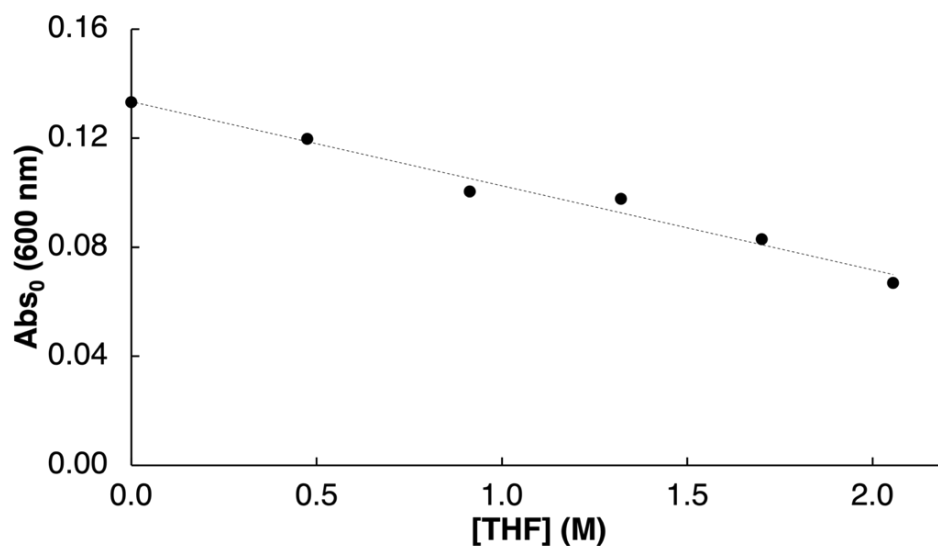
Figure 4.9. Significant decrease of jump in absorption at 600 nm immediately after laser excitation of **2SS** in deoxygenated $CHCl_3$ with increasing concentration of THF.
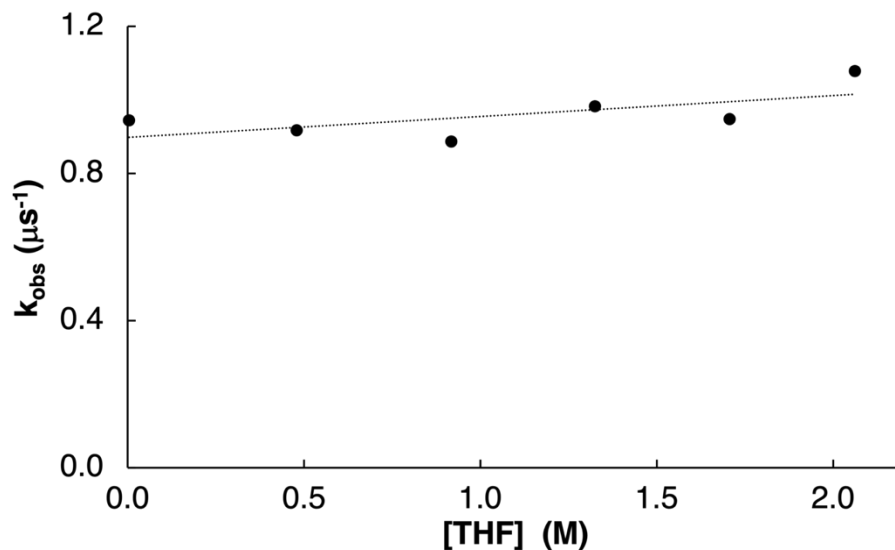
Figure 4.10. The rate constant for the triplet decay of **2SS** in $CHCl_3$ appears largely unaffected by increasing concentrations of THF.

Following the absorption of a photon, thiones are well known to rapidly undergo intersystem crossing to form triplet excited states (De Melo and Fernandes, 2001). From this triplet excited state, thiones react with molecular ground state oxygen and ketones are often an end product (Maciejewski and Steer, 1993). In our system, however, molecular oxygen is not present in the

stoichiometric quantities necessary for this conversion. The photochemical conversion at the heart of this chapter, **2SS → 2OO,** appears to begin with the direct reaction of [1][**2SS**]* with THF. Since we observe that the lifetime of [3][**2SS**]* is not shortened in increasing concentration of THF, we conclude that the triplet is (relatively) unreactive to THF. Finally, due to the relatively short lifetime of a singlet excited state (10^{-10} -10^{-7} s), **2SS** would only have time to react with the solvent. We cannot imply a reaction with oxygen, water, or other impurities during the initial photochemical step. These results strongly suggest that the initial reaction of **2SS** following photoexcitation must be with the solvent directly.

4.6.4 Evolution of the Reaction in Various Ethers Through Identification of Reaction Side Products

Reverse-phase HPLC-UV and GC-MS techniques were unsuccessful in the direct detection of **2SS**, **2OS** or **2OO** due to their highly lipophilic nature and high molecular weight, respectively. Instead, to try and further understand the reaction mechanism, we explored how altering the structure of the ethereal solvent would influence the reaction. The reaction was performed in the presence of different ethereal solvents with the goal of identifying the reaction side products via GC-MS. Since THF and diethyl ether are difficult to study via GC-MS due to their short retention times and co-elution with other solvents, we aimed to study the photochemical reaction of **2SS** with higher molecular weight ether-containing molecules. The reaction was attempted in dibenzyl ether and phthalane as potential ethereal solvents. In the photochemical reaction between **2SS** and dibenzyl ether, we looked for the formation of benzyl mercaptan ($PhCH_2SH$) or dibenzyl sulfide ($PhCH_2SCH_2Ph$) to explain the loss of sulfur during the reaction; both products were not observed by GC-MS and no evidence of C-O bond breaking could be confirmed in these experiments.

Another ether as potential source of oxygen used was 2,3-dihydrobenzofuran. When analyzing the reaction mixture, we identified an increasing amount of the dehydrogenated side product, benzofuran. The ratio of benzofuran formed to **2SS** consumed is approximately a 2:1 ratio suggesting that 2 benzofurans are formed for every **2SS** molecule that has been consumed (Figure 4.11). Strangely, the final yellow solution did not appear to contain **2OS** or **2OO** according to TLC analysis.
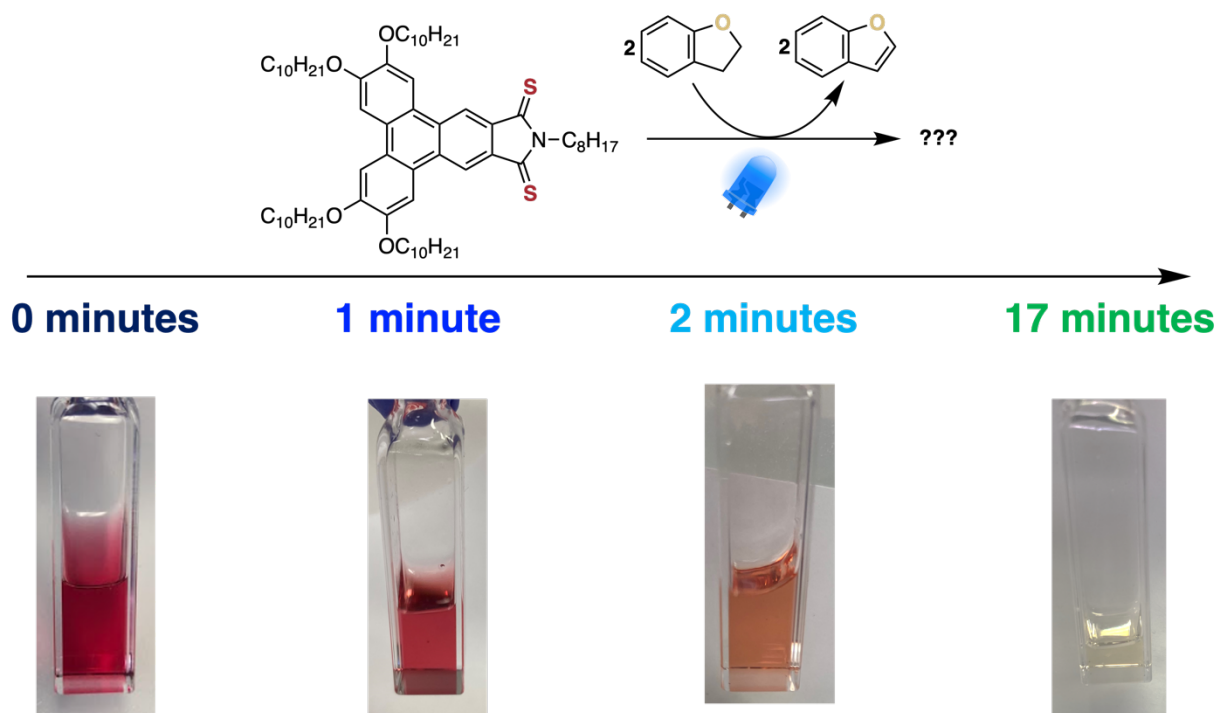
Figure 4.11. Evolution of the **2SS** in 2,3-dihydrobenzofuran with irradiation time (0 – 17 minutes).

The photoreduction reaction resulted in an increase from 0.21 mM benzofuran (impurity from initial solvent) to 0.63 mM benzofuran over 17 minutes of irradiation (Figure 4.12).
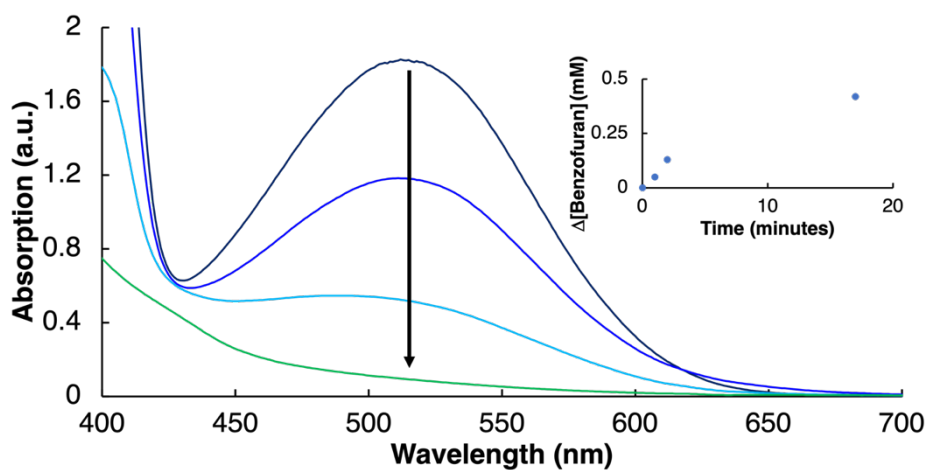
Figure 4.12. Decreasing absorption of **2SS** in 2,3-dihydrobenzofuran. Inset: Increasing concentration of the side product benzofuran with irradiation time determined via GC-MS.

4.7 Conclusion

Our experiments have demonstrated that the photochemical conversion of **2SS → 2OO** is most efficient in THF and diethyl ether with quantum yields of 0.36 and 0.07 respectively. Laser flash photolysis experiments have shown [3][**2SS**]* to be relatively unreactive to THF, however, its precursor [1][**2SS**]* does react directly with the solvent as the initiating photochemical step. The addition of known exogenous sources of oxygen atoms, e.g., water, molecular oxygen or peroxides, does not accelerate the rate of this photochemical reaction.

In an attempt to obtain direct evidence for C-O bond breaking in ethers during the photochemical conversion of **2SS →2OO**, we studied ether degradation products using GC-MS. While no direct evidence for C-O bond breaking has at this point been detected, the dehydrogenation reaction of 2 equivalents of dihydrobenzofuran into benzofuran per **2SS** reacted does indicate a likely C-H abstraction as the initiating step in this transformation. At the time of writing, the ultimate source of oxygen atoms in the efficient formation of **2OO** from **2SS** remains elusive, as does the mechanism for its formation. New experiments are being carried out by PhD candidate Steven Mauries in the Frenette lab for the determination of side products and the reaction with other ether sources.

CHAPITRE 5

MECHANISTIC INSIGHT INTO FE CATALYZED α-C-H OXIDATION OF TERITARY AMINES: NON-RADICAL PATHWAYS FOR BASE-METAL CATALYSIS

5.1   Résumé

Nous rapportons une analyse mécaniste approfondie d'un système catalytique à base de fer qui prend en charge l'oxydation α-C-H des amines en amides. Le système utilise des esters peroxy comme oxydants, contrairement à d'autres catalyseurs qui effectuent des oxydations α-C-H d'amines tertiaires. Lorsqu'ils sont utilisés avec le système catalytique décrit, des oxydants courants tels que tBuOOH, qui ont été précédemment signalés comme des amines oxydées par des voies radicalaires, ne produisent pas de produits d'oxydation α-C-H. Les calculs DFT indiquent qu'un mécanisme Fe(IV)-oxo sera la voie privilégiée.
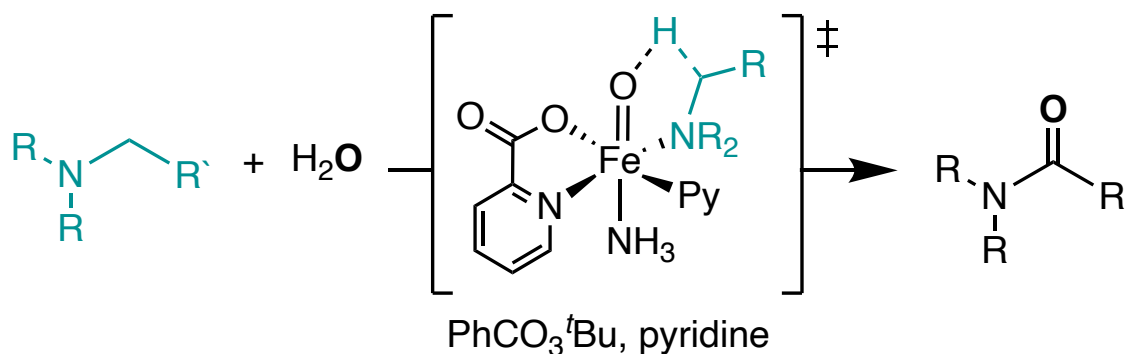
Figure 5.1. Oxydation de α-C-H d'amines aliphatiques tertiaires catalysée par Fe (Fe catalyzed α-C-H oxidation of tertiary aliphatic amines).

Supplemental information is available in Annexe C and includes DFT energies and coordinates.

5.2 Foreword

The work presented in this chapter is the result of a collaboration with researchers at the Department of Chemistry and Biochemistry at Worcester Polytechnic Institute, Gustaf H. Carlson School of Chemistry at Clark University, and the Department of Process Research & Development, Discovery Process Chemistry at Merck & Co., Inc. in West Point, Pennsylvania. The original concept, the optimization of the reaction and its conditions, and the experimental mechanistic work was completed by our collaborators Christopher J. Legacy, Frederick T. Greenaway, Marion H. Emmert.

The DFT studies were performed by Yohann Gagné, Mathieu Frenette and me.

As a lead author from my research group on this study, the objective of this collaboration was to compliment the reaction developed by Marion H. Emmert and her colleagues with an in-depth DFT mechanistic study.

The work was submitted to *ChemCatChem* where we were offered the cover image (See Annexe C, Figure C.1 for cover art). This contribution was selected as a "***Very*** Important Paper".

5.3 Abstract

We report a thorough mechanistic analyses of an iron-based catalyst system that supports the α-C-H oxidation of amines to amides. The system uses peroxy esters as oxidants, unlike other catalysts that effect α-C-H oxidations of tertiary amines. When used with the described catalyst system, common oxidants such as ^{t}BuOOH, which have been previously reported to oxidized amines via free radical routes, do not produce α-C-H oxidation products. DFT calculations indicate an Fe(IV)-oxo mechanism will be the preferred mechanistic route.

5.4 Introduction

Organic molecule C-H oxidation is of particular interest due to its abundance in drug metabolism (Genovino *et al.,* 2016) as well as biosynthetic pathways (Chen *et al.,* 2009). In particular, the direct oxidation of amines has gained attention from the pharmaceutical industry due to the conversion of amines to amides of active pharmaceuticals in the liver. Using transition metal

catalyzed C-H oxidation is an attractive approach due to the high atom economy of the reaction and green nature of using water as the oxygen source. Enzymes with iron cofactors catalyse these amine-to-amide process already in nature. The family of cytochrome P_{450} is a common example, which has non-heme dioxygenases, hydroxylases, and halogenases (Nam, 2007) as well as Fe-porphyrin cofactors (Genovino *et al.,* 2016; Oscarson *et al.,* 2001; Walsh *et al.,* 2013). Many of these systems catalyse oxidations via Fe(IV)-oxo intermediates, which attack aliphatic C-H bonds in a radical rebound manner and cleave the C-H bond through a hydrogen abstraction mechanism (Chen *et al.,* 2001; Genovino *et al.,* 2016; Groves, 2015; Huang and Groves, 2017; Nam, 2007; Schlichting *et al.,* 2000).

Based on research from Chiavarino *et al.,* (2008) an alternative mechanistic possibility to Fe-oxo routes has been put up for enzyme-catalyzed amine α-C-H oxidations. This process uses proton and single electron transfers to produce iminium or imine products from radical intermediates.

For a long time, researchers have debated the mechanism of synthetic systems that functionally mimic the metabolic pathways of amine α-C-H oxidations in using O_2, H_2O, or ^{t}BuOOH as oxidants. Proposed pathways include free or solvent-caged radicals, hemiaminals, peroxyhemiaminals, and/or metal-coordinated iminium ions (Barton and Doller, 1992; Barton *et al*., 1989; Boess *et al.,* 2012; Boivin *et al.,* 1990; Catino *et al.,* 2006 ; Kiani et al., 2000; Li et al., 2006 ; Perkins, 1996). Ratnikov *et al*. (2013) has demonstrated that, regardless of the type of metal catalyst utilised, using ^{t}BuOOH as an oxidant likely favours oxidations via free radical pathways and hemiaminal intermediates. Aniline-type substrates were used in this investigation, with both precious metal catalyst systems ($Rh_2(cap)_4$, $RuCl_3$) and base-metal as the catalysts (CuBr, $FeCl_3$, $Co(OAc)_2$). However, amine-to-amide conversion has previously been effective for primary amines using copper (Xu *et al.,* 2012) or ruthenium (Kim *et al.,* 2008) based catalysts. The conversion of secondary amines to lactams has been catalyzed with gold-nanoparticles (Preedasuriyachai *et al.,* 2011) and ruthenium pincers (Khusnutdinova *et al.,* 2014). Unfortunately, many of the catalysts that are active in primary, secondary, cyclic, or aniline oxidations are unreactive towards tertiary aliphatic amines. This leads to the questions as to if these mechanistic insights are transferable to our collaborators α-C-H functionalizations of tertiary aliphatic amines (Legacy *et al.,* 2015).

Motivated by the absence of such mechanistic studies, we set out to elucidate the reaction mechanism for the α-C-H oxidations of aliphatic amines using a Fe-based catalyst system, specifically FeCl₃ (Legacy *et al.,* 2015) using a synthetic model system. This work is an in-depth experimental and computational study based on the previous publication from our collaborators where they explored the reaction scope of aliphatic tertiary (Figure 5.2).
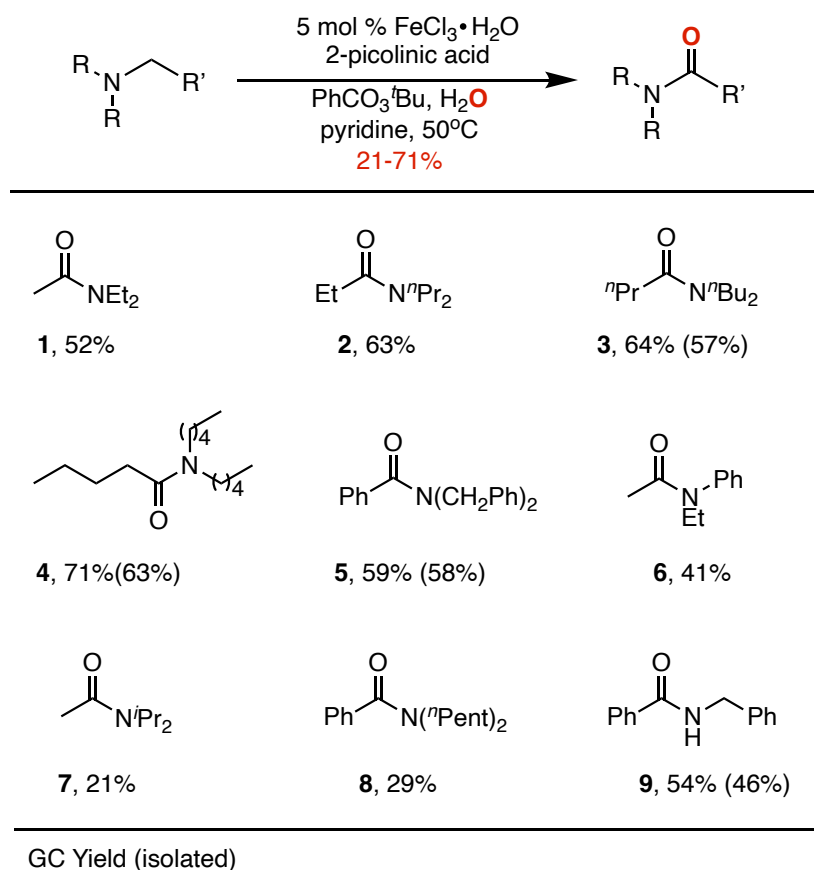
Figure 5.2. Substrate scope of amide formation from tertiary amines.

Based on the mechanistic studies performed we propose that, as opposed to the free radical mechanism frequently suggested for Fe catalysts, such as in Fenton-type chemistry, the α-C-H cleavage occurs via a radical rebound or coordinated process (Sawyer *et al.,* 1996; MacFaul *et al.,* 1998; Goldstein and Meyerstein, 1999). It's interesting to note that the experimental values for the Eyring plot and the kinetic isotope effect (KIE) ($\Delta H^{\ddagger} = + 14.1$ kcal/mol, $\Delta S^{\ddagger} = -10.8$ cal/mol and $k_H/k_D = 1.7 \pm 0.1$) are more in line with the values frequently found with β-hydride elimination/ hydride shift and concerted metalation deprotonation (involvement of a heteroatom of the oxidant).

For C-H cleavage that proceed via a 2-electron process, often a precious metal catalyst such as Pd and Ir (Boutadla *et al.,* 2009; Davies *et al.,* 2005) is involved. Overall, the mechanistic pathway provides a rationale for the selectivity of amine α-C-H oxidation with the established Fe catalyst system.

In Figure 5.3A, the mechanism is characterized by a series of coordination/dissociation steps between resting state **9** and rate determining step (rds), with the rds proceeding through a hybrid mechanism between β-hydride elimination and concerted metalation/deprotonation, which also cleaves the peroxide O-O bond. For mechanism A, we calculated the kinetic barrier for the rate-determining step (rds) **11→12**. The energy barrier to undergo a β-hydride elimination was studied computationally where it was determined that the energy barrier was prohibitively high for this mechanism.

In mechanism B (Figure 5.3B) which also proceeds through a series of coordination/dissociation steps between the resting state **9** and the rds, in addition to a two electron-oxidation of Fe^{+2} to Fe^{+4}. This oxidation of resting state **9** proceeds upon heterolytic O-O bond cleavage of $PhCO_3{}^t Bu$ to form **13**. The rds in mechanism B is formulated analogous to typical radical-rebound mechanisms at Fe-oxo species. Intramolecular α-C-H abstraction by the Fe(IV)-oxo generates intermediate **14** and the subsequent hydroxyl transfer occurred to form **15**. Several ligand exchange steps are then required to reform the resting state **9.**

Under the reaction conditions, the hemiaminal product **2** generated by both catalytic cycles will oxidize to yield the final amide product. This final transformation is assumed to be rapid and will not contribute to the initial reaction kinetics.
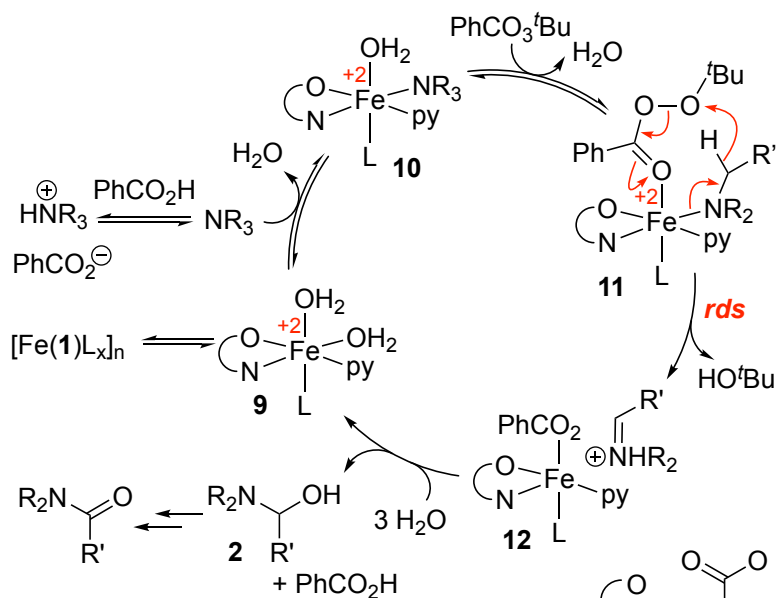
Figure 5.3. Proposed catalytic cycles based on experimental and computational mechanistic studies a) β-hydride elimination mechanism b) Fe(IV)-oxo mechanism and c) the empirical rate law of the reaction.

Both mechanisms A and B are consistent with experimental data, however only mechanism B is also consistent with reaction energies as determined by DFT. Neither mechanism suggests a role

for free radicals in the reaction mechanism outside of the catalyst activation pathway. This fundamentally distinguishes the investigated catalyst system from the systems investigated previously by Ratnikov *et al.,* (2013). This mechanistic study attempts to explain why the catalyst system allows for the selective α-C-H oxidation of a wide range of tertiary aliphatic amines: the substrates are activated to undergo α-C-H cleavage by coordination to the Fe catalyst. In contrast, earlier systems using free radical processes are limited to substrates of the secondary amine and benzylic/aniline types, which are more easily activated. As a result, the mechanistic information gained supports a non-classical amine α-C-H oxidation pathway that involves substrate binding, which also promotes selectivity and facilitates reactivity.

5.5 Experimental Method

5.5.1 Computational Methods

Density Functional Theory (DFT) calculations were performed using the Gaussian 09, (2016) suite with 3 different functionals. The functionals used were B3LYP, M06-2X and ωB97XD with the basis set 6-311+G(2d,2p) using the conductor-like polarizable continuum model (CPCM) to simulate the pyridine solvent (Barone and Cossi, 1998).

The B3LYP level of theory uses Becke's 3-parameter exchange and Lee, Yang and Parr's correlation function (Becke, 1992; Becke 1993; Lee *et al.,* 1998). All geometry optimization and frequency calculation used were conducted at the B3LYP/6-311+G(2d,2p)//CPCM(pyridine).

The M06-2X level of theory is part of the Minnesota Functionals developed from *Zhao et al.* (2008). The geometries were optimized using B3LYP/6-311+G(2d,2p)//CPCM(pyridine) followed by frequency calculations using M06-2X/6-311+G(2d,2p)//CPCM(pyridine).

The ωB97XD level of theory was developed by Chai *et al.* (2008). The geometries were optimized using B3LYP/6-311+G(2d,2p)//CPCM(pyridine) followed by frequency calculations using ωB97XD/6-311+G(2d,2p)//CPCM(pyridine).

Resulting outputs were verified for imaginary frequencies to ensure the optimized structures were local minima for ground states (no imaginary frequency) or saddle points for transition states (one

imaginary frequency). The free energies (ΔG) were calculated using the zero-point energy corrected Gibbs free energy at 298.15 K (Sum of Thermal and Free Energies in Gaussian Output), and free enthalpies (ΔH) were calculated using the zero-point energy corrected Enthalpy at 298.15K (Sum of electronic and thermal Enthalpies in Gaussian Output).

5.6   Results And Discussion

5.6.1   β-Hydride Elimination Mechanism

We were contacted to provide DFT evidence for their proposed mechanism (Figure 5.3A). An Fe^{2+} 7 or 8-membered ring structure intermediate was proposed. We attempted to calculate the transition state barrier for the rds between **11 → 12** (Figure 5.3). For both high spin (S=2) and low spin (S=0) electronic configurations, the energy barrier to undergo a β-hydride elimination was studied computationally by forcing an approach of the leaving hydride towards the peroxide oxygen of compound **11** which is highlight in red. The ligands on the peroxy ester were simplified to -CH_3 to save on computational resources but still maintain an accurate depiction of the reaction conditions. In both spin states, the energy barrier exceeded 35 kcal/mol (Figure 5.4A).

The β-hydride elimination could also occur via a reaction with the other peroxide oxygen, i.e., forming a 7-membered ring instead of the 8-membered ring. The calculation for the transition state barrier was done in similar fashion to the 8-membered ring scan by forcing an approach of the leaving hydride towards the other peroxide oxygen. The barrier for an approach of the β-hydride towards this peroxide oxygen gave a similarly large barrier which exceeded 35 kcal/mol (Figure 5.4B).
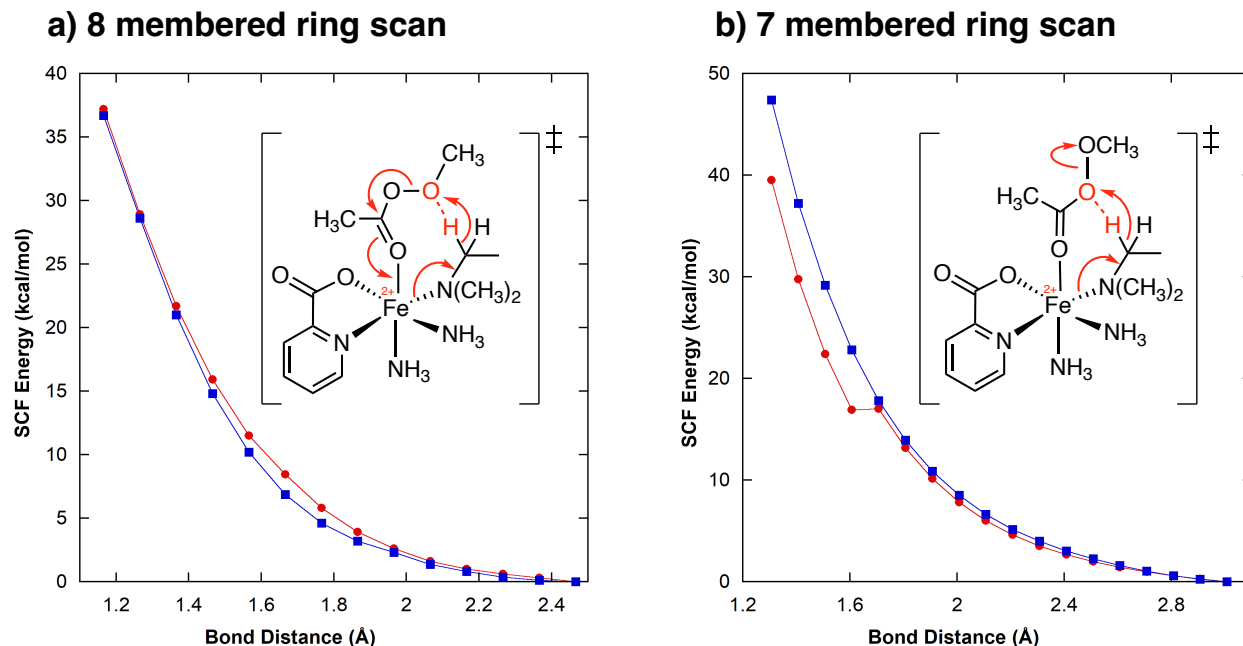
Figure 5.4. SCF energy vs highlighted O---H bond distance for the proposed a) 8-membered rings transition states and b) 7-membered rings transition states. High spin (S=2, red) and low spin (S=0, blue).

These DFT predicted transition state barriers of both the 7 membered ring transition state and 8 membered ring transition state are too large to overcome for a reaction that takes place at 50°C, suggesting that another less energetically demanding pathway is taking place.

5.6.2 Determining Catalytic Structure from Thermodynamic Parameters

To perform DFT calculation we first needed to determine the structure of the catalyst. Common Fe-centered catalytic intermediates are metal-oxo structures which appeared favourable for oxidation reactions (Meunier, 2003).

Our collaborators determined from the experimental evidence that a 1:1 ratio of Fe:2-picolinic acid resulted in the highest initial rates and the largest yields, suggesting that the active catalyst most likely does not change throughout the reaction with one 2-picolinic acid molecule remaining coordinated. The next step was establishing the kinetic orders of the different components of the catalytic system. A first order rate dependence was determined for the peroxy ester oxidant and amine substrate, while a zero-order dependence was determined for the pyridine solvent.

Interestingly, the kinetic order for H_2O was not as clear, depending on the concentration it could either be first, second, or approaching zero-order by saturation kinetics.

From these experimental results it was determined that the number of coordinated pyridine ligands does not change from the resting state to the transition state structure, which is in agreement with a zero-order dependence. While in the rds at least one peroxy ester oxidant and amine substrate are involved. The number of coordinated H_2O ligands was considered in the mechanistic studies.

In these calculations, the trialkylamine reagent was simplified to dimethyl-ethylamine and the unspecified ligand L was a chosen as a simple $-NH_3$ group. We believe that the $-NH_3$ group provided a suitable balance between being a good representative of a range of the possible ligands in solution (water, pyridine, amine, hemiaminal, etc.) while also conserving on computational cost.

Different permutations of ligands/geometries were investigated to approach the global minimum geometry for **13**, however, this was not an exhaustive search. Our choice of an $-NH_3$ ligand forced the orientation of this ligand to be oriented opposite (axial) to the oxo. Placing the $-NH_3$ group adjacent (equatorial) to the oxo resulted in an H-bonding interaction that would not be representative of the reaction.

To further understand the rds, our collaborators did an Eyring plot analysis to determine the entropy and enthalpy of activation. They experimentally measured how the initial rate of reaction varies as a function of temperature to determine the entropy of activation and enthalpy of activation which give insight into the reaction mechanism. The activation parameters measured were: $\Delta H^{\ddagger} = + 14.1$ kcal/mol and $\Delta S^{\ddagger} = -10.8$ cal/mol. The positive enthalpy of activation suggests a highly ordered transition state structure, consistent with other metal-oxo C-H abstraction mechanisms (Gardner and Mayer, 1995). From these values, $\Delta G^{\ddagger}$ was calculated to be $+ 17.3$ kcal/mol. These values were instrumental to our contribution to the mechanistic studies as they acted as a guide for the computational studies. When calculating the transition state barrier for the rds in the mechanism, the goal was to obtain theoretical values similar to those determined experimentally. From these values we refined our thinking and determined a catalyst structure and mechanism with similar thermodynamic parameters.

5.6.3 *Intra*molecular H-Atom Abstraction Mechanism

The mechanism was initially investigated computationally using the B3LYP/6-311+G(2d,2p)//CPCM(pyridine) level of theory. We began the investigation of this mechanism from the rds due to the experimentally determined activation parameters.

Intramolecular α-C-H-abstraction from the Fe(IV)-oxo species **13** afforded activation energy parameters that closely matched those obtained experimentally: $\Delta G^{\ddagger} = 19.4$ kcal/mol by DFT calculations for the high spin quintet form (S = 2), whereas the experimental results show a value of 17.3 kcal/mol (Figure 5.5). At this level of theory, the intermediate spin triplet form (S = 1) and the low spin singlet form (S = 0) for compound **13** were higher in energy than the quintet form by 3.1 and 32.5 kcal/mol, respectively.

Intramolecular α-C-H abstraction by the Fe(IV)-oxo generates intermediate **14** and the subsequent hydroxyl transfer occurred with no kinetic barrier to form **15**. The intramolecular H-abstraction/hydroxyl transfer step from **13**→**15** is highly favorable with $\Delta G^0 = -50.3$ kcal/mol. Several endergonic ligand exchange steps are then required to form the resting state **9** ($\Delta G^0 = +7.3$ kcal/mol); this compound also favors a high spin quintet electronic structure (S = 2). The oxidation of the Fe center from an oxidation state of +2 to +4 (**9** to **13**) using $PhCO_3{}^tBu$ as the oxidant is thermodynamically favorable ($\Delta G^0 = -17.5$ kcal/mol); however, the exact mechanism for this step is not yet known. The overall ΔG^0 for the catalytic cycle in mechanism B is -60.5 kcal/mol.
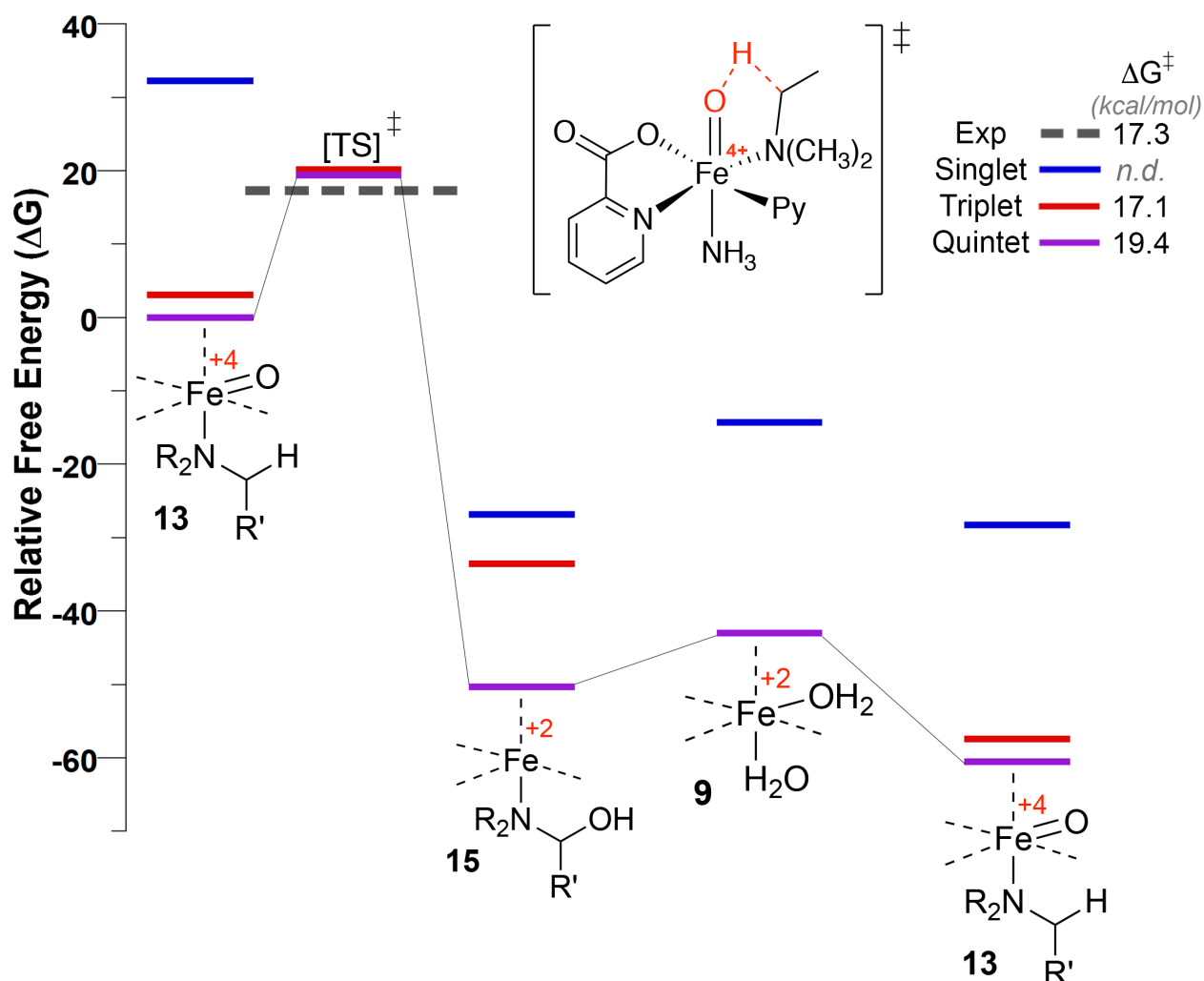
Figure 5.5. DFT-calculated free energies of the proposed Fe(IV)-oxo mechanism shown in Figure 5.3 using B3LYP/6-311++G(2d,2p)//CPCM(pyridine). High-spin quintet (S = 2) is the favored electronic configuration throughout the mechanism.

Alternative DFT functionals were investigated for the intramolecular α-C-H-abstraction mechanism, comparing M06-2X and ωB97X-D to B3LYP. The basis set of 6-311+G(2d,2p) was maintained for all calculations. The goal of comparing various functionals was to theoretically determine the most similar activation parameters to those determined experimentally. The DFT thermodynamic values for the individual steps proposed in each alternative reaction mechanism can be found in Annexe C.

The energy of the Fe(IV)-oxo is too high for the calculations using M06-2X (Figure 5.6). This is inferred from the fact that the ligand exchange from **15 → 9** and the formation of this Fe(IV)-oxo

species **13** is thermodynamically unfavorable from the reaction of the peroxy ester and the Fe^{2+} compound **9** ($\Delta G^0 = + 6.9$ and $+ 14.5$ kcal/mol, respectively). This result is somewhat expected as M06-2X is parameterized only for non-metals (Zhao *et al.,* 2008). The activation energy for the rds was calculated to be: $\Delta H^{\ddagger} = 12.8$ kcal/mol and $\Delta S^{\ddagger} = -5.4$ kcal/mol.
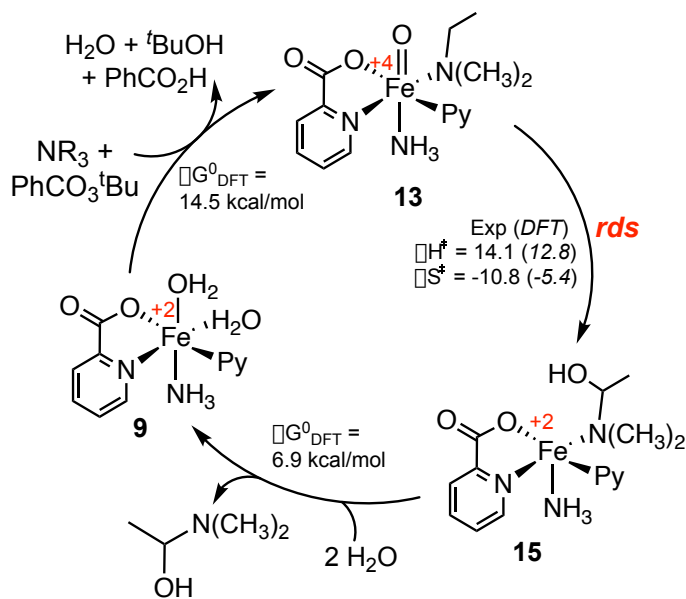
Figure 5.6. Catalytic cycle with representative geometries that were used for M06-2X/6-311+G(2d,2p)//CPCM(pyridine) calculations.

For the functional ωB97X-D, we initially calculated the rds of the for the intramolecular α-C-H-abstraction mechanism. The enthalpy for this proposed rate determining step is close in value to that obtained using B3LYP/6-311+G(2d,2p). The entropy value using the ωB97X-D functional, however, is less similar to the value determined experimentally (Figure 5.7).
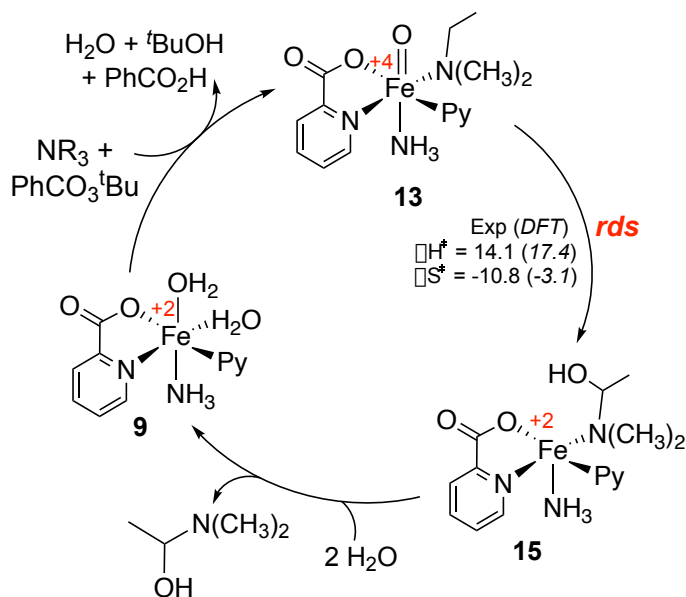
Figure 5.7. Catalytic cycle with representative geometries that were used for ωB97X-D/6-311+G(2d,2p)//CPCM(pyridine) calculations.

We ultimately decided to use the functional B3LYP, as it gave both entropy and enthalpy values most similar to those determined experimentally, as shown in Table 5.1 below.

5.6.4 *Inter*molecular H-Atom Abstraction Mechanism

While the proposed mechanism involves an *intra*molecular α-C-H abstraction between an Fe(IV)-oxo species and the alkyl amine, *inter*molecular reactivity was also considered. An intermolecular H-atom abstraction mechanism could possibly better explain the experimentally calculated entropy value (Figure 5.8). The ligands on the Fe catalyst were modified to better fit an intermolecular H-atom abstraction and dimethyl-ethylamine was exchanged to a trimethyl amine, the other ligands remained unchanged. To simulate an unbound outside amine undergoing α-C-H with the Fe(IV)-oxo complex, and fairly compare it to the *intra*molecular mechanism, a dimethyl-ethylamine was used. The H-atom abstraction was simulated by scanning the oxygen on the Fe(IV)-oxo and the ethyl group on the incoming amine as a secondary hydrogen.
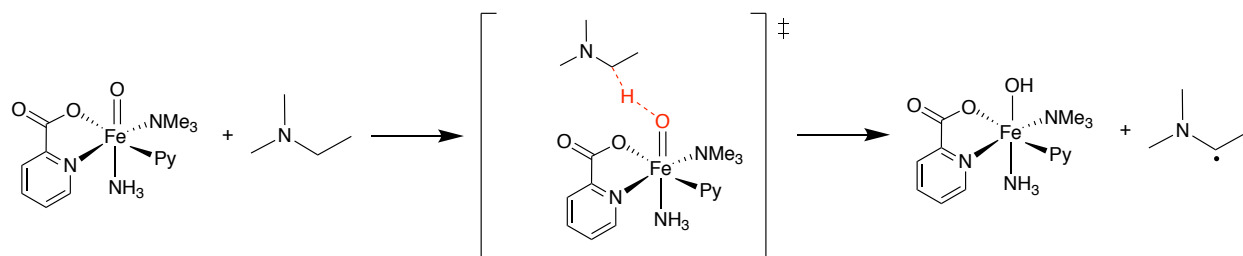
Figure 5.8. *Inter*molecular α-C-H-abstraction between Fe(IV)-oxo and dimethyl-ethylamine.

The transition state entropy for *inter*molecular reactivity, as calculated by DFT, was -33.7 cal/(mol•K). This deviated significantly from the experimentally determined $\Delta S^{\ddagger}$ of -10.8 cal/(mol•K). For comparison, the DFT-calculated $\Delta S^{\ddagger}$ for the *intra*molecular α-C-H abstraction shown in Figure 5.3B was -5.1 cal/(mol•K) and thus, in better agreement with the experimentally measured value, as shown in Table 5.1

Table 5.1. Comparison of 3 different DFT functionals for intramolecular α-C-H-abstraction and one intermolecular α-C-H-abstraction calculated with B3LYP for the proposed rds in Figure 5.3B.

	$\Delta G^{\ddagger}$ (kcal/mol)	$\Delta H^{\ddagger}$ (kcal/mol)	$\Delta S^{\ddagger}$ (cal/mol)
Experimental	17.3	14.1	-10.7
B3LYP	19.4	17.9	-5.1
ωB96X-D	18.4	17.4	-3.1
M06-2X	14.4	12.8	-5.4
*Inter*molecular	22.3	12.3	-33.7

5.7 Conclusion

Collaboration on this project has allowed me to branch out upon my previous knowledge and to investigate non-photochemical reaction mechanisms. DFT calculations reject the β-hydride elimination mechanism which gave prohibitively large energy barriers (>35 kcal/mol) for the rds in Figure 5.3A. Alternatively, DFT calculations lend strong evidence for the Fe(IV)-oxo mechanism in Figure 5.3B. Experimentally determined activation energies and those calculated for the Fe(IV)-oxo in the rds of the intramolecular α-C-H-abstraction mechanism were in good agreement. While the formation of the Fe(IV)-oxo species by reaction with $PhCO_3{}^tBu$ is

thermodynamically favorable, the exact mechanism for this transformation remains under investigation.

The intramolecular α-C-H-abstraction mechanism, which is consistent with both experimental data and reaction energies as determined by DFT, does not suggest a role for free radicals in the reaction mechanism outside of the catalyst activation pathway. This fundamentally distinguishes the investigated catalyst system from the systems investigated previously by Ratnikov *et al*. (2013).

The presented work provides an explanation for why the selective α-C-H oxidation of a wide variety of tertiary aliphatic amines is possible with this catalyst system: coordination to Fe activates the substrates to undergo α-C-H cleavage. In contrast, previous systems proceeding through free radical mechanisms are restricted to more activated substrates (secondary amines, benzylic/aniline-type substrates). Thus, the obtained mechanistic data support a non-classical amine α-C-H oxidation pathway proceeding via substrate binding, which concurrently induces selectivity and enables reactivity.

CHAPITRE 6

MECHANISTIC EVIDENCE FOR A RADICAL-RADICAL RECOMBINATION PATHWAY OF FLAVIN-BASED PHOTOCATALYTIC TYROSINE LABELING

6.1 Résumé

Nous décrivons la photocatalyse à base de flavine comme une plate-forme robuste pour le marquage des protéines à médiation lumineuse via le couplage tyrosine-phénol sur des cellules vivantes. L'étiquetage sélectif s'est avéré possible dans les approches ciblées par rapport aux approches non ciblées, et nous avons observé un rayon d'étiquetage de proximité plus étroit qu'une stratégie d'étiquetage à base de peroxydase bien connue. Pour mieux comprendre, nous avons effectué une analyse mécaniste détaillée de l'activation photomédiée par le tétraacétate de riboflavine des phénols pour le marquage de la tyrosine. Contrairement aux mécanismes précédemment proposés, nous constatons que l'étape de liaison covalente initiale entre l'étiquette et la tyrosine n'est pas une addition radicale, mais plutôt une recombinaison radical-radical. L'addition radicale aux phénols, bien que souvent proposée, est extrêmement défavorable selon les calculs DFT. La recombinaison radicalaire-radicale, suivie d'une réaromatisation, est la voie préférée pour le couplage phénol-phénol présenté ici, mais peut également expliquer le mécanisme d'autres approches de marquage de tyrosine rapportées. Des expériences de cinétique compétitive montrent que les radicaux phénoxyles sont générés par la réaction des phénols avec plusieurs intermédiaires réactifs dans le mécanisme proposé, principalement avec le photocatalyseur de riboflavine excité ou l'oxygène singulet, et ces multiples voies de génération de radicaux phénoxyles augmentent la probabilité de recombinaison radical-radical.
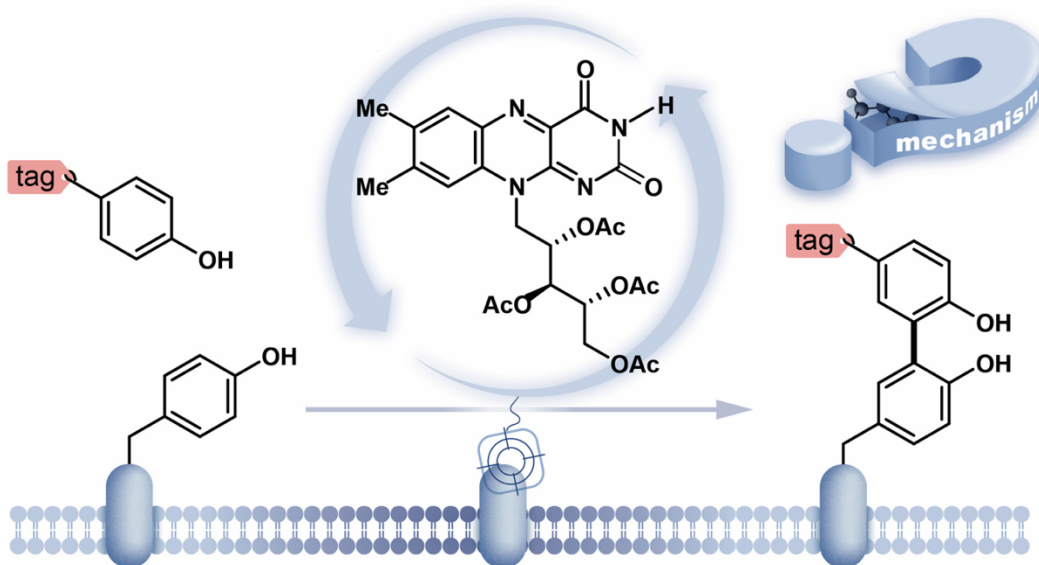
Figure 6.1. Biophotocatalyse flavin pour le couplage phénol-phénol (Flavin biophotocatalysis for phenol-phenol coupling).

Supplemental information is available in Annexe D and includes absorption and emission spectra, quantum yield of fluorescence experiments, reference system spectra and kinetic traces, time-resolved Stern-Volmer quenching results, laser flash photolysis, cyclic voltammograms, and DFT energies and atomic coordinates.

6.2   Foreword

The work presented in this chapter is the result of a collaboration with researchers at Merck Exploratory Science Center/InduPro, in Cambridge, Massachusetts, USA. The optimization of the reaction and its conditions, the control experiments, NMR compound characterization and in general the biological chemistry aspect was completed by our collaborators at Tamara Reyes-Robles, Keun Ah Ryu, Rob C. Oslund and Olugbeminiyi O. Fadeyi

Cyclic voltammetry experiments were performed by me. DFT studies were performed by Nicole Removski, Steven Mauries, Mathieu Frenette, and me. Laser flash photolysis experiments were performed by Mathieu Frenette and me. Measuring the kinetics between phenol and singlet oxygen was performed by Jacinthe Maisonneuve, Mathieu Frenette, and myself. Note: The calculations in this thesis did not contain dispersion corrections which are included in the final manuscript.

As a lead author on this study, my objective in this collaboration was to provide an in-depth mechanistic understanding of a phenol-phenol coupling reaction photocatalyzed by riboflavin tetraacetate.

6.3   Abstract

We describe flavin-based photocatalysis as a robust platform for light-mediated protein labeling via tyrosine-phenol coupling on live cells. Selective labeling was shown possible in targeted versus non-targeted approaches, and we observed a tighter proximity labeling radius than a well-known peroxidase-based labeling strategy. To gain insight, we conducted detailed mechanistic analysis for riboflavin tetraacetate-photomediated activation of phenols for tyrosine labeling. Contrary to previously proposed mechanisms, we find that the initial covalent binding step between the tag and tyrosine is not radical addition, but rather radical-radical recombination. Radical addition to phenols, while often proposed, is prohibitively unfavorable according to DFT calculations. Radical-radical recombination, followed by rearomatization, is the preferred pathway for the phenol-phenol coupling presented herein, but may also explain the mechanism of other reported tyrosine-tagging approaches. Competitive kinetics experiments show that phenoxyl radicals are generated by the reaction of phenols with several reactive intermediates in the proposed mechanism, primarily with the excited riboflavin-photocatalyst or singlet oxygen, and these multiple pathways for phenoxyl radical generation increase the likelihood of radical-radical recombination.

6.4   Introduction

Technologies that identify interacting proteins are crucial to understand fundamental biological processes and to enable new drug target discoveries. Visible light photocatalysis has emerged as an attractive platform for this purpose to achieve selective chemical transformations on and within biological materials with spatiotemporal control (Ryu *et al.,* 2021; Buksh *et al.,* 2022; Oslund *et al.,* 2022; Muller *et al.,* 2021; Wang *et al.,* 2021; Tamura *et al.,* 2020; Trowbridge *et al.,* 2022; Geri *et al.,* 2020; Tay *et al.,* 2021; Sato and Nakamura, 2013; Li *et al.,* 2021). A key feature is that visible light selectively excites a photocatalyst; the excited photocatalyst then activates chemical tags for covalent protein labeling. Tag molecules are usually activated to become reactive intermediates with short lifetimes, such as radicals, (Sato and Nakamura, 2013; Li *et al.,* 2021) carbenes (Geri *et al.,* 2020), or nitrenes (Tay *et al.,* 2021) to limit the labelling radius within a

complex biological environment. Importantly, a single photocatalyst can activate multiple tags resulting in substantial signal amplification for labeling with bioorthogonal handles such as biotin, azides, alkynes, or fluorophores for downstream protein analysis (Ryu *et al.,* 2021; Stephanopoulos *et al.,* 2011).

A major trend in proximity protein tagging is to exploit the reactivity of tyrosine at a protein's surface. Notably, peroxidase-enabled tyrosine labeling has been developed for profiling protein environments in numerous cellular contexts (Hung *et al.,* 2016). In this system, initiated by exogenous hydrogen peroxide, a phenol-containing tag is oxidized to phenoxyl radicals by heme-containing peroxidases resulting in the labeling of nearby proteins. Recently, our collaborators reported on the use of a flavin-based cofactor, riboflavin tetraacetate (**RFT**), as a photocatalyst for the generation of phenoxyl radical intermediates for tyrosine-based protein labeling (Figure 6.2A, Oslund *et al.,* 2022). Blue-light activated **RFT** was shown to achieve proximity labeling of proteins, live cells, and cell-cell contact regions (Figure 6.2B). Similar to other reported tyrosine tagging methods, radical addition onto a neutral tyrosine is traditionally proposed as a key step in the mechanism (Sato and Nakamura, 2013; Li *et al.,* 2021; Tsushima *et al.,* 2017; Fancy *et al.,* 1999; Niederer *et al.,* 2020). However, to date, no direct evidence has been reported for this mechanism. In light of this, the present collaboration is a mechanistic study on flavin-photocatalyzed phenol-phenol coupling. The result is a collaboration between Merck Exploratory Science Center/InduPro and the Frenette group where we examine a radical addition mechanism and a radical-radical recombination pathway (Figure 6.2C).
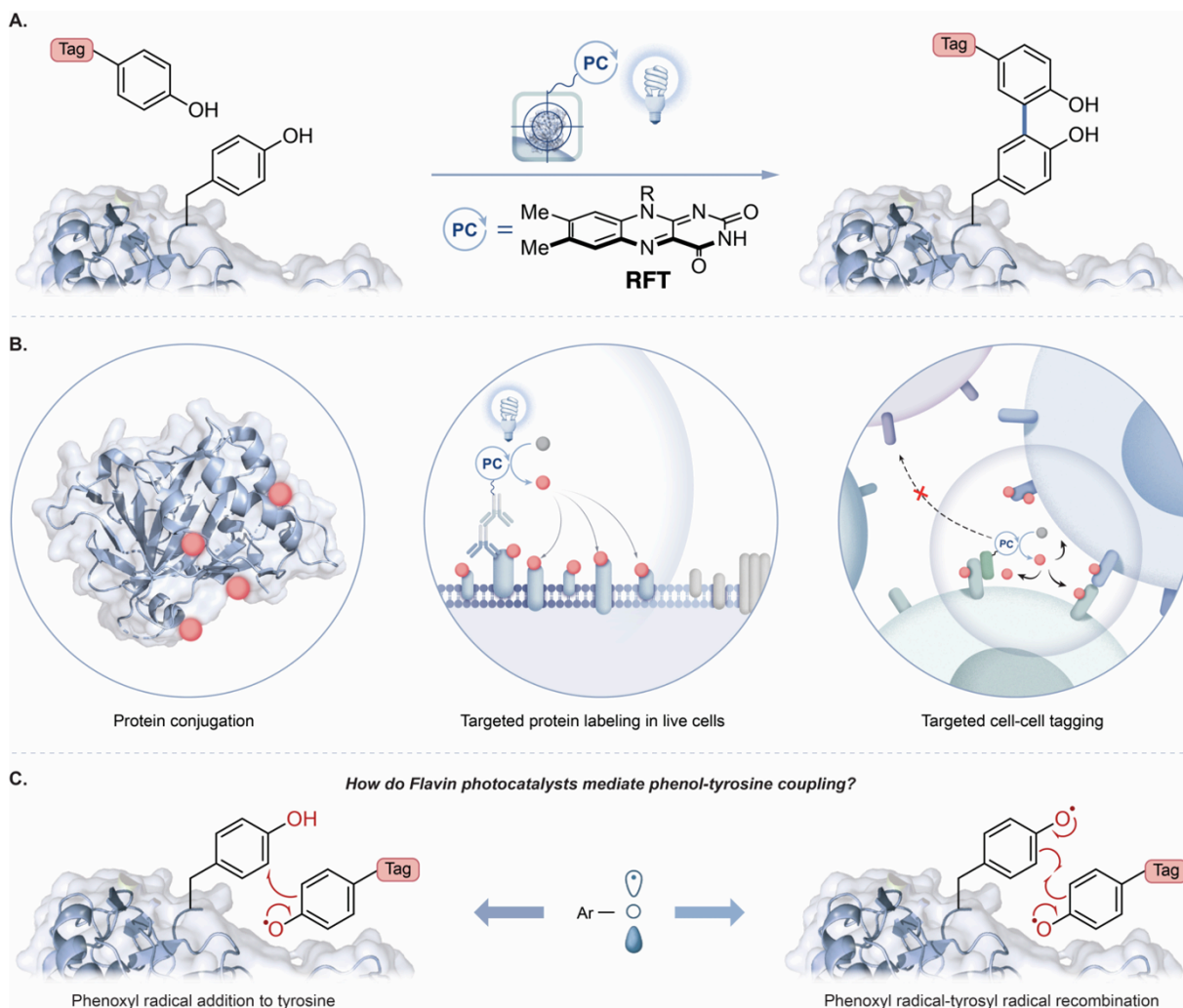
Figure 6.2. a) Flavin-based photocatalytic tyrosine-tagging by phenol containing tags. b) biological applications of **RFT**-mediated photocatalysis in protein and cellular environments. c) Competing mechanistic proposals for the labeling of tyrosine by phenoxyl radicals: radical addition to tyrosine versus radical recombination.

This photocatalytic coupling method was employed on a small variety of nucleophilic phenol substrates. The yield for the product is produced in moderate yields for the tyrosine-phenol cross-coupling reaction (Figure 6.3).
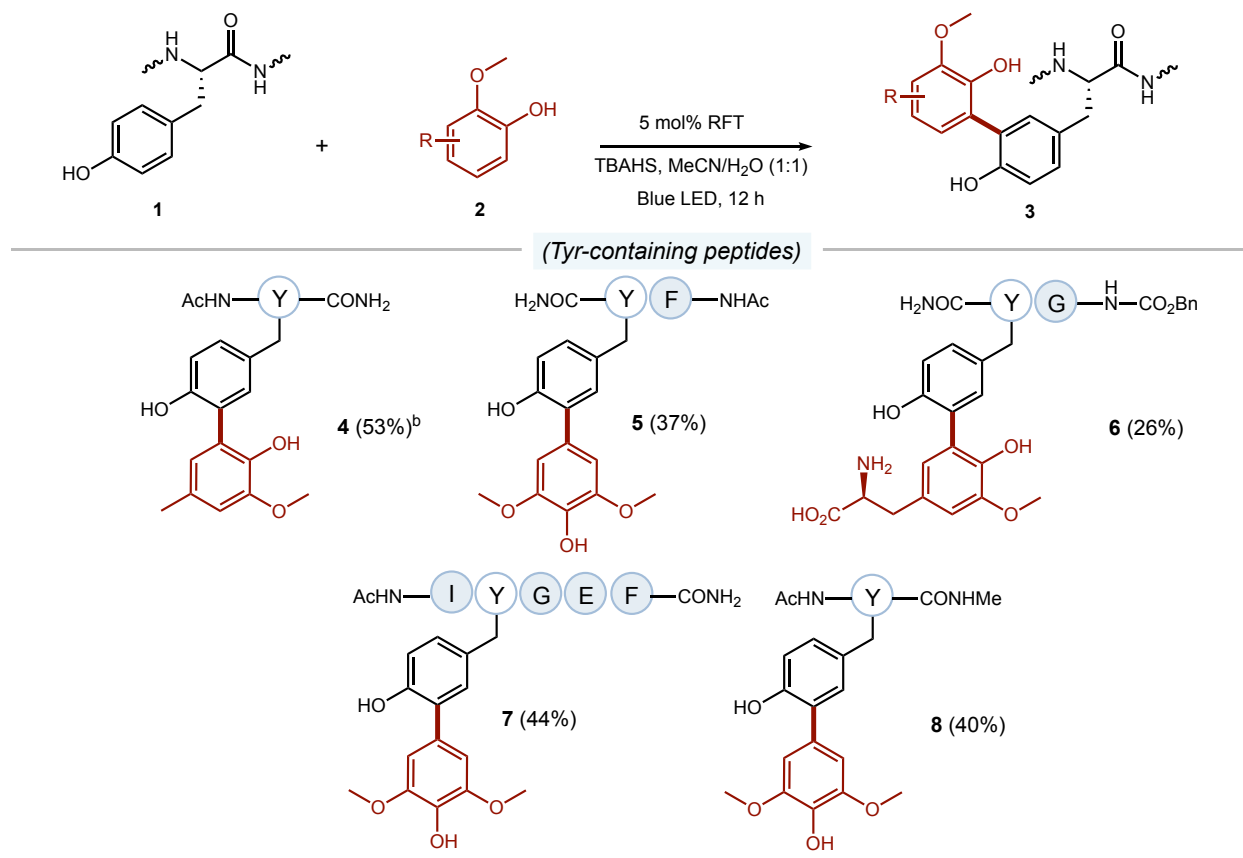
Figure 6.3. **RFT**-mediated coupling substrate scope.

For tyrosine-tagging methods, radical addition onto a neutral tyrosine has often been proposed as a key step in the mechanism (Sato and Nakamura, 2013; Li *et al.,* 2021; Tsushima *et al.,* 2017; Fancy *et al.,* 1999; Niederer *et al.,* 2020). Initially, our collaborators even proposed their reaction mechanism based on this (Figure 6.4).
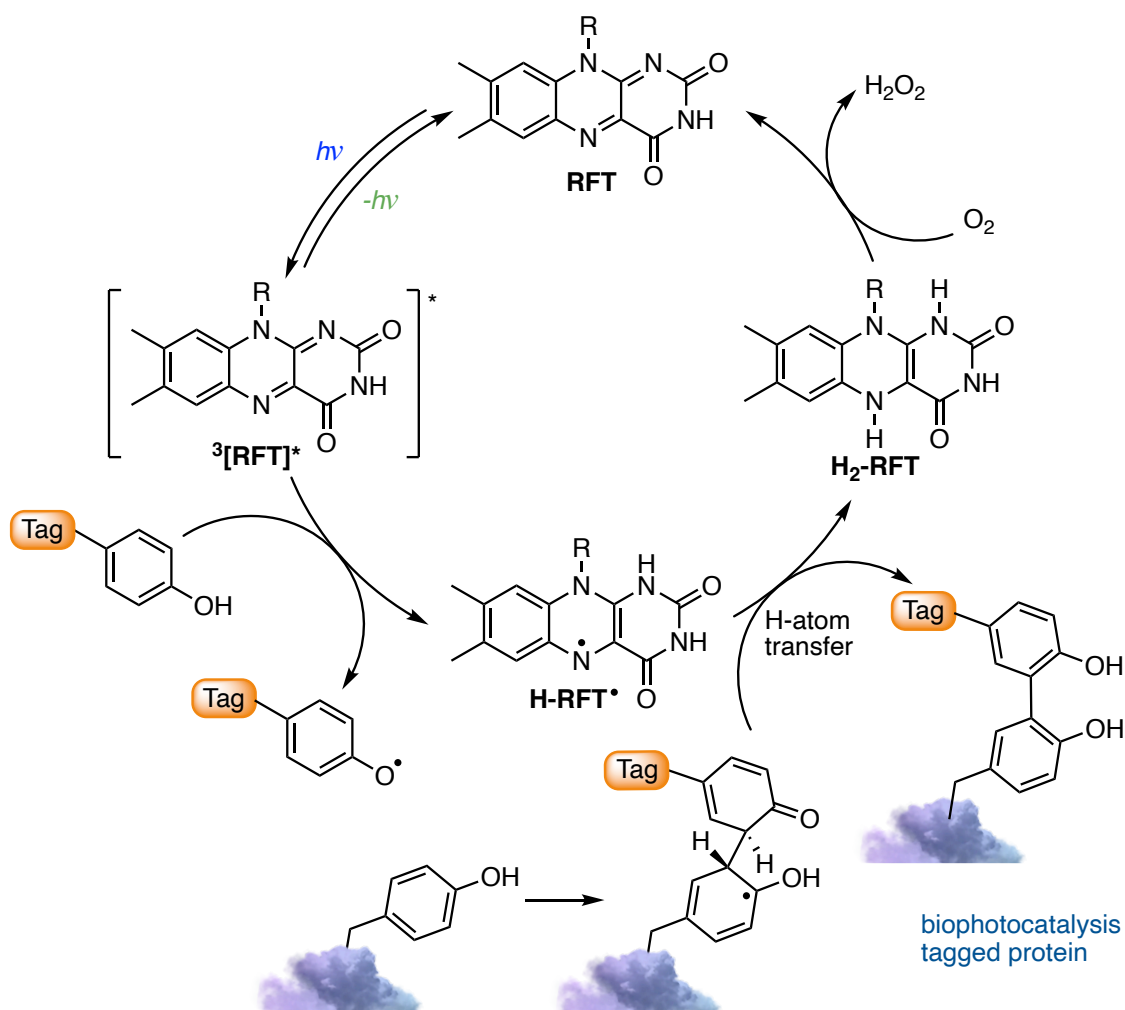
Figure 6.4. Initially considered reaction mechanism.

A major contribution of this study is to bring convincing evidence against radical addition to tyrosine; the thermodynamic cost of this radical addition step is prohibitively unfavorable (Figure 6.5A). The recombination of phenoxyl radicals, however, is much more probable (Figure 6.5B). The slight endergonic recombination is a testament to phenoxyl radical stability, but the recombination product will rapidly tautomerize to regenerate aromaticity for a largely favorable phenol-phenol coupled product.

A. Radical addition to tyrosine

$\Delta G_{add} > +44$ kcal/mol

B. Phenoxyl radical-radical recombination

$\Delta G_{rec} = +7$ to 12 kcal/mol
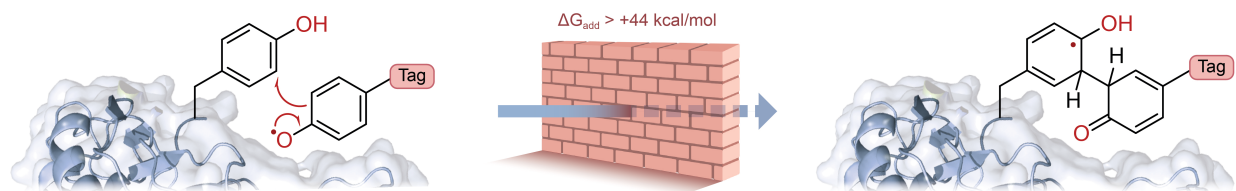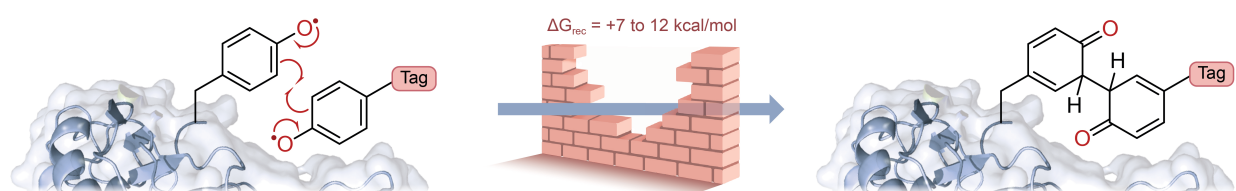
Figure 6.5. A) The addition of a phenoxyl radical tag to tyrosine is highly unfavorable (Table D.4). B) Radical-radical recombination of phenoxyl radicals is more favorable, and rearromatization leads to a strong covalent bond (Table D.3).

Photocatalysis often employs metal-based complexes due to their long-lived excited state lifetimes and tunable redox potentials, (Juneau *et al.,* 2022; Hernandez-Perez and Collins, 2016; Glaser and Wenger, 2020) however, more bio-compatible photocatalysts such as **RFT** are desirable in protein labeling. We explored **RFT** photochemistry and found several pathways by which phenoxyl radicals, from tags and tyrosine, could be generated. The multiple pathways that generate phenoxyl radicals support evidence of radical-radical recombination as the likely mechanism in these systems.

As depicted in Figure 6.6A, the photocatalytic cycle begins with blue light absorption by **RFT** followed by formation of a triplet excited state, **³[RFT]***. Flavins are well-known singlet oxygen ($^1O_2$) sensitizers (Zhuang *et al*., 2022; Grosheva *et al.,* 2021), **³[RFT]*** can generate $^1O_2$ which can oxidize phenols to phenoxyl radicals (DeRosa and Crutchley, 2002; Thomas and Foote, 1978; Scully Jr and Hoigné, 1987; Al-Nu'airat *et al.,* 2019). It is also possible for **³[RFT]*** to directly react with phenols to form phenoxyl radicals and **H-RFT˙**. To regenerate **RFT** from **H-RFT˙** two pathways are considered. As often proposed in the literature for flavins, **H-RFT˙** can be further reduced to **H₂-RFT** (Li *et al.,* 2021; Zhuang *et al*., 2022; Grosheva *et al.,* 2021; Chen *et al.,* 2014), via reduction from phenols to phenoxyl radicals. A second pathway can bypass the need to generate **H₂-RFT**, as oxygen can directly oxidize **H-RFT˙** back to **RFT** with the formation of HOO˙.

The detection of H_2O_2 as a by-product has been used as evidence for the catalytic cycle to involve **H₂-RFT** (Niederer *et al.,* 2020). Indeed, the reduction of **H₂-RFT**, in a presumably multistep process, could favorably generate H_2O_2 in the presence of oxygen. However, H_2O_2 can also be generated in pathways that do not include **H₂-RFT**. The reaction of $^1O_2$ with phenols will generate HOO• as could the reaction of $^3O_2$ with **H-RFT˙**. Both H-abstraction by HOO• and recombination of two HOO˙ can explain the presence of H_2O_2. Finally, as proposed in Figure 5.6B the phenoxyl radicals will recombine and favourably tautomerize.
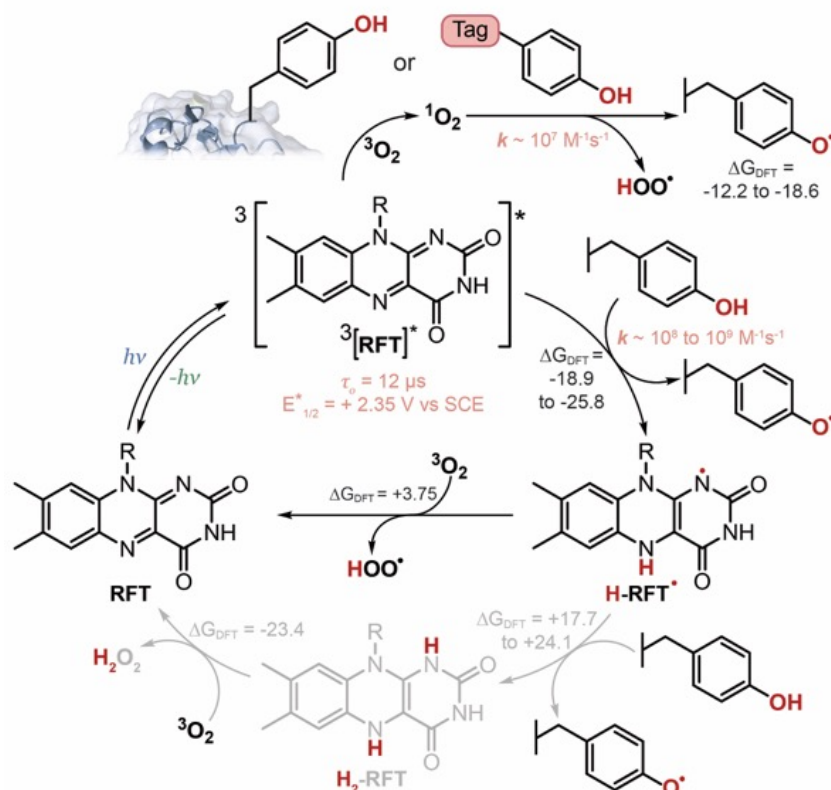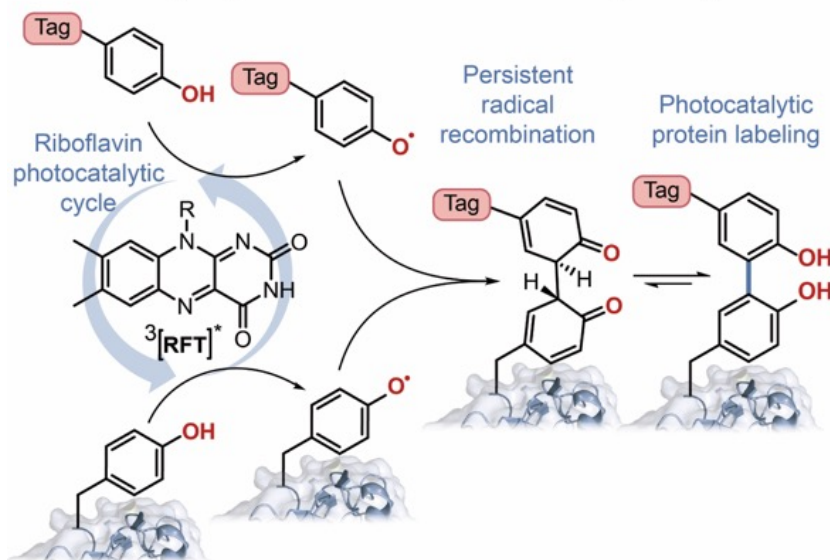
Figure 6.6. a) Proposed photocatalytic reaction mechanism for the generation of phenoxyl radicals from tyrosine-containing protein and phenol-containing tag molecules. b) Phenoxyl radical are persistent radicals, and as such will selectively recombine, followed by rearomatization, as the preferred pathway for phenol-phenol coupling.

6.5 Experimental Methods

6.5.1 Cyclic Voltammetry

Riboflavin tetraacetate

A solution of **RFT** (0.25 mM) and tetraethylammonium tetrafluoroborate (0.09 M, as the supporting electrolyte), was prepared in 1:1 water:acetonitrile and deoxygenated with N_2. The cyclic voltammograms were measured using an Ag/AgCl pseudo-reference electrode, a gold working electrode, and a platinum counter electrode. An internal standard of ferrocene (0.25 mM) was added to reference the value against Fc/Fc^+. The scanning rate was 50 mV/s. For re-calculation, Fc/Fc^+ was taken to be 0.380 V vs. SCE. **RFT** was measured to have a reduction potential of -0.185 V vs SCE.

6.5.2 Excited State Redox Potentials

The excited state redox potentials were calculated using the Rehm and Weller equation (Rehm and Weller, 1970):

$$E^*_{1/2}\,^{red} = E_{1/2}\,^{red} + E_{00} \qquad\qquad \text{eq. 6.1}$$

$$E^*_{1/2}\,^{oxi} = E_{1/2}\,^{oxi} - E_{00} \qquad\qquad \text{eq. 6.2}$$

The excited state potential is the sum of the ground state reduction potential of **RFT** ($E_{1/2}^{red}$) and the energy difference between the ground state and the excited state (E_{00}). This refers to the transition from the lowest energy vibrational state, which is estimated to the intersection between the absorption and emission spectra (See Annexe D, Figure D.1 for spectroscopic details of **RFT**) after converting wavelength to electron volts.

6.5.3 Time Resolved Stern-Volmer Quenching Studies and Triplet Excited State Lifetime Measurements

RTA and phenols

The transient absorption spectra and excited state lifetime of **RFT** was measured after pulsed laser irradiation at 355 nm (~20 mJ/pulse) from the third harmonic of a Surelite II Nd:YAG laser (Continuum).

To measure the quenching rates of various phenols, time-resolved emission following the laser excitation was measured at 700 nm using a fiber-optic based laser-flash photolysis system (miniLFP from Luzchem Research, Ottawa, Canada), fits to mono-exponential decays and the resulting lifetimes were analyzed using Stern-Volmer quenching kinetics analysis using eq. 2.8.

To a 1 x 1 cm quartz cuvette under argon, a pre-degassed solution of phenol quencher (2,6-dimethoxyphenol, biotin tyramide, and Ac-Tyr-NHMe) was added neat via syringe to a 1:1 water:acetonitrile solution containing RFT under argon (0.06 mM A_{355} = 0.5) that was sealed with a rubber septum under N_2.

When using the protein bovine serum albumin (BSA), the solutions (0.101 mM, 0.204 mM and 0.297 mM) were prepared in individual 1 x 1 cm quartz cuvettes in phosphate-buffered saline (PBS) under vacuum and N_2. A degassed solution of RFT (0.07 mM in PBS, A_{355nm} = 0.3) was added to each BSA containing cuvette to a final volume of 2.5 mL and sealed with a rubber septum under vacuum and N_2.

Biotin Tyramide

Transient absorption spectra of biotin tyramide (A_{266} = 0.5) measured in deoxygenated phosphate buffer saline (pH = 7.4, with 10% acetonitrile for solubility) after pulsed laser irradiation at 266 nm (~27 mJ/pulse) from the fourth harmonic of a Nd:YAG laser (Continuum).

Direct photolysis of the phenol at this wavelength forms a phenoxyl radical that can be followed by its absorption at 430 nm as measured using a fiber-optic based laser-flash photolysis system

(miniLFP from Luzchem Research, Ottawa, Canada). The transient absorption decay monitored at 430 nm fits to a second order decay.

6.5.4   Measuring The Rate of Reaction Between Phenol and Singlet Oxygen

Experiments were performed using 16 W blue outdoor LED by Feit Electricity. Quartz cuvettes were held by an in-house built support secured to a platform shaker set at 360 rpm, air-cooled using a fan (Figure D.13). The optimization of the reaction setup was tested with a known protocol by Pitre *et al.* (2015), used to measure chemical actinometry. The experiments were performed in a 1 x 1 cm quartz cuvette using a Cary-60 to record the absorption spectra.

RFT and 9,10-diphenylanthracene

A solution (2.5 mL) of (9,10-diphenylanthracene) **DPA** (0.1 mM) and **RFT** (A_{454nm} = ~0.4, 42 µM) was added to a quartz cuvette under air in 1:1 water:acetonitrile. The cuvettes were irradiated with blue LEDs and the change in absorption at 372 nm due to $^1O_2$ reaction with **DPA** was recorded as a function of irradiation time.

RFT, Phenol and DPA

A solution (2.5 mL) of **DPA** (0.1 mM), **RFT** (A_{454nm} = ~0.4, 42 µM) and phenol (1.31 mM, 0.66 mM, and 0.33 mM) was added to a quartz cuvette under air in 1:1 water:acetonitrile. The cuvettes were irradiated with blue LEDs and the change in absorption at 372 nm due to $^1O_2$ reaction with **DPA** and PhOH was recorded as a function of irradiation time.

6.5.5   Computational Methods

Density Functional Theory (DFT) calculations were performed using the Gaussian 09 (2009) and Gaussian 16 (2016) suite at the B3LYP level of theory which uses Becke's 3-parameter exchange and Lee, Yang and Parr's correlation function (Becke, 1992; Becke 1993; Lee *et al.,* 1998). All geometry optimization and frequency calculation used the conductor-like polarizable continuum model (CPCM) to simulate the water solvent (Barone and Cossi, 1998).

Resulting outputs were verified for imaginary frequencies to ensure the optimized structures were local minima for ground states (no imaginary frequency) or saddle points for transition states (one imaginary frequency). Reaction free energies (ΔG) were calculated using the zero-point energy corrected Gibbs free energy at 298.15 K (Sum of Thermal and Free Energies in Gaussian Output), and enthalpies (ΔH) were calculated using the zero-point energy corrected Enthalpy at 298.15K (Sum of electronic and thermal Enthalpies in Gaussian Output). Both geometry and frequency calculations were conducted at the B3LYP/6-311+G(2d,2p) level of theory in solvent, i.e., CPCM(water).

6.6   Results And Discussion

6.6.1   Cyclic Voltammetry and Excited State Redox Potentials

We experimentally validated just how strong of an oxidizing agent the excited state triple is by examining the single electron transfer (SET) step between ^{3}[RFT]* and phenol via cyclic voltammetry (Figure 6.7)
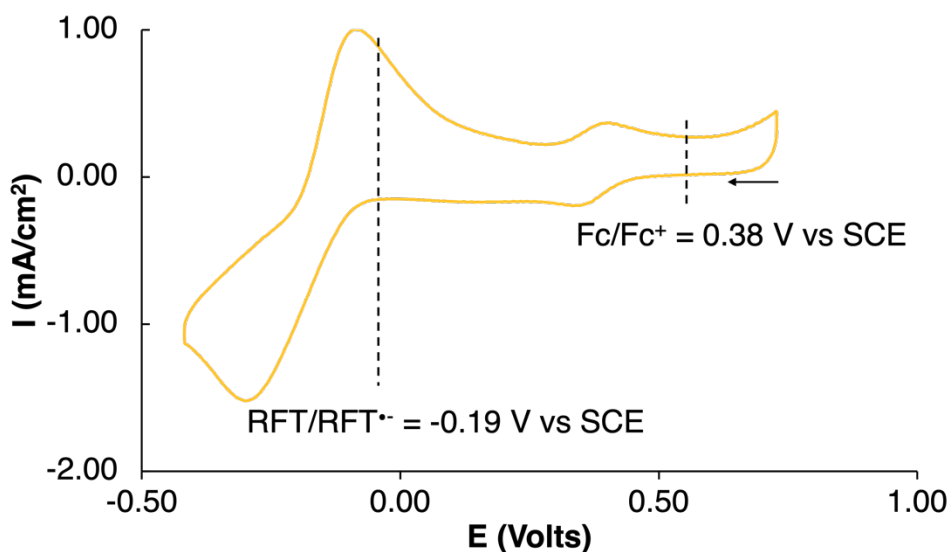
Figure 6.7. Cyclic voltammogram of **RFT**.

Although ^{1}[**RFT**]*, is higher in energy than ^{3}[**RFT**]*, and will produce a stronger oxidant, **RFT** is known to undergo ISC to the triplet. The triplet has a significantly longer lifetime than the singlet which results in the active oxidizing agent being ^{3}[**RFT**]*. In acetonitrile:water (1:1 v/v) ^{3}[**RFT**]*

has an oxidizing potential of 2.35 V *vs* SCE (Table 6.1). The oxidation of phenols by ^{3}[**RFT**]*, is generally thermodynamically favorable—for example, the tyrosine/tyrosyl radical redox potential is 1.08 V *vs* SCE (Close and Wardman, 2018; Lind *et al.,* 1990), which makes tyrosine oxidation by ^{3}[**RFT**]* favorable by 1.27 V.

Table 6.1. Summary of redox potentials and excited state redox potentials for ^{3}[**RFT**]*.

$E_{1/2}^{red}$ (RFT/RFT$^{\cdot-}$) *vs* SCE (V)	E_{00} (eV) 488 nm	$E^*_{1/2}^{red}$ (RFT+/RFT$^{\cdot-}$) *vs* SCE (V)
-0.19	2.54	2.35

6.6.2 Time Resolved Stern-Volmer Quenching Studies and Triplet Excited State Lifetime Measurements

The photocatalytic cycle begins with irradiation of **RFT** into the singlet excited state ^{1}[**RFT**]*, followed by rapid intersystem crossing (ISC) to the triplet excited state, ^{3}[**RFT**]*. After a 355 nm laser pulse, the transient absorption measurements of **RFT** in deoxygenated solution shows positive changes in absorbance at 400 nm, 520 nm, 700 nm and negative changes in absorbance at 460 nm (Figure 6.8). The negative absorption at 460 nm is attributed to ground state bleaching and coincides with the absorption profile of ground state **RFT** (Figure D.1).
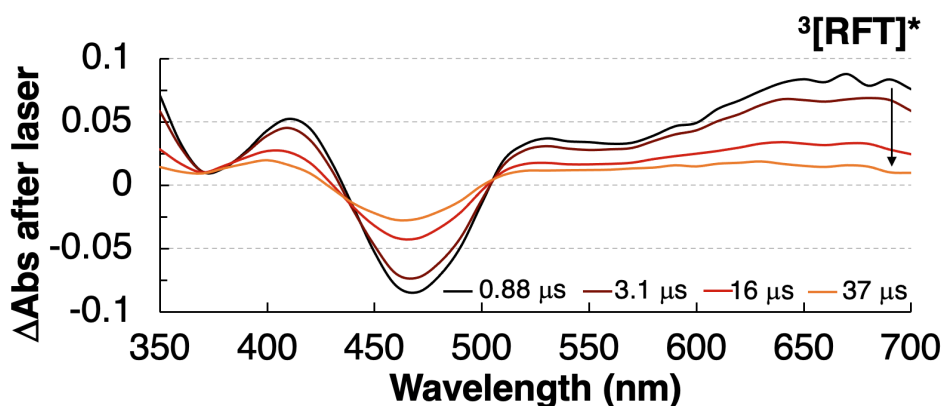
Figure 6.8. Transient absorption of **RFT** after laser excitation in deoxygenated solution.

We observed ^{3}[RFT]* to display a relatively long excited state lifetime of 12 µs in deoxygenated solution, as determined by following its characteristic absorption at 700 nm in laser-flash photolysis experiments (Figure 6.8). We also measured the lifetime of ^{3}[RFT]* in deoxygenated phosphate buffer saline (pH = 7.4) as 16 µs.

Due to its strongly oxidizing nature, ^{3}[RFT]* can initiate radical chemistry. In our system, phenol-containing tags or tyrosine groups on a protein will be rapidly oxidized by ^{3}[RFT]* to generate phenoxyl radicals. The rate constant (k_q) for this bimolecular process is determined by monitoring the rate constant of triplet decay for ^{3}[RFT]* as a function of increasing phenol concentration, known as a Stern-Volmer kinetic analysis (Figure 6.9). The oxidation of phenols with ^{3}[RFT]* is unsurprisingly fast in all cases (10^8 to 10^9 M^{-1}s^{-1}) as this electron transfer process is quite favorable.
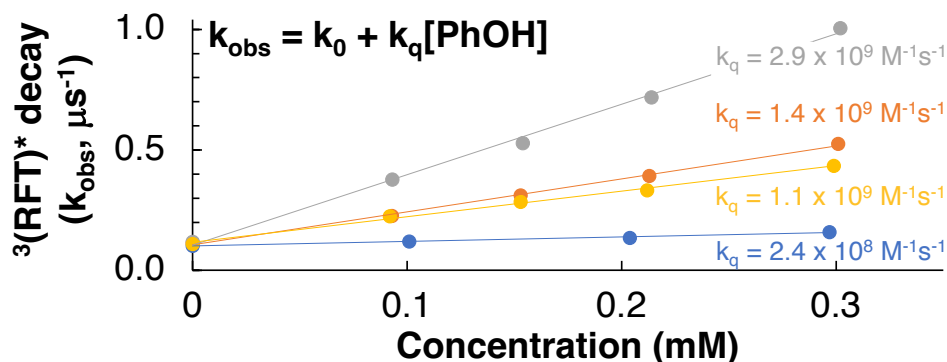
Figure 6.9. Stern-Volmer quenching of ^{3}[RFT]* with 2,6-dimethoxyphenol (grey), biotin tyramine (orange), Ac-Tyr-NHMe (yellow) and BSA (blue, measured in PBS).

When ^{3}[RFT]* is in a deoxygenated solution it will quickly be reduced by phenols, either from the tag or a tyrosine moiety. Laser-flash photolysis experiments of **RFT** and phenols shows a rapid disappearance of ^{3}[RFT]* at 700 nm and a relatively stable intermediate with an absorption centered at 600 nm (Figure 6.10A). We identify this peak as the semi reduced form, **H-RFT•**, with supporting evidence provided by TD-DFT predicted spectra (Figure 6.10C). Semi-reduced flavins with slightly different chemical structures were reported to have similar absorption peaks (Zhuang *et al.,* 2022, Grosheva *et al.,* 2021). Both transient absorption peaks associated of ^{3}[RFT]* and **H-RFT•** are strongly attenuated by the introduction of molecular oxygen from air (Figure 6.10B).

a) RFT and biotin tyramide (deoxygenated)
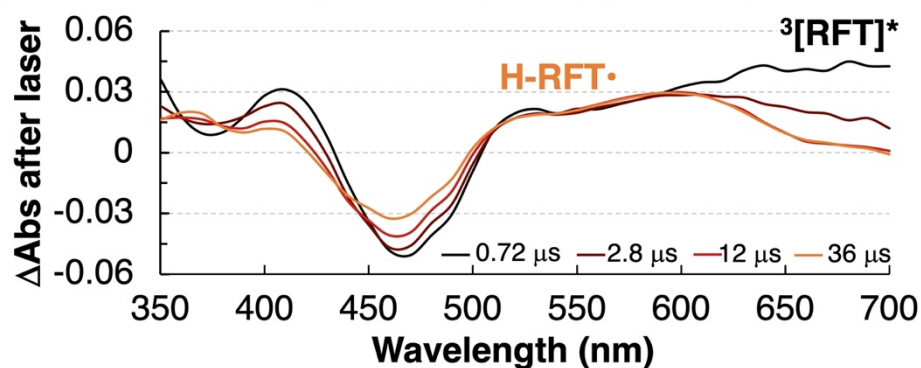
b) RFT and biotin tyramide (under air)
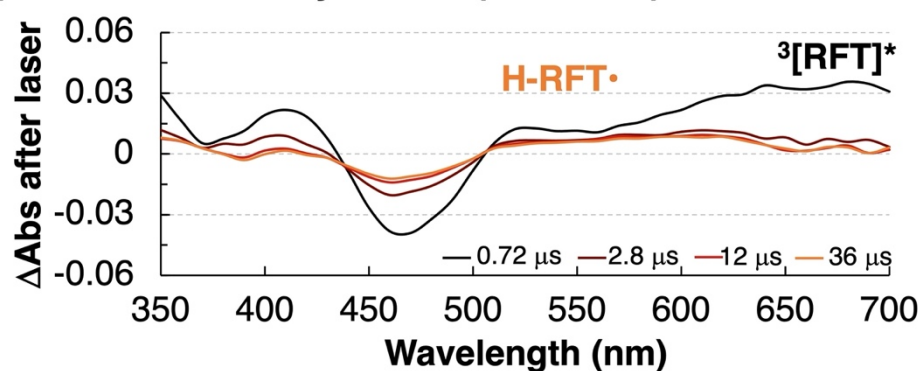
c) TD-DFT predictions
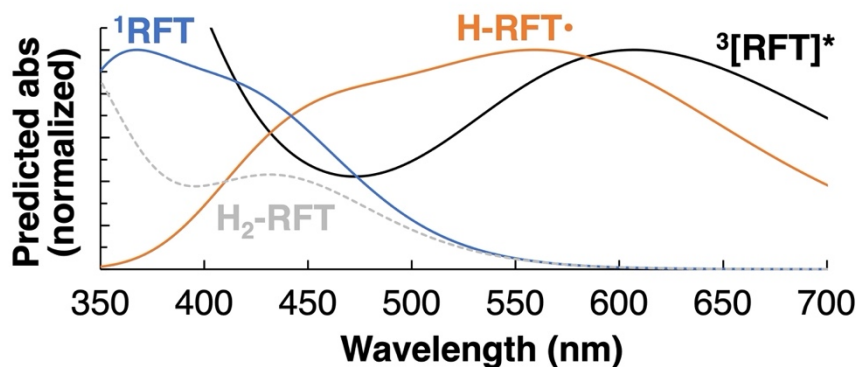
Figure 6.10. a) Transient absorption of **RFT** (0.06 mM) and biotin tyramide (biotin tyramide**,** 0.3 mM) in deoxygenated solution after a 355 nm laser pulse. b) Transient absorption of the same **RFT** (0.06 mM) and biotin tyramide (0.3 mM) solution open to air. c) TD-DFT predicted absorption spectra of ground state **RFT** (blue), **³[RFT]*** (black), **H-RFT·** (orange) and **H₂-RFT** (dashed grey), calculated using B3LYP/6-311+G(2d,2p) in CPCM(H₂O).

To directly observe the formation of phenoxyl radicals, biotin tyramide was pulsed with a 266 nm laser where the transient absorption measurements show a positive change at 430 nm (Figure 6.11A). The transient absorption decay monitored at 430 nm fits to a second order decays implying a phenoxyl radical-radical recombination mechanism (6.11B)

a) Biotin tyramide (deoxygenated)   **b) Second order decay of PhO·**
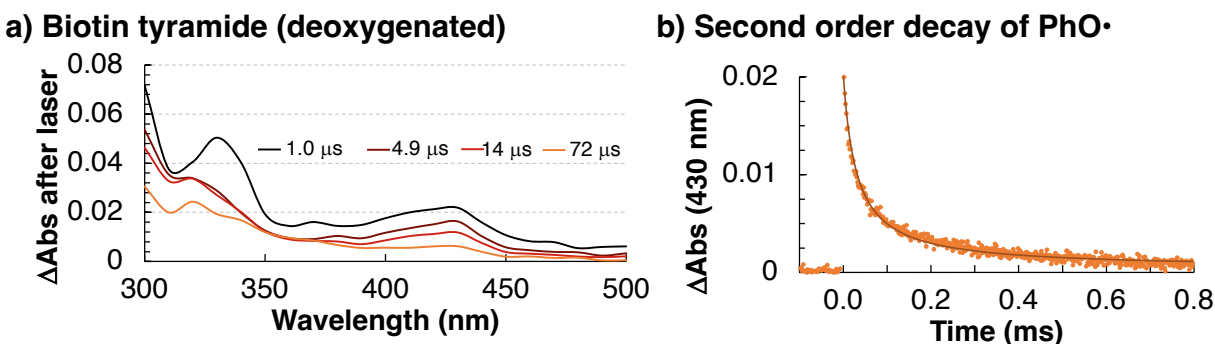
Figure 6.11. a) Transient absorption of biotin tyramide after laser excitation in deoxygenated PBS buffer saline (with 10% acetonitrile for solubility). b) Transient absorption of phenoxyl radicals and fit to second order decay kinetics.

6.6.3   Measuring The Rate of Reaction Between Phenol and Singlet Oxygen

During the optimization of our synthetic method, our collaborators found oxygen to be crucially important in maximizing the conversion efficiency. This observation led us to investigative the role oxygen plays in this reaction mechanism.

Flavins are well known $^1O_2$ sensitizers (Zhuang *et al.,* 2022, Grosheva *et al.,* 2021). We have previously shown that **^{3}[RFT]*** can generate phenoxyl radicals by direct reaction with phenols (*vide infra*), however, it is also known that $^1O_2$ can oxidize phenols to phenoxyl radicals (DeRosa *et al.,* 2002, Thomas and Foote, 1987; Scully and Hoigné, 1987; Al-Nu'airat *et al.,* 2019).

Pitre *et al*. (2015) showed that DPA will selectively react with $^1O_2$ via a [4+2] cycloaddition and cause a quantifiable decrease in its characteristic absorption at 372 nm (Figure 6.12). Since the rate constants for the reaction between $^1O_2$ and DPA is known (k_{DPA}, eq 6.4) and the rate of decay (k_d) from singlet oxygen to triplet oxygen is also reported (k_d, eq 6.3, Wilkinson *et al.,* 1995), we can use competitive kinetics to estimate the rate constant for the reaction of $^1O_2$ with phenols in our system (eq 6.5).

$$^1O_2 \xrightarrow{k_d} {}^3O_2 \qquad\qquad (k_d = 4.5 \times 10^4 \text{ s}^{-1}) \text{ eq } 6.3$$

$$^1O_2 + DPA \xrightarrow{k_q} DPA\text{-}O_2. \qquad\qquad (k_{DPA} = 2.0 \times 10^6 \text{ M}^{-1} \text{ s}^{-1}) \text{ eq } 6.4$$

$$^1O_2 + PhOH \xrightarrow{k_r} PhO^\bullet + HOO^\bullet \qquad\qquad (k_r = ?) \text{ eq } 6.5$$
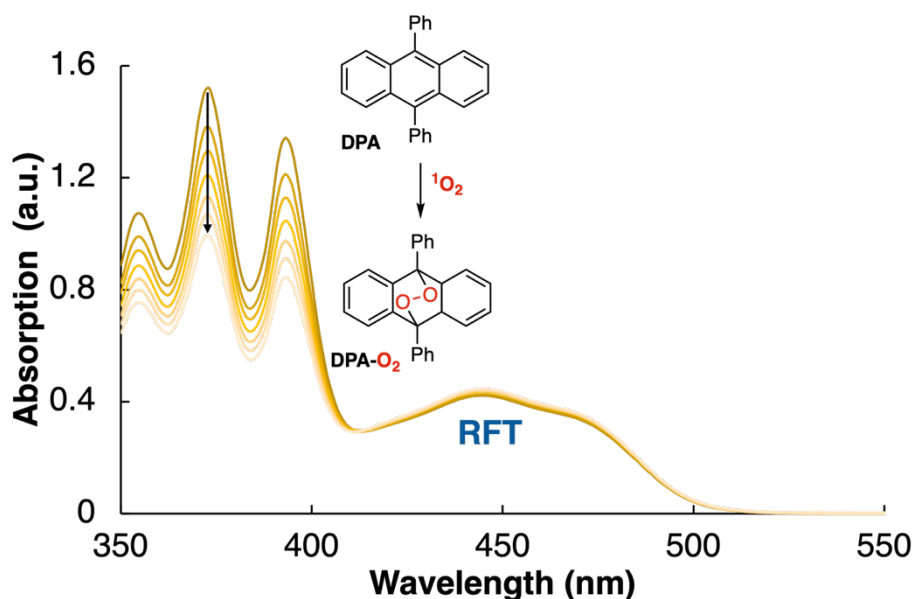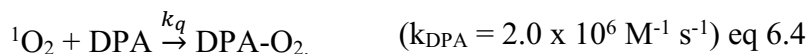
Figure 6.12. Absorption spectra of **DPA** (initial concentration = 0.1 mM) and **RFT** (initial concentration = 42 µM) during 85 seconds of blue-light irradiation.

The absorption decrease seen at 372 nm is caused by the loss of DPA's π conjugation as it reacts with $^1O_2$. When phenol is added to the cuvette a new reaction pathway for $^1O_2$ is introduced to form phenoxyl radicals (Burton, G.W. and Ingold, 1986) and the change in absorption of DPA at 372 nm as a function of irritation time decreases (Figure 6.13). The rate of reaction between $^1O_2$ and phenols is estimated to be (eq 6.6 and Figure 6.14):

$$\frac{Slope_{DPA}}{Slope_{DPA+PhOH}} = \frac{\Phi_0}{\Phi} = 1 + \frac{k_r[PhOH]}{k_d + k_q[DPA]} \qquad\qquad \text{eq } 6.6$$

96
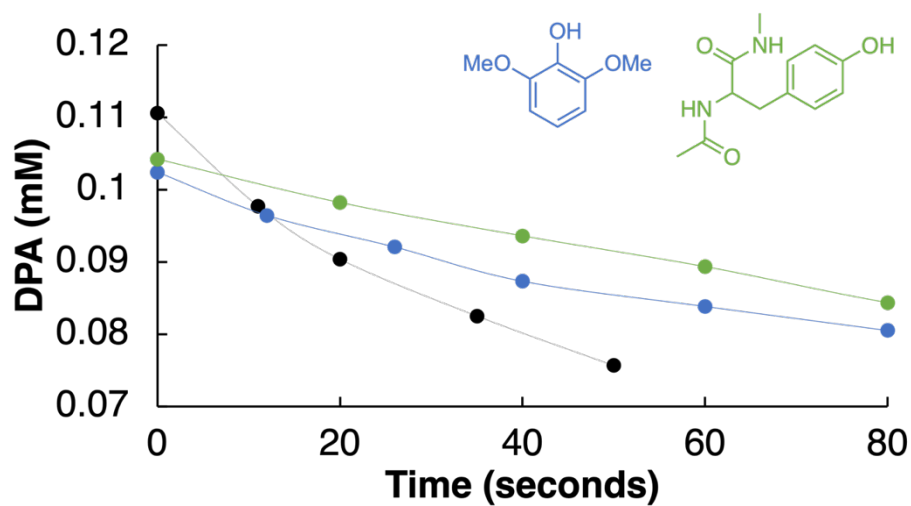
Figure 6.13. Concentration of **DPA** during irradiation of **RFT** (42 µM) and **DPA** (~ 0.1 mM) in 1:1 water:acetonitrile. Conditions: Gray trace, no phenol added; blue trace, addition of 1.31 mM 2,6-dimethoxylphenol; green trace, addition of 1.3 mM Ac-Tyr-NHMe.
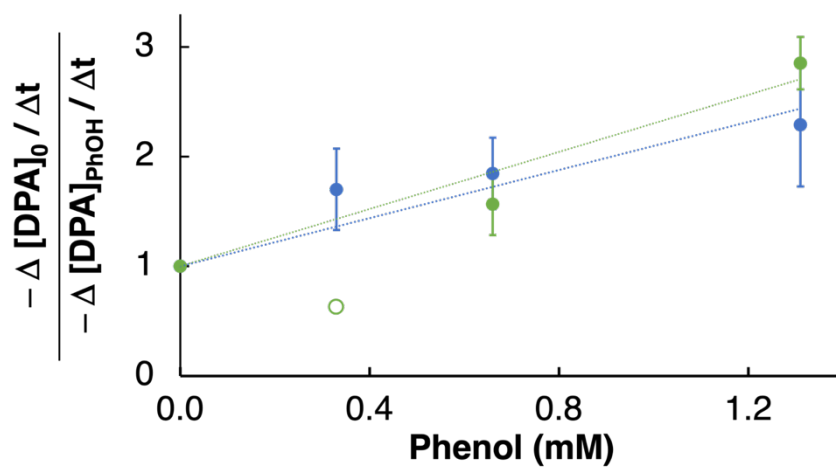
Figure 6.14. Graph showing ratio of consumption of **DPA** vs PhOH form Figure 6.13.

Using equation 6.6, the rate constant for the reaction between $^1O_2$ and phenols (k_r) can be estimated as shown in Table 6.2.

Table 6.2. Rate constant (k_r) between $^1O_2$ and phenols.

Phenol	k_r (M^{-1} s^{-1})
2,6-dimethoxyphenol	$(5.0 \pm 0.7) \times 10^7$
Ac-Tyr-NHMe	$(5.9 \pm 0.7) \times 10^7$

6.6.4 Computational Methods

The mechanism was calculated using riboflavin with a tetraacetate side chain. The experimental aspect of the study was done with biotin tyramide, 2,6-dimethoxyphenol, or Ac-Tyr-NHMe. To match theoretical values with experimental work, biotin tyramide and 2,6-dimethoxyphenol were used to represent the phenol tags and Ac-Tyr-NHMe represented a simplified version of a tyrosine containing protein for the formation of phenoxyl radicals. Additional phenols were calculated for the radical-radical recombination step to match the substrate scope and the radical-radical recombination step is summarized in Table D.4 whereas the radical additional onto neutral tyrosine is summarized in Table D.5.

The RFT mediated mechanism for phenoxyl radical generation is shown in Figure 6.6A. DFT calculations support that ^{3}[RFT]* can directly oxidize tyrosine in proteins and the phenol-containing tags to generate phenoxyl radicals and the semi-reduced **H-RFT$^\bullet$**. The exergonic nature of this reaction has a DFT-calculated ΔG ranging from -18.9 to -25.8 kcal/mol for various phenols (For more information see Annexe D, Table D.1). The H-abstraction by singlet oxygen is favorable with a ΔG_{DFT} ranging from -12.2 to -18.6 kcal/mol for various phenols and a and tyrosine analogues (For more information see Annexe D, Table D.3.). Two pathways to regenerate **RFT** from **H-RFT$^\bullet$** are considered. A second reduction from **H-RFT$^\bullet$** to **H$_2$-RFT** is proposed, however we calculate this reduction to be significantly unfavorable in our system. Phenoxyl radical generation from the reaction between various phenols and **H-RFT$^\bullet$** gave ΔG_{DFT} values in the range of +17.7 to +24.1 kcal/mol (For more information see Annexe D, Table D.2). To close the catalytic cycle **H$_2$-RFT**, could favorably generate H$_2$O$_2$ in the presence of oxygen (ΔG_{DFT} = -23.4 kcal/mol).

The proposed addition of a phenoxyl radical onto a neutral tyrosine is unfavourable in the range of +44 to + 49 (For more information see Annexe D, Table D.5). Whereas, if phenoxyl radicals recombine to form a diketone, it is slightly endergonic in the range of +7 to +12 kcal/mol. Then followed by tautomerize in the range of -36 to -39 kcal/mol (For more information see Annexe D, Table D.4) to form the desired phenol-phenol coupled product (Figure 6.6B).

6.7   Conclusion

Traditionally, the need for two radicals to recombine in a synthetically useful transformation is rare—the concentration of transient radicals is often too low to explain high yielding reactions. In this case, however, the persistence of phenoxyl radicals is well-documented—several antioxidants are based on phenoxyl radical persistence (Burton and Ingold, 1986). In biological systems, phenoxyl radicals are relatively persistent due to their low reactivity with oxygen and their inability to perform H-abstraction with most biomolecules—their estimated lifetime is ~0.1 ms in cell media (Geri *et al.,* 2020).

The proposed mechanism described herein helps explain the success of phenoxyl radical labelling methods. Radical-radical recombination follows bimolecular kinetics, and the efficiency of this process will dramatically decrease as the distance increases away from the photochemical source of phenoxyl radicals. Another important factor in the success of this protein tagging method is the strength of the bonds formed. Radical-radical recombination becomes more predominant with increasing radical persistence; however, the recombination of persistent radicals can lead to weak and reversible bonds. The recombination of phenoxyl radical is followed by tautomeric aromatization leading to bond strengthening. Altogether, these mechanistic insights will be an important consideration as different tag motifs are considered in photochemical protein tagging. Furthermore, the radical-radical recombination mechanism described here might be a potential pathway that occurs in the case of peroxidase-based labeling systems where peroxide radicals and other reactive species are likely involved in the generation of tyrosyl radicals that could potentially explain the increased labeling radius (Michon *et al.,* 1997; Oakley *et al.,* 2022).

We envision that the insights gained from our mechanistic analysis will lead to improved catalytic performance of these flavin-based systems and further encourage the development of new and effective light-mediated labeling strategies in the field of chemical biology.

CHAPITRE 7
CONCLUSION

The goal of my research was to elucidate (photo)catalytic reaction mechanisms in tandem with their development. By understanding the mechanism behind exactly how starting material becomes the desired product, the reaction can be intentionally optimized in real time with its development. We use a combination of spectroscopic techniques such as absorption, emission, and laser flash photolysis along with electrochemistry and computational chemistry to inform our decisions. We have studied interestingly difficult chemical reactions step-by-step and demonstrated how our "mechanistic insight and innovative solutions" approach has helped several synthetic and biological chemists explain reactions.

Photoredox catalysis typically favours metal-based complexes, due to their long-lived excited state lifetimes and large redox windows. Alternatively metal-free photocatalysts eliminates the potential for metal toxicity, while also having excitation wavelengths in the visible region. Prior to our publication in collaboration with Pfizer (Chapter 3) many photoredox catalysed Minisci reactions assumed an incorrect intermediate in the proposed mechanisms. Guided by electrochemistry, DFT and time-resolved photochemical results, we proposed the formation of a highly reducing species (α-amino radical) that can turn-over a catalytic chain reaction with various oxidants. We showed that the low quantum yield is most likely a result of an inefficient initiation step or inefficient chain propagation resulting from imperfect oxidation of carboxylates.

In the presence of molecular oxygen, thione to ketone photoconversions are well understood. For the dithioimide synthesized by our collaborators at Wilfred Laurier University, however, the photoconversion still proceeds in the absence of oxygen and other common oxygen sources (Chapter 4). This suggests that the solvent is the source of oxygen, which is unprecedented for this type of reaction. Spectroscopic and kinetic studies have thus far not been successful is elucidating this the reaction mechanism but have rather provided more questions than answers.

A mechanistic investigation into the transformation of alkyl amines to amides catalyzed by an iron complex is a biologically relevant reaction, similar to that of cytochrome P450 in the liver. This

simplified reaction aims to help understand how active pharmaceutical agents make drug metabolites of unknown toxicity. Our work will therefore explain with great precision how to produce certain metabolites of pharmaceutical products. The reaction mechanism under investigation was an α-C-H oxidation in collaboration with Merck (Chapter 5). The structure of the iron centred catalyst was guided by experimental mechanistic studies and determined with high level DFT calculations. An in-depth computational look at the mechanism was performed where we examined several potential mechanisms, along with numerous spin states. Finally, the Fe(IV)-oxo as a quintet showed the best agreement between experimental and computational results.

A growing interest in photochemical methods to tag proteins has exploited tyrosine's unique phenol group to develop interesting phenol-phenol coupling reactions. However, there is an important need to understand the processes at play before accepting this tool as a simple "click process". We undertook a systemic study of a phenol-phenol coupling reaction photocatalyzed by an organic molecule: riboflavin (Chapter 6). While investigating the simplified mechanism of this biophotocatalytic reaction computationally, we noted that the mechanism usually proposed in the literature, a radical addition onto a phenol, is very thermodynamically demanding. Riboflavin can oxidize phenols via several different pathways leading to persistent phenoxyl radicals, that can favourably recombine via radical recombination. The enhanced understanding gained from our mechanistic studies can lead to more efficient photochemical protein labeling reactions.

Mechanistic studies have shed new light on the inner workings of the reactions explore in this thesis, even if the final mechanism remains undetermined. The proposed mechanisms were significantly altered, and our hope is that by investigating reaction mechanism, informed changes can be made resulting in intelligent development in future reactions. Traditionally, these mechanistic studies are left to the final stages of the project, much to the detriment of reaction optimization. The characterization of excited and ground state intermediates as well as the identification of transient species provides fundamental information for fully exploiting newly identified reactivity concepts. In addition, there is an educationally satisfying component that a refined and supported mechanistic proposal adds to a synthetic study. To sustain additional innovation, we anticipate that the combination of experimental and mechanistic studies will

become increasingly important. By thoroughly understanding a reaction mechanism, more efficient and intelligent reaction design will follow.

The overall increase in interest in photochemical methods to explore synthetic reaction is both exciting and promising. Using photochemistry to explore previously synthetically difficult reactions showcases its utility. My hope is that by demonstrating how mechanistic studies complement our understanding of reaction mechanisms, a more conscious effort will be put forward into its elucidation in the future.

CHAPITRE 8
CONTRIBUTIONS

Throughout my time at UQAM as a graduate student, I have had the opportunity to collaborate on work outside of my thesis projects. The first contribution is a photocatalyzed hydroboration of alkynes and alkenes using a Cu-photocatalyst and B_2Pin_2. This project was in collaboration with researchers at the Institut National des Sciences Appliquées de Rouen Normandie in Saint-Étienne-du-Rouvray, France. The original concept, the optimization of the reaction and its conditions, and in general the organic chemistry aspect was completed by our collaborators Mingbing Zhong, Xavier Pannecoucke, Philippe Jubault, and Thomas Poisson.

Cyclic voltammetry, absorption and emission spectra of Cu-PC-1 experiments were performed by me.

Using B_2Pin_2 and a unique copper photocatalyst, this experiment generated an unprecedented photocatalytic hydroboration process. With excellent functional group tolerance, the reaction was used with a variety of alkynes and alkenes. To allow an easy scale up of the reaction, the methodology was extended to continuous flow conditions. The mechanism of the transformation was investigated, and the oxidation of a transient borate species to form a boryl radical is suggested as a crucial step in the hydroboration of the unsaturated C-C bond.

Zhong, M., Gagné, Y., **Hope, T. O.,** Pannecoucke, X., Frenette, M., Jubault, P., & Poisson, T. (2021). Copper-Photocatalyzed Hydroboration of Alkynes and Alkenes. *Angewandte Chemie International Edition*, *60*(26), 14498-14503.

The next collaboration came within the Frenette group, where we developed a tool based on ionization energies to predict reagents for an electron transfer with an iridium-based photocatalyst.

The project focused on the development of a DFT-based tool to estimate the quenching rate constant of the excited state of the photocatalyst $Ir[dF(CF_3)ppy]_2(dtbpy)^+$ by various organic molecules in acetonitrile. By interpolation, potential quenchers with particular a DFT-calculated ionization energy should feature high quenching rate constants with this iridium photocatalyst.

These compounds are predicted to be a viable source of radical cations in photoredox reactions. Our method is compatible with the rapid screening of potential reagents *in silico*. Simple C–C bond formation photoredox mechanisms utilizing 2,4-pentanedione and malononitrile anions were developed as a proof of concept to demonstrate the utility of fast screening for predicting reagents in photoredox catalysis.

Juneau, A., **Hope, T. O**., Malenfant, J., Mesko, M., McNeill, J., & Frenette, M. (2022). Methods to Predict Potential Reagents in Iridium-Based Photoredox Catalysis Calibrated with Stern–Volmer Quenching Rate Constants. *ACS Catalysis*, *12*(4), 2348-2356.

My research studies have been complimented with the opportunity to participate in and co-organize several chemistry conferences, Chemistry Olympics, and become an executive committee member of the Electrochemistry Society (ECS) Montreal Student Chapter. My research experience has been enhanced with a wide range of both local and national conference presentations :

(*Oral*) **Mechanistic Insight into Flavin Biophotocatalysis for Protein Tagging and Phenol-Phenol Coupling (graduate student oral presentation prize)**
105th Canadian Chemistry Conference and Exhibition; Calgary, AB
T.O. Hope, N. Removski, J. Maisonneuve, R. Oslund, O. Fadeyi, M. Frenette. June 2022

(*Oral*) **Mechanistic Insight into Flavin Biophotocatalysis for Protein Tagging and Phenol-Phenol Coupling**
6th Annual Meeting on for the Centre for Advanced Materials (CQMF), Virtual Conference
T.O. Hope, N. Removski, J. Maisonneuve, R. Oslund, O. Fadeyi, M. Frenette. March 2022

(*Oral*) **Mechanistic Insights into Metal-Free Visible Light C-H Functionalization**
104th Canadian Chemistry Conference and Exhibition; Virtual Conference
T.O. Hope, A. Juneau, Y. Gagne, N. Removski, J. Maisonneuve, J. Genovino, Y. Lian, Y. Zhang, G. Ingle, R. Oslund, O. Fadeyi, M. Frenette, August 2021

(*Poster*) **Mechanistic Insights into Fe Catalyzed α-C-H Oxidations of Tertiary Amines: Non-Radical Pathways for Base-Metal Catalyst**
47th Physical Organic Mini-Symposium, Toronto, ON
T.O. Hope, C.T. Legacy, Y. Gagne, F.T. Greenaway, M.H. Emmert, M. Frenette, November 2019

(Oral) **Mechanistic Insights into Fe Catalyzed α-C-H Oxidations of Tertiary Amines: Non-Radical Pathways for Base-Metal Catalyst**
102nd Canadian Chemistry Conference and Exhibition; Quebec City, QC
T.O. Hope, *C.T. Legacy, Y. Gagne, F.T. Greenaway, M.H. Emmert, M. Frenette,* June 2019

(Oral) **Mechanistic Insights into Fe Catalyzed α-C-H Oxidations of Tertiary Amines: Non-Radical Pathways for Base-Metal Catalyst (conference co-organizer)**
46th Physical Organic Mini-Symposium, Montreal, QC
T.O. Hope, *C.T. Legacy, Y. Gagne, F.T. Greenaway, M.H. Emmert, M. Frenette*, November 2018

(Oral) **Metal-Free Visible Light C−H Alkylation of Heteroaromatics via Hypervalent Iodine-Promoted Decarboxylation (1st place prize oral presentation)**
8th Annual ECS Montreal Student Symposium; Montreal, QC
T.O. Hope, *A. Juneau, Y. Gagne, J. Genovino, Y. Lian, Y. Zhang, G. Ingle, M. Frenette*, June 2018

(Oral) **Manganese-Based and Metal-Free Visible Light C−H Alkylation of Heteroaromatics via Hypervalent Iodine-Promoted Decarboxylation**
101st Canadian Chemistry Conference and Exhibition; Edmonton, AB
T.O. Hope, *A. Juneau, Y. Gagne, J. Genovino, Y. Lian, Y. Zhang, G. Ingle, M. Frenette,* May 2018

(Poster) **Manganese-Based and Metal-Free Visible Light C−H Alkylation of Heteroaromatics via Hypervalent Iodine-Promoted Decarboxylation**
Symposium du réseau de l'Université du Québec sur la Recherche Biomédicale et Biopharmaceutique; Sainte-Adele, QC
T.O. Hope, *A. Juneau, Y. Gagne, J. Genovino, Y. Lian, Y. Zhang, G. Ingle, M. Frenette*, May 2018

SUPPORTING INFORMATION: METAL FREE VISIBLE LIGHT C-H ALKYLATION OF HETEROAROMATICS VIA HYPERVALENT IODINE PROMOTED DECARBOXYLATION

Quantum Yield
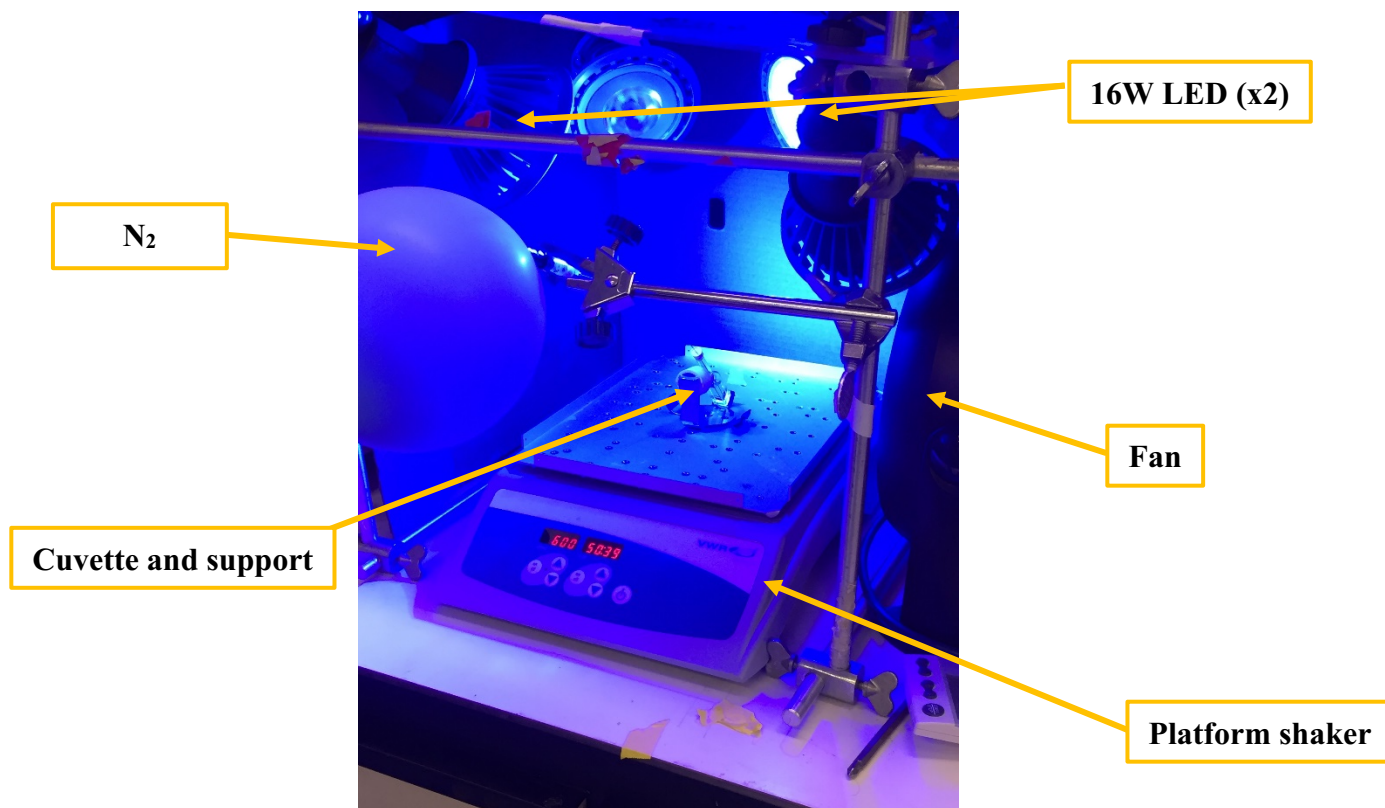
Figure A.1 – Chemical Actinometer Setup.
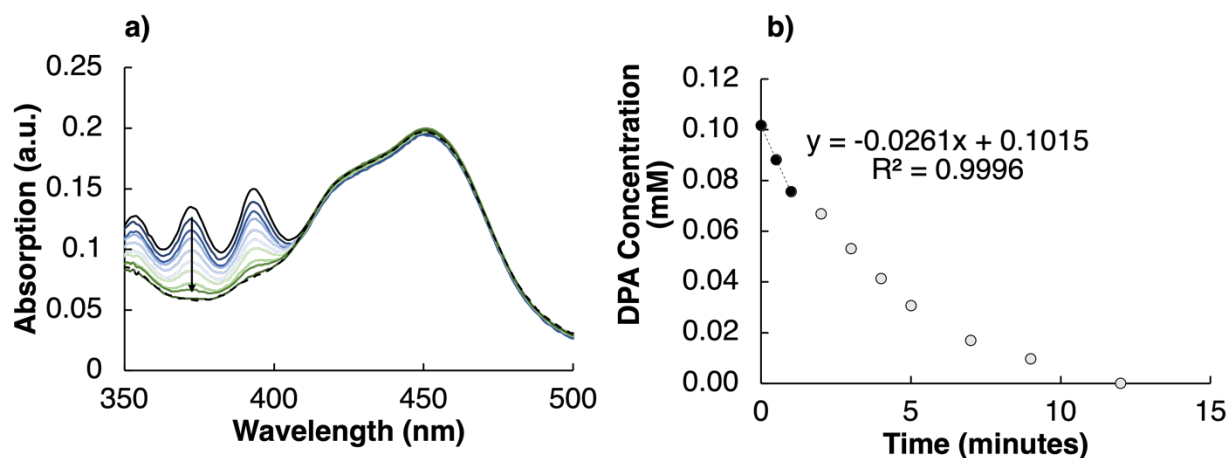
Figure A.2 – a) UV-Visible spectra at different irradiation times showing the decay of DPA over 12 minutes. b) Kinetics of the reaction at 372 nm with the first two minutes used in the actinometry measurements.
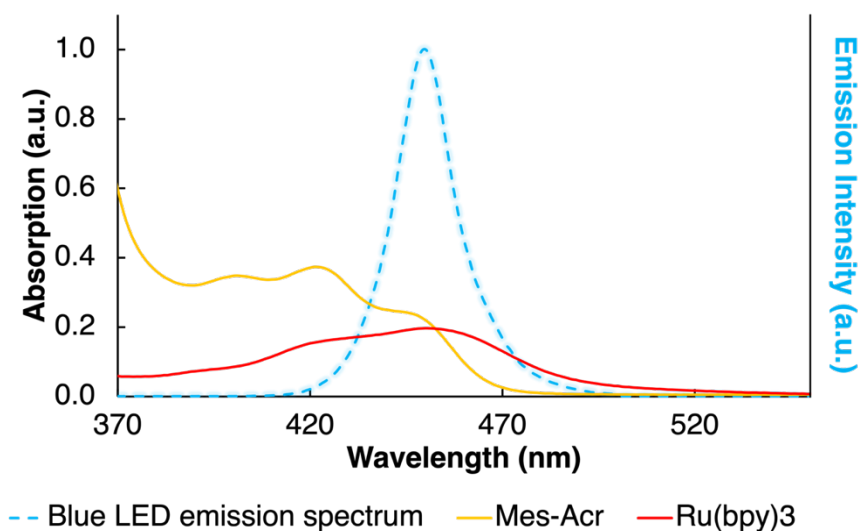
Figure A.3 – UV-Vis of the chemical actinometry samples (from dilutions, not actual absorbance of the irradiated sample) and emission spectrum of the blue LED.
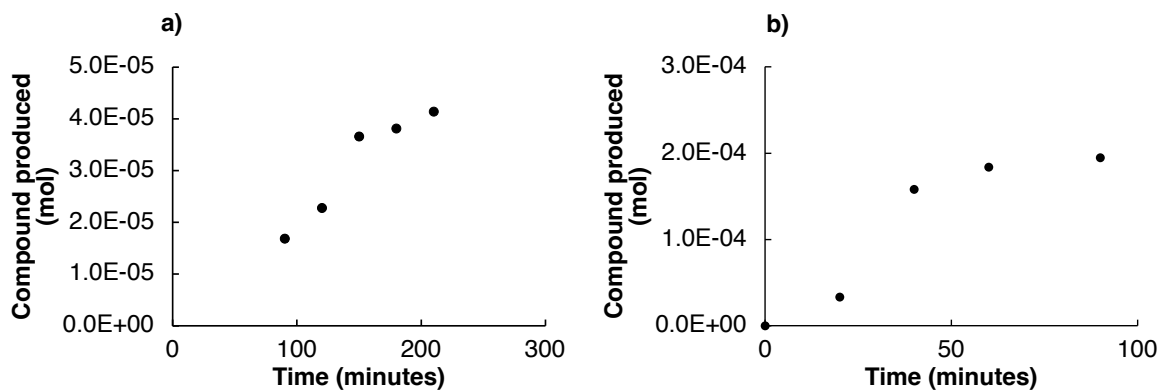
Figure A.4 – Kinetics for the formation of 2-cyclohexyl-4-methylquinoline at a) low and b) high light intensity.

Cyclic Voltammetry
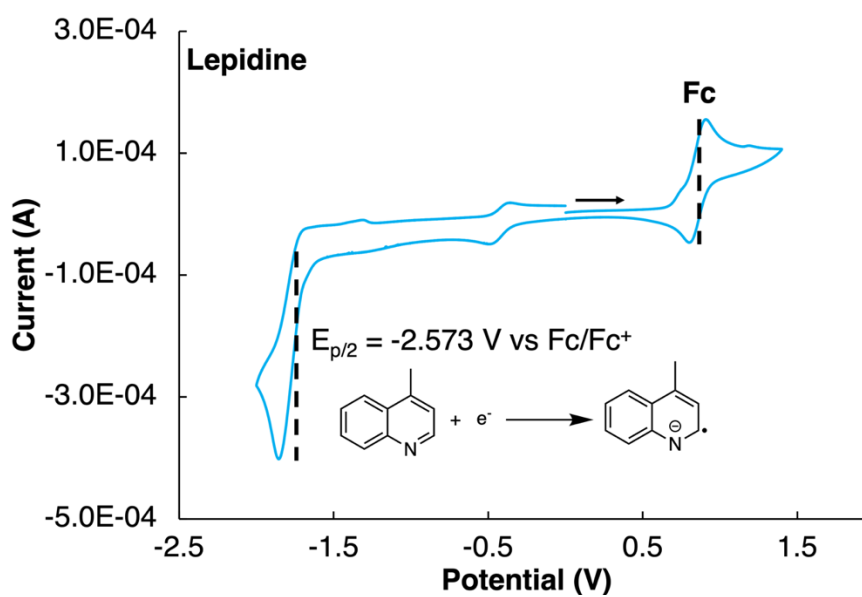
Figure A.5. Cyclic voltammetry of neutral lepidine.

Theoretical potentials and computational methods
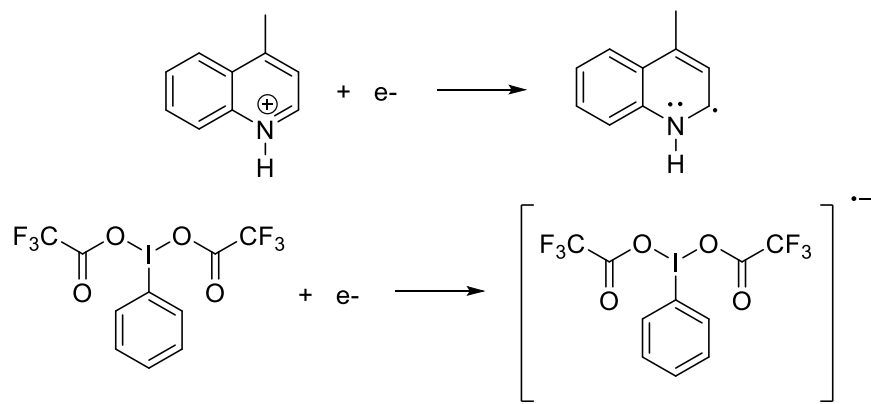
	Experimental $E_{p/2}$ (V) vs Fc/Fc⁺	Theoretical $E_{p/2}$ (V) vs Fc/Fc⁺
	-1.340	-1.297
	-0.527	
+ 0.813 V		
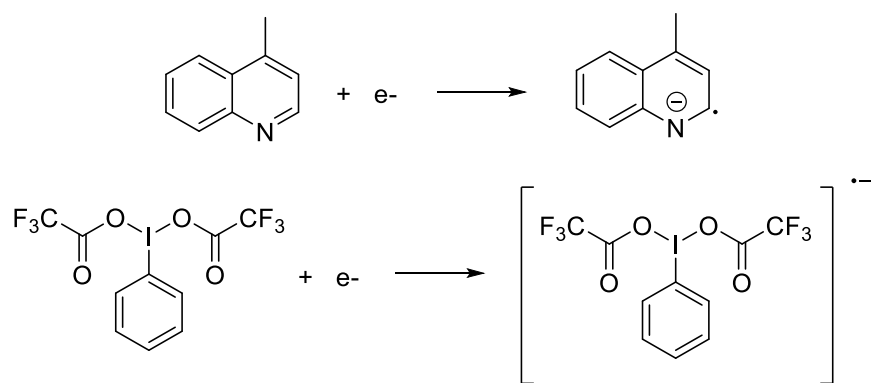
	Experimental $E_{p/2}$ (V) vs Fc/Fc⁺	Theoretical $E_{p/2}$ (V) vs Fc/Fc⁺
	-2.573	-2.574
	-0.527	
+ 2.056 V		

Initiation step
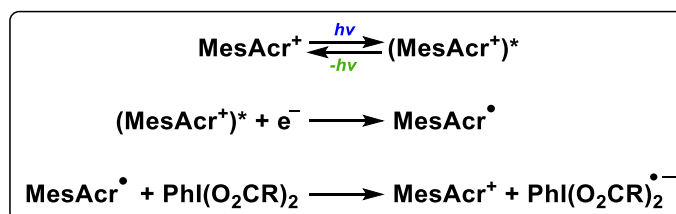
Chain reaction
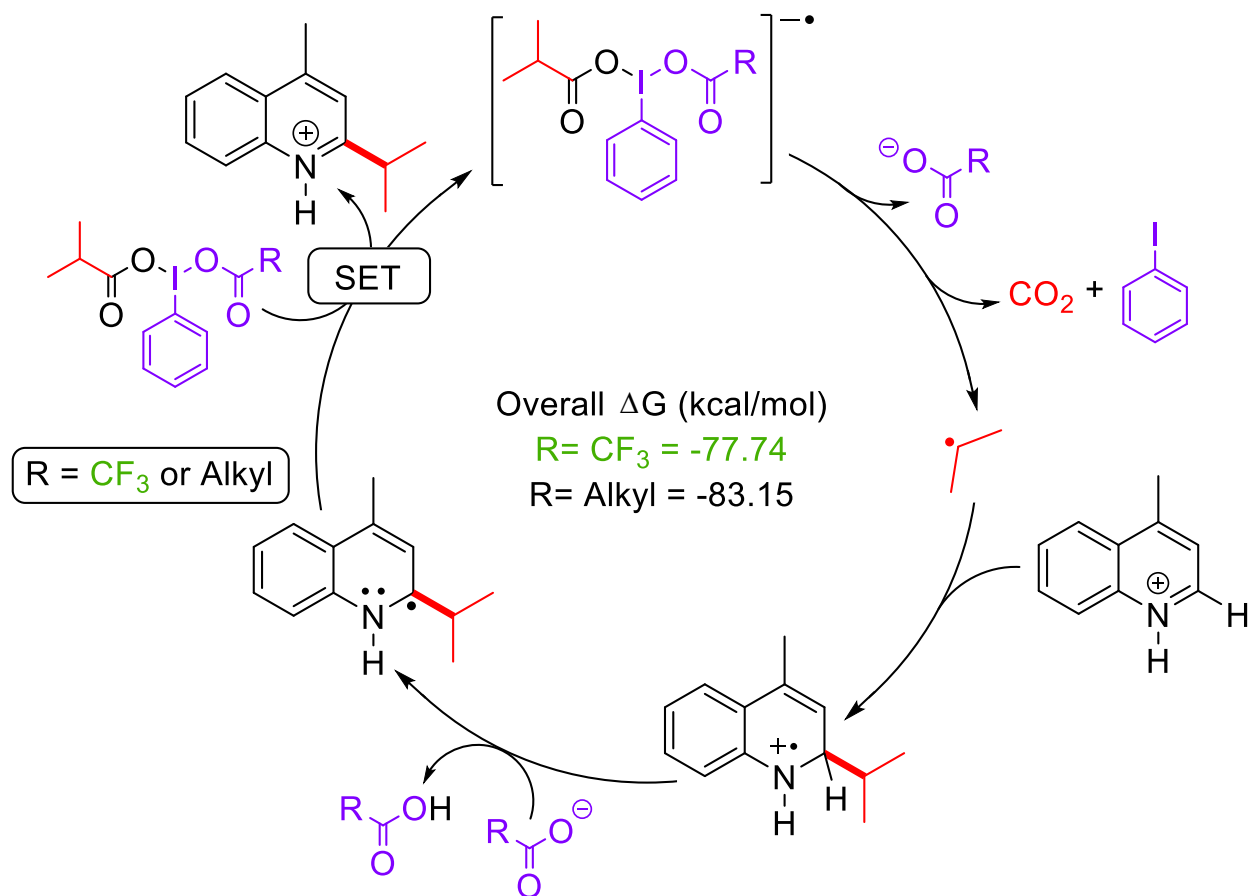
Figure A.6. Proposed mechanism ΔG^o for the overall catalytic cycle.

Energies obtained from DFT calculations and basis set used for each atom for step A + B → [TS1] → C
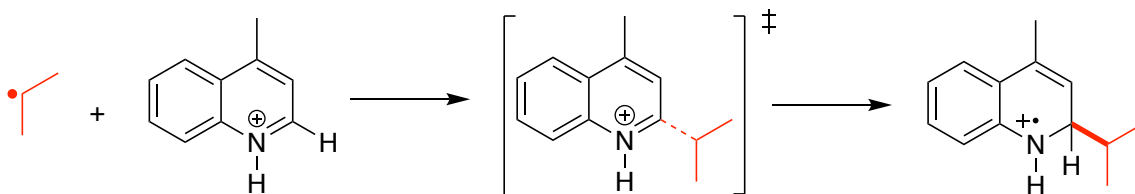
C, H, N	$\Delta G^{\ddagger}$ (kcal/mol)	ΔG°_{RX} (kcal/mol)
6-311++G(2d,2p)	18.08	7.73

C, H, N	$\Delta H^{\ddagger}$ (kcal/mol)	ΔH°_{RX} (kcal/mol)
6-311++G(2d,2p)	4.91	-5.81

Energies obtained from DFT calculations and basis set used for each atom for step C + D → [TS2] → E + F
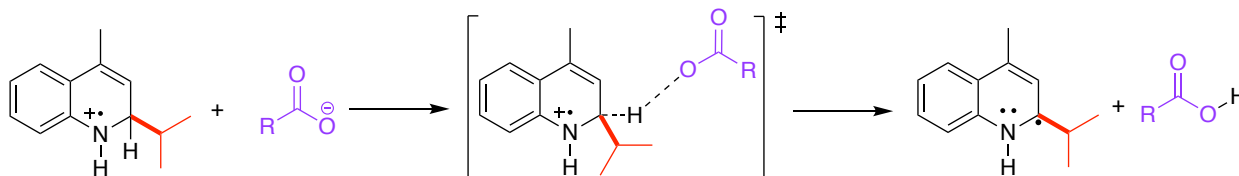
C, H, N, O, F	$\Delta G^{\ddagger}$ (kcal/mol)	ΔG°_{RX} (kcal/mol)
6-311++G(2d,2p) R= CF₃	10.73	-7.74
6-311++G(2d,2p) R= Alkyl	4.19	-24.51

C, H, N, O, F	$\Delta H^{\ddagger}$ (kcal/mol)	ΔH°_{RX} (kcal/mol)
6-311++G(2d,2p) R= CF₃	-0.63	-8.19
6-311++G(2d,2p) R= Alkyl	-8.20	-24.79

Energies obtained from DFT calculations and basis set used for each atom for step E + G → H + I
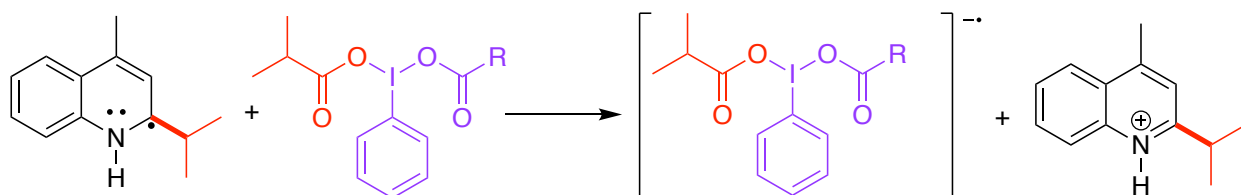
C, H, N, O, F	I	ΔG‡(kcal/mol)	ΔG°$_{RX}$ (kcal/mol)
6-311++G(2d,2p) **R= CF$_3$**	LanL2DZ+ p-diff. + d-pol.	N/A	-37.60
6-311++G(2d,2p) **R= Alkyl**	LanL2DZ+ p-diff. + d-pol.	N/A	-24.25

C, H, N, O, F	I	ΔH‡(kcal/mol)	ΔH°$_{RX}$ (kcal/mol)
6-311++G(2d,2p) **R= CF$_3$**	LanL2DZ+ p-diff. + d-pol.	N/A	-30.15
6-311++G(2d,2p) **R= Alkyl**	LanL2DZ+ p-diff. + d-pol.	N/A	-18.60

Energies obtained from DFT calculations and basis set used for each atom for step H → A + D + J + K
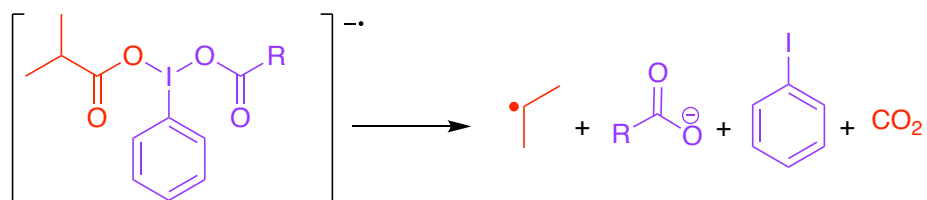
C, H, N, O, F	I	ΔG‡(kcal/mol)	ΔG°$_{RX}$ (kcal/mol)
6-311++G(2d,2p) **R= CF$_3$**	LanL2DZ+ p-diff. + d-pol.	N/A	-40.13
6-311++G(2d,2p) **R = Alkyl**	LanL2DZ+ p-diff. + d-pol.	N/A	-42.12

C, H, N, O, F	I	ΔH‡(kcal/mol)	ΔH°$_{RX}$ (kcal/mol)
6-311++G(2d,2p) **R= CF$_3$**	LanL2DZ+ p-diff. + d-pol.	N/A	-14.34
6-311++G(2d,2p) **R= Alkyl**	LanL2DZ+ p-diff. + d-pol.	N/A	-12.58

DFT energies and coordinates as obtained from 6-311++G(2d,2p) for C, H, N, O, F and LanL2DZ+ p-diff + d.pol. for iodine
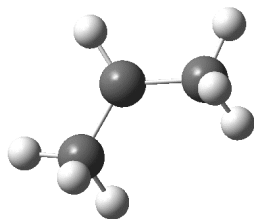
Isopropyl (Radical)
(A)
Zero-point correction=   0.087494 (Hartree/Particle)
Thermal correction to Energy=   0.092685
Thermal correction to Enthalpy=   0.093629
Thermal correction to Gibbs Free Energy=   0.060282
Sum of electronic and zero-point Energies=   -118.434316
Sum of electronic and thermal Energies=   -118.429125
Sum of electronic and thermal Enthalpies=   -118.428181
Sum of electronic and thermal Free Energies= -118.461528

C	0.00000000	0.53442200	-0.04546000
H	0.00000000	1.60642400	0.10196600
C	1.29508400	-0.19771000	0.00255900
H	2.14198900	0.45332100	-0.21381700
H	1.47605300	-0.64364300	0.99233200
H	1.31278700	-1.02989800	-0.70847400
C	-1.29508400	-0.19771000	0.00255900
H	-1.47605400	-0.64364300	0.99233200
H	-2.14198900	0.45332100	-0.21381700
H	-1.31278700	-1.02989800	-0.70847300

H⁺-4-methylquinoline
(B)

Zero-point correction=   0.177161 (Hartree/Particle)
Thermal correction to Energy=   0.185624
Thermal correction to Enthalpy=   0.186568
Thermal correction to Gibbs Free Energy=   0.143944
Sum of electronic and zero-point Energies=   -441.655129
Sum of electronic and thermal Energies=   -441.646667
Sum of electronic and thermal Enthalpies=   -441.645723
Sum of electronic and thermal Free Energies= -441.688346

```
C      -2.74710300 -0.14791700  0.00000100
C      -1.84315400 -1.18100100  0.00000000
C      -0.47008000 -0.88540000 -0.00000100
C       0.00107300  0.45438400 -0.00000100
C      -0.96732000  1.48804200  0.00000000
C      -2.30726500  1.19203000  0.00000200
H      -3.80559100 -0.36375100  0.00000200
H      -2.16965100 -2.21129500  0.00000000
C       1.40838000  0.69386700 -0.00000100
H      -0.64485800  2.51750800  0.00000100
H      -3.03500500  1.99026200  0.00000300
C       2.26497800 -0.39527200  0.00000000
C       1.76397800 -1.68908700 -0.00000100
H       3.33443800 -0.25703500  0.00000000
H       2.39597300 -2.56264900  0.00000000
N       0.45256700 -1.90011100  0.00000000
C       1.95788600  2.08583600  0.00000000
H       1.61626600  2.63613300 -0.87770900
H       1.61629500  2.63611800  0.87773000
H       3.04389400  2.07587200 -0.00001600
H       0.11203000 -2.85327700 -0.00000500
```

TS1

Zero-point correction=   0.267875 (Hartree/Particle)
Thermal correction to Energy=   0.281383
Thermal correction to Enthalpy=   0.282327
Thermal correction to Gibbs Free Energy=   0.227343
Sum of electronic and zero-point Energies=   -560.080525
Sum of electronic and thermal Energies=   -560.067018
Sum of electronic and thermal Enthalpies=   -560.066074
Sum of electronic and thermal Free Energies= -560.121058

C   1.77497700 -1.86031000 0.32589800
C   0.89529500 -0.77094500 0.43098900
C   1.28711900 0.53022500 0.01888800
C   2.58313100 0.68670800 -0.51219700
C   3.43937100 -0.38770800 -0.62066800
C   3.03358500 -1.66458100 -0.19605800
H   1.45466100 -2.84037700 0.65089700
H   2.90754900 1.66311700 -0.83744600
H   4.42879300 -0.24918000 -1.03156700
H   3.71235400 -2.50087000 -0.28148700
C   0.36226500 1.62215400 0.18872600
C   -0.88831900 1.35338400 0.67554300
C   -1.30258400 0.03157300 0.98256800
H   -1.60184300 2.14999600 0.81666300
H   -2.14017900 -0.14966300 1.63783100
N   -0.35904400 -0.94499500 0.95979200
C   0.76470700 3.02644500 -0.15049500
H   1.64401700 3.33126400 0.41842900
H   1.01929000 3.11394700 -1.20810200
H   -0.04240600 3.72173200 0.06414900
C   -2.87354100 -1.86111400 -0.64896600
C   -2.68675200 -0.38166600 -0.69589600
C   -3.86546900 0.49006900 -0.41742000
H   -1.99899900 -0.02134200 -1.45169100
H   -3.37588400 -2.18527000 0.26352700
H   -1.93878000 -2.40630900 -0.76519800

```
H      -4.36246500  0.22039800  0.51568000
H      -3.61142700  1.54754900  -0.39779500
H      -0.60486000  -1.86083400  1.30730900
H      -3.51748600  -2.15556400  -1.48675600
H      -4.60173500  0.35096300  -1.21846500
```


4-methylquinolinium-isopropyl (Radical Cation) (C)

Zero-point correction=   0.270544 (Hartree/Particle)
Thermal correction to Energy=   0.283827
Thermal correction to Enthalpy=   0.284771
Thermal correction to Gibbs Free Energy=   0.230389
Sum of electronic and zero-point Energies=   -560.097395
Sum of electronic and thermal Energies=   -560.084112
Sum of electronic and thermal Enthalpies=   -560.083168
Sum of electronic and thermal Free Energies= -560.137550

```
C      1.75148600  -1.92403300  -0.17121900
C      0.85634700  -0.82285600  -0.24771300
C      1.32458300  0.51721100  -0.01307700
C      2.67600700  0.68746900  0.30698100
C      3.53218900  -0.39550000  0.38896000
C      3.06372800  -1.70627500  0.14464500
H      1.37629700  -2.92039100  -0.35758100
H      3.05739100  1.67960200  0.49051200
H      4.57131900  -0.24033200  0.63934800
H      3.74743200  -2.53981900  0.21034600
C      0.39056100  1.61231200  -0.14680600
C      -0.90490400  1.33761600  -0.42598800
C      -1.46816000  -0.02492500  -0.58360300
H      -1.60368700  2.15119600  -0.54633800
H      -1.95036100  -0.09485500  -1.56811200
N      -0.42825200  -1.03400200  -0.54775900
C      0.86409500  3.02932500  0.01294500
H      1.27250600  3.19653300  1.01066700
H      1.65173900  3.26353700  -0.70441400
H      0.04419100  3.72623000  -0.13935800
C      -3.13627400  -1.78070000  0.27360000
```

```
C     -2.59949400 -0.35878600 0.46767800
C     -3.73915600 0.66039200 0.37647300
H     -2.13230000 -0.28612000 1.45144400
H     -3.94880700 -1.95808000 0.97715200
H     -2.38601000 -2.54839000 0.46130900
H     -4.52878300 0.37864900 1.07220100
H     -3.42229700 1.66891600 0.63393000
H     -0.71180100 -1.98543000 -0.73482700
H     -3.53332200 -1.92076100 -0.73364900
H     -4.17180100 0.68003500 -0.62557500
```
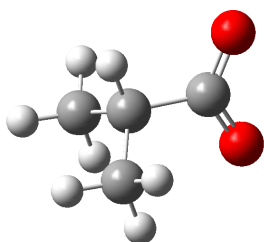

i-PrCOO⁻ (Anion)
(D)

Zero-point correction=   0.104971 (Hartree/Particle)
Thermal correction to Energy=   0.111843
Thermal correction to Enthalpy=   0.112787
Thermal correction to Gibbs Free Energy=   0.072937 Sum of electronic and zero-point
Energies=   -307.256448
Sum of electronic and thermal Energies=   -307.249576
Sum of electronic and thermal Enthalpies=   -307.248632
Sum of electronic and thermal Free Energies= -307.288482

```
C     -0.90040100 -0.03707700 0.00731200
C     0.57655100 0.11541000 -0.43551900
O     -1.78685100 0.31911100 -0.81876700
O     -1.11426000 -0.48998700 1.16409900
C     1.24713500 1.26210100 0.33425100
H     1.27891700 1.04300000 1.40242200
H     2.27278200 1.41166200 -0.00981300
H     0.70941100 2.20214300 0.19795600
C     1.36020300 -1.19071800 -0.26919600
H     1.39173900 -1.49079400 0.77835400
H     0.90539900 -2.00419700 -0.83768600
H     2.38763700 -1.07233600 -0.62067100
H     0.56207200 0.37923200 -1.49431100
```
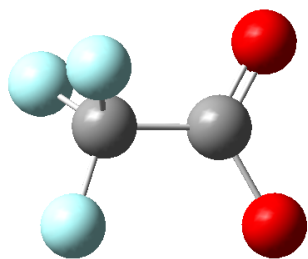
CF$_3$COO$^-$ (Anion)
(D)

Zero-point correction=   0.025286 (Hartree/Particle)
Thermal correction to Energy=   0.031357
Thermal correction to Enthalpy=   0.032301
Thermal correction to Gibbs Free Energy=   -0.006638
Sum of electronic and zero-point Energies=   -526.519229
Sum of electronic and thermal Energies=   -526.513159
Sum of electronic and thermal Enthalpies=   -526.512215
Sum of electronic and thermal Free Energies= -526.551154

C   1.04659700 0.01158800 0.00003100
C   -0.52479200 0.01316500 -0.00001000
O   1.53343500 -1.13426000 -0.00003800
O   1.58849100 1.12943100 0.00009400
F   -1.02362800 -0.62878400 -1.08717400
F   -1.07559800 1.24505900 -0.00019500
F   -1.02368900 -0.62848500 1.08730500

TS2
R= CF$_3$

Zero-point correction=   0.291712 (Hartree/Particle)
Thermal correction to Energy=   0.312558
Thermal correction to Enthalpy=   0.313502
Thermal correction to Gibbs Free Energy=   0.238282
Sum of electronic and zero-point Energies= -1086.618175
Sum of electronic and thermal Energies=   -1086.597329
Sum of electronic and thermal Enthalpies=   -1086.596385

Sum of electronic and thermal Free Energies= -1086.671606

C	-2.32261100	-1.38826800	-1.76789800
C	-1.98933600	-0.40610600	-0.81799200
C	-2.63809000	-0.37966100	0.44652100
C	-3.61269200	-1.35501600	0.70798700
C	-3.93537100	-2.31914800	-0.23208000
C	-3.28538700	-2.33222000	-1.47332700
H	-1.81809500	-1.39420000	-2.72448600
H	-4.11823400	-1.35324300	1.66187200
H	-4.68733800	-3.06198800	-0.00808800
H	-3.53569100	-3.08591800	-2.20653100
C	-2.26112300	0.65194400	1.39299400
C	-1.27436500	1.52550100	1.05259700
C	-0.52062200	1.46330600	-0.18127800
H	-0.98680300	2.28619700	1.76265300
H	0.62397100	0.87575100	0.23322000
N	-1.05290200	0.54297500	-1.11261900
C	-2.95351200	0.74650300	2.72315000
H	-4.02975700	0.88289600	2.60251600
H	-2.81056500	-0.16421200	3.30862200
H	-2.56655400	1.58325200	3.29989600
C	0.77286800	3.63889400	0.19422000
C	-0.02412600	2.79455600	-0.80799000
C	0.79731200	2.58177200	-2.08632500
H	-0.92482900	3.35437600	-1.08132600
H	1.67068800	3.11556500	0.52509900
H	0.19086100	3.90714500	1.07410800
H	1.67915800	1.96853800	-1.89876600
H	0.22007600	2.11854500	-2.88707200
H	-0.54310200	0.42275800	-1.97454100
O	1.69752100	0.29263700	0.66970800
C	2.21068100	-0.53195900	-0.16584500
O	1.86794000	-0.80142000	-1.30380500
C	3.45258400	-1.25448500	0.44247800
F	4.40567200	-0.36818200	0.79945200
F	3.11555200	-1.95011900	1.54896700
F	4.00848100	-2.11662200	-0.41987300
H	1.08395100	4.56800200	-0.28240300
H	1.13427700	3.54659300	-2.46385500

TS2
R = alkyl

Zero-point correction=   0.372087 (Hartree/Particle)
Thermal correction to Energy=   0.393383
Thermal correction to Enthalpy=   0.394327
Thermal correction to Gibbs Free Energy=   0.319837
Sum of electronic and zero-point Energies=   -867.367111
Sum of electronic and thermal Energies=   -867.345815
Sum of electronic and thermal Enthalpies=   -867.344871
Sum of electronic and thermal Free Energies= -867.419360

```
C      1.70355500 -1.74482500  1.57244900
C      1.59476700 -0.59800300  0.76029600
C      2.54196500 -0.36080500 -0.27506900
C      3.58824400 -1.28220700 -0.43742500
C      3.69382700 -2.39870000  0.37369000
C      2.74209500 -2.62967000  1.37848900
H      0.96982500 -1.91349700  2.34867400
H      4.31973200 -1.11967800 -1.21465000
H      4.50647300 -3.09608900  0.22969400
H      2.82234300 -3.50596500  2.00618100
C      2.35997400  0.80398800 -1.11821300
C      1.29458300  1.61661700 -0.89249700
C      0.28233600  1.38783700  0.12744300
H      1.16217000  2.48470200 -1.52121800
H     -0.76491500  0.98886000 -0.45217600
N      0.58794800  0.29089300  0.97719200
C      3.33942500  1.09760900 -2.21984600
H      4.35184600  1.21705400 -1.82989900
H      3.37088500  0.28376300 -2.94699000
H      3.06717200  2.01048000 -2.74436900
C     -0.84938600  3.67791800 -0.07033800
C     -0.21022900  2.66554000  0.88666200
C     -1.16953000  2.34864600  2.03845400
H      0.68801100  3.11928100  1.31729700
H     -1.74189900  3.26180400 -0.53889200
H     -0.17103700  4.00131700 -0.85832700
```

```
H      -2.06913500  1.84715000  1.68305500
H      -0.70828300  1.72180900  2.80126300
H      -0.20354900 -0.04848700  1.51615100
O      -1.94647600  0.45036400 -1.01846800
C      -2.50054700 -0.44087300 -0.26603900
O      -2.11209900 -0.74985500  0.87208800
C      -3.70115500 -1.15858200 -0.89859200
H      -1.14576500  4.56731300  0.48569200
H      -1.46831800  3.27821800  2.52296900
C      -4.81740600 -1.41264800  0.11728800
H      -5.16968700 -0.48250000  0.56484000
H      -5.66646000 -1.89383800 -0.37041600
H      -4.47137200 -2.06275000  0.92008700
C      -3.21686500 -2.46917500 -1.54177500
H      -4.04591700 -2.97494000 -2.03833200
H      -2.44017000 -2.28578500 -2.28456000
H      -2.81462500 -3.14425400 -0.78502700
H      -4.07828100 -0.51029300 -1.69021400
```
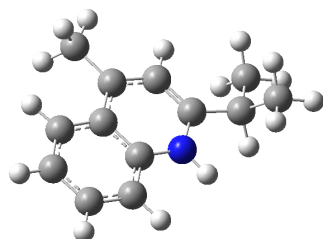

4-methylquinolinium-isopropyl (Radical)
(E)

Zero-point correction=   0.256599 (Hartree/Particle)
Thermal correction to Energy=   0.269967
Thermal correction to Enthalpy=   0.270911
Thermal correction to Gibbs Free Energy=   0.216749
Sum of electronic and zero-point Energies=   -559.681484
Sum of electronic and thermal Energies=   -559.668116
Sum of electronic and thermal Enthalpies=   -559.667172
Sum of electronic and thermal Free Energies= -559.721334

```
C       1.77497700 -1.86031000  0.32589800
C       0.89529500 -0.77094500  0.43098900
C       1.28711900  0.53022500  0.01888800
C       2.58313100  0.68670800 -0.51219700
C       3.43937100 -0.38770800 -0.62066800
C       3.03358500 -1.66458100 -0.19605800
H       1.45466100 -2.84037700  0.65089700
H       2.90754900  1.66311700 -0.83744600
```

```
H        4.42879300 -0.24918000 -1.03156700
H        3.71235400 -2.50087000 -0.28148700
C        0.36226500  1.62215400  0.18872600
C       -0.88831900  1.35338400  0.67554300
C       -1.30258400  0.03157300  0.98256800
H       -1.60184300  2.14999600  0.81666300
H       -2.14017900 -0.14966300  1.63783100
N       -0.35904400 -0.94499500  0.95979200
C        0.76470700  3.02644500 -0.15049500
H        1.64401700  3.33126400  0.41842900
H        1.01929000  3.11394700 -1.20810200
H       -0.04240600  3.72173200  0.06414900
C       -2.87354100 -1.86111400 -0.64896600
C       -2.68675200 -0.38166600 -0.69589600
C       -3.86546900  0.49006900 -0.41742000
H       -1.99899900 -0.02134200 -1.45169100
H       -3.37588400 -2.18527000  0.26352700
H       -1.93878000 -2.40630900 -0.76519800
H       -4.36246500  0.22039800  0.51568000
H       -3.61142700  1.54754900 -0.39779500
H       -0.60486000 -1.86083400  1.30730900
H       -3.51748600 -2.15556400 -1.48675600
H       -4.60173500  0.35096300 -1.21846500
```


i-PrCOOH
(F)

```
Zero-point correction=             0.118230 (Hartree/Particle)
Thermal correction to Energy=              0.125352
Thermal correction to Enthalpy=           0.126297
Thermal correction to Gibbs Free Energy=      0.086676
Sum of electronic and zero-point Energies=    -307.712196
Sum of electronic and thermal Energies=       -307.705074
Sum of electronic and thermal Enthalpies=     -307.704130
Sum of electronic and thermal Free Energies=  -307.743751
```

```
C        0.83439500  0.00005900 -0.13168000
C       -0.64203100  0.00028800 -0.46703200
```

```
O        1.73441200  0.00076800 -0.94313000
O        1.07371500 -0.00100800  1.19657300
C       -1.32721000 -1.27225600  0.05633900
H       -1.31720100 -1.30379500  1.14513800
H       -2.36507700 -1.28754000 -0.27542800
H       -0.83985500 -2.17212200 -0.31886400
C       -1.32707100  1.27229500  0.05783100
H       -1.31704400  1.30256200  1.14666700
H       -0.83963000  2.17254700 -0.31633200
H       -2.36494200  1.28807600 -0.27390200
H       -0.68348700  0.00093700 -1.55529700
H        2.03373100 -0.00106300  1.32772500
```


CF₃COOH
(F)

Zero-point correction=   0.038370 (Hartree/Particle)
Thermal correction to Energy=   0.044613
Thermal correction to Enthalpy=   0.045558
Thermal correction to Gibbs Free Energy=   0.007128
Sum of electronic and zero-point Energies=   -526.948456
Sum of electronic and thermal Energies=   -526.942213
Sum of electronic and thermal Enthalpies=   -526.941269
Sum of electronic and thermal Free Energies= -526.979698

```
C       -0.94824700  0.15611900  0.00004700
C        0.59404600 -0.00217700  0.00010600
O       -1.52230200 -1.03952600  0.00006900
O       -1.48904800  1.22398500 -0.00002500
F        1.00238900 -0.67788600  1.08640400
F        1.18458400  1.19205800  0.00064900
F        1.00231400 -0.67676100 -1.08719700
H       -2.48758100 -0.93602900  0.00002300
```
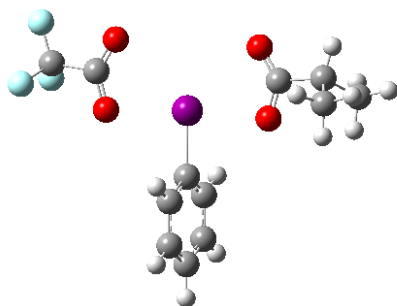
PIFA *(bis(trifluoroacetoxy)iodo benzene)*
(G)
R = CF₃

Zero-point correction=   0.224811 (Hartree/Particle)
Thermal correction to Energy=   0.246703
Thermal correction to Enthalpy=   0.247648
Thermal correction to Gibbs Free Energy=   0.166277
Sum of electronic and zero-point Energies=   -1076.417266
Sum of electronic and thermal Energies=   -1076.395373
Sum of electronic and thermal Enthalpies=   -1076.394429
Sum of electronic and thermal Free Energies= -1076.475799

C	0.55493600	4.46010100	0.00000000
C	0.50586000	3.77007800	-1.20779600
C	0.40744600	2.38200200	-1.21841700
C	0.36148000	1.71707000	-0.00002200
C	0.40779800	2.38195800	1.21838400
C	0.50621300	3.77003400	1.20778500
H	0.63059800	5.53819000	0.00000900
H	0.54338900	4.30594600	-2.14530900
H	0.36807900	1.84476400	-2.15353300
H	0.36869700	1.84468600	2.15349200
H	0.54401500	4.30586700	2.14530600
I	0.21817800	-0.38299200	-0.00003700
O	-2.01716700	0.05015300	0.00004700
O	2.35681800	-0.33366300	-0.00006200
C	-2.70284000	-1.03657000	-0.00006200
C	2.82509600	-1.56833700	-0.00001200
C	4.34348000	-1.66876000	0.00004500
C	-4.23394500	-0.75037500	0.00006900
O	2.07769400	-2.53906700	-0.00002600
O	-2.29590200	-2.18363600	-0.00020400
F	-4.58967300	-0.03974600	1.08724200
F	-4.58978700	-0.03928100	-1.08676000
F	-4.94701400	-1.88177400	-0.00013700
C	4.93351700	-1.04316800	-1.27240500
H	4.74722700	0.02970700	-1.30290200

```
H        6.01125800 -1.20380600 -1.28956500
H        4.51167500 -1.49193000 -2.17174000
C        4.93342000 -1.04311000  1.27250900
H        4.51150800 -1.49182900  2.17183300
H        6.01115900 -1.20374700  1.28976100
H        4.74712900  0.02976800  1.30294200
H        4.55377400 -2.73768300  0.00007700
```
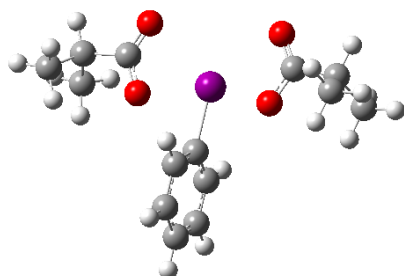

(bis(isobutylcarboxylate)iodo benzene)
(G)
R = alkyl

Zero-point correction=   0.304814 (Hartree/Particle)
Thermal correction to Energy=   0.326484
Thermal correction to Enthalpy=   0.327428
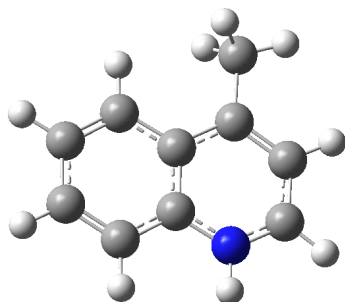Thermal correction to Gibbs Free Energy=   0.248287
Sum of electronic and zero-point Energies=   -857.174707
Sum of electronic and thermal Energies=   -857.153038
Sum of electronic and thermal Enthalpies=   -857.152093
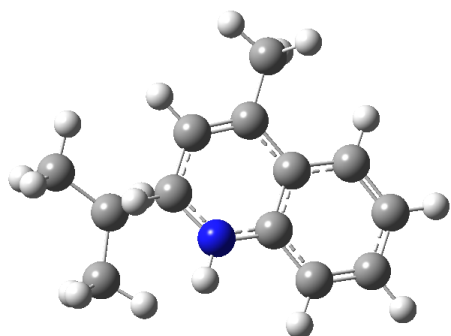Sum of electronic and thermal Free Energies= -857.231235

```
C       -0.00041200  4.39703400 -0.00293800
C        0.00010800  3.70318100 -1.20941100
C        0.00019100  2.31120300 -1.21750800
C       -0.00029900  1.64205000 -0.00061200
C       -0.00078700  2.31326900  1.21514400
C       -0.00087800  3.70522900  1.20470900
H       -0.00045200  5.47785200 -0.00385600
H        0.00045900  4.23930100 -2.14770700
H        0.00055900  1.77253600 -2.15289600
H       -0.00114000  1.77616800  2.15142900
H       -0.00129000  4.24293200  2.14209800
I        0.00015200 -0.46723700  0.00132100
O       -2.18087200 -0.20456800  0.00163700
O        2.18082600 -0.20444100  0.00026900
C       -2.76491600 -1.37800500  0.00350100
C        2.76511400 -1.37788600  0.00131600
C        4.28935900 -1.33729600  0.00047400
C       -4.28920600 -1.33771700  0.00276800
```

```
O      2.12699400 -2.42932000  0.00268900
O     -2.12669900 -2.42942900  0.00485400
C      4.81867600 -0.66288500 -1.27335600
H      4.52720100  0.38630500 -1.30891500
H      5.90734700 -0.71571300 -1.29110200
H      4.44341200 -1.15403700 -2.17147600
C      4.82051600 -0.65442700  1.26896600
H      4.44607400 -1.13919300  2.17089200
H      5.90918300 -0.70771700  1.28578300
H      4.52964600  0.39513800  1.29769700
H      4.60184100 -2.38115800  0.00366500
H     -4.60151800 -2.38158500  0.01226100
C     -4.81798300 -0.67138000 -1.27562600
H     -4.44278500 -1.16863300 -2.17040000
H     -4.52590100  0.37739300 -1.31793000
H     -5.90666900 -0.72374100 -1.29319000
C     -4.82101000 -0.64686900  1.26661500
H     -5.90966400 -0.70039500  1.28335200
H     -4.53045800  0.40293300  1.28871100
H     -4.44673100 -1.12575400  2.17173800
```
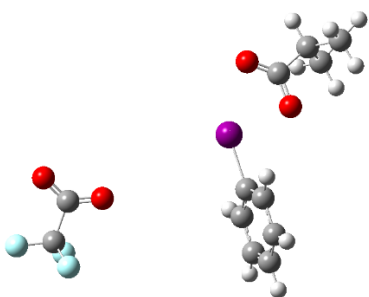

PIFA radical anion
(I-(trifluoroacetoxy), I-(isobutylcarboxylate)iodo benzene) radical anion; collapse observed during optimization via DFT)
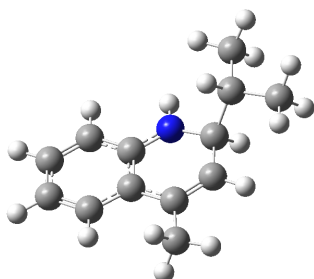**(H)**
R = CF₃

```
Zero-point correction=              0.221571 (Hartree/Particle)
Thermal correction to Energy=            0.244955
Thermal correction to Enthalpy=          0.245900
Thermal correction to Gibbs Free Energy=     0.151886
Sum of electronic and zero-point Energies=  -1076.589268
Sum of electronic and thermal Energies=     -1076.565884
Sum of electronic and thermal Enthalpies=   -1076.564939
Sum of electronic and thermal Free Energies= -1076.658953
```

```
C     -0.15331900  4.31705100  0.14896700
C      0.29646100  3.85643700 -1.08596900
```

```
C      0.71433500  2.53835800  -1.23325700
C      0.67060800  1.68817900  -0.12941700
C      0.22831600  2.13754400   1.11379000
C     -0.18637500  3.45831800   1.24482700
H     -0.47634100  5.34276700   0.25718700
H      0.32328000  4.52051500  -1.93831400
H      1.06244200  2.18316000  -2.19144300
H      0.20213700  1.47346400   1.96449100
H     -0.53499900  3.81285800   2.20451200
I      1.27734800 -0.31079300  -0.34447100
O     -3.92259800 -0.86034900  -0.47981700
O      3.85915900 -0.08447700   0.23662800
C     -5.00320300 -1.47619500  -0.43075100
C      4.18868700 -1.31331700   0.10001000
C      5.68921900 -1.60710200   0.36137700
C     -6.12782800 -0.68368200   0.32834100
O      3.42530300 -2.23596900  -0.21650100
O     -5.32916000 -2.59058900  -0.87220000
F     -5.77615200 -0.43384100   1.61587000
F     -6.36320200  0.52311800  -0.24671900
F     -7.31657800 -1.32016600   0.37577900
C      6.56344200 -0.91721400  -0.69164800
H      6.49671000  0.16690300  -0.60528500
H      7.60526200 -1.20765300  -0.55084800
H      6.27080500 -1.19977400  -1.70322600
C      6.08933000 -1.21772800   1.78790100
H      5.45416200 -1.70346900   2.52916700
H      7.11878400 -1.52482500   1.97627000
H      6.02256100 -0.14001700   1.93317000
H      5.77948400 -2.68673500   0.24699900
```
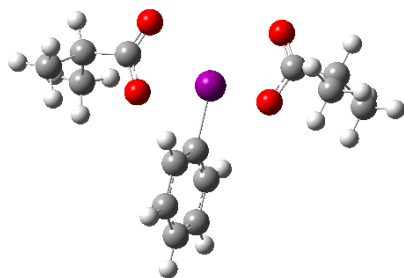

*(bis(isobutylcarboxylate)iodo benzene) radical anion **(H)***
R = alkyl

Zero-point correction=   0.301567 (Hartree/Particle)
Thermal correction to Energy=   0.325438
Thermal correction to Enthalpy=   0.326383
Thermal correction to Gibbs Free Energy=   0.237460
Sum of electronic and zero-point Energies=   -857.329003

Sum of electronic and thermal Energies=   -857.305132
Sum of electronic and thermal Enthalpies=   -857.304187
Sum of electronic and thermal Free Energies= -857.393110

C	-0.01566300	4.90712500	0.08179800
C	-0.01391800	4.18338400	1.27161100
C	-0.00903600	2.79256500	1.24712300
C	-0.00594700	2.12902700	0.02005100
C	-0.00759200	2.84649600	-1.17619500
C	-0.01249400	4.23702500	-1.13902000
H	-0.01943000	5.98781800	0.10588300
H	-0.01635500	4.69873800	2.22201100
H	-0.00766300	2.23611000	2.17280900
H	-0.00509000	2.33140500	-2.12547000
H	-0.01380900	4.79412900	-2.06556000
I	0.00165700	0.02856000	-0.02703500
O	2.86255600	-0.19946100	-0.03088000
O	-2.85717400	-0.21048900	-0.03402400
C	2.93202200	-1.46364700	-0.06167200
C	-2.92442600	-1.47491600	-0.06232700
C	-4.34714900	-2.08873600	-0.05452200
C	4.35563300	-2.07531300	-0.05426400
O	-1.94680000	-2.25964700	-0.08086600
O	1.95557600	-2.24994200	-0.08257400
C	-4.99903300	-1.88856000	1.32017500
H	-5.14635900	-0.82831100	1.52804900
H	-5.97360100	-2.37880000	1.35197900
H	-4.38643300	-2.31017300	2.11838700
C	-5.21822000	-1.51598600	-1.17654700
H	-4.75912100	-1.66541300	-2.15498700
H	-6.19315400	-2.00688200	-1.18621000
H	-5.37651300	-0.44674100	-1.03717400
H	-4.21273700	-3.15774400	-0.22207400
H	4.22285800	-3.14453800	-0.22173500
C	5.00807400	-1.87403400	1.31998700
H	4.39664400	-2.29654200	2.11862800
H	5.15388200	-0.81355400	1.52770600
H	5.98341400	-2.36277500	1.35120300
C	5.22510500	-1.50118500	-1.17687500
H	6.20086200	-1.99042700	-1.18707600
H	5.38167500	-0.43166500	-1.03763400
H	4.76569000	-1.65145600	-2.15503800
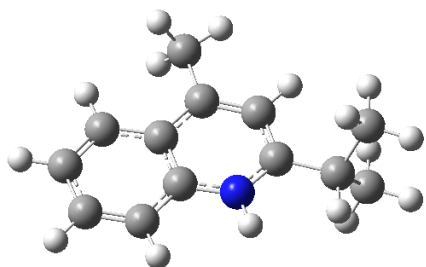
4-methylquinolinium-isopropyl (Cation)
(I)

Zero-point correction=   0.260797 (Hartree/Particle)
Thermal correction to Energy=   0.273800
Thermal correction to Enthalpy=   0.274744
Thermal correction to Gibbs Free Energy=   0.221353
Sum of electronic and zero-point Energies=   -559.558664
Sum of electronic and thermal Energies=   -559.545660
Sum of electronic and thermal Enthalpies=   -559.544716
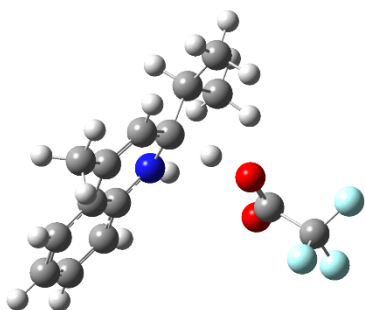Sum of electronic and thermal Free Energies= -559.598107

C   -1.90411500 -1.88530300 -0.00028700
C   -0.94748600 -0.85806200 -0.00015400
C   -1.32787700 0.50564800 0.00007900
C   -2.71074800 0.80278000 0.00017000
C   -3.64343400 -0.20556600 0.00003800
C   -3.23830900 -1.55450400 -0.00019000
H   -1.58651400 -2.91849400 -0.00046300
H   -3.03281700 1.83245700 0.00034700
H   -4.69662600 0.03448600 0.00011100
H   -3.98255600 -2.33758400 -0.00028800
C   -0.30335000 1.50236000 0.00021500
C   1.01523300 1.09780800 0.00011100
C   1.37157300 -0.25579300 -0.00013400
H   1.80331300 1.83435700 0.00021900
N   0.39421100 -1.16226500 -0.00025300
C   -0.64635700 2.96015400 0.00047000
H   -1.24063100 3.21757800 -0.87730700
H   -1.24055500 3.21728500 0.87838400
H   0.25164300 3.57108700 0.00053200
C   3.53339800 -0.28939700 1.27415000
C   2.79830400 -0.74150900 -0.00022500
C   3.53364200 -0.28842000 -1.27410400
H   2.76738100 -1.83277400 -0.00065400
H   3.02092300 -0.63188000 2.17210000
H   3.02131800 -0.63017300 -2.17241800
H   0.65348300 -2.14115300 -0.00043200
H   3.62038500 0.79692600 -1.31889800

H   3.62007200 0.79591900 1.31980400
H   4.53954100 -0.70621100 -1.27437100
H   4.53931400 -0.70714600 1.27427000
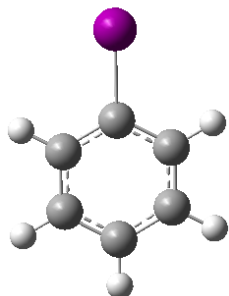
Iodobenzene
(J)
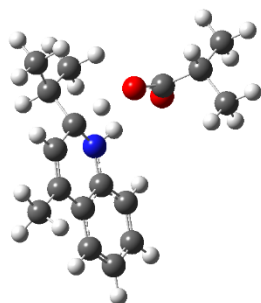Zero-point correction=   0.090032 (Hartree/Particle)
Thermal correction to Energy=   0.095894
Thermal correction to Enthalpy=   0.096838
Thermal correction to Gibbs Free Energy=   0.058304
Sum of electronic and zero-point Energies=   -243.016288
Sum of electronic and thermal Energies=   -243.010426
Sum of electronic and thermal Enthalpies=   -243.009482
Sum of electronic and thermal Free Energies= -243.048016

C   -3.33914300 0.00000300 0.00000400
C   -2.64063600 1.20358100 0.00000600
C   -1.24764000 1.21100500 -0.00000300
C   -0.56461300 -0.00001300 0.00000200
C   -1.24764600 -1.21100800 0.00000400
C   -2.64065800 -1.20356900 -0.00000200
H   -4.41999100 0.00002000 0.00000400
H   -3.17414100 2.14402400 0.00000700
H   -0.71293300 2.14890200 -0.00000400
H   -0.71296900 -2.14892200 0.00000300
H   -3.17415300 -2.14401700 -0.00000100
I   1.55238100 0.00000000 -0.000000

SUPPORTING INFORMATION: EFFICIENT PHOTOCONVERSION OF THIONES TO KETONES: EXPLORING ETHERS AS A SOURSE OF OXYGEN

Quantum Yield of the Reaction: Visible Light Actinometry
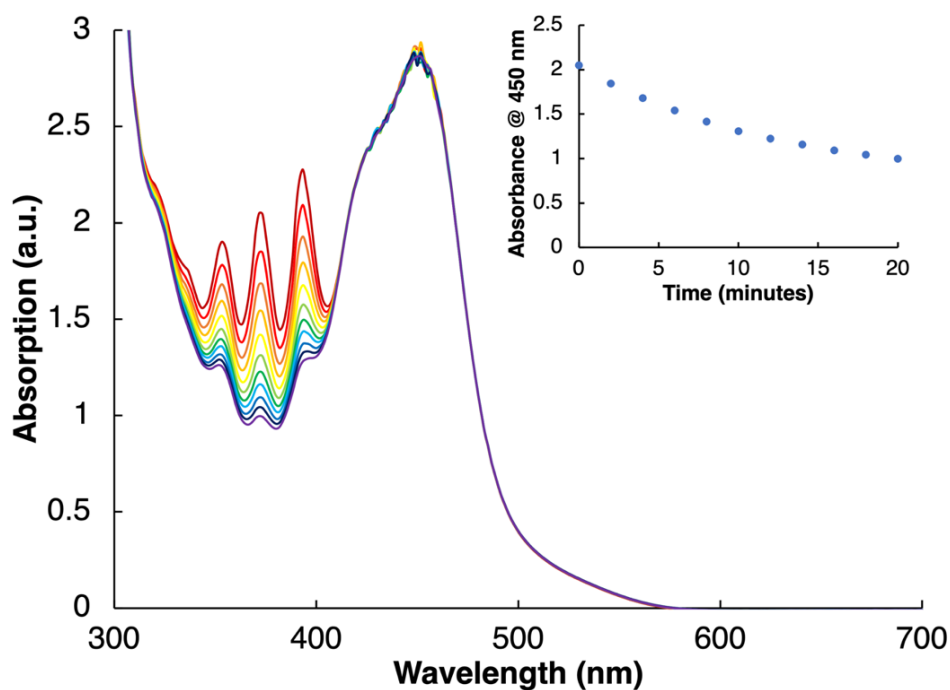
Figure B.1. Absorption spectra of the actinometry experiment performed with Ru(bpy)$_3$Cl$_2$ (0.19 mM) and DPA (0.10 mM) in acetonitrile and irradiated at 450 nm. Inset: Absorption at 450 nm vs. irradiation time corresponding to data from absorption vs wavelength graph. Data recorded according to conditions from protocol (Pitre *et al.,* 2015).
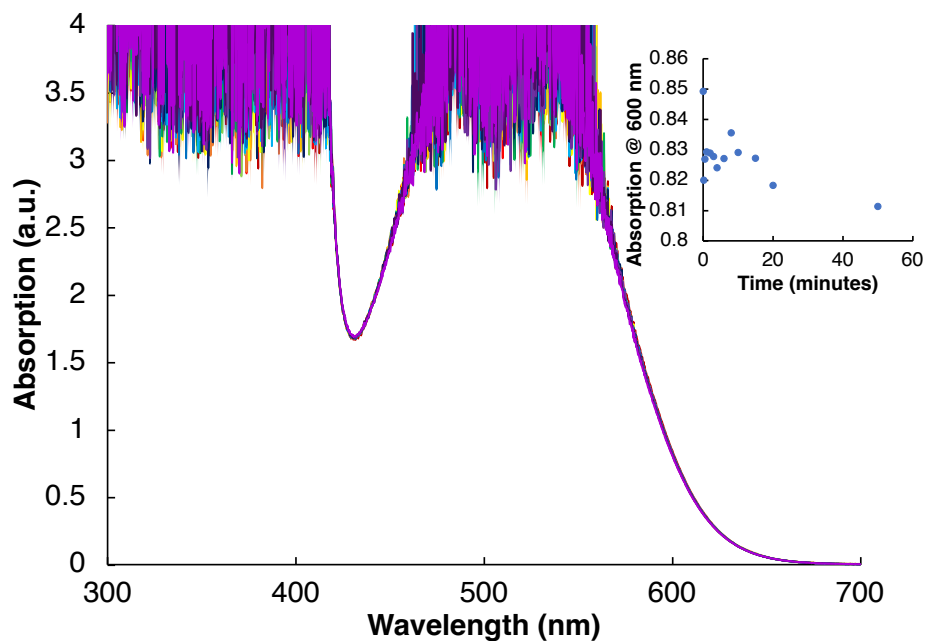
Figure B.2. Absorption spectra of the actinometry experiment performed with **2SS** (0.545 mM) in dichloromethane and irradiated at 450 nm. Inset: Absorption at 600 nm vs. irradiation time corresponding to data from absorption vs wavelength graph.
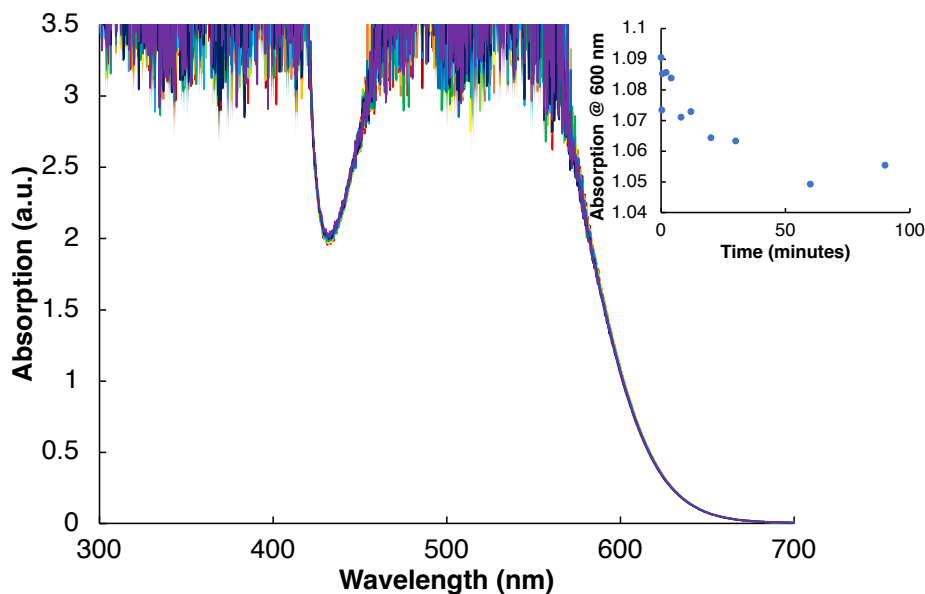
Figure B.3. Absorption spectra of the actinometry experiment performed with **2SS** (0.545 mM) in chloroform and irradiated at 450 nm. Inset: Absorption at 600 nm vs. irradiation time corresponding to data from absorption vs wavelength graph.
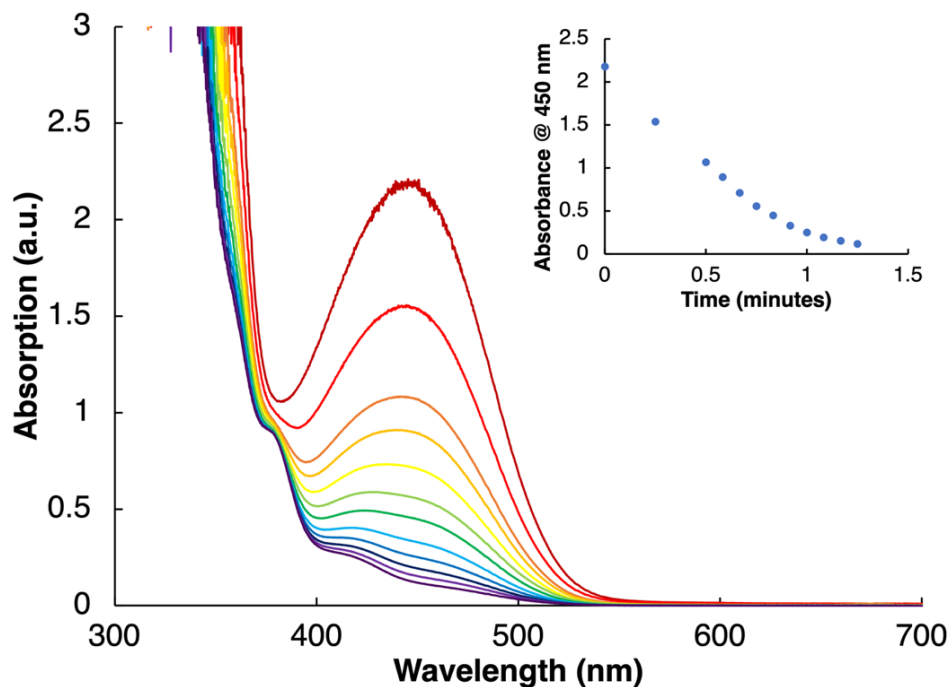
Figure B.4. Absorption spectra of the actinometry experiment performed with **2OS** (0.545 mM) in THF and irradiated at 450 nm. Inset: Absorption at 450 nm vs. irradiation time corresponding to data from absorption vs wavelength graph.

Table B.1. Quantum yield for the loss of starting material during 450 nm irradiation in various solvents under N_2.

Molecule (Monitoring λ)	Solvents	Reaction Quantum Yield (ϕ)
2SS (600 nm)	THF	0.36
2SS (600 nm)	ET_2O	0.07
2SS (600 nm)	DCM	< 0.001
2SS (600 nm)	Chloroform	< 0.001
2OS (450 nm)	THF	0.43

Solvent Scope

Stock solutions of **2SS, 2OS** and **2OO** (~ 0.25 mM in DCM) were used to create 0.01 mM samples in various solvents (hexane, toluene, Et_2O, THF, chloroform, dichloromethane, DMSO and acetonitrile). A solution of 3 mL of each molecule (**2SS, 2OS** and **2OO** 0.01 mM) was added to a quartz cuvette with the solvents and a spectrum was collected using the Cary 60 (Figure B.5-B.7).
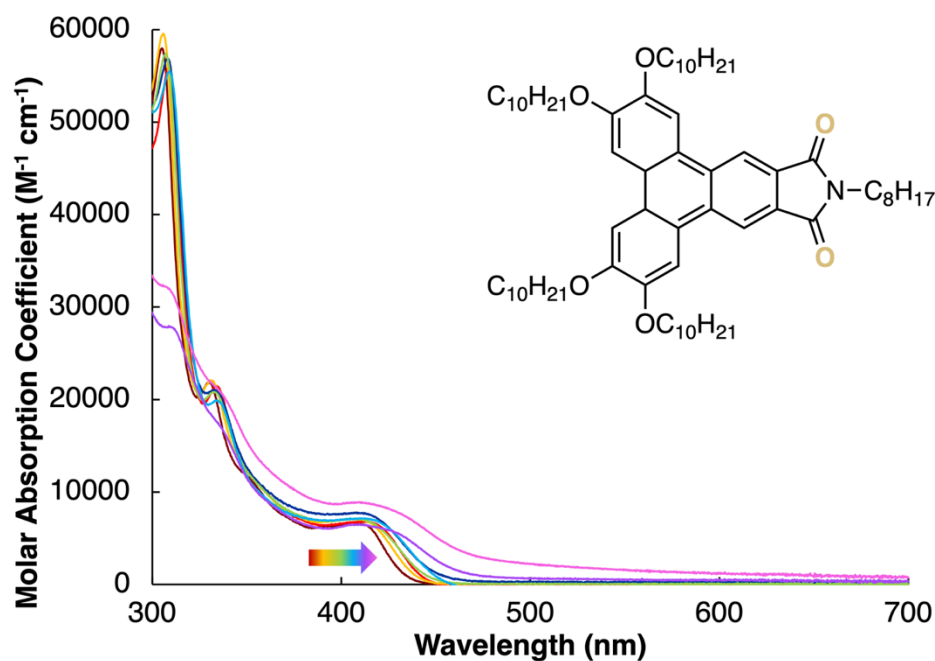
Figure B.5. Molar absorption coefficient of **2OO** in solvents of ranging polarities. Hexane (brown), toluene (red), Et₂O (orange), THF (green), chloroform (blue), dichloromethane (navy), DMSO (purple) and acetonitrile (pink).
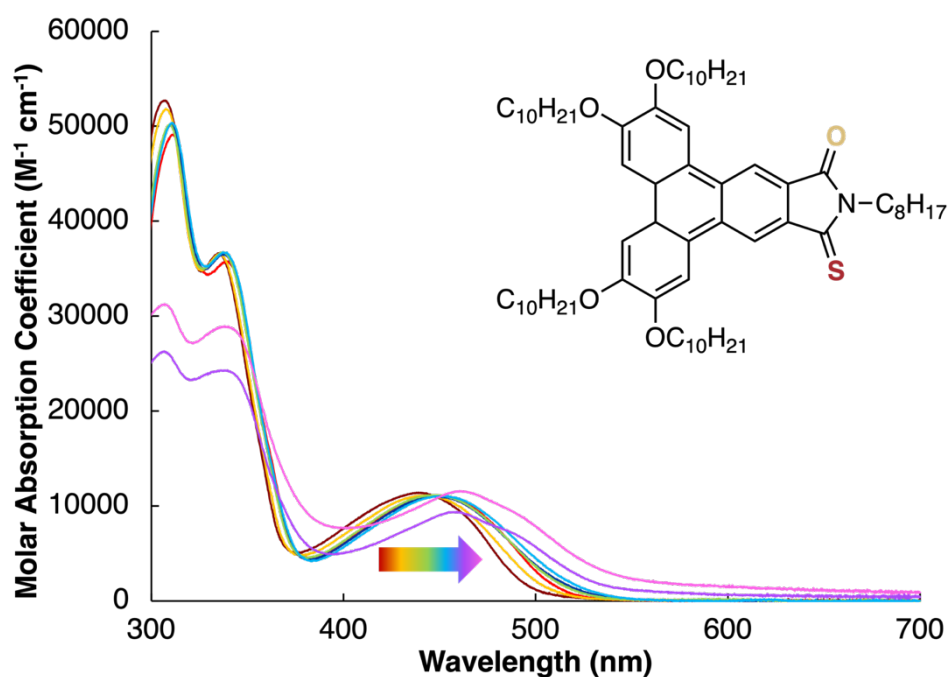
Figure B.6. Molar absorption coefficient of **2OS** in solvents of ranging polarities. Hexane (brown), toluene (red), Et₂O (orange), THF (green), chloroform (blue), dichloromethane (navy), DMSO (purple) and acetonitrile (pink).
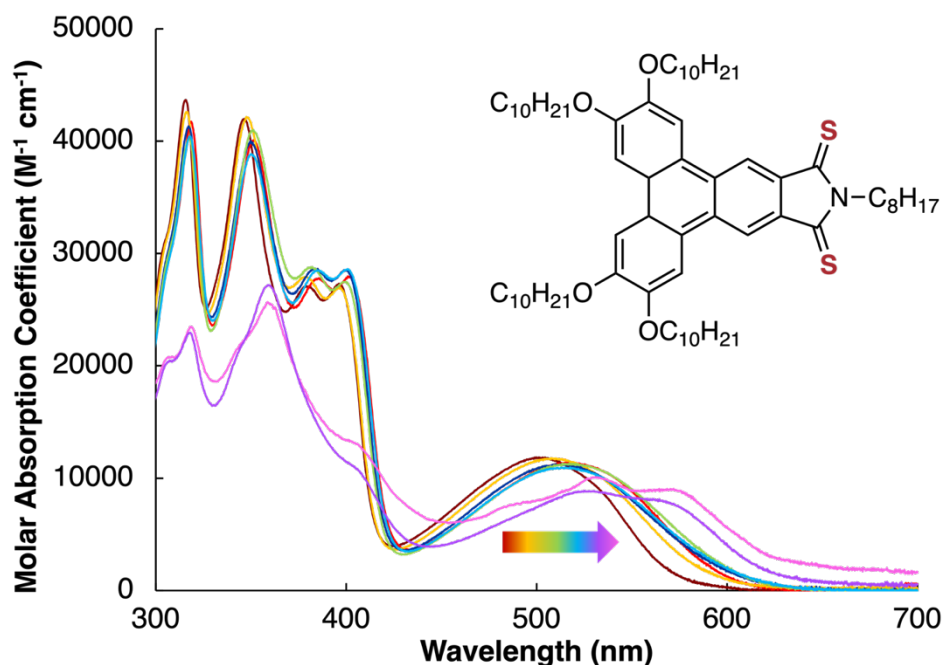
Figure B.7. Molar absorption coefficient of **2SS** in solvents of ranging polarities. Hexane (brown), toluene (red), Et$_2$O (orange), THF (green), chloroform (blue), dichloromethane (navy), DMSO (purple) and acetonitrile (pink).

It can be noted that by increasing the solvent polarity, the absorption maximum slightly red shifted,

a summary of the absorption maximum can be found in Table B.2.

Table B.2. Absorption maximum of **2SS, 2OS** and **2OO** in hexane, toluene, ether, chloroform, dichloromethane, THF, DMSO, and acetonitrile.

	Hexane	Toluene	Ether	THF	Chloro-form	Dichloro-methane	DMSO	Aceto-nitrile
Solvent polarity (ET$_{30}$)[*]	30.9	33.9	34.6	37.4	39.1	41.1	45.1[**]	46.0
2OO	413	419	416	417	421	419	428	416
2OS	443	448	445	450	452	449	457	561
2SS	503	502	509	523	517	513	526	531

(header spanning: λ$_{max}$ (nm))

[*] Values from Reichardt (1979)

[**] Value from Cerón-Carrasco *et al.* (2014)

DFT Calculations

Density Functional Theory (DFT) calculations were performed using the Gaussian 09, (2016) suite at the B3LYP level of theory which uses Becke's 3-parameter exchange and Lee, Yang and Parr's correlation function (Becke, 1992; Becke 1993; Lee *et al.,* 1998). Resulting outputs were verified for imaginary frequencies to ensure the optimized structures were local minima for ground states (no imaginary frequency). All atoms were calculated at B3LYP/6-311+G(d,p) level of theory in the gas phase. The long alkyl chains on the molecule were simplified for the calculations to -CH_3 groups.

The red-shift in absorption is due to the decreasing HOMO-LUMO gap in increasingly polar solvents. DFT calculations predict a significant charge-transfer character to the first singlet excited state. Typically, charge-transfer excited states will be more stabilized in more polar solvents (Figure B.8). A further red shift in acetonitrile solvent can also be explained via dimerization/agglomeration of the molecules.
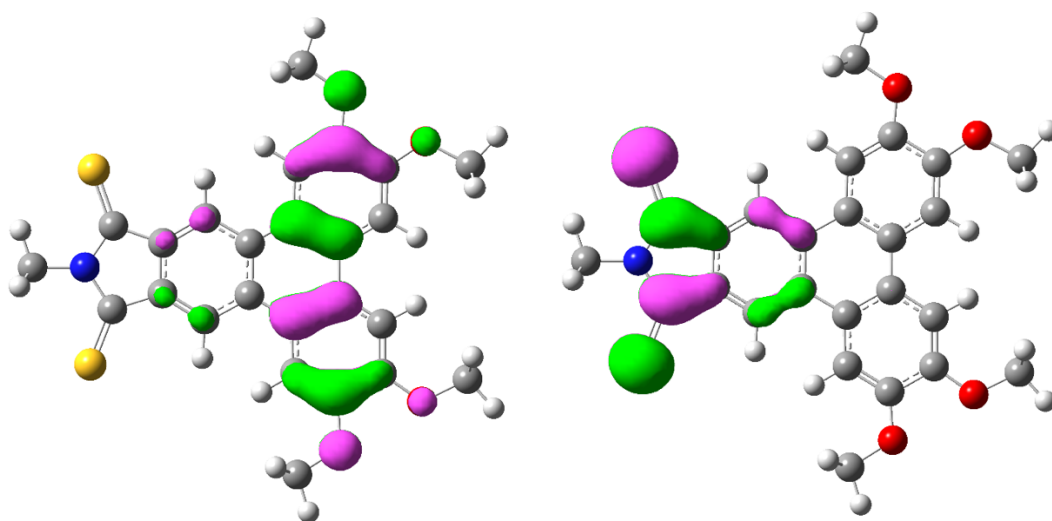
Figure B.8. HOMO (left) and LUMO (right) of **2SS**.
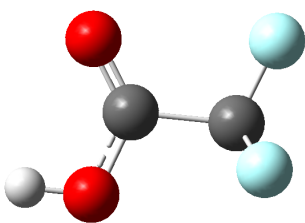
DFT energies and atomic coordinates

Zero-point correction=   0.409305 (Hartree/Particle)
Thermal correction to Energy=   0.438587
Thermal correction to Enthalpy=   0.439531
Thermal correction to Gibbs Free Energy=   0.348486
Sum of electronic and zero-point Energies=   -2117.002388
Sum of electronic and thermal Energies=   -2116.973106
Sum of electronic and thermal Enthalpies=   -2116.972162
Sum of electronic and thermal Free Energies=   -2117.063207

C   -1.62584 -3.56774 0.00002
C   -0.44024 -2.86053 0.00005
C   -0.40311 -1.44027 -0.00001
C   -1.62697 -0.72918 -0.00007
C   -2.83806 -1.46992 -0.00009
C   -2.85909 -2.85168 -0.00005
C   0.86448 -0.71688 -0.00001
C   -1.62616 0.73084 -0.00007
C   -0.40148 1.44056 0.00002
C   0.86526 0.71581 0.00002
C   -0.43698 2.86087 0.00008
H   0.48868 3.41643 0.00018
C   -1.62174 3.56944 0.00003
C   -2.85582 2.85477 -0.0001
C   -2.83639 1.47297 -0.00014
H   0.48479 -3.41714 0.00013
H   -3.78218 -0.94582 -0.00012
H   -3.78112 0.94997 -0.00024
C   2.10431 -1.41149 -0.00004
C   2.1059 1.4091 0.00004
C   3.28231 0.69957 0.00002
C   3.28154 -0.7031 -0.00002
H   2.15102 2.49054 0.00005
H   2.14828 -2.49297 -0.00009
C   4.69659 1.16364 0.00004
C   4.69427 -1.17152 -0.00005
N   5.47843 -0.00302 0.0001
C   6.93121 0.00422 0.00031
H   7.30913 0.51821 -0.88782
H   7.2665 -1.03356 0.00024
O   -1.72805 4.92448 0.00009
O   -3.97604 3.62356 -0.00017
O   -3.98023 -3.61918 -0.00007
O   -1.73369 -4.92266 0.00007
C   -0.5331 5.69717 0.00018
H   0.0686 5.50162 -0.8962

```
H        0.0685  5.50157  0.89661
C       -5.2431   2.97902 -0.0004
H       -5.37645  2.36062  0.89634
H       -5.37615  2.36068 -0.89723
C       -5.2465  -2.97311 -0.00023
H       -5.37885 -2.3546  -0.89704
H       -5.37905 -2.35455  0.89652
C       -0.53964 -5.69672  0.00013
H        0.06221 -5.50181  0.89655
H        0.06227 -5.50185 -0.89626
H       -5.98602 -3.77452 -0.00028
H       -0.85637  6.73855  0.00019
H       -5.98163  3.78133 -0.0005
H       -0.86409 -6.73773  0.00014
H        7.30889  0.518    0.88867
S        5.25603 -2.63372  0.00008
S        5.26911  2.62167  0.00025
```

Quantum yield of fluorescence *(Φ_f)*

The relative fluorescence quantum yield of **2SS, 2OS** and **2OO** in THF and chloroform was determined by comparing the change in fluorescence to that of fluorescein which has a known absolute quantum yield of 0.925 in 0.1 M NaOH (Sjöback *et al.,* 1995).

In a 1 x 1 cm quartz cuvette, emission spectra were recorded at using an excitation wavelength of 450 nm, first collecting a blank to correct for any emission arising from the solvent. The samples were then added into the cuvettes in small increments, without exceeding an absorption of 0.11 to minimize non-linear effects. The relative quantum yield was then calculated using the equation:

$$F = F_{std} * \left(\frac{m_{molecule}}{m_{std}}\right) * \left(\frac{\eta_{molecule}}{\eta_{std}}\right)^2 \qquad \text{eq B.1}$$

Where F is quantum yield, m is the gradient of the plot of integrated fluorescence intensity against absorbance, and η is the refractive index of the solvent (Perkin Elmer, 2022). The refractive index for water, chloroform and THF is 1.33, 1.45 and 1.45 respectively.

2OO has the largest fluorescence quantum yield in both chloroform and THF, 0.46 and 0.60, respectively. **2SS** and **2OS** is very weakly fluorescent with a quantum yield of fluorescence < 0.01 in chloroform and THF. The results are summarized in tables B.3 and Figures B.9 and B.10.

Table B.3. Quantum yields of fluorescence in chloroform and THF.

Molecule	Solvent	Quantum Yield of Fluorescence (Φ_f)
2OO	chloroform	0.46
2OS	chloroform	0.0077
2SS	chloroform	0.0017
2OO	THF	0.60
2OS	THF	0.0008
2SS	THF	0.0016
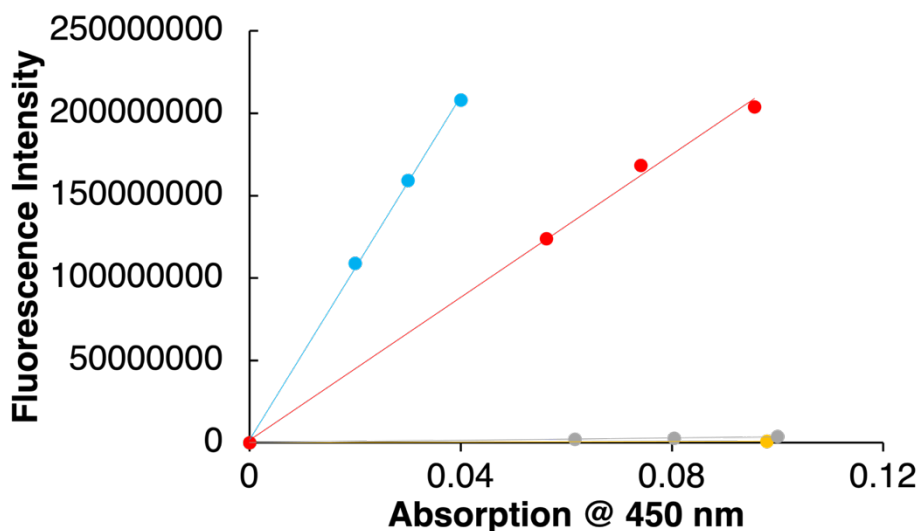
Figure B.9. Integrated fluorescence intensity of **2SS** (orange), **2OS** (grey), and **2OO** (red) in chloroform and fluorescein (blue) in 0.1 M NaOH.
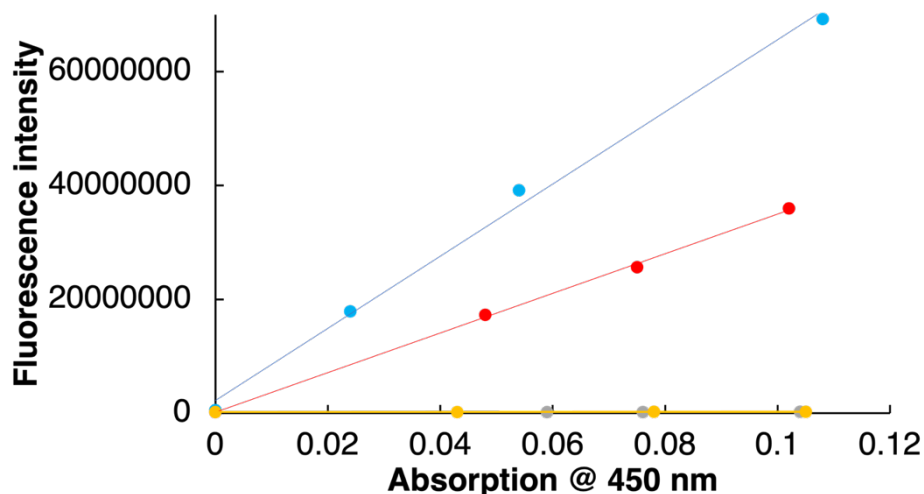
Figure B.10. Integrated fluorescence intensity of **2SS** (orange), **2OS** (grey), and **2OO** (red) in THF and fluorescein (blue) in 0.1 M NaOH.

Direct identification of the imide

The experiments carried out so far have not allowed for the direct identification of **2OO** at its absorption maximum of 410 nm, despite the disappearance of the peak at 515 nm attributed to the disappearance of **2SS**. In an attempt to directly observe an increase at 410 nm from irritation of **2SS**, a spectrum of **2SS** in THF was taken after irritation in short time intervals. By using a less intense light source, the goal was to identify small absorption increases at 410 nm while a simultaneous decrease in the absorption maximum at 515 nm.

The spectrum obtained in Figure B.11 shows the gradual decrease in the peak at 515 nm attributed to the disappearance of **2SS**. However, it is not possible to observe an increase at 410 nm which would indicate the formation of **2OO**. One of the reasons for this is due to **2SS** having an absorption in the region of 350 - 400 nm with a much larger molar absorption coefficient (ε) than **2OO** (Figure B.12).
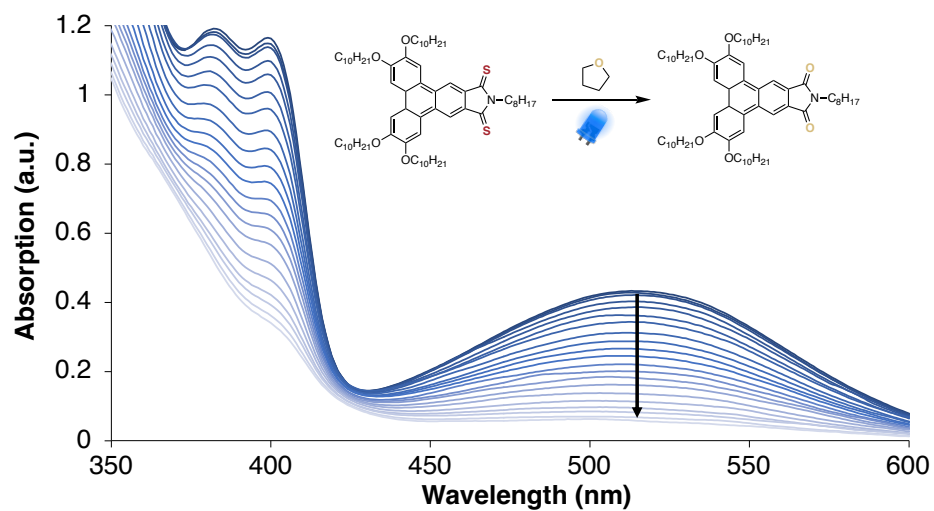
Figure B.11. UV-Visible spectra of 2SS in chloroform with THF from 0 -112 minutes of irritation.
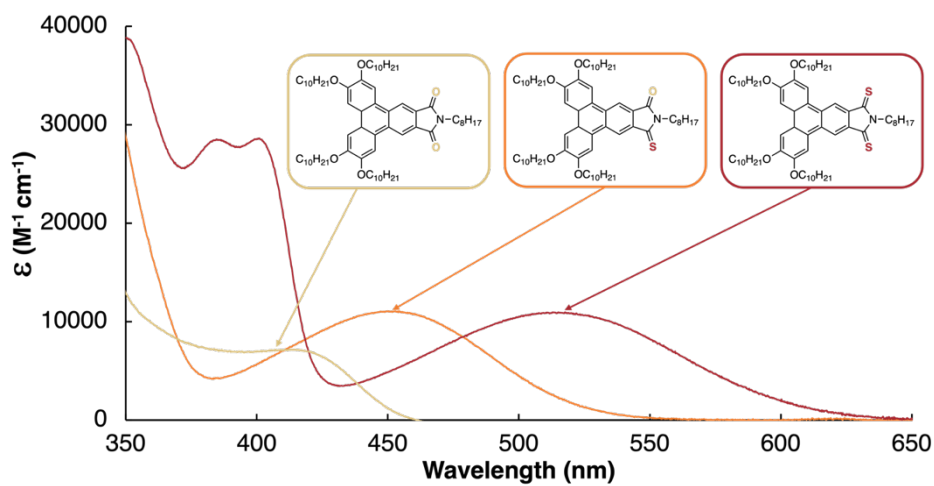
Figure B.12. Molar absorption coefficients (ε) of **2SS, 2OS** and **2OO** in THF.

ANNEXE C

SUPPORTING INFORMATION : MECHANISTIC INSIGHT INTO FE CATALYZED ALPHA-C-H OXIDATION OF TERITARY AMINES: NON-RADICAL PATHWAYS FOR BASE-METAL CATALYSIS

Figure C.1. Cover of *ChemCatChem*. 2020, DOI: 10.1002/cctc.202001382.

Thermochemical data from an alternative DFT functional: intramolecular H-atom abstraction using B3LYP/6-311+G (2d,2p)

Thermochemical data obtained from DFT calculations for the reaction **13** → **[TS]** → **15**. Compound **[TS]** was converted to **15** with no barrier during geometry optimization.
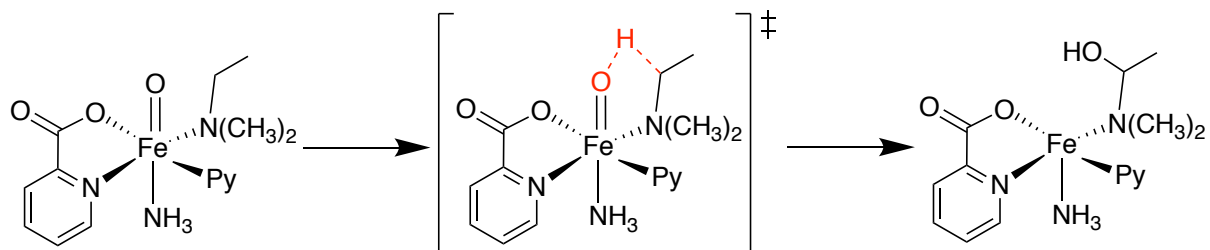
ΔG‡(kcal/mol)	ΔG°$_{RX}$ (kcal/mol)
19.4	-50.3

ΔH‡(kcal/mol)	ΔH°$_{RX}$ (kcal/mol)
17.9	-48.4

ΔS‡(cal/mol)
-5.1

Thermochemical data obtained from DFT calculations for the ligand exchange reactions **15 + 2 H₂O → 9 + hemiaminal.**
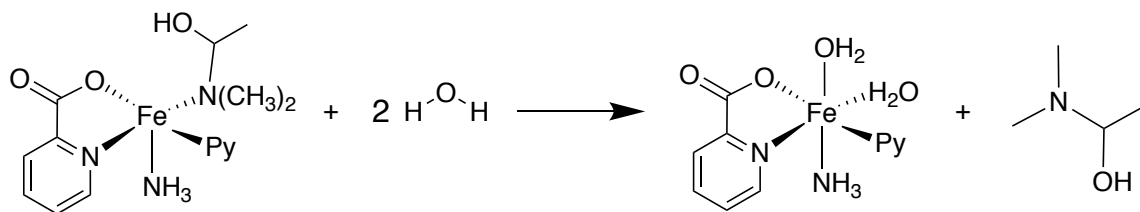
ΔG°$_{RX}$ (kcal/mol)	ΔH°$_{RX}$ (kcal/mol)
7.3	0.9

Thermochemical data obtained from DFT calculations for the redox/ligand exchange reaction **9 +
Me₂NEt + PhCO₃ᵗBu → 13 + PhCO₂H + ᵗBuOH + H₂O.**
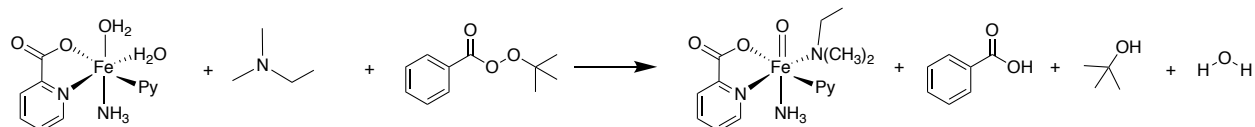
ΔG°$_{RX}$ (kcal/mol)	ΔH°$_{RX}$ (kcal/mol)
-17.5	-12.4

Thermochemical data from an alternative DFT functional: intramolecular H-atom abstraction
using M06-2X/6-311+G (2d,2p)

Thermochemical data obtained from DFT calculations for the reaction **13 → [TS] → 15**
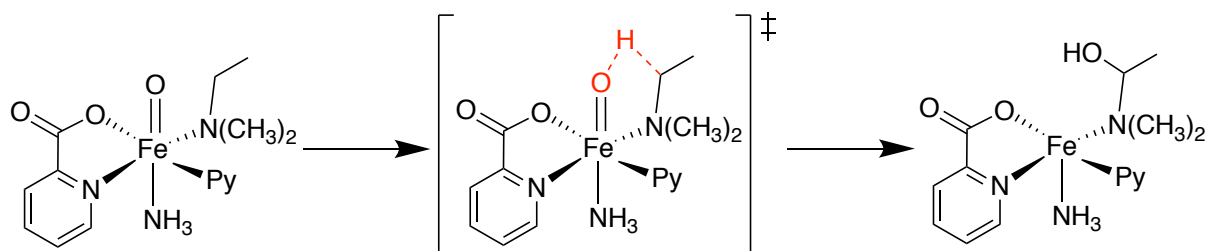
ΔG‡ (kcal/mol)	ΔG°$_{RX}$ (kcal/mol)
14.4	-84.1

ΔH‡ (kcal/mol)	ΔH°$_{RX}$ (kcal/mol)
12.8	-82.3

ΔS‡ (cal/mol)
-5.4

Thermochemical data obtained from DFT calculations for the ligand exchange reactions **15 + 2 H₂O → 9 + hemiaminal.**
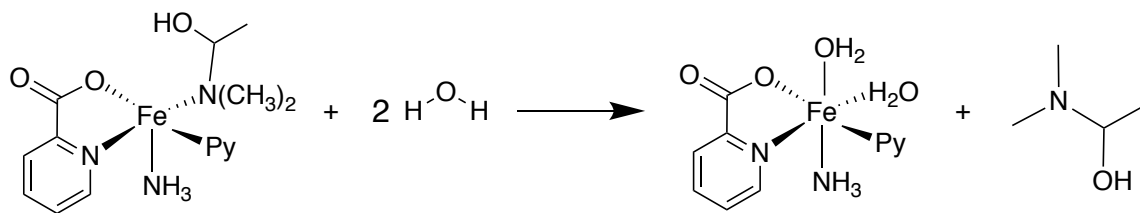
ΔG°$_{RX}$ (kcal/mol)	ΔH°$_{RX}$ (kcal/mol)
6.9	-0.2

Thermochemical data obtained from DFT calculations for the redox/ligand exchange reaction **9 + Me₂NEt + PhCO₃^{t}Bu → 13 + PhCO₂H + ^{t}BuOH + H₂O.**
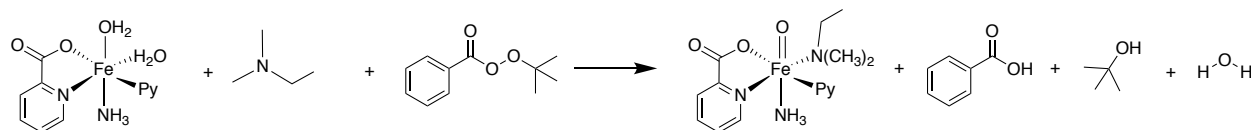
ΔG°$_{RX}$ (kcal/mol)	ΔH°$_{RX}$ (kcal/mol)
14.5	20.4

Thermochemical data from an alternative DFT functional: intramolecular H-atom abstraction using ωB97XD/6-311+G (2d,2p)

Thermochemical data obtained from DFT calculations for the reaction **13** → **[TS]** → **15**
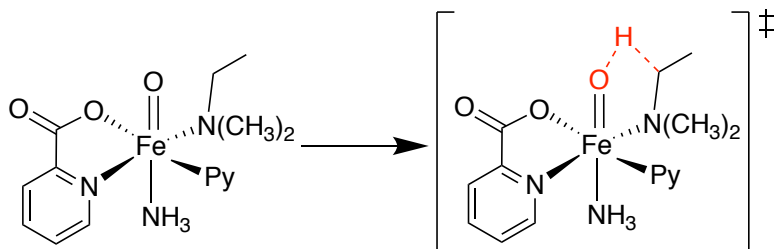
ΔG‡ (kcal/mol)	ΔH‡ (kcal/mol)
18.4	17.4

ΔS‡ (cal/mol)
-3.1

Thermochemical data from an alternative DFT functional: *inter*molecular H-atom abstraction using B3LYP/6-311+G (2d,2p)
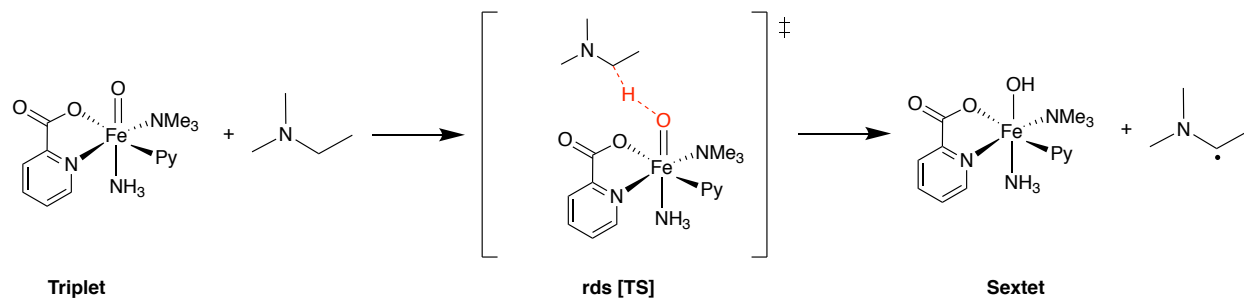
ΔG‡ (kcal/mol)	ΔG°$_{RX}$ (kcal/mol)
22.3	-10.7

ΔH‡ (kcal/mol)	ΔH°$_{RX}$ (kcal/mol)
12.3	-5.5

ΔS‡ (cal/mol)
-33.7

DFT energies and coordinates for selected compounds as obtained from B3LYP/6-311+G(2d,2p)//CPCM(pyridine)
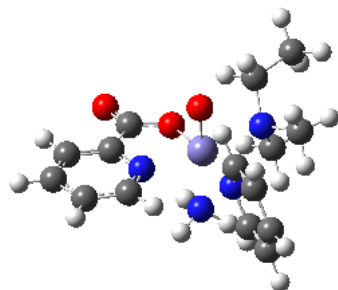
(13)

Zero-point correction=   0.381541 (Hartree/Particle)
Thermal correction to Energy=   0.405657
Thermal correction to Enthalpy=   0.406601
Thermal correction to Gibbs Free Energy=   0.327897
Sum of electronic and zero-point Energies= -2293.714864
Sum of electronic and thermal Energies=   -2293.690748
Sum of electronic and thermal Enthalpies=   -2293.689804
Sum of electronic and thermal Free Energies= -2293.768509

Fe   0.09019600 -0.32572800 0.03409200
O   -0.90518500 -1.95573600 0.25448100
C   -2.71019500 -0.47672000 -0.06363600
C   -2.12823700 1.76423100 -0.13341900
C   -4.05343500 -0.17937200 -0.21225100
C   -3.45756100 2.13620100 -0.28094100
H   -1.34431200 2.50324400 -0.10184600
C   -4.43550700 1.15175400 -0.32473700
H   -4.76743700 -0.98794500 -0.23557100
H   -3.70766700 3.18295200 -0.36195000
H   -5.47626800 1.41592900 -0.44275800
N   -1.76603700 0.48188700 -0.02593500
C   -2.19478200 -1.88198500 0.09391800
O   -2.94976400 -2.84186000 0.09639600
O   0.14782400 -0.36804900 -1.59372500
C   3.09290400 -0.70917300 -0.21123600
H   3.21372900 0.08556700 0.51679000
H   3.98840900 -1.32875500 -0.18934900
H   2.97781500 -0.28197000 -1.20257200
C   2.08608800 -2.12320900 1.46426800
H   2.95284500 -2.78237300 1.46554500
H   2.27509600 -1.34270600 2.19424900
H   1.20613800 -2.69612000 1.74146900
C   1.72930700 -2.61813300 -0.90821100
H   1.57540800 -2.11372700 -1.85676600

```
H        0.80779100  -3.13328800  -0.65937000
N        1.89399100  -1.52102800   0.12001400
H        0.66456300  -0.17432300   2.79973300
H       -0.74730900   0.56208000   2.46922300
H       -0.64332000  -1.05943500   2.43810000
N       -0.14644200  -0.20823000   2.19144000
C        2.86972300  -3.62768300  -1.03365500
H        3.01922300  -4.21805700  -0.13158400
H        2.59749400  -4.32120000  -1.82957400
H        3.81743000  -3.17179600  -1.31434000
N        1.05598000   1.53336100   0.02273900
C        1.47237500   2.18294700   1.12567900
C        1.24914400   2.13719900  -1.16616400
C        2.07859500   3.42724900   1.08458600
H        1.32592000   1.69742900   2.07393200
C        1.84661600   3.38090700  -1.28654500
H        0.90961700   1.58772900  -2.02912100
C        2.27161700   4.04409400  -0.14377900
H        2.39032100   3.89263800   2.00719200
H        1.97229600   3.81173800  -2.26832400
H        2.74177100   5.01470200  -0.20779400
```
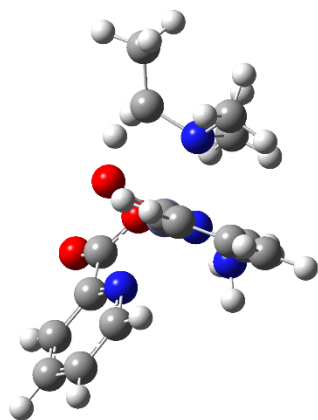

(TS)

Zero-point correction=   0.374641 (Hartree/Particle)
Thermal correction to Energy=   0.398259
Thermal correction to Enthalpy=   0.399203
Thermal correction to Gibbs Free Energy=   0.322250
Sum of electronic and zero-point Energies= -2293.688897
Sum of electronic and thermal Energies=   -2293.665279
Sum of electronic and thermal Enthalpies=   -2293.664335
Sum of electronic and thermal Free Energies= -2293.741289

```
Fe       0.04842800  -0.35930400   0.19999400
```

O	-1.16462300	-1.83522700	0.42742400
C	-2.72721100	-0.14325400	-0.08475400
C	-1.86498200	2.00114900	-0.18501500
C	-4.01294000	0.31449800	-0.31628400
C	-3.12684600	2.53299800	-0.41489400
H	-0.99697700	2.63800900	-0.12808300
C	-4.21795600	1.67811100	-0.48671900
H	-4.82203000	-0.39816000	-0.35483600
H	-3.23822400	3.59972200	-0.53574800
H	-5.20967800	2.06593200	-0.66860100
N	-1.66888400	0.68825200	-0.02581800
C	-2.41343400	-1.59843100	0.15265400
O	-3.29004600	-2.44952300	0.11288600
O	0.14736400	-0.56073100	-1.54839000
C	2.99825100	-1.18752100	0.16694100
H	3.15491200	-0.58621200	1.05654200
H	3.77757500	-1.94852100	0.12792900
H	3.07314600	-0.55261600	-0.70925300
C	1.59598700	-2.72589400	1.40329900
H	2.31470900	-3.53862300	1.28811400
H	1.85377800	-2.17253900	2.30276100
H	0.59568100	-3.13428400	1.49558100
C	1.34993800	-2.57077000	-1.00872800
H	0.74314400	-1.61997200	-1.65416300
H	0.52689500	-3.24823900	-0.81066800
N	1.65554400	-1.81769600	0.22303700
H	0.68532500	-0.29804800	2.86703300
H	-0.56039200	0.70904900	2.57213200
H	-0.78416300	-0.90285300	2.54997200
N	-0.13519900	-0.16736300	2.28402100
C	2.45667600	-3.17200400	-1.83457500
H	3.03172200	-3.90608800	-1.26037300
H	2.01194100	-3.69742900	-2.67836200
H	3.15228000	-2.43230900	-2.22549600
N	1.24622100	1.34208500	0.09484300
C	1.78825000	1.95812600	1.16143100
C	1.46581700	1.88718300	-1.11787800
C	2.54739900	3.11214800	1.06152000
H	1.61893900	1.51865300	2.12907900
C	2.21171800	3.04050300	-1.29686400
H	1.02857200	1.35982600	-1.95043100
C	2.76576600	3.66987000	-0.19063200
H	2.95554300	3.55500300	1.95726500
H	2.35060200	3.42860100	-2.29460600
H	3.35364000	4.56964600	-0.30059700
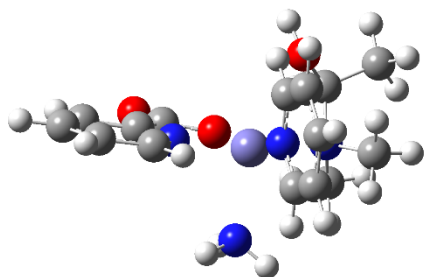
(15)

Zero-point correction=   0.377703 (Hartree/Particle)
Thermal correction to Energy=   0.403986
Thermal correction to Enthalpy=   0.404930
Thermal correction to Gibbs Free Energy=   0.317992
Sum of electronic and zero-point Energies= -2293.793822
Sum of electronic and thermal Energies=   -2293.767539
Sum of electronic and thermal Enthalpies= -2293.766595
Sum of electronic and thermal Free Energies=   -2293.853533

```
Fe     -0.28420600  -0.15139400  0.43119400
O      -0.01409300  -1.23269500  -1.22653600
C       2.21632800  -1.53394700  -0.47435200
C       2.80637700  -0.44282700  1.47072500
C       3.49474200  -2.05475600  -0.62069900
C       4.10739100  -0.92322100  1.39722900
H       2.50052800  0.20565700  2.28070500
C       4.45662500  -1.74519400  0.33275400
H       3.71347200  -2.68376700  -1.46929300
H       4.82392600  -0.65332800  2.15847800
H       5.46071000  -2.13512900  0.24600200
N       1.87791800  -0.74412800  0.55743200
C       1.11515700  -1.80833200  -1.48145500
O       1.34207100  -2.52426100  -2.45246900
C      -3.34844500  0.71013000  0.87826600
H      -2.84164700  1.65954700  1.03585500
H      -4.36593600  0.91975900  0.54048800
H      -3.39629900  0.17225200  1.82017100
C      -2.68960600  0.57486900  -1.44282300
H      -3.72480800  0.64845700  -1.78558000
H      -2.28862700  1.58191700  -1.36686600
H      -2.10760200  0.01613400  -2.17089400
C      -3.05358400  -1.48602700  -0.21056800
H      -2.50307600  -1.91359400  -1.04871200
N      -2.59094400  -0.07950800  -0.12042100
H      -1.03798200  0.23987500  3.08312900
H      -1.34659300  -1.25778400  2.49830200
H       0.15796700  -0.86393500  3.02145500
```

```
N      -0.65254200 -0.51298800 2.52236500
O      -2.61746100 -2.10805900 1.00280100
H      -3.04215000 -2.96802700 1.08242900
C      -4.54906600 -1.69817300 -0.41529900
H      -4.74193100 -2.76383100 -0.54270800
H      -5.12690500 -1.34515700 0.43671300
H      -4.90054300 -1.19765200 -1.31596100
N      0.19835700 1.90102500 -0.03827000
C      0.15191300 2.88959000 0.87103500
C      0.63090100 2.20122300 -1.27559500
C      0.52386000 4.19342200 0.58307900
H      -0.19403600 2.62419100 1.85989000
C      1.01994900 3.47917000 -1.64312100
H      0.66094400 1.38647100 -1.98502400
C      0.96588100 4.49680600 -0.69821100
H      0.46539600 4.94828700 1.35273300
H      1.35774100 3.66515000 -2.65149700
H      1.26260600 5.50367400 -0.95475700
```
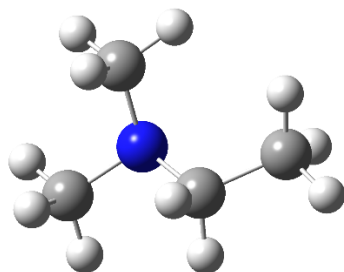

(Me₂NEt)

Zero-point correction=   0.148123 (Hartree/Particle)
Thermal correction to Energy=   0.154913
Thermal correction to Enthalpy=   0.155857
Thermal correction to Gibbs Free Energy=   0.118482
Sum of electronic and zero-point Energies=   -213.715925
Sum of electronic and thermal Energies=   -213.709134
Sum of electronic and thermal Enthalpies=   -213.708190
Sum of electronic and thermal Free Energies=   -213.745565

```
N      -0.45504400 -0.00353400 -0.32895900
C      0.71750200 -0.61721300 0.30314200
H      0.69947400 -1.67834300 0.05025500
H      0.64350600 -0.55500400 1.40283700
C      -0.65487100 1.37952500 0.09369500
H      0.20384100 1.99159900 -0.17347600
H      -0.81441000 1.46650900 1.18154000
C      -1.65454200 -0.79213500 -0.06537400
H      -2.50646700 -0.35280100 -0.58393600
```

```
C        2.04699800 -0.02560300 -0.15413700
H        2.16509500  1.01393100  0.14995300
H        2.13995800 -0.07656300 -1.23958000
H       -1.51783900 -1.80921700 -0.43179500
H       -1.52886000  1.79119400 -0.41004600
H        2.87091800 -0.58935700  0.28471500
H       -1.90042800 -0.84465400  1.00828500
```

(H₂O)
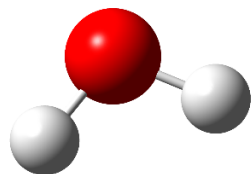
Zero-point correction=   0.021267 (Hartree/Particle)
Thermal correction to Energy=   0.024102
Thermal correction to Enthalpy=   0.025046
Thermal correction to Gibbs Free Energy=   0.003622
Sum of electronic and zero-point Energies=   -76.447253
Sum of electronic and thermal Energies=   -76.444418
Sum of electronic and thermal Enthalpies=   -76.443473
Sum of electronic and thermal Free Energies= -76.464898

```
O        0.00000000  0.00000000  0.11758300
H        0.00000000  0.76175400 -0.47033300
H        0.00000000 -0.76175400 -0.47033300
```
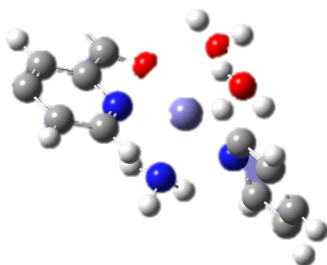
(9)

Zero-point correction=   0.271290 (Hartree/Particle)
Thermal correction to Energy=   0.294577
Thermal correction to Enthalpy=   0.295521
Thermal correction to Gibbs Free Energy=   0.216261
Sum of electronic and zero-point Energies= -2157.721034
Sum of electronic and thermal Energies=   -2157.697747
Sum of electronic and thermal Enthalpies=   -2157.696803
Sum of electronic and thermal Free Energies= -2157.776062

```
Fe    -0.14169000 -0.82879500 -0.09360900
N      1.29127300  0.84243600 -0.13554300
C      2.56080700  0.41574900 -0.00778300
C      1.06215000  2.15311800 -0.27629700
C      3.63682500  1.29229500 -0.00899300
C      2.08501600  3.09159600 -0.28905800
H      0.03023700  2.45688500 -0.38392700
C      3.39591200  2.65312900 -0.15027300
H      4.63462700  0.89680900  0.09803100
H      1.85078200  4.13916900 -0.40454500
H      4.21494900  3.35806000 -0.15386100
C      2.75250800 -1.08715300  0.12799600
O      3.88918300 -1.54063100  0.24669600
O      1.66519300 -1.77639500  0.10071700
H      0.78048200 -1.31088700 -2.55330400
H     -0.74940800 -1.84183700 -2.65500800
H     -0.42529700 -0.25212200 -2.81715600
O     -0.26106500 -0.79302400  2.21035400
N     -0.17551700 -1.08598100 -2.29465700
H      0.55734300 -0.60381900  2.68284100
C     -2.39292400  1.04829600  0.92107300
C     -3.61958200  1.68689000  1.00852700
C     -4.62205100  1.34233500  0.11066900
C     -4.35707200  0.36898100 -0.84463800
C     -3.10163900 -0.21658300 -0.87039000
N     -2.12643700  0.11111800 -0.00556900
H     -5.58999800  1.82067500  0.15552600
H     -1.59865100  1.27713700  1.61471900
H     -3.77900500  2.43531100  1.77003600
H     -5.10477000  0.06420400 -1.56114600
H     -2.86702100 -0.97642200 -1.60103400
H     -0.49367800 -1.70115000  2.44091700
O     -0.76045100 -2.99394300  0.46913700
H     -1.43682000 -3.48458800 -0.01092500
H      0.07235800 -3.46175700  0.32282300
```
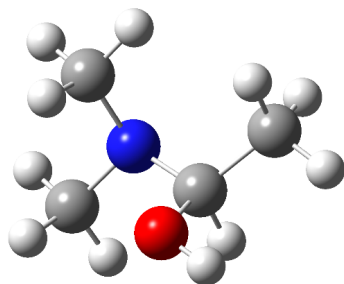
(Me₂NCH(OH)Me)

Zero-point correction=   0.152433 (Hartree/Particle)
Thermal correction to Energy=   0.160526
Thermal correction to Enthalpy=   0.161471
Thermal correction to Gibbs Free Energy=   0.121033
Sum of electronic and zero-point Energies=   -288.964309
Sum of electronic and thermal Energies=   -288.956216
Sum of electronic and thermal Enthalpies=   -288.955272
Sum of electronic and thermal Free Energies= -288.995709

N	-0.65433800	0.25215800	-0.38163900
C	0.64933800	-0.35183300	-0.32438100
H	0.67963100	-1.09127400	-1.12868100
C	-0.93218000	1.27684300	0.62424600
H	-0.16899900	2.05082500	0.60579000
H	-0.99603900	0.87392800	1.64264900
C	-1.73709400	-0.72697600	-0.45766600
H	-2.66493500	-0.21717600	-0.71716700
C	1.79258500	0.63552600	-0.51941500
H	1.85914200	1.34131300	0.30648400
H	1.66283700	1.18734600	-1.44997100
H	-1.51912600	-1.45538300	-1.23819800
H	-1.88632500	1.74691300	0.38744400
H	2.73773200	0.09503300	-0.57446500
H	-1.89666100	-1.26753300	0.48380000
O	0.81004200	-1.06367600	0.93679100
H	1.65687100	-1.52105000	0.92275400

155
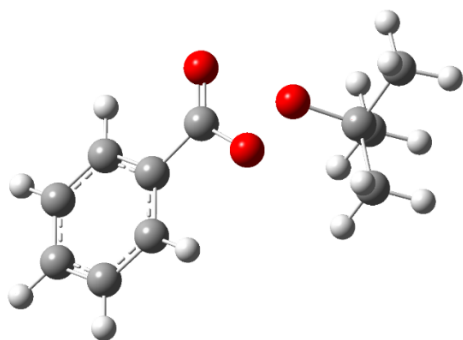
(PhCO₃ᵗBu)

Zero-point correction=   0.229044 (Hartree/Particle)
Thermal correction to Energy=   0.243171
Thermal correction to Enthalpy=   0.244116
Thermal correction to Gibbs Free Energy=   0.186484
Sum of electronic and zero-point Energies=   -653.193858
Sum of electronic and thermal Energies=   -653.179730
Sum of electronic and thermal Enthalpies=   -653.178786
Sum of electronic and thermal Free Energies=   -653.236417


```
C      -4.25694400  0.69089400  0.21871300
C      -3.23191400  1.57920300 -0.09683100
C      -1.93545600  1.11378200 -0.27809700
C      -1.65987600 -0.25152200 -0.14522300
C      -2.69226500 -1.13974000  0.16965300
C      -3.98537000 -0.66891900  0.35191800
H      -5.26460000  1.05707700  0.35892200
H      -3.44218800  2.63409800 -0.20317300
H      -1.14542200  1.80547600 -0.52639200
H      -2.46937800 -2.19170200  0.26846000
H      -4.77988600 -1.35975900  0.59644200
C      -0.29488600 -0.82261200 -0.32843500
O      -0.02579900 -1.99695300 -0.32480300
O       0.61628000  0.17736100 -0.50636900
O       1.93658000 -0.34944000 -0.78041200
C       2.89256500  0.23994200  0.16222300
C       4.19580100 -0.39746900 -0.32097400
H       4.40480500 -0.12173300 -1.35373100
H       5.01643500 -0.04481100  0.30218500
H       4.14937700 -1.48306400 -0.24707600
C       2.92016300  1.75792800  0.00220200
H       3.11574000  2.03051700 -1.03435300
H       1.97588600  2.20334000  0.30982200
H       3.71007500  2.17863400  0.62407200
C       2.55879000 -0.18447800  1.58946500
H       2.52285100 -1.26986300  1.67060800
```

H   3.32435800 0.18683200 2.27041500
H   1.60182200 0.22516700 1.90878200
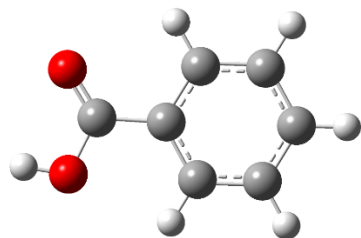
(PhCO₂H)

Zero-point correction=   0.115132 (Hartree/Particle)
Thermal correction to Energy=   0.122286
Thermal correction to Enthalpy=   0.123230
Thermal correction to Gibbs Free Energy=   0.082947
Sum of electronic and zero-point Energies=   -420.854281
Sum of electronic and thermal Energies=   -420.847127
Sum of electronic and thermal Enthalpies=   -420.846183
Sum of electronic and thermal Free Energies= -420.886466

C   1.83592800 -1.23276500 -0.00001800
C   0.44692900 -1.19758000 -0.00003000
C   -0.21989300 0.03169200 -0.00002700
C   0.51599800 1.22035400 -0.00001000
C   1.90332700 1.18067100 0.00000200
C   2.56463900 -0.04599300 -0.00000200
H   2.34912000 -2.18407200 -0.00002100
H   -0.11839600 -2.11684400 -0.00004400
H   -0.00903400 2.16413400 -0.00000800
H   2.46887500 2.10179100 0.00001400
H   3.64551500 -0.07655600 0.00000800
C   -1.70150800 0.12030800 -0.00004600
O   -2.33194300 1.15712200 0.00002700
O   -2.31082000 -1.08468200 0.00006300
H   -3.26649400 -0.92810400 0.00012300
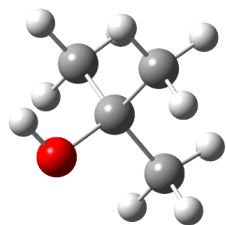
(ᵗBuOH)

Zero-point correction=   0.134988 (Hartree/Particle)
Thermal correction to Energy=   0.141764
Thermal correction to Enthalpy=   0.142708
Thermal correction to Gibbs Free Energy=   0.105947
Sum of electronic and zero-point Energies=   -233.632105
Sum of electronic and thermal Energies=   -233.625328
Sum of electronic and thermal Enthalpies=   -233.624384
Sum of electronic and thermal Free Energies= -233.661146

C	0.00314500	0.01142100	0.00000000
C	0.00314500	-0.85611600	1.26153000
H	0.87566300	-1.51199800	1.27854500
H	0.02597800	-0.23026000	2.15353500
H	-0.88793100	-1.48340400	1.30275500
C	0.00314500	-0.85611600	-1.26153000
H	-0.88793100	-1.48340400	-1.30275500
H	0.02597800	-0.23026000	-2.15353500
H	0.87566300	-1.51199800	-1.27854500
C	-1.17890800	0.97688900	0.00000000
H	-1.15211200	1.61346000	0.88449300
H	-1.15211200	1.61346000	-0.88449300
H	-2.12015000	0.42793200	0.00000000
O	1.18174300	0.85640200	0.00000000
H	1.95984600	0.28879400	0.00000000

MECHANISTIC EVIDENCE FOR A RADICAL-RADICAL RECOMBINATION PATHWAY OF FLAVIN-BASED PHOTOCATALYTIC TYROSINE LABELING

Absorption and Emission Spectra

Absorption and emission spectra were recorded in 1:1 water:acetonitrile in quartz cuvettes.

λ_{ex} = 445 nm

ε = 11638 $M^{-1} s^{-1}$

λ_{00} = 488 nm

(E_{00} = 2.54 eV)

λ_{em} = 520 nm

Φ_{fluor} = 0.31

$\tau_{0\ fluor}$ = 3.2 ns
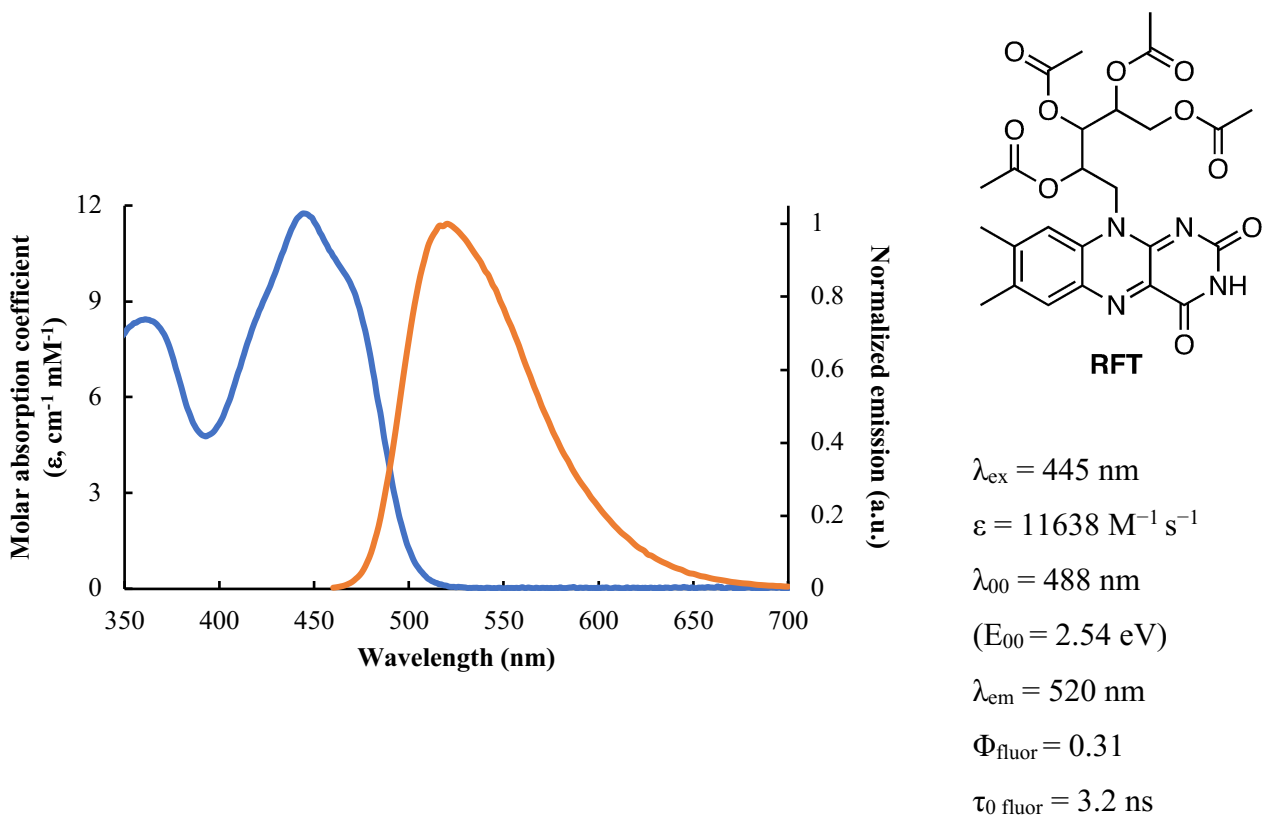
Figure D.1. Normalized absorption (blue) and emission (solvent corrected, orange λ_{ex} = 445 nm) spectrum of **RFT** in 1:1 water:acetonitrile.
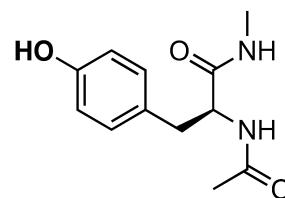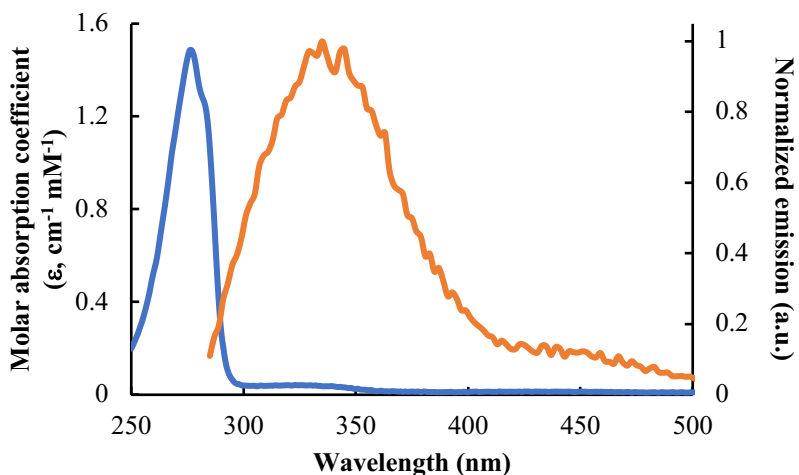
λ_{max} = 276 nm

(ε = 1471 M^{-1} cm^{-1})

λ_{em} = 335 nm

Figure D.2. Normalized absorption (blue) and emission (solvent corrected, orange λ_{ex} = 276 nm) spectrum of **Ac-Tyr-NHMe** in 1:1 water:acetonitrile.
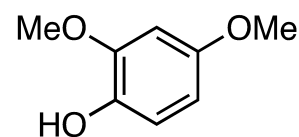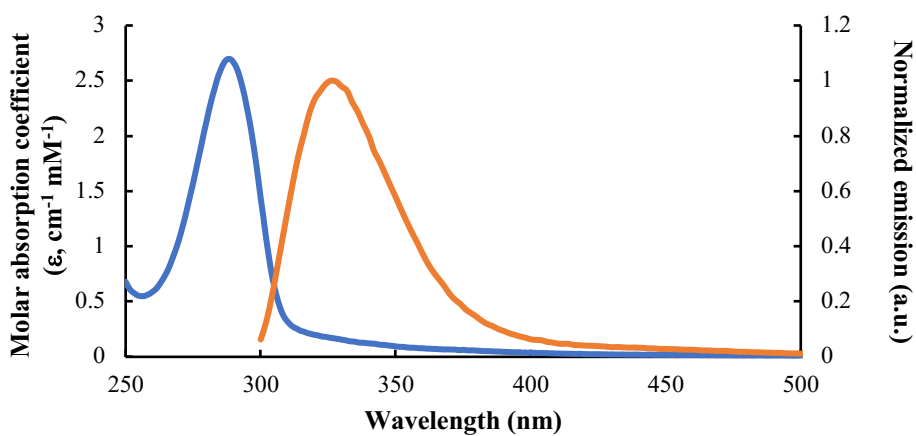
λ_{max} = 288 nm

(ε = 2829 M^{-1} cm^{-1})

λ_{em} = 323 nm

Figure D.3. Normalized absorption (blue) and emission (solvent corrected, orange λ_{ex} = 288 nm) spectrum of **2,4-dimethoxyphenol** in 1:1 water:acetonitrile
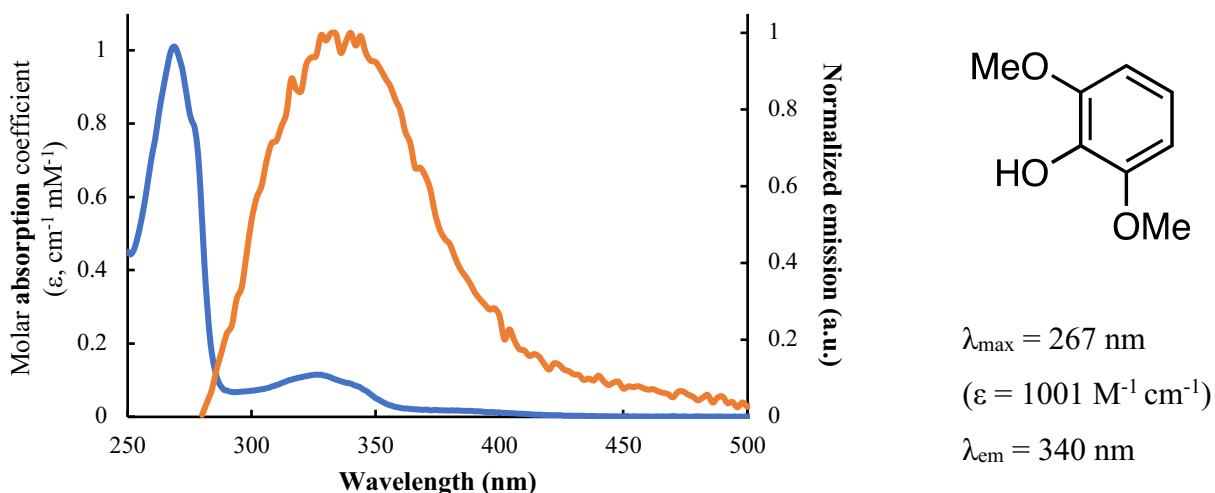
Figure D.4. Normalized absorption (blue) and emission (solvent corrected, orange λ_{ex} = 267 nm) spectrum of **2,6-dimethoxyphenol** in 1:1 water:acetonitrile

Fluorescence Lifetime Measurements

Fluorescence lifetime measurement was performed using time resolved fluorescence on a PTI QuantaMaster 40 (Horiba). In a 1 x 1 cm quartz cuvette a solution of RFT (0.0093 mM in 1:1 water:acetonitrile) was excited at 456 nm and the emission was measured at 520 nm; the irritation wavelength was chosen due to the limited selection of pulsed LED lights available. To the trace a mono-exponential decay was fitted and corrected for the instrument response factor (IRF) using LUDOX® and setting the emission wavelength to the excitation wavelength (456 nm). The fluorescence lifetime of **RFT** in 1:1 water:acetonitrile is 3.2 ns (Figure D.5).

The lifetime was measured with a start delay of 55 ns and an end delay of 90ns. The integration was set to 20 seconds in random collection mode with the slits at 1.00 mm 1.00 mm.
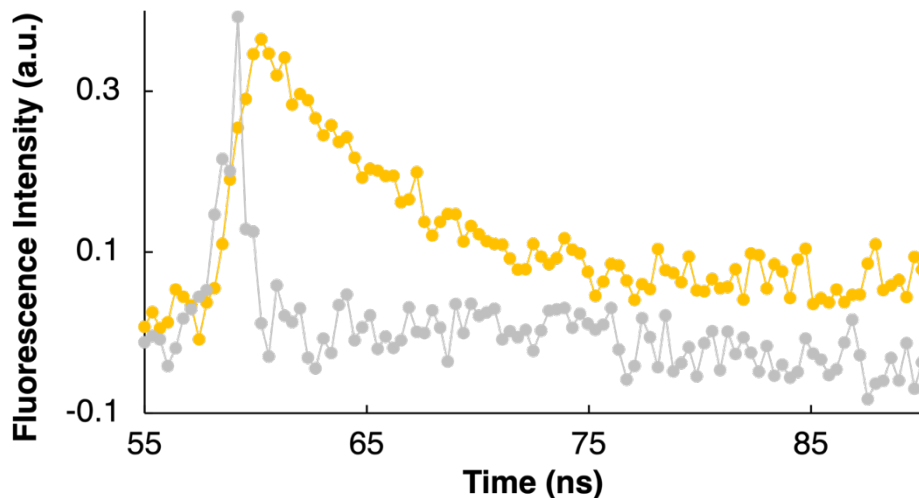
Figure D.5. Fluorescence lifetime measurement of **RFT** (orange) in 1:1 water:acetonitrile and the IRF (grey).

Relative Fluorescence Quantum Yield

The relative fluorescence quantum yield of **RFT** was determined by comparing an unknown quantum yield to that of fluorescein which has a known absolute quantum yield of 0.925 (Sjöback *et al.,* 1995). The slits were set to 0.5 mm corresponding to a 2 nm resolution.

In a 1 x 1 cm quartz cuvette, emission spectra were recorded at 450 nm, first collecting a blank to correct for any emission arising from the solvent. The samples were then added into the cuvettes in small increments, without exceeding an absorption of 0.1 to minimize non-linear effects. The blank for fluorescein is 0.1M NaOH, and for **RFT** the blank used was the solvent (1:1 water:acetonitrile). The integrated fluorescence was then graphed vs the absorbance at 450 nm (Figure D.6) and based on the equation below <u>the fluorescence quantum yield of RFT was found to be 0.31</u>.

The relative quantum yield was then calculated using the equation:

$$\Phi_{RFT} = \Phi_{std} * \left(\frac{m_{RFT}}{m_{std}}\right) * \left(\frac{\eta_{RFT}}{\eta_{std}}\right)^2 \qquad \text{Eq D.1}$$

Where Φ is quantum yield, m is the gradient of the plot of integrated fluorescence intensity against absorbance, and η is the refractive index of the solvent (Perkin Elmer, 2022). The refractive index for 0.1 M NaOH is 1.33 (water) and for acetonitrile is 1.34.
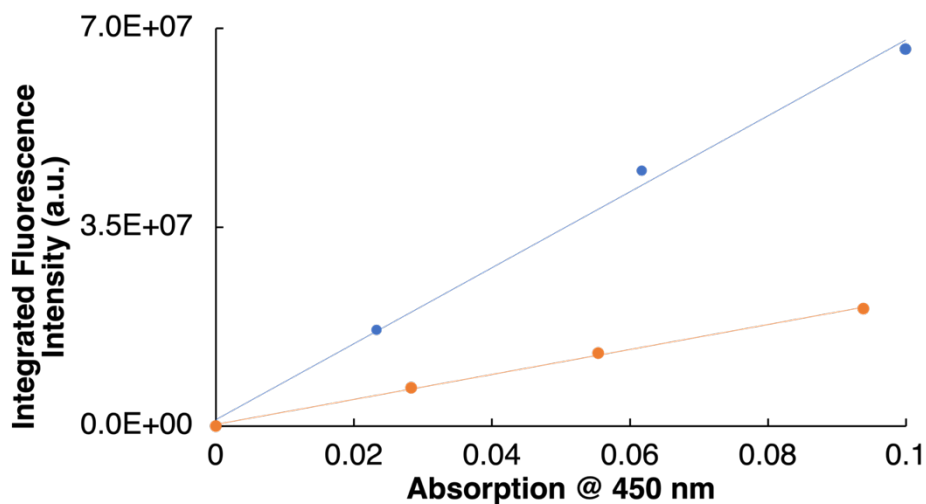
Figure D.6. Integrated fluorescence intensity of **RFT** (orange) and fluorescein (blue).

Catalyst Photostability

Photocatalyst stability was measured using the time-based option on the PTI QuantaMaster 40 (Horiba). In a 1 x 1 cm quartz cuvette a solution of **RFT** ($A_{445 \, nm}$ = 0.093 in 1:1 water:acetonitrile) with constant stirring via a stir bar was excited at 445 nm and the emission was measured at 520 nm. The scan took place over 7200 seconds, collecting ~1 data point every minute. The slits were set to 0.25 mm 0.25 mm 4.00 mm 4.00 mm.

The scans were also run with only solvent to ensure that the change in photocatalyst stability was due to the change in fluorescence of the photocatalyst, and a final test was done with **LUDOX**® in the cuvette to ensure that the light intensity remained constant over the 2 hour scan where the excitation wavelength was set to 445 nm and emission wavelength was set to 458 nm, and the slits were adjusted to match the initial fluorescence intensity (IRF).

RFT photostability was measured in the presence and absence of various phenol (2,6-dimethoxyphenol and 2,4-dimethoxyphenol, 84.4 mM in 1:1 water:acetonitrile), the results are summarized in Figure D.7.
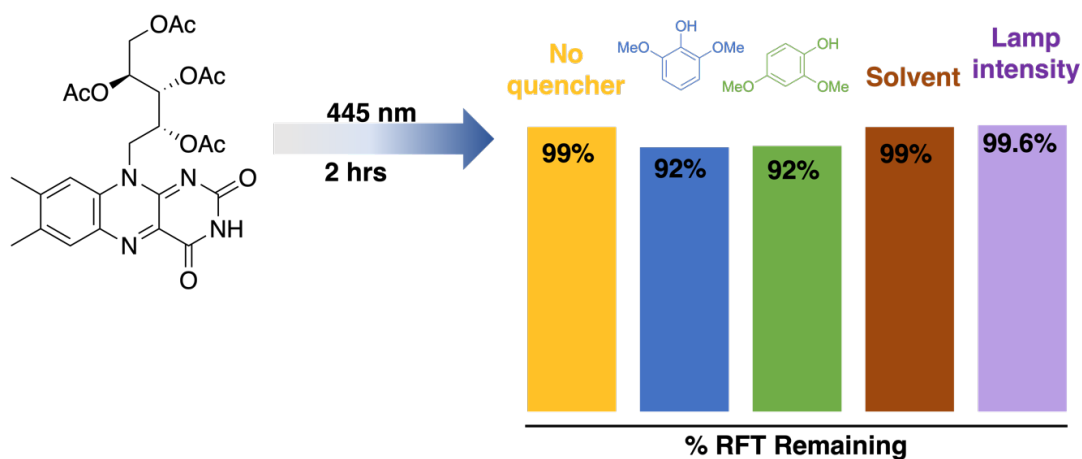
Figure D.7. **RFT** Photocatalyst stability over 2 hours with and without phenols.

Laser Flash Photolysis

The transient absorption decay monitored at 700 nm (Figure D.8 – D.11) fits to mono-exponential decays and the resulting lifetimes were analyzed using Stern-Volmer quenching kinetics analysis, $\tau_0/\tau = 1 + k_q\tau_0[\text{phenol}]$, where τ_0 and τ are the observed lifetime without and with added phenol.
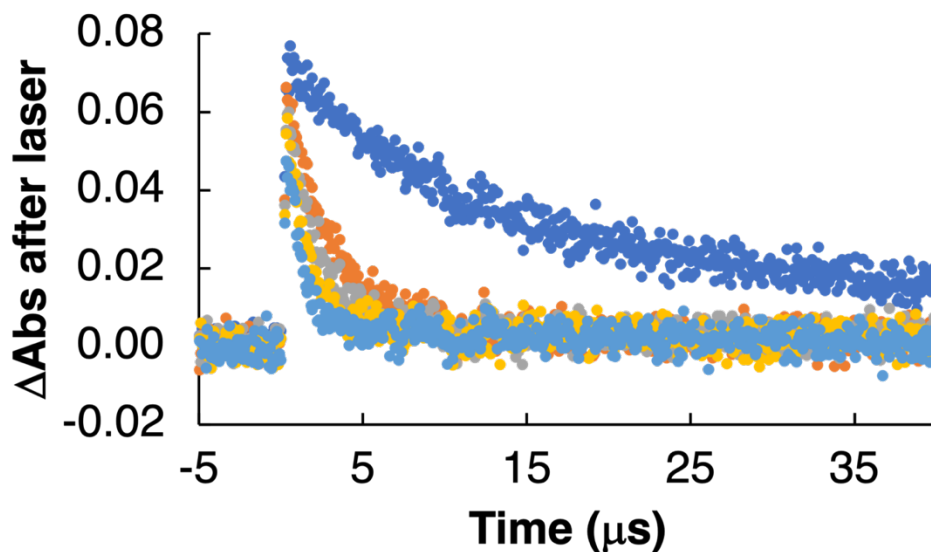
Figure D.8. Excited-state lifetime measurements for ^{3}**RFT*** ($\lambda_{mon} = 700$ nm) in the presence of 2,6-dimethoxyphenol (— 0, — 0.09, — 0.15, — 0.21, — 0.30 mM) in 1:1 water:acetonitrile under argon atmosphere.
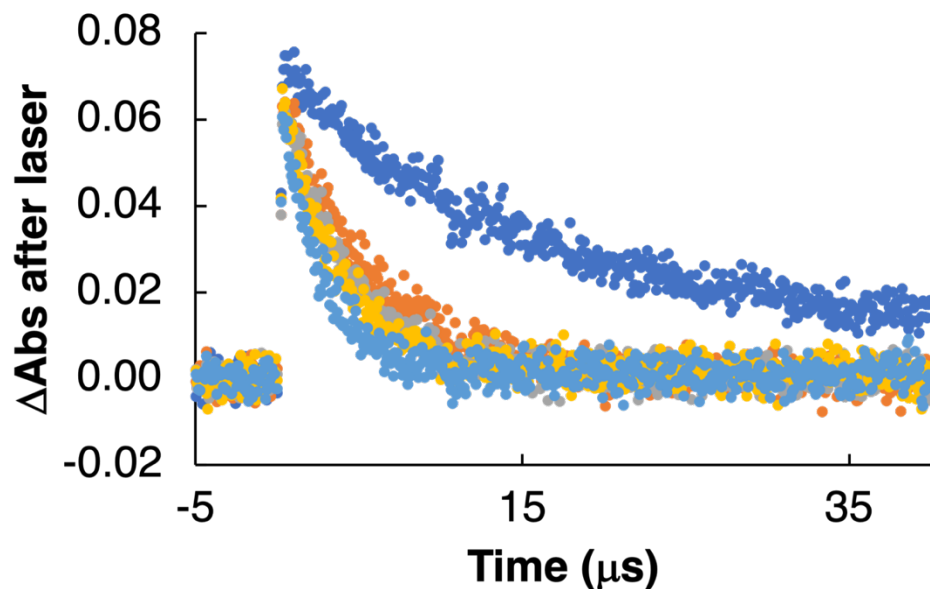
Figure D.9. Excited-state lifetime measurements for ^{3}**RFT*** (λ_{mon} = 700 nm) in the presence of Ac-Tyr-NHMe (— 0, — 0.09, — 0.15, — 0.21, — 0.30 mM) in 1:1 water:acetonitrile under argon atmosphere.
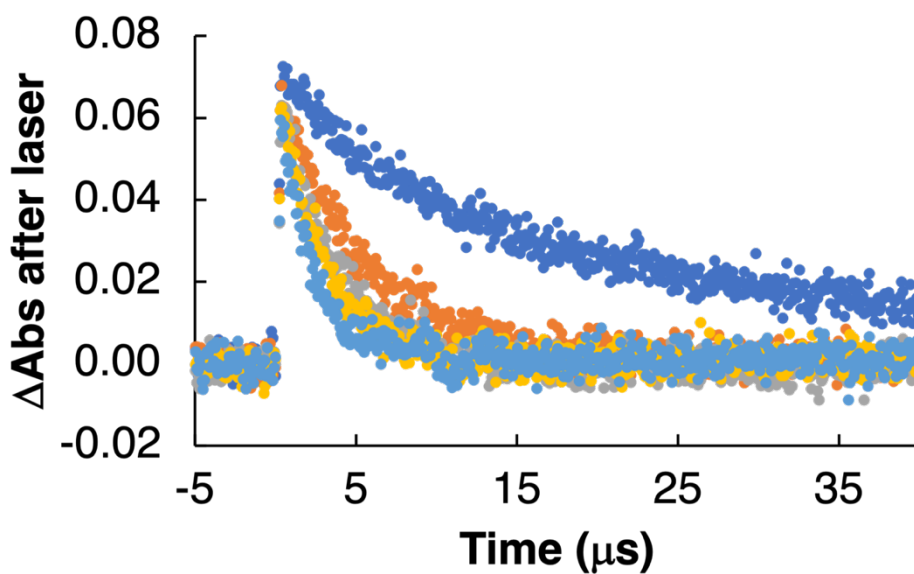
Figure D.10. Excited-state lifetime measurements for ^{3}**RFT*** (λ_{mon} = 700 nm) in the presence of biotin tyramine (— 0, — 0.09, — 0.15, — 0.21, — 0.30 mM) in 1:1 water:acetonitrile under argon atmosphere.
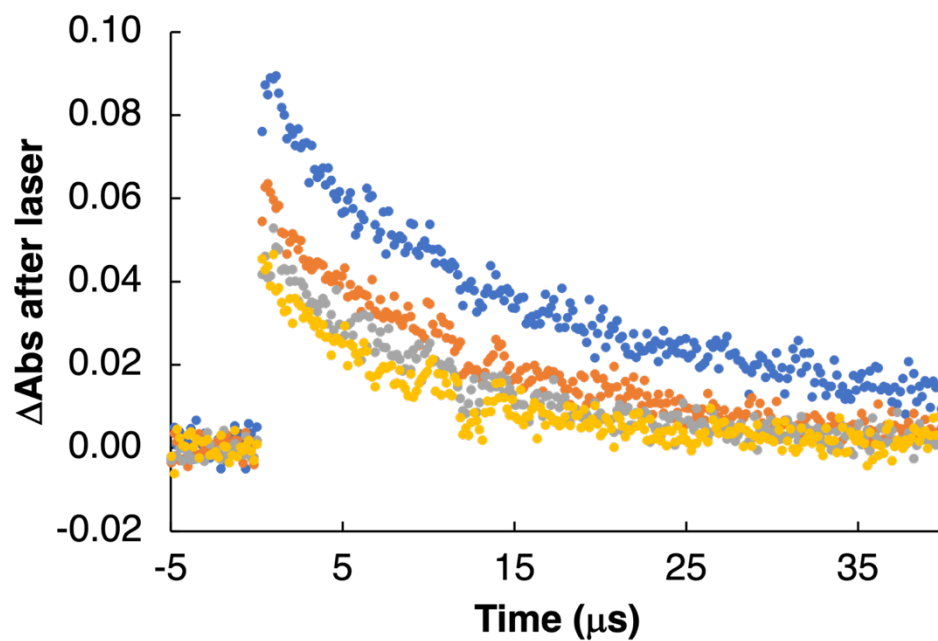
Figure D.11. Excited-state lifetime measurements for ^{3}**RFT*** (λ_{mon} = 700 nm) in the presence of BSA (— 0, — 0.101, — 0.204, — 0.297 mM) in PBS under argon atmosphere.

Reaction Between Phenols and Singlet Oxygen ($^1O_2$)
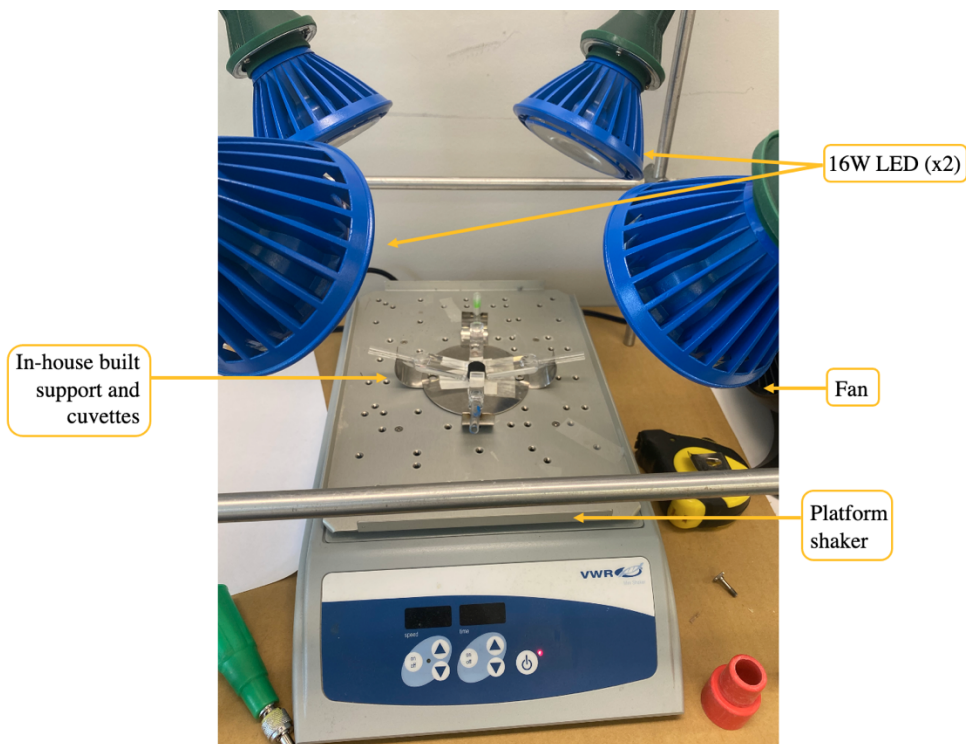
Figure D.13. Experimental Setup.
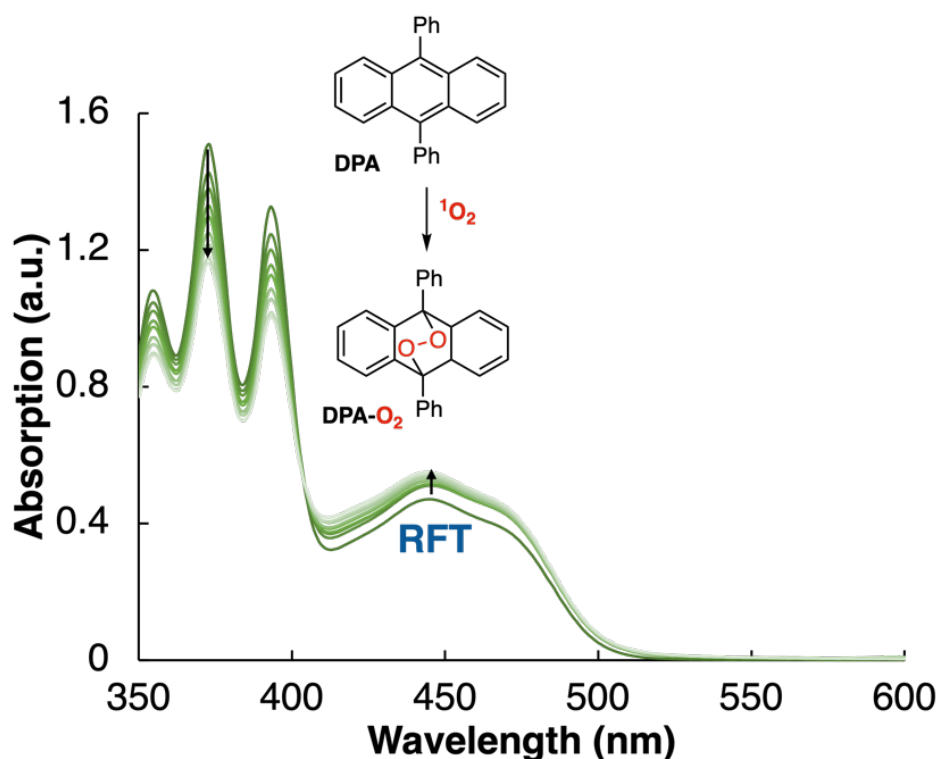
Figure D.14. Example of the simultaneous increase in absorption of **RFT** and decrease in absorption of **DPA** during blue-light irradiation caused by the cycloaddition of singlet oxygen and breaking of π-system conjugation. Impure reduced **RFT** oxidizes to the neutral form during irradiation causing the absorption of **RFT** to increase over 160 seconds. [RFT] = 0.042 mM, [DPA] = 0.1 mM and [2,6-dimethoxyphenol] = 1.31 mM (green cuvette).

Strangely, there was a slight absorption increase accounted for by the apparent *formation* of **RFT** during the irradiation at 450 nm. We postulate the increase of **RFT** is due to the oxidation of reduced **RFT** impurities in the photocatalyst, e.g., **RFT-H₂**, during irradiation. The reaction product between $^1O_2$ and phenols—HOO*—could explain the oxidation reaction and absorption increase. To properly quantify the change in **DPA** concentration during irradiation, it became necessary to deconvolute the contribution of **DPA**, **RFT** and phenol from the absorption spectra (Figure D.15).
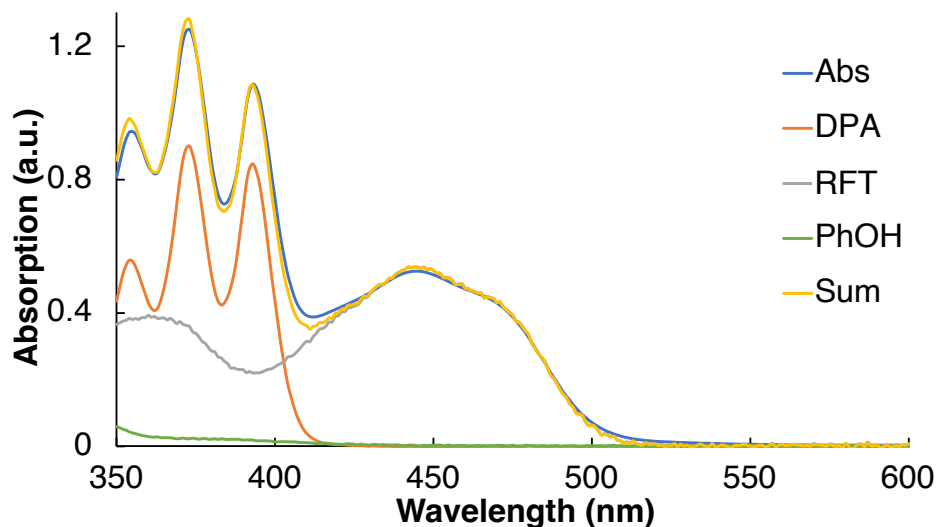
Figure D.15. Deconvolution of a UV-visible absorption spectrum (using 80 second irradiation time point as an example) using spectra corresponding to [RFT] = 0.042 mM, [DPA] = 0.1 mM and [2,6-dimethoxyphenol] = 1.31 mM (green cuvette). Similar deconvolutions were done for each irradiation time point to obtain the change in concentration of DPA over time.

To deconvolute the spectra we compared the sum of the absorption of each individual molecule using its molar absorption coefficient to recreate the absorption spectra and solve for the smallest difference in the absorption and sum by changing the concentration of DPA and RFT. (i.e. solving the (sum-abs)^2 and minimizing the concentration of DPA and RFT using the "solver" tool in excel). The equation was derived the following way:

$$\tau_0 = \frac{1}{k_d + k_q[DPA]}$$
Eq D.2

$$\tau_{PhOH} = \frac{1}{k_d + k_q[DPA] + k_r[PhOH]}$$
Eq D.3

$$\frac{\tau_0}{\tau_{PhOH}} = \frac{k_d + k_q[DPA] + k_r[PhOH]}{k_d + k_q[DPA]} = 1 + \frac{k_r[PhOH]}{k_d + k_q[DPA]}$$
Eq D.4

Φ_0 = fraction of excited states that react with DPA in the absence of PhOH

Φ_{PhOH} = fraction of excited states that react with DPA in the presence of PhOH

$$\Phi_0 = \frac{k_q[DPA]}{k_d + k_q[DPA]} \qquad \text{Eq D.5}$$

$$\Phi_{PhOH} = \frac{k_q[DPA]}{k_d + k_q[DPA] + k_r[PhOH]} \qquad \text{Eq D.6}$$

$$\frac{\Phi_0}{\Phi_{PhOH}} = \frac{k_d + k_q[DPA] + k_r[PhOH]}{k_d + k_q[DPA]} = 1 + \frac{k_r[PhOH]}{k_d + k_q[DPA]} \qquad \text{Eq D.7}$$

$$\frac{\tau_0}{\tau_{PhOH}} = \frac{\Phi_0}{\Phi_{PhOH}} \qquad \text{Eq D.8}$$

$$\frac{\Phi_0}{\Phi_{PhOH}} = \frac{-\Delta[DPA]_0/\Delta t}{-\Delta[DPA]_{PhOH}/\Delta t} = \frac{Slope_{DPA}}{Slope_{DPA+PhOH}} \qquad \text{Eq D.9}$$

$$\frac{Slope_{DPA}}{Slope_{DPA+PhOH}} = 1 + \frac{k_r[PhOH]}{k_d + k_q[DPA]} \qquad \text{Eq D.10}$$

Computational methods

Calculated energies key reactions using B3LYP/6-311+G(2d,2p)//CPCM(water)

Thermodynamic data obtained from DFT calculations. (R = tetraacetate side chain)

Table D.1. Oxidation of ^{3}[RFT]* with phenol.
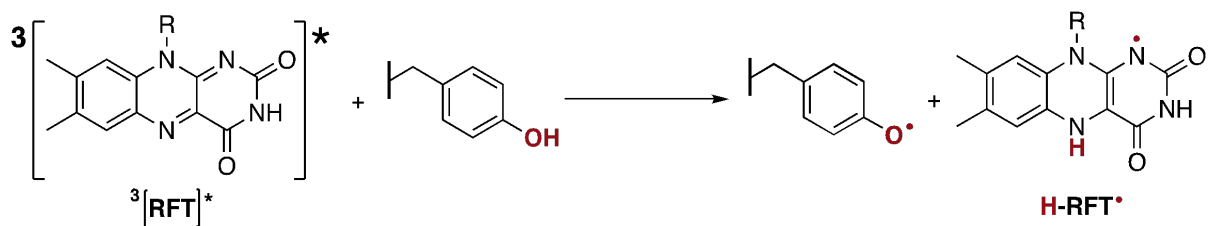
Phenol	ΔG (kcal/mol)	ΔH (kcal/mol)
Biotin tyramide	-18.9	-19.7
Ac-Tyr-NHMe	-19.2	-19.4
2,6-dimethoxyphenol	-25.3	-25.8

Table D.2. H-atom abstraction between **H-RFT•** and phenol.
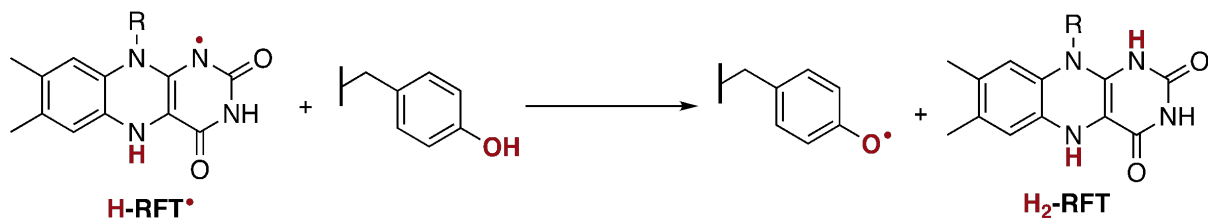
Phenol	ΔG (kcal/mol)	ΔH (kcal/mol)
Biotin tyramide	24.1	24.6
Ac-Tyr-NHMe	23.8	24.8
2,6-dimethoxyphenol	17.7	18.4

Table D.3. H-atom abstraction between $^1O_2$ and phenol.
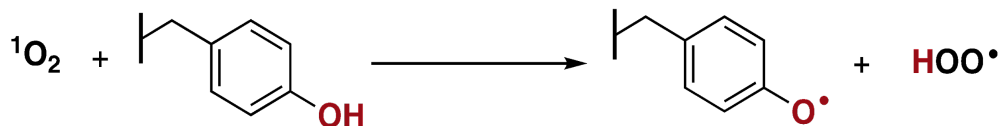
Phenol	ΔG (kcal/mol)	ΔH (kcal/mol)
Biotin tyramide	-12.2	-10.2
Ac-Tyr-NHMe	-12.5	-9.9
2,6-dimethoxyphenol	-18.6	-16.3

Table D.4 Calculated energies for phenoxyl radical-radical recombination pathway using B3LYP/6-311+G(2d,2p)//CPCM(water).

Phenoxyl radical   Tyrosyl radical   Diketone intermediate   Final coupled product
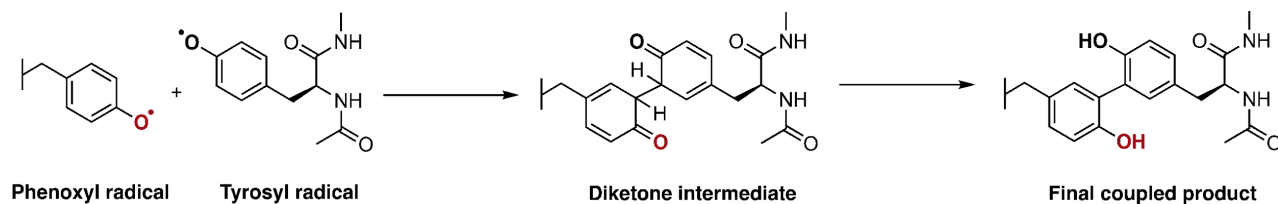
Entry	Phenoxyl radical	Diketone intermediate		Final Coupled Product	
		ΔG (kcal/mol)	ΔH (kcal/mol)	ΔG (kcal/mol)	ΔH (kcal/mol)
1		+11.37	-1.57	-36.30	-39.94
2		+9.44	-4.32	-37.75	-38.52
3		+6.53	-6.09	-38.89	-39.04
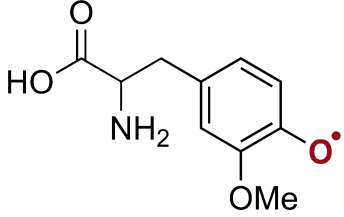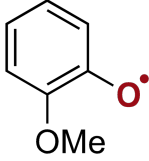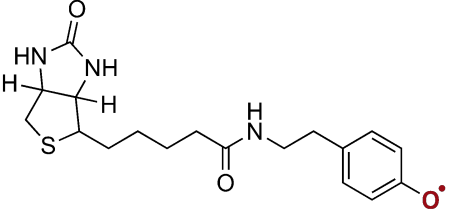
4		+8.25	-5.49	-39.27	-39.98
5		+7.61	-5.29	-37.84	-38.50
6		+8.15	-6.98	-39.08	-37.54

Table D.5. Calculated energies for the addition of a phenoxyl radical onto a neutral tyrosine using B3LYP/6-311+G(2d,2p)//CPCM(water).
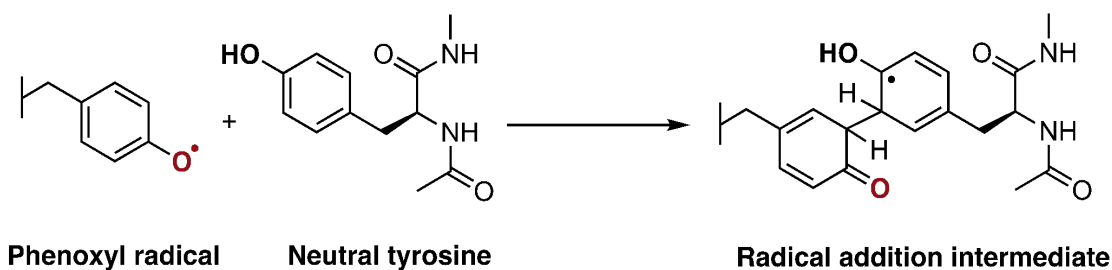
Entry	Phenoxyl radical (#)	ΔG (kcal/mol)	ΔH (kcal/mol)
1		+49.46	+37.47
2		+ 44.22	+ 30.71

173

Table D.6. Comparing DFT functionals: B3LYP vs ωB97XD to calculate energies for phenoxyl radical addition onto neutral tyrosine.
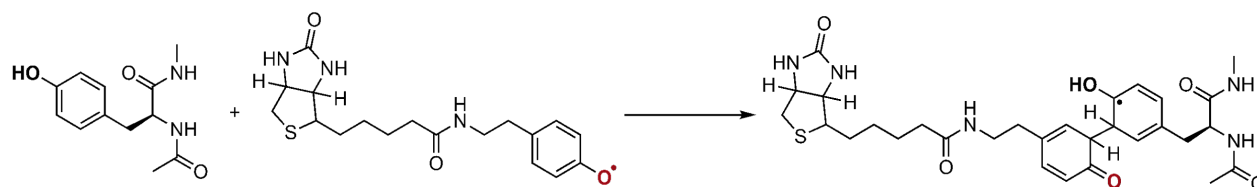
Functional	ΔH (kcal/mol)	ΔG (kcal/mol)
B3LYP	+ 30.71	+ 44.22
ωB97XD	+ 18.12	+ 32.02

The geometries were optimized at ωB97XD/6-311+G(2d,2p)//CPCM(water). The basis set used for both functionals was 6-311+G(2d,2p). The Gibbs free energy for this proposed step is not significantly different from the value obtained using B3LYP/6-311+G(2d,2p). Both functional's show that the energy for this step is prohibitively unfavorable.

Calculated energies for the phenoxyl radical and probe recombination pathway using B3LYP/6-311+G(2d,2p)//CPCM(water) from Sato and Nakamura

The addition of a phenoxyl radical onto a neutral aromatic system appears in the literature in several instances (Sato and Nakamura, 2013; Tsushima et al., 2017). We postulate this step is almost never favorable as the intermediate formed following phenoxyl radical addition will be prohibitively endergonic. Sato and Nakamura's "phenoxyl radical trap" (Table D.7) could possibly occur via the addition of a phenoxyl radical onto the oxidized trap (Table D.8), but this reaction is also significantly costly in ΔG. As expected, the recombination of two radicals will be more favorable (Table D.9) and the tautomerization to regenerate aromaticity is expected to yield a stable covalent bond.

174

Table D.7. Sato and Nakamura's "phenoxyl radical trap".
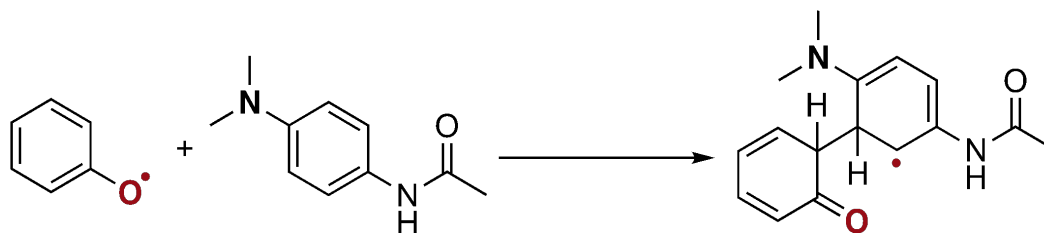
ΔH (kcal/mol)	ΔG (kcal/mol)
+29.1	+41.8

Table D.8. Addition of a phenoxyl radical onto the oxidized "phenoxyl radical trap".
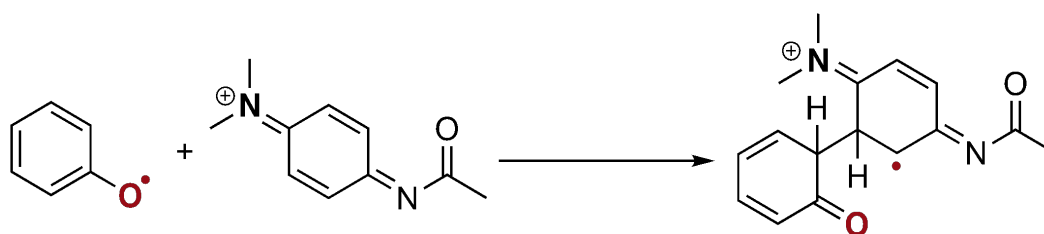
ΔH (kcal/mol)	ΔG (kcal/mol)
+19.4	+32.0

Table D.9. Radical recombination between phenoxyl radical onto the "phenoxyl radical trap".
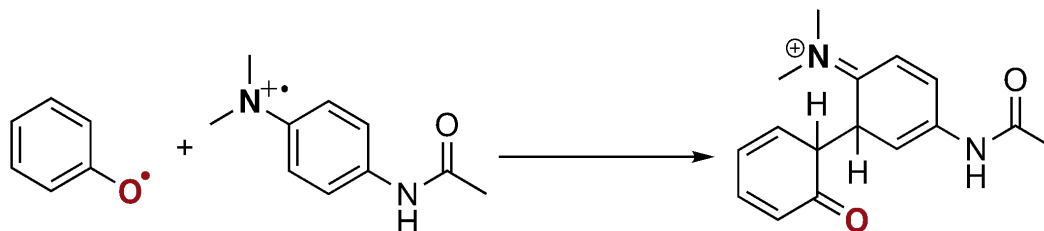
ΔH (kcal/mol)	ΔG (kcal/mol)
+6.4	+20.2

Calculated energies for proposed coupling of a peptide and probe using B3LYP/6-311+G(2d,2p)//CPCM(water) from MacMillan Site Selective Flavin Photoredox

In a recent article, Li *et al.* (2021). proposed a radical addition onto a neutral tyrosine which we also find to be energetically unfavorable (Table D.10); the recombination of these two persistent radicals is more favorable and the final product, following a tautomerization to regenerate aromaticity, yields a strong covalent bond (Table D.11).

Table D.10. Calculated energies for the addition of a lumiflavin radical onto a neutral tyrosine using B3LYP/6-311+G(2d,2p)//CPCM(water).
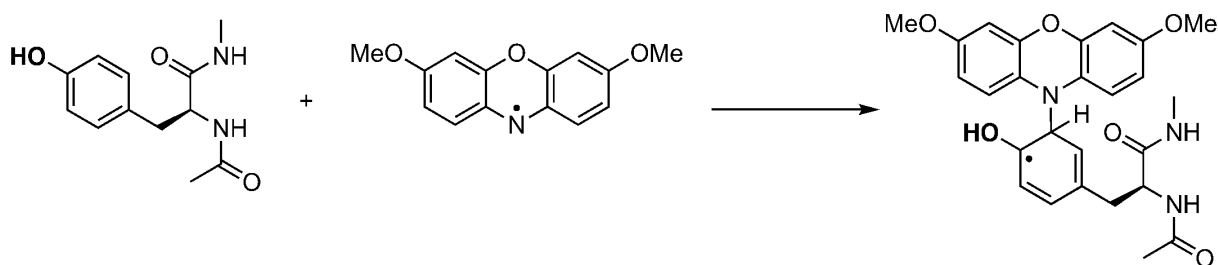
ΔH (kcal/mol)	ΔG (kcal/mol)
+31.77	+44.54

Table D.11. Calculated energies for the radical-radical recombination between lumiflavin radical and tyrosyl radical using B3LYP/6-311+G(2d,2p)//CPCM(water).
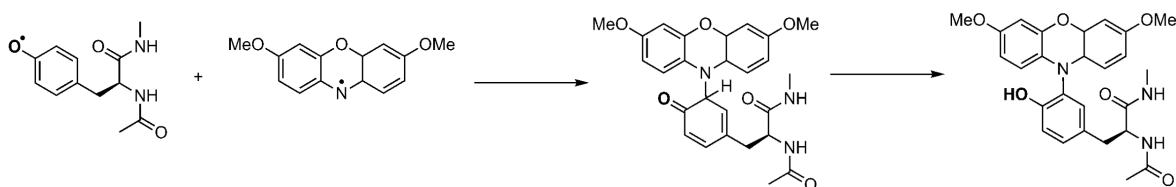
	Ketone intermediate	Final product
ΔH (kcal/mol)	-7.60	-23.49
ΔG (kcal/mol)	+6.31	-23.46

DFT energies and coordinates for selected compounds as obtained from B3LYP/6-311+G (2d,2p) //CPCM(water)
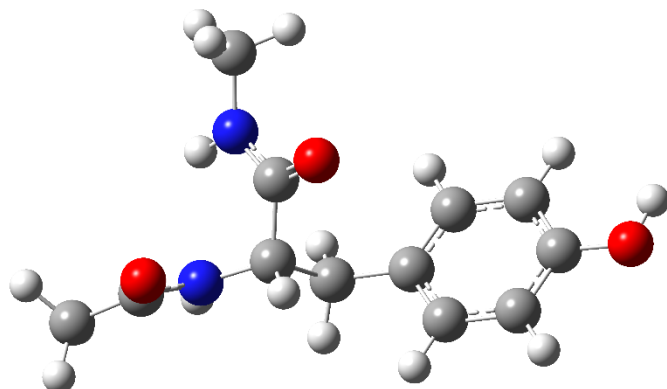
phenol-peptide_b3lyp_6311gplus2d2p_H2O
Zero-point correction=   0.270479 (Hartree/Particle)
Thermal correction to Energy=   0.288520
Thermal correction to Enthalpy=   0.289464
Thermal correction to Gibbs Free Energy=   0.221608
Sum of electronic and zero-point Energies=   -802.137994
Sum of electronic and thermal Energies=   -802.119953
Sum of electronic and thermal Enthalpies=   -802.119009
Sum of electronic and thermal Free Energies=   -802.186865

C	1.15299	-0.51079	-0.58708
C	1.99404	0.53426	-0.99567
C	3.35529	0.53736	-0.67216
C	3.88934	-0.51765	0.07452
C	3.06913	-1.57267	0.49164
C	1.71564	-1.56411	0.15999
H	1.58643	1.35709	-1.57638
H	1.08078	-2.38571	0.47949
O	5.23433	-0.58582	0.43258
H	3.99155	1.35543	-1.00044
H	3.50753	-2.38066	1.0651
C	-0.32538	-0.5191	-0.91407
C	-1.21815	-0.04354	0.273
H	-0.6505	-1.53626	-1.15149
H	-0.52838	0.10257	-1.79585
H	-0.94046	-0.61594	1.1621
C	-3.1908	-1.53482	0.01001
C	-4.69486	-1.61602	-0.1662
H	-5.15177	-1.93836	0.77589
C	-1.0132	1.43229	0.62612
N	-1.40113	2.32608	-0.34613
H	-1.67479	1.97501	-1.25277

```
O        -0.54802  1.79325  1.72558
N        -2.6496  -0.27303 -0.006
H        -3.26235  0.52837 -0.04892
O        -2.48356 -2.55533  0.17181
H         5.72964  0.19599  0.12173
H        -5.14815 -0.66724 -0.46889
H        -4.92476 -2.37699 -0.91673
C        -1.26669  3.77202 -0.17145
H        -0.47769  4.18255 -0.81248
H        -2.20912  4.28114 -0.39799
H        -0.99903  3.95123  0.87091
```


phenol-rad-peptide_b3lyp_6311gplus2d2p_H2O
Zero-point correction=   0.257838 (Hartree/Particle)
Thermal correction to Energy=   0.275551
Thermal correction to Enthalpy=   0.276495
Thermal correction to Gibbs Free Energy=   0.208283
Sum of electronic and zero-point Energies=   -801.508559
Sum of electronic and thermal Energies=   -801.490846
Sum of electronic and thermal Enthalpies=   -801.489902
Sum of electronic and thermal Free Energies=   -801.558114

```
C         1.21091 -0.46264 -0.58316
C         2.07049  0.57592 -1.01607
C         3.41373  0.5704  -0.68775
C         3.97441 -0.49577  0.106
C         3.08277 -1.54514  0.53913
C         1.74478 -1.52089  0.19865
H         1.66064  1.38412 -1.61515
H         1.07985 -2.31774  0.52001
O         5.2317  -0.51219  0.41306
H         4.08509  1.35775 -1.01178
H         3.50665 -2.34742  1.13263
C        -0.25857 -0.46263 -0.92557
```

```
C        -1.16128 -0.02735  0.27631
H        -0.57412 -1.47624 -1.18988
H        -0.45641  0.18867 -1.78505
H        -0.84174 -0.58028  1.16389
C        -3.04283 -1.62364  0.00234
C        -4.54195 -1.79443 -0.13539
H        -4.95217 -2.16324  0.81119
C        -1.00666  1.45841  0.61168
N        -1.52735  2.32902 -0.3165
H        -1.88138  1.96337 -1.18922
O        -0.44518  1.83916  1.65811
N        -2.5791  -0.3293   0.01238
H        -3.24165  0.43256  0.03613
O        -2.26626 -2.59987  0.11158
H        -5.06029 -0.8696  -0.40546
H        -4.74554 -2.55309 -0.89563
C        -1.44338  3.78121 -0.15384
H        -0.75085  4.22536 -0.87798
H        -2.4284   4.24341 -0.27352
H        -1.07105  3.97684  0.8527
```


biotin-tyramide_b3lyp_6311gplus2d2p_h2o_optfreqtight
Zero-point correction=   0.419227 (Hartree/Particle)
Thermal correction to Energy=   0.444183
Thermal correction to Enthalpy=   0.445127
Thermal correction to Gibbs Free Energy=   0.357200
Sum of electronic and zero-point Energies=   -1489.127771
Sum of electronic and thermal Energies=   -1489.102815
Sum of electronic and thermal Enthalpies=   -1489.101871
Sum of electronic and thermal Free Energies=   -1489.189798

```
C        -6.11755 -0.4006   0.1426
C        -4.8422  -0.70386 -0.33829
C        -6.73649 -1.32436  0.99616
C        -4.1649  -1.87533  0.00506
```

```
H     -4.36617  0.0064  -1.0028
C     -6.08054 -2.50047  1.35177
C     -4.8077  -2.76865  0.86248
H     -6.57403 -3.21153  2.00283
H     -4.31739 -3.69072  1.14728
O     -8.00369 -1.04521  1.43548
H     -8.31404 -1.75994  2.00169
C     -2.76799 -2.14126 -0.50419
C     -1.68762 -1.55684  0.42577
H     -2.64201 -1.70683 -1.49662
H     -2.60468 -3.21602 -0.5996
H     -1.82328 -0.48222  0.52275
H     -1.77539 -1.99702  1.41855
C      0.35499 -0.91684 -0.82253
C      1.75253 -1.34566 -1.23473
C      2.83214 -0.41127 -0.66959
H      1.785  -1.32185 -2.32611
H      1.9498 -2.3734  -0.9269
C      4.2403  -0.79489 -1.12968
H      2.60918  0.61276 -0.97393
H      2.7888  -0.43104  0.42276
C      5.31737  0.133  -0.56328
H      4.45317 -1.82442 -0.83368
H      4.28282 -0.7704  -2.22289
H      5.09768  1.15544 -0.8808
H      5.26787  0.13433  0.52775
N     -0.33346 -1.79213 -0.05517
H      0.09555 -2.67745  0.15408
O     -0.10906  0.17582 -1.15957
C      7.91752 -1.03022  1.19345
C      8.37943  0.38982  0.82697
C      6.7344  -0.21431 -1.02758
C      7.85439  0.77113 -0.59432
C      7.38753  2.51916  0.91207
S      7.36155 -1.82285 -0.3704
H      8.65958  0.69387 -1.3208
H      9.46796  0.44087  0.84488
N      7.47113  2.1601  -0.40584
H      7.00937  2.71069 -1.10878
N      7.80326  1.44102  1.66448
H      8.18424  1.63246  2.57657
O      7.00784  3.60208  1.34881
H      6.74324 -0.31304 -2.11253
H      8.71597 -1.63488  1.61304
H      7.09515 -0.99328  1.90325
H     -6.60784  0.50987 -0.13227
```
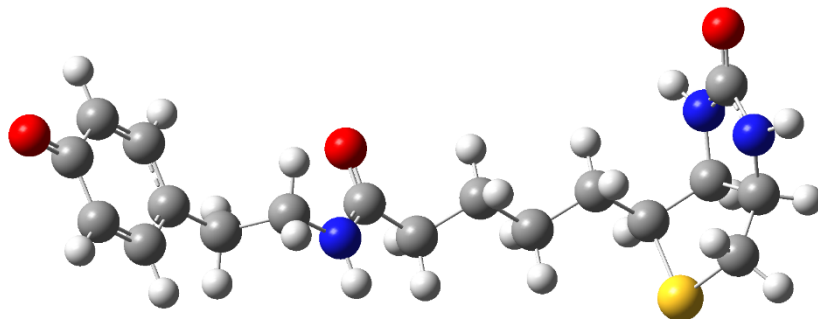
biotin-tyramide_rad_b3lyp_6311gplus2d2p_h2o_optfreqtight_geom2
Zero-point correction=   0.406670 (Hartree/Particle)
Thermal correction to Energy=   0.431277
Thermal correction to Enthalpy=   0.432222
Thermal correction to Gibbs Free Energy=   0.344855
Sum of electronic and zero-point Energies=   -1488.498724
Sum of electronic and thermal Energies=   -1488.474117
Sum of electronic and thermal Enthalpies=   -1488.473172
Sum of electronic and thermal Free Energies=   -1488.560539

C	-7.82747	1.32158	-0.48127
C	-6.59537	0.75645	-0.78679
C	-8.62974	0.74023	0.49781
C	-6.13402	-0.39084	-0.13435
H	-5.98461	1.21598	-1.55357
C	-8.19265	-0.40348	1.16176
C	-6.9561	-0.95618	0.84247
H	-8.81549	-0.86168	1.91969
H	-6.63269	-1.84872	1.36292
O	-9.83898	1.33137	0.76256
C	-4.7783	-0.97653	-0.45057
C	-3.66154	-0.36861	0.41938
H	-4.53143	-0.8053	-1.49903
H	-4.79339	-2.05659	-0.29539
H	-3.61353	0.70675	0.26426
H	-3.87395	-0.54619	1.47309
C	-1.48768	-0.38324	-0.77014
C	-0.17393	-1.12167	-0.96025
C	1.03845	-0.24887	-0.60722
H	-0.12051	-1.40997	-2.01257
H	-0.15762	-2.0405	-0.37256
C	2.36818	-0.96242	-0.86082
H	0.99426	0.6712	-1.19219
H	0.97742	0.04408	0.44443
C	3.57941	-0.09181	-0.51893
H	2.40477	-1.88471	-0.27687
H	2.42436	-1.25822	-1.91293

H	3.5337	0.81899	-1.12122
H	3.52348	0.22831	0.52376
N	-2.34679	-0.92115	0.12501
H	-2.08714	-1.78522	0.56948
O	-1.74137	0.6522	-1.39163
C	5.95105	-1.07217	1.62722
C	6.6422	0.084	0.88576
C	4.92195	-0.77592	-0.79094
C	6.18767	0.1061	-0.60888
C	6.01534	2.27207	0.2981
S	5.27607	-2.19555	0.33672
H	6.96975	-0.30716	-1.24107
H	7.72406	-0.03506	0.9416
N	6.03734	1.53087	-0.85212
H	5.6737	1.91483	-1.70708
N	6.24823	1.41308	1.35125
H	6.65588	1.8025	2.18551
O	5.81966	3.4814	0.3812
H	4.91615	-1.19075	-1.79831
H	6.63732	-1.64245	2.24609
H	5.14393	-0.69739	2.25144
H	-8.17571	2.20571	-0.99701
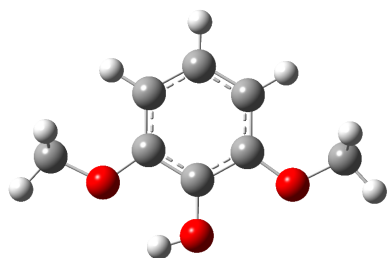
2-6-dimethoxyphenol_b3lyp_6311gplus2d2p_H2O
Zero-point correction=   0.169367 (Hartree/Particle)
Thermal correction to Energy=   0.180108
Thermal correction to Enthalpy=   0.181052
Thermal correction to Gibbs Free Energy=   0.133176
Sum of electronic and zero-point Energies=   -536.527363
Sum of electronic and thermal Energies=   -536.516622
Sum of electronic and thermal Enthalpies=   -536.515677
Sum of electronic and thermal Free Energies=   -536.563553

C	-0.04156	2.1028	0.00001
C	1.18633	1.44319	0.00003
C	1.1995	0.04799	0.00003
C	0.00217	-0.68108	0.00002
C	-1.22608	-0.00572	0.00002
C	-1.24152	1.39407	0.

```
H          2.10923  2.00647  0.00006
H         -2.18036  1.92983 -0.00003
O          0.02182 -2.04714 0.
O          2.31575 -0.74654  0.00006
C          3.60014 -0.12133 -0.00007
H          4.32576 -0.93191 -0.00022
H          3.73767  0.49326 -0.89432
H          3.73789  0.49316  0.89419
H         -0.06437  3.186   -0.00002
O         -2.3324  -0.8043   0.00003
C         -3.61358 -0.17576 -0.00005
H         -4.33993 -0.98621 -0.00005
H         -3.75632  0.43988  0.89348
H         -3.75625  0.43982 -0.89364
H          0.93143 -2.35409 -0.00001
```


2-6-dimethoxyphenol_rad_b3lyp_6311gplus2d2p_H2O
Zero-point correction=   0.156989 (Hartree/Particle)
Thermal correction to Energy=   0.167383
Thermal correction to Enthalpy=   0.168328
Thermal correction to Gibbs Free Energy=   0.120557
Sum of electronic and zero-point Energies=   -535.908096
Sum of electronic and thermal Energies=   -535.897702
Sum of electronic and thermal Enthalpies=   -535.896758
Sum of electronic and thermal Free Energies=   -535.944528

```
C         -0.04156  2.1028   0.00001
C          1.18633  1.44319  0.00003
C          1.1995   0.04799  0.00003
C          0.00217 -0.68108  0.00002
C         -1.22608 -0.00572  0.00002
C         -1.24152  1.39407  0.
H          2.10923  2.00647  0.00006
H         -2.18036  1.92983 -0.00003
O          0.02182 -2.04714 0.
O          2.31575 -0.74654  0.00006
C          3.60014 -0.12133 -0.00007
H          4.32576 -0.93191 -0.00022
H          3.73767  0.49326 -0.89432
```

H	3.73789	0.49316	0.89419
H	-0.06437	3.186	-0.00002
O	-2.3324	-0.8043	0.00003
C	-3.61358	-0.17576	-0.00005
H	-4.33993	-0.98621	-0.00005
H	-3.75632	0.43988	0.89348
H	-3.75625	0.43982	-0.89364

2-methoxy4-methyl-phenol_rad_b3lyp_6311gplus2d2p_H2O_2
Zero-point correction=   0.151694 (Hartree/Particle)
Thermal correction to Energy=   0.161325
Thermal correction to Enthalpy=   0.162269
Thermal correction to Gibbs Free Energy=   0.116003
Sum of electronic and zero-point Energies=   -460.680697
Sum of electronic and thermal Energies=   -460.671065
Sum of electronic and thermal Enthalpies=   -460.670121
Sum of electronic and thermal Free Energies=   -460.716387

C	1.639	-0.46022	-0.0001
C	0.35319	-0.91943	0.3158
C	-0.73046	-0.05876	0.32325
C	-0.55826	1.36612	-0.00184
C	0.78398	1.78607	-0.3193
C	1.83101	0.9076	-0.31677
H	0.22031	-1.96375	0.55519
H	2.82707	1.25246	-0.55926
O	-1.52742	2.15933	-0.00005
O	-1.98866	-0.40932	0.61186
C	-2.26963	-1.77647	0.94361
H	-3.33625	-1.81615	1.13485
H	-2.01744	-2.43377	0.11219
H	-1.72163	-2.07623	1.83621
H	0.92388	2.83082	-0.56002
C	2.79553	-1.41665	0.00001
H	2.62834	-2.22766	0.71184
H	2.91692	-1.87904	-0.98173
H	3.72636	-0.91867	0.2612
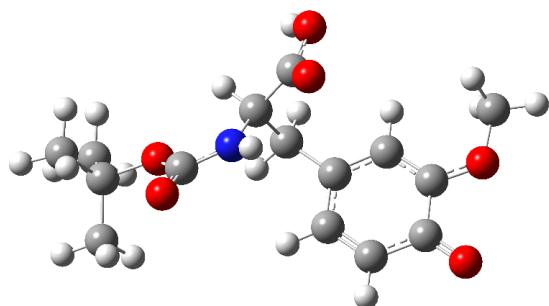
2-methoxy-4ethyl-COOH-NHBoc-phenol_rad_b3lyp_6311gplus2d2p_H2O
Zero-point correction=   0.338743 (Hartree/Particle)
Thermal correction to Energy=   0.361862
Thermal correction to Enthalpy=   0.362806
Thermal correction to Gibbs Free Energy=   0.283347
Sum of electronic and zero-point Energies=   -1089.774401
Sum of electronic and thermal Energies=   -1089.751282
Sum of electronic and thermal Enthalpies=   -1089.750338
Sum of electronic and thermal Free Energies=   -1089.829797

C   -1.29945 -0.30655 0.6762
C   -2.58291 0.2579 0.71627
C   -3.6872 -0.46118 0.27969
C   -3.52347 -1.7686 -0.20731
C   -2.261 -2.33417 -0.24238
C   -1.15597 -1.60676 0.19852
H   -2.71254 1.25853 1.10098
H   -0.17833 -2.06707 0.17347
O   -4.60709 -2.48453 -0.6348
O   -4.98118 -0.01999 0.27727
C   -5.25336 1.2972 0.76213
H   -6.32564 1.43245 0.6668
H   -4.96313 1.39324 1.80876
H   -4.73425 2.04634 0.16387
H   -2.14954 -3.34498 -0.60962
C   -0.10342 0.4903 1.13937
H   -0.39953 1.19395 1.91866
H   0.63897 -0.16971 1.58491
C   0.64955 1.27939 0.02072
H   1.45156 1.8364 0.50494
C   -0.27077 2.28155 -0.66995
O   -0.6699 3.33558 0.0644
H   -0.24661 3.35714 0.93271
O   -0.66612 2.16042 -1.80234
N   1.22388 0.42844 -0.99937
H   0.71935 0.34335 -1.8667
C   2.44226 -0.1751 -0.95775

185

```
O        2.88401 -0.83524 -1.88656
O        3.05729  0.05021  0.21607
C        4.41338 -0.47478  0.51063
C        4.39707 -2.00165  0.49614
H        5.35955 -2.37217  0.84912
H        3.62352 -2.37979  1.1645
H        4.22142 -2.38818 -0.5033
C        5.42533  0.11346 -0.47006
H        6.43099 -0.16754 -0.15711
H        5.2612  -0.25261 -1.47926
H        5.36382  1.20177 -0.4723
C        4.66514  0.04793  1.92274
H        4.63381  1.1368   1.94235
H        3.91633 -0.33548  2.615
H        5.64767 -0.27482  2.26443
```


2-methoxy-4ethyl-COOH-NH2-phenol_rad_b3lyp_6311gplus2d2p_H2O
Zero-point correction=   0.213190 (Hartree/Particle)
Thermal correction to Energy=   0.227851
Thermal correction to Enthalpy=   0.228795
Thermal correction to Gibbs Free Energy=   0.169116
Sum of electronic and zero-point Energies=   -743.952612
Sum of electronic and thermal Energies=   -743.937951
Sum of electronic and thermal Enthalpies=   -743.937007
Sum of electronic and thermal Free Energies=   -743.996686

```
C        0.31822  2.08065  0.19356
C        1.50088  1.3646  -0.0356
C        1.50481 -0.03305  0.06679
C        0.32607 -0.71465  0.39834
C       -0.85659  0.00139  0.6275
C       -0.86051  1.39904  0.52511
H        2.40087  1.88502 -0.28874
H       -1.7635   1.94576  0.70008
O        0.33008 -2.14083  0.50282
O        2.7116  -0.76371 -0.16705
C        3.52298 -0.05544 -1.10775
H        4.42596 -0.60216 -1.28272
H        2.98852  0.05444 -2.02818
```

186

H	3.76156	0.91136	-0.71624
H	-1.75658	-0.51903	0.88064
C	0.31391	3.61652	0.08105
H	1.04611	3.92366	-0.63619
H	-0.65375	3.94846	-0.23257
C	0.64847	4.23262	1.45222
H	0.64548	5.29976	1.37404
C	2.04118	3.75488	1.90359
O	2.85043	4.59282	2.73298
H	3.77771	4.42179	2.55274
O	2.46708	2.62713	1.54257
N	-0.35745	3.81066	2.43759
H	-0.1402	4.21073	3.32796
H	-1.2618	4.12088	2.14449

2-methoxyphenol_rad_b3lyp_6311gplus2d2p_H2O
Zero-point correction=   0.124431 (Hartree/Particle)
Thermal correction to Energy=   0.132223
Thermal correction to Enthalpy=   0.133168
Thermal correction to Gibbs Free Energy=   0.091430
Sum of electronic and zero-point Energies=   -421.375763
Sum of electronic and thermal Energies=   -421.367970
Sum of electronic and thermal Enthalpies=   -421.367026
Sum of electronic and thermal Free Energies=   -421.408763

C	-0.04156	2.1028	0.00001
C	1.18633	1.44319	0.00003
C	1.1995	0.04799	0.00003
C	0.00217	-0.68108	0.00002
C	-1.22608	-0.00572	0.00002
C	-1.24152	1.39407	0.
H	2.10923	2.00647	0.00006
H	-2.18036	1.92983	-0.00003
O	0.02182	-2.04714	0.
O	2.31575	-0.74654	0.00006
C	3.60014	-0.12133	-0.00007
H	4.32576	-0.93191	-0.00022
H	3.73767	0.49326	-0.89432
H	3.73789	0.49316	0.89419

H   -2.14408 -0.55543 0.00004
H   -0.06325 3.17258 0.
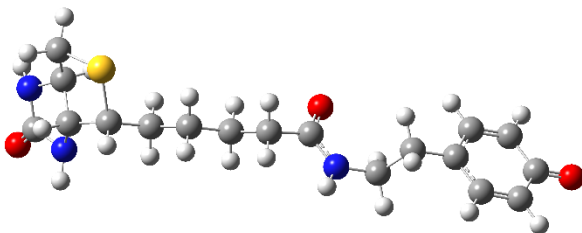
biotin-tyramide_rad_b3lyp_6311gplus2d2p_H2O
Zero-point correction=   0.407064 (Hartree/Particle)
Thermal correction to Energy=   0.431451
Thermal correction to Enthalpy=   0.432395
Thermal correction to Gibbs Free Energy=   0.344994
Sum of electronic and zero-point Energies=   -1488.487157
Sum of electronic and thermal Energies=   -1488.462770
Sum of electronic and thermal Enthalpies=   -1488.461826
Sum of electronic and thermal Free Energies=   -1488.549227

C   3.79493 -2.5059 -0.08852
C   2.4705 -2.36775 0.35037
C   4.49412 -3.67366 0.27628
C   1.82322 -3.35293 1.11637
H   1.92864 -1.46695 0.07588
C   3.8698 -4.66807 1.03487
C   2.54392 -4.50903 1.44762
H   4.4236 -5.56075 1.31584
H   2.07343 -5.28743 2.04229
O   5.82493 -3.77124 -0.11426
C   0.37336 -3.18375 1.52324
C   -0.60097 -3.59888 0.39247
H   0.16605 -2.13738 1.77596
H   0.15954 -3.78323 2.41788
H   -0.41499 -2.98066 -0.48995
H   -0.43437 -4.64571 0.1166
C   -2.67146 -2.24439 0.58584
C   -4.11558 -2.2078 1.07419
C   -5.00753 -1.33141 0.17859
H   -4.11161 -1.7937 2.09399
H   -4.52434 -3.2249 1.1494
C   -6.42038 -1.1348 0.75297
H   -4.51052 -0.36301 0.0478
H   -5.07224 -1.78216 -0.82207
C   -7.30043 -0.24343 -0.14086

```
H        -6.90833 -2.11361  0.88425
H        -6.34954 -0.68345  1.75278
H        -6.81614  0.73159 -0.27176
H        -7.37205 -0.68995 -1.14501
N        -2.01104 -3.43257  0.75783
H        -2.49245 -4.20344  1.19671
O        -2.11637 -1.24486  0.07222
C        -8.7234  -0.06604  0.38735
C        -9.67619  0.79398 -0.44219
H        -9.16733 -1.03808  0.62048
C        -9.61059  2.49826  1.29833
C        -9.31941  2.27229 -0.17322
H       -10.67822  2.50676  1.5224
C       -10.13043  2.05428 -2.35909
S        -8.79921  0.92159  2.09137
H        -8.23943  2.41157 -0.33456
H       -10.69394  0.62528 -0.05091
N       -10.07356  2.9157  -1.25239
H       -10.09304  3.91135 -1.41088
N        -9.70333  0.79415 -1.90704
H        -9.91813 -0.01665 -2.46699
O       -10.48996  2.34608 -3.50955
H        -9.11587  3.36747  1.73186
H         4.26067 -1.74752 -0.68253
```
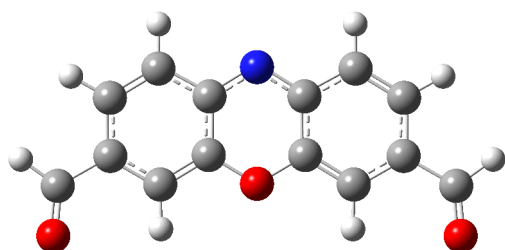

flavin-rad_b3lyp_6311gplus2d2p_H2O
Zero-point correction=   0.185571 (Hartree/Particle)
Thermal correction to Energy=   0.199194
Thermal correction to Enthalpy=   0.200139
Thermal correction to Gibbs Free Energy=   0.144012
Sum of electronic and zero-point Energies=   -818.768758
Sum of electronic and thermal Energies=   -818.755135
Sum of electronic and thermal Enthalpies=   -818.754191
Sum of electronic and thermal Free Energies=   -818.810317

```
C        -5.73748 -3.67964  0.36997
C        -4.38081 -3.69111  0.3758
C        -3.67195 -2.48441  0.37193
```

```
C      -4.36821 -1.27213  0.36206
C      -5.76808 -1.28233  0.35617
C      -6.43851 -2.46229  0.36005
C      -2.41678 -0.12013  0.36378
C      -1.69176 -1.31543  0.37368
C      -0.29277 -1.27778  0.37941
H       0.26737 -2.18942  0.38699
C       0.35263 -0.08441  0.37535
C      -0.37451  1.11753  0.36541
C      -1.73153  1.10061  0.35974
H      -6.27692 -4.60371  0.37295
H      -3.85326 -4.62199  0.38335
H      -6.30962 -0.35952  0.34861
H       1.42231 -0.05855  0.37975
H      -2.27785  2.02059  0.35217
O      -3.72098 -0.13968  0.35836
N      -2.3373  -2.48359  0.3776
C      -7.97849 -2.46678  0.35354
H      -8.51081 -3.39496  0.35657
C       0.37343  2.46369  0.36092
H       1.44328  2.48133  0.36536
O      -8.61083 -1.37883  0.34465
O      -0.27361  3.54297  0.35202
```


phenol-peptide_plus_2-6-dimethoxyphenol_b3lyp_6311gplus2d2p_H2O
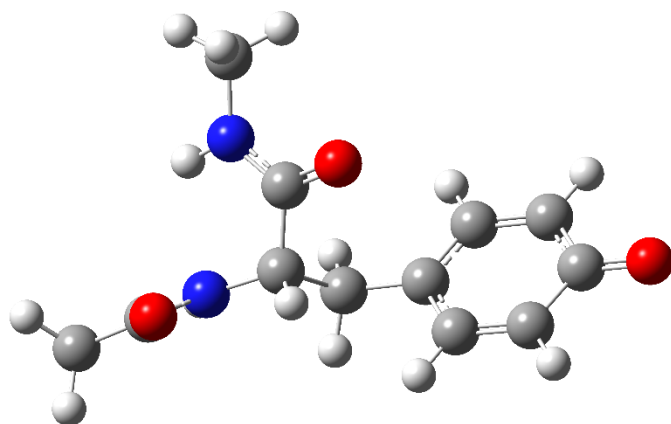Zero-point correction=   0.419783 (Hartree/Particle)
Thermal correction to Energy=   0.449176
Thermal correction to Enthalpy=   0.450120
Thermal correction to Gibbs Free Energy=   0.355799
Sum of electronic and zero-point Energies=   -1337.478376
Sum of electronic and thermal Energies=   -1337.448983
Sum of electronic and thermal Enthalpies=   -1337.448039
Sum of electronic and thermal Free Energies=   -1337.542360

```
C       1.45774 -0.53409 -0.63505
C       2.30269  0.44931 -1.19328
C       3.60534  0.57851 -0.7901
```

```
C        4.15961 -0.29351  0.22355
C        3.27586 -1.30071  0.77458
C        1.98065 -1.40569  0.35109
H        1.90629  1.10989 -1.95266
H        1.34069 -2.17101  0.77041
O        5.35249 -0.18491  0.60491
H        3.68008 -1.96563  1.525
C        0.04184 -0.69317 -1.11339
C       -1.05115 -0.35282 -0.06755
H       -0.11442 -1.73733 -1.39381
H       -0.11717 -0.09047 -2.00771
H       -0.86896 -0.91512  0.84604
C       -3.35655 -1.18544  0.22103
C       -4.59581 -1.69859 -0.47405
H       -5.46041 -1.15591 -0.09562
C       -0.97654  1.12802  0.3466
N       -1.92095  1.94723 -0.13724
H       -2.66383  1.5478  -0.68484
O       -0.05794  1.50906  1.07277
N       -2.34666 -0.76112 -0.58763
H       -2.45209 -0.8755  -1.58251
O       -3.26424 -1.14848  1.44569
H       -4.55574 -1.59877 -1.55619
H       -4.72632 -2.74998 -0.21934
C       -1.95699  3.36845  0.17395
H       -1.0381   3.85609 -0.14772
H       -2.79729  3.81486 -0.34877
H       -2.07713  3.5301   1.2448
C        4.53081  1.65092 -1.39427
C        5.1069   1.44868 -2.64874
C        4.79302  2.82447 -0.68745
C        5.94554  2.41952 -3.19589
H        4.90059  0.52304 -3.20539
C        5.63111  3.79613 -1.23506
H        4.33891  2.9841   0.3012
C        6.20748  3.5938  -2.48901
H        6.07023 -0.35952 -0.00825
O        7.06732  4.58905 -3.05031
H        7.98298  4.33069 -2.92214
O        5.89928  4.99937 -0.51035
O        6.53672  2.21196 -4.48132
C        7.28514  5.04744 -0.16107
H        7.78939  5.74428 -0.7975
H        7.38556  5.35782  0.85798
H        7.71742  4.07619 -0.28236
C        7.86622  1.71067 -4.31996
H        7.96106  0.77847 -4.83659
```

H   8.56413 2.41446 -4.72306
H   8.06826 1.56399 -3.2795

phenol-peptide_plus_2-methoxy4-methyl-phenol_b3lyp_6311gplus2d2p_H2O
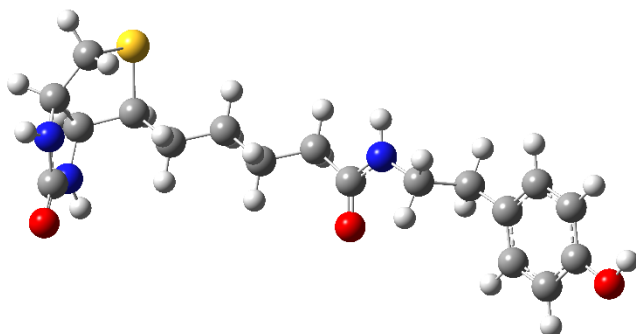Zero-point correction=   0.415548 (Hartree/Particle)
Thermal correction to Energy=   0.443625
Thermal correction to Enthalpy=   0.444570
Thermal correction to Gibbs Free Energy=   0.353253
Sum of electronic and zero-point Energies=   -1262.257325
Sum of electronic and thermal Energies=   -1262.229248
Sum of electronic and thermal Enthalpies=   -1262.228304
Sum of electronic and thermal Free Energies=   -1262.319620

C   1.45774 -0.53409 -0.63505
C   2.30269 0.44931 -1.19328
C   3.60534 0.57851 -0.7901
C   4.15961 -0.29351 0.22355
C   3.27586 -1.30071 0.77458
C   1.98065 -1.40569 0.35109
H   1.90629 1.10989 -1.95266
H   1.34069 -2.17101 0.77041
O   5.35249 -0.18491 0.60491
H   3.68008 -1.96563 1.525
C   0.04184 -0.69317 -1.11339
C   -1.05115 -0.35282 -0.06755
H   -0.11442 -1.73733 -1.39381
H   -0.11717 -0.09047 -2.00771
H   -0.86896 -0.91512 0.84604
C   -3.35655 -1.18544 0.22103
C   -4.59581 -1.69859 -0.47405
H   -5.46041 -1.15591 -0.09562
C   -0.97654 1.12802 0.3466
N   -1.92095 1.94723 -0.13724
H   -2.66383 1.5478 -0.68484
O   -0.05794 1.50906 1.07277
N   -2.34666 -0.76112 -0.58763

192

H	-2.45209	-0.8755	-1.58251
O	-3.26424	-1.14848	1.44569
H	-4.55574	-1.59877	-1.55619
H	-4.72632	-2.74998	-0.21934
C	-1.95699	3.36845	0.17395
H	-1.0381	3.85609	-0.14772
H	-2.79729	3.81486	-0.34877
H	-2.07713	3.5301	1.2448
C	4.53081	1.65092	-1.39427
C	5.1069	1.44868	-2.64874
C	4.79302	2.82447	-0.68745
C	5.94554	2.41952	-3.19589
H	4.90059	0.52304	-3.20539
C	5.63111	3.79613	-1.23506
C	6.20748	3.5938	-2.48901
H	6.07023	-0.35952	-0.00825
H	6.85042	4.33895	-2.90888
O	4.20247	3.03207	0.59826
H	4.61965	3.78411	1.02487
O	5.89927	4.9996	-0.51072
C	6.97706	5.70227	-1.13482
H	6.67315	6.03117	-2.1066
H	7.24303	6.54989	-0.53841
H	7.82148	5.05153	-1.22644
C	6.58241	2.19557	-4.58003
H	6.21843	2.93375	-5.26377
H	7.64635	2.27688	-4.50047
H	6.32497	1.22048	-4.93755

phenol-peptide_plus_2-methoxy-4ethyl-COOH-NHBoc-phenol_b3lyp_6311gplus2d2p_H2O
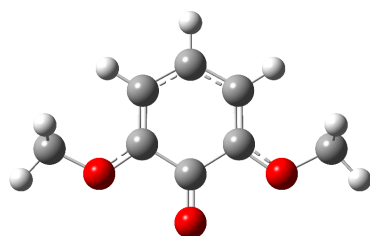Zero-point correction=   0.601853 (Hartree/Particle)
Thermal correction to Energy=   0.644120
Thermal correction to Enthalpy=   0.645064

Thermal correction to Gibbs Free Energy=   0.517758
Sum of electronic and zero-point Energies=   -1891.355380
Sum of electronic and thermal Energies=   -1891.313113
Sum of electronic and thermal Enthalpies=   -1891.312169
Sum of electronic and thermal Free Energies=   -1891.439475

C	1.45774	-0.53409	-0.63505
C	2.30269	0.44931	-1.19328
C	3.60534	0.57851	-0.7901
C	4.15961	-0.29351	0.22355
C	3.27586	-1.30071	0.77458
C	1.98065	-1.40569	0.35109
H	1.90629	1.10989	-1.95266
H	1.34069	-2.17101	0.77041
O	5.35249	-0.18491	0.60491
H	3.68008	-1.96563	1.525
C	0.04184	-0.69317	-1.11339
C	-1.05115	-0.35282	-0.06755
H	-0.11442	-1.73733	-1.39381
H	-0.11717	-0.09047	-2.00771
H	-0.86896	-0.91512	0.84604
C	-3.35655	-1.18544	0.22103
C	-4.59581	-1.69859	-0.47405
H	-5.46041	-1.15591	-0.09562
C	-0.97654	1.12802	0.3466
N	-1.92095	1.94723	-0.13724
H	-2.66383	1.5478	-0.68484
O	-0.05794	1.50906	1.07277
N	-2.34666	-0.76112	-0.58763
H	-2.45209	-0.8755	-1.58251
O	-3.26424	-1.14848	1.44569
H	-4.55574	-1.59877	-1.55619
H	-4.72632	-2.74998	-0.21934
C	-1.95699	3.36845	0.17395
H	-1.0381	3.85609	-0.14772
H	-2.79729	3.81486	-0.34877
H	-2.07713	3.5301	1.2448
C	4.53081	1.65092	-1.39427
C	5.1069	1.44868	-2.64874
C	4.79302	2.82447	-0.68745
C	5.94554	2.41952	-3.19589
H	4.90059	0.52304	-3.20539
C	5.63111	3.79613	-1.23506
C	6.20748	3.5938	-2.48901
H	6.07023	-0.35952	-0.00825
H	6.85042	4.33895	-2.90888
O	4.20247	3.03207	0.59826

```
H       4.61965  3.78411  1.02487
O       5.89927  4.9996  -0.51072
C       6.97706  5.70227 -1.13482
H       6.67315  6.03117 -2.1066
H       7.24303  6.54989 -0.53841
H       7.82148  5.05153 -1.22644
C       6.58241  2.19557 -4.58003
H       7.64635  2.27688 -4.50047
H       6.32497  1.22048 -4.93755
C       6.05855  3.258   -5.56411
H       5.0158   3.42258 -5.38948
C       6.82825  4.57535 -5.35494
O       5.99614  5.50857 -4.66097
O       7.19733  5.11862 -6.62519
H       8.13219  5.33684 -6.62098
N       6.25634  2.78856 -6.94302
H       7.21279  2.91728 -7.205
C       5.39202  3.55653 -7.85081
O       4.57272  2.65772 -8.60299
O       4.56027  4.43463 -7.08791
C       3.80932  5.26975 -7.97311
C       3.38957  6.55421 -7.23449
H       2.94726  6.29693 -6.29478
H       4.25056  7.16718 -7.06753
H       2.67926  7.09099 -7.82798
C       4.67698  5.63811 -9.19092
H       4.81999  4.77161 -9.80216
H       4.18686  6.39965 -9.76079
H       5.62695  5.99903 -8.85595
C       2.5527   4.51626 -8.44719
H       1.74611  5.20879 -8.56848
H       2.75547  4.03756 -9.38241
H       2.28342  3.7789  -7.72008
```
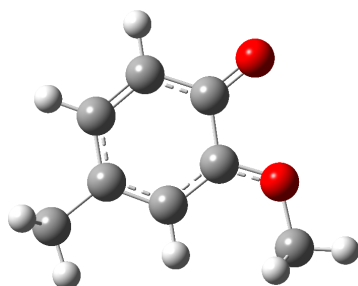
phenol-peptide_plus_2-methoxy-4ethyl-COOH-NH2-phenol_b3lyp_6311gplus2d2p_H2O
Zero-point correction=   0.476894 (Hartree/Particle)
Thermal correction to Energy=   0.510193
Thermal correction to Enthalpy=   0.511137
Thermal correction to Gibbs Free Energy=   0.406247
Sum of electronic and zero-point Energies=   -1545.533583
Sum of electronic and thermal Energies=   -1545.500284
Sum of electronic and thermal Enthalpies=   -1545.499340
Sum of electronic and thermal Free Energies=   -1545.604230

C	1.45774	-0.53409	-0.63505
C	2.30269	0.44931	-1.19328
C	3.60534	0.57851	-0.7901
C	4.15961	-0.29351	0.22355
C	3.27586	-1.30071	0.77458
C	1.98065	-1.40569	0.35109
H	1.90629	1.10989	-1.95266
H	1.34069	-2.17101	0.77041
O	5.35249	-0.18491	0.60491
H	3.68008	-1.96563	1.525
C	0.04184	-0.69317	-1.11339
C	-1.05115	-0.35282	-0.06755
H	-0.11442	-1.73733	-1.39381
H	-0.11717	-0.09047	-2.00771
H	-0.86896	-0.91512	0.84604
C	-3.35655	-1.18544	0.22103
C	-4.59581	-1.69859	-0.47405
H	-5.46041	-1.15591	-0.09562
C	-0.97654	1.12802	0.3466
N	-1.92095	1.94723	-0.13724
H	-2.66383	1.5478	-0.68484
O	-0.05794	1.50906	1.07277
N	-2.34666	-0.76112	-0.58763
H	-2.45209	-0.8755	-1.58251
O	-3.26424	-1.14848	1.44569
H	-4.55574	-1.59877	-1.55619

196

```
H        -4.72632 -2.74998 -0.21934
C        -1.95699  3.36845  0.17395
H        -1.0381   3.85609 -0.14772
H        -2.79729  3.81486 -0.34877
H        -2.07713  3.5301   1.2448
C         4.53081  1.65092 -1.39427
C         5.1069   1.44868 -2.64874
C         4.79302  2.82447 -0.68745
C         5.94554  2.41952 -3.19589
H         4.90059  0.52304 -3.20539
C         5.63111  3.79613 -1.23506
C         6.20748  3.5938  -2.48901
H         6.07023 -0.35952 -0.00825
H         6.85042  4.33895 -2.90888
O         4.20247  3.03207  0.59826
H         4.61965  3.78411  1.02487
O         5.89927  4.9996  -0.51072
C         6.97706  5.70227 -1.13482
H         6.67315  6.03117 -2.1066
H         7.24303  6.54989 -0.53841
H         7.82148  5.05153 -1.22644
C         6.58241  2.19557 -4.58003
H         7.64635  2.27688 -4.50047
H         6.32497  1.22048 -4.93755
C         6.05855  3.258   -5.56411
H         5.0158   3.42258 -5.38948
C         6.82825  4.57535 -5.35494
O         5.99614  5.50857 -4.66097
O         7.19733  5.11862 -6.62519
H         8.13219  5.33684 -6.62098
N         6.25634  2.78856 -6.94302
H         6.97599  3.32888 -7.37909
H         5.40425  2.89253 -7.45599
```
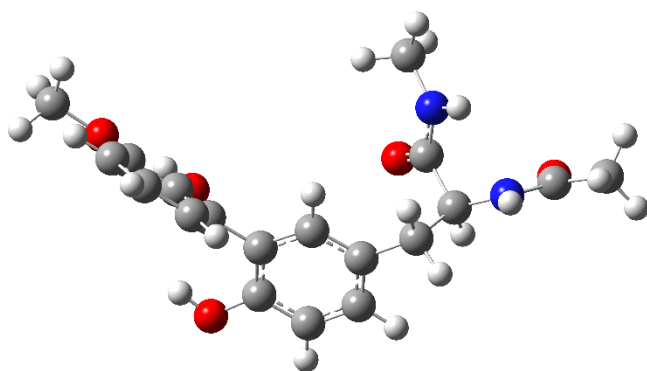
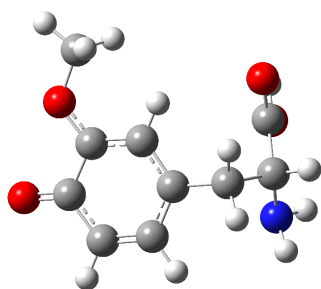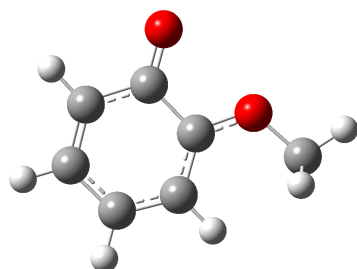**phenol-peptide_plus_2-methoxyphenol_b3lyp_6311gplus2d2p_H2O**
Zero-point correction=   0.387726 (Hartree/Particle)
Thermal correction to Energy=   0.414369
Thermal correction to Enthalpy=   0.415313
Thermal correction to Gibbs Free Energy=   0.326959
Sum of electronic and zero-point Energies=   -1222.954287
Sum of electronic and thermal Energies=   -1222.927644
Sum of electronic and thermal Enthalpies=   -1222.926700
Sum of electronic and thermal Free Energies=   -1223.015055

C   1.45774 -0.53409 -0.63505
C   2.30269 0.44931 -1.19328
C   3.60534 0.57851 -0.7901
C   4.15961 -0.29351 0.22355
C   3.27586 -1.30071 0.77458
C   1.98065 -1.40569 0.35109
H   1.90629 1.10989 -1.95266
H   1.34069 -2.17101 0.77041
O   5.35249 -0.18491 0.60491
H   3.68008 -1.96563 1.525
C   0.04184 -0.69317 -1.11339
C   -1.05115 -0.35282 -0.06755
H   -0.11442 -1.73733 -1.39381
H   -0.11717 -0.09047 -2.00771
H   -0.86896 -0.91512 0.84604
C   -3.35655 -1.18544 0.22103
C   -4.59581 -1.69859 -0.47405
H   -5.46041 -1.15591 -0.09562
C   -0.97654 1.12802 0.3466
N   -1.92095 1.94723 -0.13724
H   -2.66383 1.5478 -0.68484
O   -0.05794 1.50906 1.07277
N   -2.34666 -0.76112 -0.58763
H   -2.45209 -0.8755 -1.58251
O   -3.26424 -1.14848 1.44569
H   -4.55574 -1.59877 -1.55619

H	-4.72632	-2.74998	-0.21934
C	-1.95699	3.36845	0.17395
H	-1.0381	3.85609	-0.14772
H	-2.79729	3.81486	-0.34877
H	-2.07713	3.5301	1.2448
C	4.53081	1.65092	-1.39427
C	5.1069	1.44868	-2.64874
C	4.79302	2.82447	-0.68745
C	5.94554	2.41952	-3.19589
H	4.90059	0.52304	-3.20539
C	5.63111	3.79613	-1.23506
C	6.20748	3.5938	-2.48901
H	6.07023	-0.35952	-0.00825
H	6.85042	4.33895	-2.90888
O	4.20247	3.03207	0.59826
H	4.61965	3.78411	1.02487
O	5.89927	4.9996	-0.51072
C	6.97706	5.70227	-1.13482
H	6.67315	6.03117	-2.1066
H	7.24303	6.54989	-0.53841
H	7.82148	5.05153	-1.22644
H	6.38804	2.26392	-4.1576
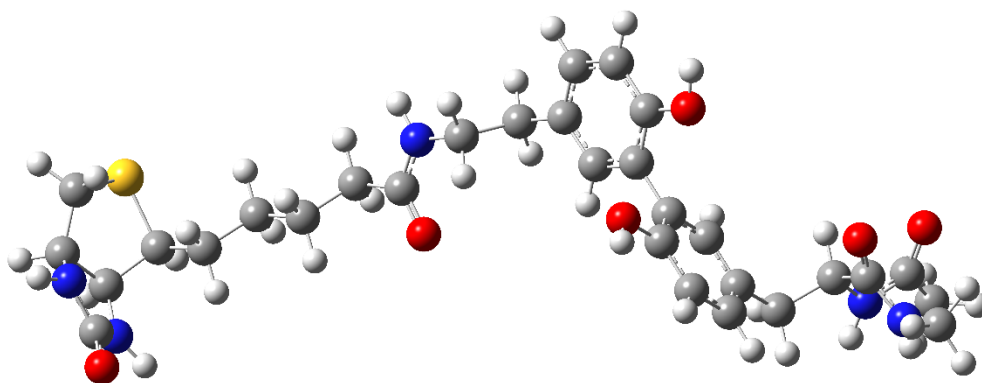
phenol-peptide_plus_biotin-tyramide_b3lyp_6311gplus2d2p_h2o_mfgeom_unfreeze1to54_optfreqtight

Zero-point correction=   0.670047 (Hartree/Particle)
Thermal correction to Energy=   0.713563
Thermal correction to Enthalpy=   0.714507
Thermal correction to Gibbs Free Energy=   0.580591
Sum of electronic and zero-point Energies=   -2290.078491
Sum of electronic and thermal Energies=   -2290.034975
Sum of electronic and thermal Enthalpies=   -2290.034031
Sum of electronic and thermal Free Energies=   -2290.167946

```
C      5.5466 -0.69835  1.17588
C      5.67115 -0.38456  2.52743
C      5.02704  0.72341  3.06571
C      4.24624  1.5435   2.25616
C      4.10159  1.2577   0.89022
C      4.7521   0.13263  0.38355
H      6.27158 -1.01048  3.17439
H      4.63257 -0.09261 -0.66887
O      3.57486  2.62507  2.76024
H      5.12212  0.94781  4.1207
C      6.23148 -1.90646  0.58259
C      7.47658 -1.60258 -0.2866
H      5.5288  -2.44194 -0.05881
H      6.52009 -2.5917   1.38111
H      7.20697 -0.90035 -1.07335
C      8.72518 -2.86911 -1.99808
C      9.0015  -4.2281  -2.59848
H      10.07897 -4.37665 -2.6498
C      8.58142 -0.89922  0.52134
N      9.47682 -1.69246  1.13316
H      9.44941 -2.67951  0.94194
O      8.59508  0.32776  0.6194
N      7.9217  -2.84626 -0.90319
H      7.49972 -3.70891 -0.60071
O      9.20362 -1.83873 -2.46946
H      3.7476   2.70166  3.70488
H      8.55444 -5.04516 -2.03705
H      8.61547 -4.24392 -3.61722
C      10.56931 -1.16424  1.93566
H      10.18578 -0.5536   2.75132
H      11.1282  -1.99778  2.35024
H      11.23985 -0.55173  1.33261
C      3.24972  2.09772  0.00174
C      2.0614   1.58624 -0.52383
C      3.62445  3.3991  -0.36029
C      1.23745  2.32003 -1.37917
H      1.77465  0.57883 -0.24897
C      2.81856  4.14941 -1.2132
C      1.63752  3.6142  -1.71287
H      3.12367  5.14958 -1.49453
H      1.02814  4.21265 -2.3779
O      4.80954  3.88605  0.12466
H      4.95262  4.77885 -0.20758
C     -0.06231  1.74491 -1.89014
C     -1.24038  2.0314  -0.93953
H      0.02764  0.66515 -2.01484
H     -0.29392  2.16451 -2.87052
```

```
H     -1.04599  1.59224  0.03606
H     -1.35594  3.10659 -0.80665
C     -2.98966  0.28155 -1.08391
C     -4.32031 -0.10335 -1.70669
C     -5.41931 -0.29205 -0.65096
H     -4.1632  -1.04316 -2.24028
H     -4.63266  0.63895 -2.4425
C     -6.7483  -0.74081 -1.26253
H     -5.08298 -1.02596  0.08333
H     -5.56601  0.64776 -0.11182
C     -7.84471 -0.93537 -0.21275
H     -7.0763  -0.00626 -2.00129
H     -6.59826 -1.68014 -1.80352
H     -7.50645 -1.68348  0.50861
H     -7.98709 -0.01036  0.35015
N     -2.50544  1.49754 -1.42397
H     -3.02384  2.04312 -2.09139
O     -2.40172 -0.47122 -0.30249
C     -10.78819  0.6478  -0.37815
C     -11.08165 -0.4809   0.6239
C     -9.17764 -1.40772 -0.79957
C     -10.28761 -1.76638  0.22637
C     -9.98018 -1.32949  2.51927
S     -10.01875 -0.14237 -1.85022
H     -10.95395 -2.48289 -0.24766
H     -12.15012 -0.6955   0.63687
N     -9.85133 -2.258    1.52223
H     -9.23679 -3.04449  1.64134
N     -10.59474 -0.22015  1.97793
H     -11.11845  0.37038  2.60303
O     -9.61245 -1.4561   3.68389
H     -9.00063 -2.26374 -1.44983
H     -11.68694  1.16365 -0.70279
H     -10.10352  1.37339  0.05343
```
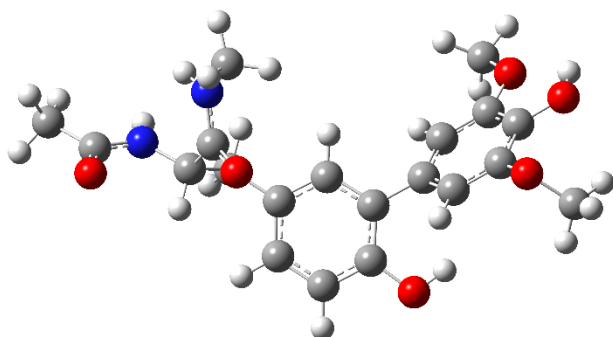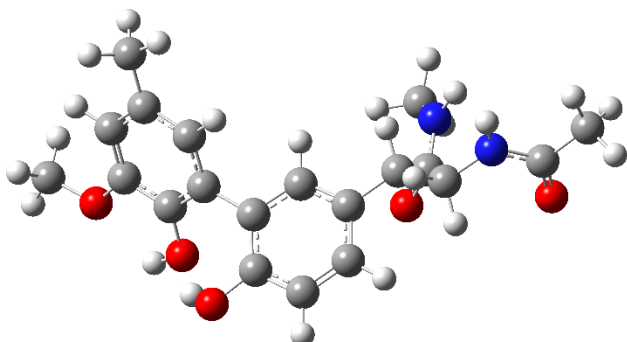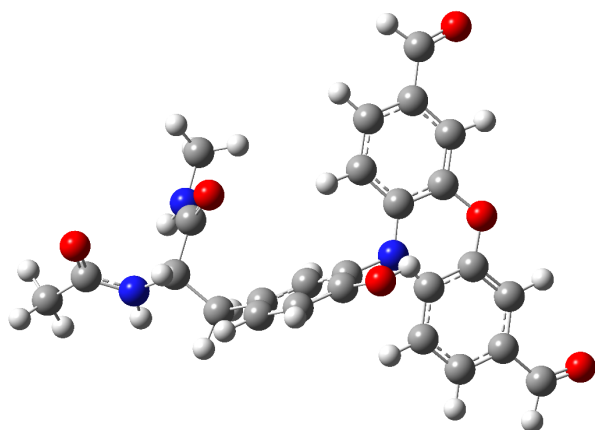
phenol-peptide_plus_flavin_b3lyp_6311gplus2d2p_H2O_noH
Zero-point correction=   0.448930 (Hartree/Particle)
Thermal correction to Energy=   0.481343
Thermal correction to Enthalpy=   0.482287
Thermal correction to Gibbs Free Energy=   0.380166
Sum of electronic and zero-point Energies=   -1620.327002
Sum of electronic and thermal Energies=   -1620.294589
Sum of electronic and thermal Enthalpies=   -1620.293644
Sum of electronic and thermal Free Energies=   -1620.395765

C	-1.99072	-1.34732	0.78866
C	-0.79356	-0.90613	0.23695
C	0.32249	-0.66333	1.03378
C	0.25947	-0.86031	2.41507
C	-0.93754	-1.30221	2.97868
C	-2.03832	-1.54309	2.17397
H	-0.7065	-0.74891	-0.82967
H	-2.95157	-1.89764	2.63361
O	1.31578	-0.64922	3.24714
H	-0.98319	-1.46103	4.04658
C	-3.19065	-1.64165	-0.07904
C	-4.34612	-0.61512	0.01244
H	-3.60925	-2.60763	0.20927
H	-2.87743	-1.7289	-1.1201
H	-4.63928	-0.48905	1.05303
C	-6.75637	-0.71401	-0.50815
C	-7.84635	-1.43877	-1.26322
H	-8.41863	-0.71159	-1.83724
C	-3.90433	0.78311	-0.45516
N	-4.10427	1.07713	-1.75027
H	-4.6224	0.42432	-2.31336
O	-3.35995	1.55565	0.33373
N	-5.48492	-1.13948	-0.7301
H	-5.34579	-1.94844	-1.31316

```
O       -7.00172  0.21342  0.26101
H        2.08968 -0.36489  2.74628
H       -7.46772 -2.20593 -1.93466
H       -8.52205 -1.8987  -0.54292
C       -3.72717  2.35762 -2.32929
H       -2.66291  2.54143 -2.19286
H       -3.94928  2.33492 -3.39192
H       -4.28038  3.17579 -1.86787
C        1.81757  1.13692  0.32206
C        2.46765 -1.16714 -0.01981
C        1.02165  2.14575  0.91748
C        2.96293  1.60485 -0.34683
C        3.6337  -0.78361 -0.70552
C        2.34942 -2.55811  0.22101
C        1.39727  3.46655  0.86008
H        0.1128   1.86423  1.42622
C        3.37486  2.89706 -0.41614
C        4.63937 -1.60862 -1.0955
H        1.46991 -2.93021  0.72302
C        3.339   -3.42866 -0.16816
C        2.58698  3.89058  0.21286
H        0.76603  4.20876  1.33064
H        4.26889  3.16742 -0.95919
C        4.52114 -2.99255 -0.82156
H        5.50053 -1.22541 -1.62342
H        3.21491 -4.48381  0.03677
N        1.5538  -0.22218  0.42815
O        3.75365  0.62467 -1.1005
C        2.97141  5.2751   0.17832
H        2.27137  5.96138  0.68449
C        5.5515  -3.91655 -1.2076
H        5.34306 -4.97101 -0.95876
O        6.61386 -3.61815 -1.77916
O        3.9944   5.72831 -0.36131
```
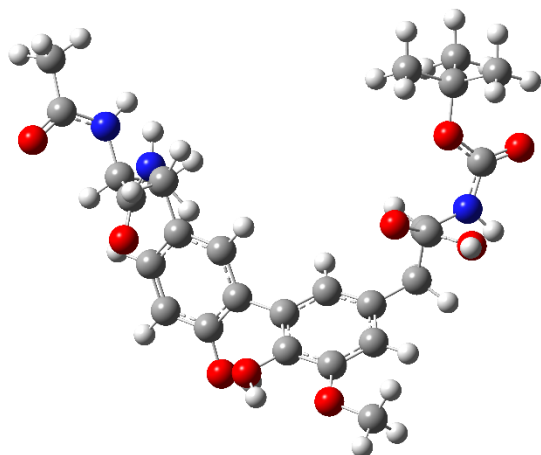
phenol-peptide_rad_plus_2-6-dimethoxyphenol_b3lyp_6311gplus2d2p_H2O
Zero-point correction=   0.428196 (Hartree/Particle)
Thermal correction to Energy=   0.458112
Thermal correction to Enthalpy=   0.459056
Thermal correction to Gibbs Free Energy=   0.362546
Sum of electronic and zero-point Energies=   -1337.986920
Sum of electronic and thermal Energies=   -1337.957005
Sum of electronic and thermal Enthalpies=   -1337.956060
Sum of electronic and thermal Free Energies=   -1338.052571

C   -1.53143 -1.02256 -1.07895
C   -0.31508 -0.40602 -0.80021
C   0.86062 -1.12823 -0.56429
C   0.79454 -2.52903 -0.63116
C   -0.41254 -3.16434 -0.91592
C   -1.56025 -2.41865 -1.13546
H   -0.26911 0.67427 -0.74975
H   -2.48634 -2.93172 -1.36091
O   1.89091 -3.33176 -0.46083
H   -0.43214 -4.24357 -0.9771
C   -2.77995 -0.2105 -1.3284
C   -3.80548 -0.19825 -0.1681
H   -3.30218 -0.61249 -2.19885
H   -2.50754 0.81854 -1.56738
H   -4.05974 -1.22167 0.10158
C   -6.2122 0.326 -0.0091
C   -7.39817 0.98826 -0.67143
H   -7.87271 1.65592 0.04609
C   -3.21631 0.42214 1.11121
N   -3.35951 1.75021 1.25659
H   -3.93166 2.24424 0.59319
O   -2.61348 -0.28018 1.92281
N   -5.01275 0.47721 -0.62838
H   -4.98859 0.94705 -1.51852
O   -6.32272 -0.31117 1.03715
H   -7.13467 1.55178 -1.56343

H	-8.12234	0.21915	-0.93794
C	-2.84746	2.46997	2.41264
H	-1.77097	2.33466	2.5034
H	-3.06135	3.52681	2.28469
H	-3.31729	2.1211	3.33239
C	2.1404	-0.42421	-0.28098
C	2.60315	0.56769	-1.1585
C	2.89413	-0.72398	0.85556
C	3.78634	1.24126	-0.89051
H	2.03596	0.79638	-2.04685
C	4.08622	-0.05181	1.12462
H	2.55067	-1.45131	1.57821
C	4.53785	0.93849	0.25749
H	2.67094	-2.78221	-0.30795
O	5.68994	1.61396	0.5291
O	4.76556	-0.32159	2.29057
O	4.33631	2.22467	-1.65998
C	5.97584	-1.08207	2.12519
H	6.68585	-0.55414	1.49001
H	6.39497	-1.20494	3.11977
H	5.75224	-2.06108	1.69844
C	3.64839	2.62974	-2.84778
H	4.25387	3.41626	-3.28544
H	3.56301	1.79862	-3.54783
H	2.65825	3.01731	-2.60816
H	2.67182	-1.17078	-0.83337
H	0.6461	-1.15874	0.48354
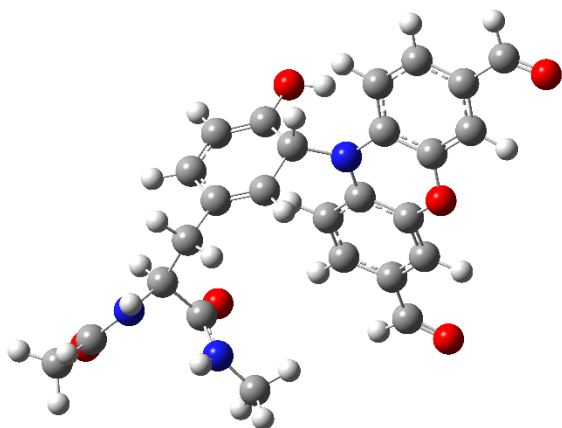
phenol-rad-peptide_plus_flavin_b3lyp_6311gplus2d2p_H2O
Zero-point correction=   0.458302 (Hartree/Particle)
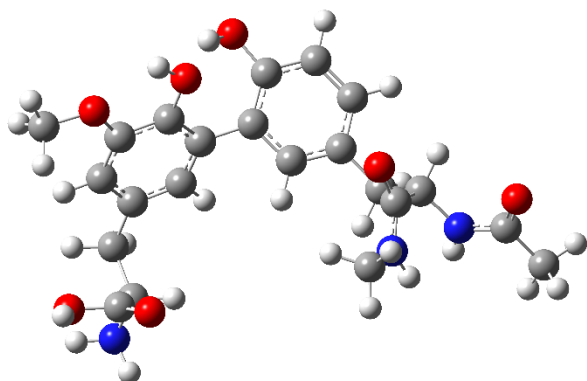Thermal correction to Energy=   0.491263
Thermal correction to Enthalpy=   0.492207
Thermal correction to Gibbs Free Energy=   0.388575

Sum of electronic and zero-point Energies=   -1620.856483
Sum of electronic and thermal Energies=   -1620.823522
Sum of electronic and thermal Enthalpies=   -1620.822578
Sum of electronic and thermal Free Energies=   -1620.926210

C	-1.99072	-1.34732	0.78866
C	-0.79356	-0.90613	0.23695
C	0.32249	-0.66333	1.03378
C	0.25947	-0.86031	2.41507
C	-0.93754	-1.30221	2.97868
C	-2.03832	-1.54309	2.17397
H	-0.7065	-0.74891	-0.82967
H	-2.95157	-1.89764	2.63361
O	1.31578	-0.64922	3.24714
H	-0.98319	-1.46103	4.04658
C	-3.19065	-1.64165	-0.07904
C	-4.34612	-0.61512	0.01244
H	-3.60925	-2.60763	0.20927
H	-2.87743	-1.7289	-1.1201
H	-4.63928	-0.48905	1.05303
C	-6.75637	-0.71401	-0.50815
C	-7.84635	-1.43877	-1.26322
H	-8.41863	-0.71159	-1.83724
C	-3.90433	0.78311	-0.45516
N	-4.10427	1.07713	-1.75027
H	-4.6224	0.42432	-2.31336
O	-3.35995	1.55565	0.33373
N	-5.48492	-1.13948	-0.7301
H	-5.34579	-1.94844	-1.31316
O	-7.00172	0.21342	0.26101
H	2.08968	-0.36489	2.74628
H	-7.46772	-2.20593	-1.93466
H	-8.52205	-1.8987	-0.54292
C	-3.72717	2.35762	-2.32929
H	-2.66291	2.54143	-2.19286
H	-3.94928	2.33492	-3.39192
H	-4.28038	3.17579	-1.86787
C	1.81757	1.13692	0.32206
C	2.46765	-1.16714	-0.01981
C	1.02165	2.14575	0.91748
C	2.96293	1.60485	-0.34683
C	3.6337	-0.78361	-0.70552
C	2.34942	-2.55811	0.22101
C	1.39727	3.46655	0.86008
H	0.1128	1.86423	1.42622
C	3.37486	2.89706	-0.41614
C	4.63937	-1.60862	-1.0955

```
H        1.46991 -2.93021  0.72302
C        3.339   -3.42866 -0.16816
C        2.58698  3.89058  0.21286
H        0.76603  4.20876  1.33064
H        4.26889  3.16742 -0.95919
C        4.52114 -2.99255 -0.82156
H        5.50053 -1.22541 -1.62342
H        3.21491 -4.48381  0.03677
N        1.5538  -0.22218  0.42815
O        3.75365  0.62467 -1.1005
C        2.97141  5.2751   0.17832
H        2.27137  5.96138  0.68449
C        5.5515  -3.91655 -1.2076
H        5.34306 -4.97101 -0.95876
O        6.61386 -3.61815 -1.77916
O        3.9944   5.72831 -0.36131
H        0.62711 -1.68129  0.90783
```


peptide-OH-rad_plus_biotin-tyramide_ketone_b3lyp_6311gplus2d2p_h2o_mfgeom_unfreeze1to54_optfreqtight_2
Zero-point correction=   0.678847 (Hartree/Particle)
Thermal correction to Energy=   0.722419
Thermal correction to Enthalpy=   0.723363
Thermal correction to Gibbs Free Energy=   0.589672
Sum of electronic and zero-point Energies=   -2290.587754
Sum of electronic and thermal Energies=   -2290.544181
Sum of electronic and thermal Enthalpies=   -2290.543237
Sum of electronic and thermal Free Energies=   -2290.676929

```
C        4.7911  -0.29125  0.20794
C        4.10186 -0.48314  1.43347
C        3.90917  0.59172  2.32417
C        4.32804  1.851    2.00532
C        4.92504  2.18898  0.66865
C        5.19808  0.96064 -0.15079
H        3.75386 -1.46902  1.70656
```

H	5.72094	1.11512	-1.08699
O	4.20536	2.85181	2.9176
H	3.4505	0.42403	3.28976
C	5.06727	-1.47651	-0.69229
C	6.49324	-2.06915	-0.58926
H	4.92862	-1.18095	-1.73312
H	4.34328	-2.26635	-0.48476
H	7.22229	-1.29123	-0.80785
C	7.82529	-3.5848	-2.01319
C	7.79748	-4.59546	-3.13643
H	8.32557	-5.49188	-2.81488
C	6.82945	-2.545	0.83593
N	6.48058	-3.80512	1.14624
H	6.13033	-4.39822	0.41338
O	7.35687	-1.77788	1.64117
N	6.62063	-3.12546	-1.58688
H	5.7948	-3.41763	-2.08318
O	8.87904	-3.20203	-1.50715
H	6.79089	-4.86604	-3.44681
H	8.33396	-4.18271	-3.99013
C	6.73531	-4.38752	2.4549
H	6.2661	-3.79245	3.23646
H	6.31828	-5.38999	2.47458
H	7.80466	-4.44363	2.65981
C	4.05539	3.21816	-0.16251
C	2.75791	2.68683	-0.68104
C	3.9754	4.61396	0.43648
C	1.69956	3.47773	-0.932
H	2.72326	1.63133	-0.91675
C	2.88071	5.44828	-0.02075
C	1.80848	4.89683	-0.63376
H	2.90493	6.49564	0.24546
H	0.97246	5.53458	-0.89517
O	4.81131	5.01801	1.25325
C	0.40649	2.95083	-1.50362
C	-0.71434	2.86887	-0.44992
H	0.56629	1.95885	-1.92402
H	0.07492	3.59887	-2.31828
H	-0.42599	2.17844	0.33924
H	-0.88305	3.84459	0.0043
C	-2.35165	1.11069	-1.04785
C	-3.69587	0.82366	-1.69373
C	-4.68159	0.1652	-0.71827
H	-3.50755	0.14838	-2.53144
H	-4.13023	1.73556	-2.1055
C	-6.01226	-0.19121	-1.38463
H	-4.22266	-0.73347	-0.30299

H	-4.86423	0.84169	0.12103
C	-6.99916	-0.85048	-0.41862
H	-6.46193	0.71022	-1.80667
H	-5.82537	-0.86764	-2.22433
H	-6.53894	-1.75595	-0.01505
H	-7.1785	-0.19228	0.43428
N	-1.97771	2.41038	-1.00775
H	-2.58145	3.09159	-1.43572
O	-1.65347	0.20772	-0.58015
C	-10.07941	0.36247	0.08854
C	-10.19205	-1.06084	0.65899
C	-8.32662	-1.24297	-1.073
C	-9.31687	-2.04357	-0.18345
C	-8.87784	-2.36478	2.10738
S	-9.35631	0.19924	-1.59472
H	-9.94982	-2.63148	-0.84358
H	-11.23244	-1.38505	0.64165
N	-8.73893	-2.88581	0.84992
H	-8.05181	-3.59723	0.6707
N	-9.62991	-1.21379	2.00032
H	-10.15821	-0.92985	2.80905
O	-8.41457	-2.83161	3.14428
H	-8.12502	-1.80809	-1.98236
H	-11.04337	0.8537	-0.00455
H	-9.43253	0.97403	0.71222
H	5.86653	2.72312	0.84532
H	4.66248	3.40507	-1.06585
H	4.57442	3.67381	2.5467
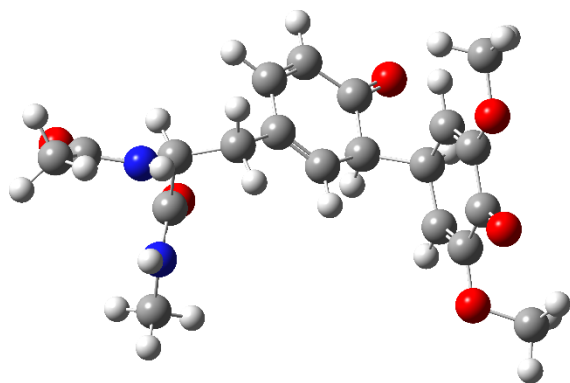
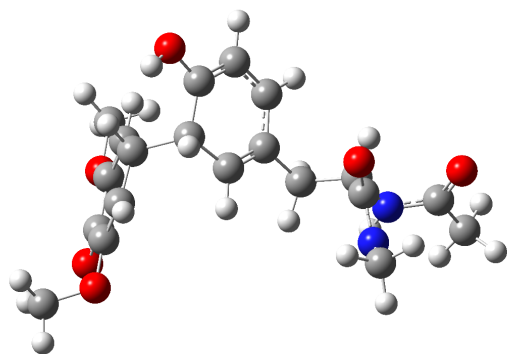**KETONE-peptide_plus_2-6-dimethoxyphenone_b3lyp_6311gplus2d2p_H2O_noH**
Zero-point correction=   0.418587 (Hartree/Particle)
Thermal correction to Energy=   0.447916
Thermal correction to Enthalpy=   0.448860
Thermal correction to Gibbs Free Energy=   0.353505

Sum of electronic and zero-point Energies=   -1337.419436
Sum of electronic and thermal Energies=   -1337.390108
Sum of electronic and thermal Enthalpies=   -1337.389164
Sum of electronic and thermal Free Energies=   -1337.484519

C	0.74493	0.90668	-0.04676
C	-0.22437	0.4181	0.74509
C	-1.20716	1.28048	1.45227
C	-0.97765	2.7761	1.34
C	0.05167	3.22976	0.42095
C	0.85178	2.34757	-0.21734
H	-0.33447	-0.65158	0.8726
H	1.61303	2.72348	-0.89057
O	-1.66675	3.56159	1.99651
H	0.16433	4.29643	0.28365
C	1.70013	0.01421	-0.79829
C	3.18075	0.10943	-0.35803
H	1.67208	0.27742	-1.85864
H	1.36993	-1.02171	-0.7157
H	3.51528	1.14426	-0.40664
C	5.32414	-0.47975	-1.42758
C	6.00566	-1.28515	-2.50931
H	6.83843	-1.83068	-2.06846
C	3.35683	-0.29802	1.11555
N	3.64532	-1.58719	1.3557
H	3.83758	-2.18699	0.57161
O	3.1928	0.53355	2.00836
N	3.98782	-0.67868	-1.27946
H	3.51808	-1.28286	-1.93359
O	5.94143	0.31003	-0.71557
H	5.34093	-1.98757	-3.00676
H	6.41399	-0.59781	-3.24964
C	3.82776	-2.11144	2.70068
H	2.93799	-1.93819	3.30354
H	4.00725	-3.18023	2.63339
H	4.67673	-1.63893	3.19495
C	-2.74017	0.94998	1.00984
C	-2.97197	1.168	-0.45121
C	-3.13213	-0.40676	1.48254
C	-3.32286	0.14538	-1.27121
H	-2.81911	2.16107	-0.84424
C	-3.48397	-1.40751	0.62725
H	-3.09834	-0.61601	2.54282
C	-3.54923	-1.17318	-0.76627
O	-3.83711	-2.19171	-1.61594
O	-3.72821	-2.67386	1.11364
O	-3.50851	0.21576	-2.62358

```
C       -5.10826 -3.07744  1.08969
H       -5.50124 -3.07888  0.07392
H       -5.13635 -4.08556  1.49344
H       -5.70588 -2.41502  1.7181
C       -3.29435  1.47258 -3.27082
H       -3.47577  1.29818 -4.32615
H       -3.99092  2.22278 -2.89606
H       -2.26949  1.81308 -3.12253
H       -3.28392  1.70852  1.58312
H       -1.20193  1.04073  2.51831
```


ketone-peptide_plus_2-methoxy4-methyl-phenone_b3lyp_6311gplus2d2p_H2O
Zero-point correction=   0.413558 (Hartree/Particle)
Thermal correction to Energy=   0.441792
Thermal correction to Enthalpy=   0.442736
Thermal correction to Gibbs Free Energy=   0.350182
Sum of electronic and zero-point Energies=   -1262.196089
Sum of electronic and thermal Energies=   -1262.167855
Sum of electronic and thermal Enthalpies=   -1262.166911
Sum of electronic and thermal Free Energies=   -1262.259465

```
C        1.26292 -1.17568  0.87152
C        0.06045 -0.48319  0.79164
C       -1.15109 -1.09029  0.42424
C       -1.11712 -2.45949  0.10079
C        0.07964 -3.17075  0.19508
C        1.25155 -2.54304  0.58268
H        0.05046  0.57393  1.02138
H        2.16418 -3.12104  0.65215
O       -2.2314  -3.17563 -0.24879
H        0.06768 -4.22637 -0.03826
C        2.53851 -0.47741  1.27935
C        3.55497 -0.2338   0.13702
H        3.05373 -1.08081  2.02936
H        2.30035  0.47861  1.74806
H        3.78071 -1.17778 -0.35553
```

```
C     5.97332  0.25326  0.0653
C     7.18063  0.72709  0.84092
H     7.66563  1.52567  0.28157
C     2.97285  0.66763 -0.9664
N     3.14998  1.99126 -0.81776
H     3.74153  2.31312 -0.07063
O     2.3456  0.17649 -1.90478
N     4.78312  0.29426  0.71855
H     4.77881  0.55854  1.69011
O     6.05906 -0.14271 -1.09598
H     6.9376  1.08632  1.83818
H     7.88801 -0.09748  0.92253
C     2.64753  2.95927 -1.78079
H     1.56766  2.87023 -1.88672
H     2.88696  3.95698 -1.42547
H     3.10311  2.81204 -2.76017
C    -2.39927 -0.27948  0.47353
C    -2.63417  0.56226  1.57906
C    -3.35394 -0.28333 -0.53709
C    -3.76173  1.36287  1.681
H    -1.9125  0.56483  2.38381
C    -4.50403  0.5183  -0.45382
C    -4.70593  1.3368  0.64404
H    -5.59014  1.95309  0.70975
O    -3.18091 -1.07524 -1.65228
O    -5.33771  0.39741 -1.52996
C    -6.53986  1.17252 -1.55217
H    -6.31312  2.23853 -1.53193
H    -7.0366  0.92116 -2.48329
H    -7.18256  0.91393 -0.71057
C    -3.98892  2.24432  2.88448
H    -4.06781  3.29399  2.59591
H    -4.91564  1.98208  3.39799
H    -3.17208  2.15277  3.59813
H    -1.00921 -0.82891 -0.6036
H    -2.90285 -1.08946  0.95854
```
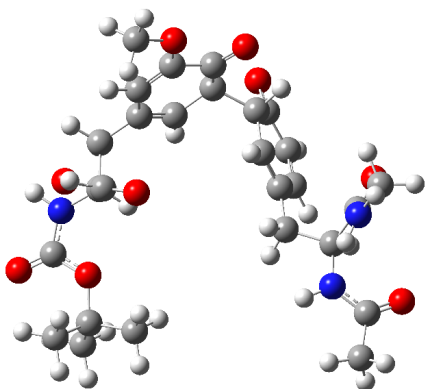
ketone-peptide_plus_2-methoxy-4ethyl-COOH-NHBoc-phenone_b3lyp_6311gplus2d2p_H2O

Zero-point correction=   0.600304 (Hartree/Particle)
Thermal correction to Energy=   0.642454
Thermal correction to Enthalpy=   0.643398
Thermal correction to Gibbs Free Energy=   0.515849
Sum of electronic and zero-point Energies=   -1891.293046
Sum of electronic and thermal Energies=   -1891.250896
Sum of electronic and thermal Enthalpies=   -1891.249951
Sum of electronic and thermal Free Energies=   -1891.377501

C	-3.1488	-0.20254	-1.49673
C	-1.95094	-0.68655	-0.97863
C	-1.50726	-1.99435	-1.204
C	-2.30598	-2.83485	-1.99163
C	-3.50434	-2.36574	-2.52747
C	-3.91752	-1.06578	-2.2823
H	-1.33433	-0.03651	-0.37138
H	-4.84861	-0.72027	-2.71289
O	-1.94983	-4.11807	-2.30394
H	-4.09514	-3.02861	-3.14425
C	-3.59441	1.21659	-1.23571
C	-4.78688	1.36868	-0.25983
H	-3.9039	1.67667	-2.17643
H	-2.75414	1.80067	-0.85704
H	-5.62821	0.77966	-0.62022
C	-6.39926	3.17984	0.2047
C	-6.70469	4.65303	0.06215
H	-6.95484	5.05576	1.04257
C	-4.46525	0.80048	1.13396
N	-3.91998	1.65153	2.0192
H	-3.86059	2.62436	1.77096
O	-4.67012	-0.38741	1.38371
N	-5.17891	2.77249	-0.23078
H	-4.58358	3.44496	-0.68568

```
O      -7.20666  2.39149  0.69389
H      -5.88104  5.22488 -0.35895
H      -7.58006  4.76703 -0.57625
C      -3.56275  1.25095  3.37146
H      -2.85999  0.41988  3.35148
H      -3.09764  2.0956   3.87078
H      -4.443    0.94462  3.9371
C      -0.19751 -2.44514 -0.65442
C       0.99126 -1.82043 -1.05913
C      -0.11612 -3.4739   0.2838
C       2.22934 -2.19912 -0.55573
H       0.9292  -1.03049 -1.79566
C       1.13104 -3.8735   0.79465
C       2.29226 -3.24127  0.37721
H       3.24925 -3.55352  0.76734
O      -1.25249 -4.09394  0.72197
O       1.05611 -4.89207  1.70066
C       2.26706 -5.36848  2.29547
H       2.76443 -4.57325  2.85088
H       1.97064 -6.16008  2.97542
H       2.93976 -5.76847  1.53668
C       3.49173 -1.50847 -1.01744
H       4.35888 -2.13313 -0.79997
H       3.46162 -1.36585 -2.09804
C       3.72554 -0.10413 -0.40576
H       2.86625  0.52468 -0.62071
C       3.81016 -0.18241  1.11902
O       2.87915  0.0334   1.85786
O       5.02567 -0.55279  1.55636
H       4.99638 -0.60814  2.52373
N       4.90663  0.47481 -1.01998
H       5.62513 -0.14802 -1.35098
C       5.29888  1.77928 -0.92173
O       6.3592   2.18409 -1.37145
O       4.36894  2.51477 -0.29284
C       4.51265  3.98165 -0.10924
C       3.22204  4.34715  0.61927
H       2.35228  4.09316  0.01438
H       3.15266  3.81949  1.56979
H       3.20332  5.418    0.81739
C       5.72889  4.2799   0.76419
H       6.65512  4.0275   0.2566
H       5.74237  5.34271  1.00585
H       5.67194  3.72134  1.69844
C       4.57856  4.67188 -1.46946
H       4.54368  5.75149 -1.32341
H       5.49369  4.42342 -1.9988
```

H   3.72402 4.38587 -2.08269
H   -0.10854 -3.15495 -1.45013
H   -2.00175 -2.33425 -0.31809
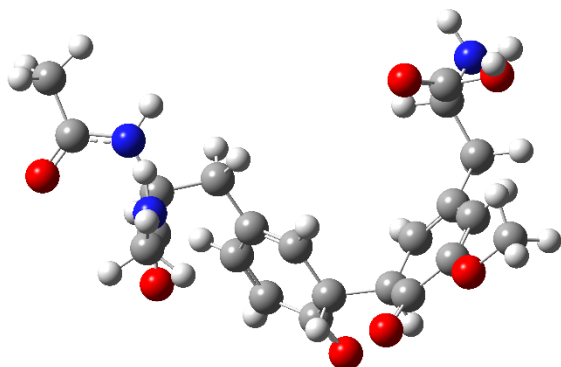
ketone-peptide_plus_2-methoxy-4ethyl-COOH-NH2-phenone_b3lyp_6311gplus2d2p_H2O
Zero-point correction=   0.474907 (Hartree/Particle)
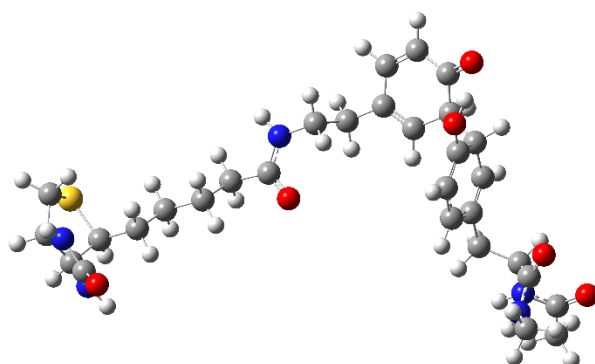Thermal correction to Energy=   0.508454
Thermal correction to Enthalpy=   0.509398
Thermal correction to Gibbs Free Energy=   0.403371
Sum of electronic and zero-point Energies=   -1545.470117
Sum of electronic and thermal Energies=   -1545.436571
Sum of electronic and thermal Enthalpies=   -1545.435627
Sum of electronic and thermal Free Energies=   -1545.541653

C   2.12535 1.09601 -1.20098
C   0.81682 0.77881 -0.85626
C   -0.19653 1.74214 -0.72803
C   0.15765 3.08775 -0.93768
C   1.4635   3.41786 -1.30176
C   2.43235 2.43826 -1.44026
H   0.56045 -0.25662 -0.67568
H   3.43612 2.72283 -1.72868
O   -0.7403   4.11998 -0.86887
H   1.69856 4.4584 -1.47752
C   3.17815 0.02199 -1.33698
C   4.22668 -0.02864 -0.19875
H   3.73427 0.18028 -2.26314
H   2.69876 -0.95484 -1.41635
H   4.69305 0.9489 -0.09098
C   6.48864 -0.99683 0.00181
C   7.4862 -1.97979 -0.5661
H   7.8573 -2.60885 0.24158
C   3.57773 -0.31926 1.16627
N   3.48055 -1.61071 1.52373
H   3.93012 -2.30045 0.94622

```
O      3.14241  0.60253  1.85631
N      5.25347 -0.99693 -0.56378
H      5.09482 -1.58321 -1.36672
O      6.77423 -0.24101  0.92902
H      7.07123 -2.6109  -1.34856
H      8.33217 -1.42391 -0.969
C      2.88606 -2.03162  2.7831
H      1.85589 -1.68701  2.85585
H      2.89991 -3.11655  2.82601
H      3.44282 -1.63523  3.63238
C     -1.58697  1.28156 -0.45857
C     -2.10234  0.18486 -1.17131
C     -2.41713  1.8698   0.49259
C     -3.38145 -0.31064 -0.95333
H     -1.48252 -0.26905 -1.93208
C     -3.71429  1.38966  0.72373
C     -4.19405  0.30424  0.00703
H     -5.19398 -0.06382  0.17883
O     -1.96942  2.94304  1.22958
O     -4.39587  2.08172  1.6839
C     -5.72813  1.67114  2.00706
H     -5.73689  0.64804  2.38287
H     -6.06581  2.34951  2.78331
H     -6.38008  1.75357  1.13746
C     -3.88824 -1.49945 -1.7395
H     -4.97865 -1.51456 -1.73308
H     -3.57449 -1.42232 -2.78048
C     -3.37101 -2.86222 -1.23353
H     -2.28353 -2.86629 -1.27339
C     -3.72563 -3.09023  0.23452
O     -2.92213 -3.22173  1.13001
O     -5.0562  -3.15713  0.43915
H     -5.21253 -3.32607  1.38049
N     -3.85892 -3.93077 -2.10961
H     -4.8665  -4.01829 -2.03899
H     -3.46393 -4.82417 -1.83979
H     -0.01475  1.84265  0.32161
H     -1.95154  1.95952 -1.20178
```
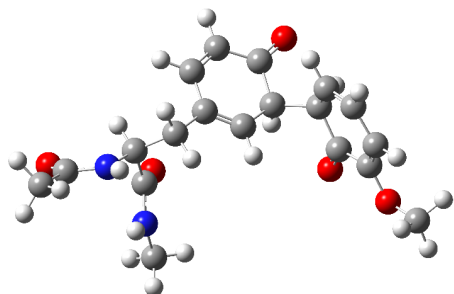
ketone-peptide_plus_2-methoxyphenone_b3lyp_6311gplus2d2p_H2O
Zero-point correction=   0.386041 (Hartree/Particle)
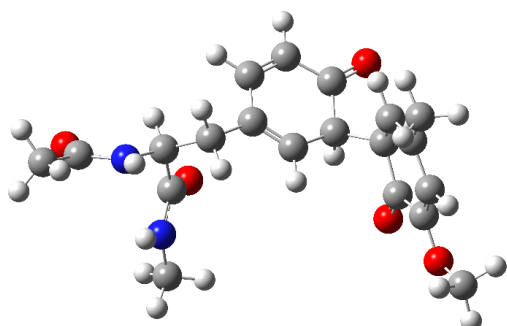Thermal correction to Energy=   0.412608
Thermal correction to Enthalpy=   0.413552
Thermal correction to Gibbs Free Energy=   0.324157
Sum of electronic and zero-point Energies=   -1222.892863
Sum of electronic and thermal Energies=   -1222.866296
Sum of electronic and thermal Enthalpies=   -1222.865352
Sum of electronic and thermal Free Energies=   -1222.954746

C	1.10501	-1.49529	0.46512
C	-0.08317	-0.83407	0.76411
C	-1.32111	-1.24447	0.25802
C	-1.35154	-2.37487	-0.57069
C	-0.17397	-3.05564	-0.87525
C	1.03779	-2.61908	-0.36267
H	-0.05851	0.03694	1.4063
H	1.93991	-3.16533	-0.6068
O	-2.51152	-2.88436	-1.08631
H	-0.22617	-3.93279	-1.50517
C	2.4229	-1.01975	1.02818
C	3.34182	-0.27755	0.02692
H	2.99097	-1.87687	1.39509
H	2.24006	-0.36849	1.88426
H	3.53695	-0.91894	-0.83063
C	5.73831	0.31641	0.00804
C	6.99716	0.47094	0.82985
H	7.43566	1.44534	0.62069
C	2.66454	0.97624	-0.55518
N	2.81328	2.11673	0.13962
H	3.44296	2.11889	0.92391
O	1.99219	0.8998	-1.58336
N	4.60581	0.01231	0.69331
H	4.67856	-0.16649	1.68147
O	5.73498	0.46202	-1.21322
H	6.82598	0.37779	1.8998
H	7.71273	-0.28898	0.51728

```
C        2.2269  3.37707 -0.29017
H        1.14861 3.2789  -0.40234
H        2.43719 4.13082 0.46269
H        2.64448 3.70127 -1.24372
C       -2.56376 -0.51538 0.63893
C       -2.97042 -0.45598 1.98228
C       -3.336   0.15268 -0.31183
C       -4.10781 0.23957 2.35548
H       -2.38058 -0.97169 2.72678
C       -4.49484 0.85688 0.06675
C       -4.88098 0.90026 1.39759
H       -5.76734 1.43821 1.69596
O       -2.95898 0.14459 -1.62564
O       -5.13759 1.46067 -0.97645
C       -6.31458 2.22529 -0.69994
H       -6.08938 3.05207 -0.02608
H       -6.64722 2.61298 -1.65701
H       -7.0926  1.59587 -0.2678
H       -4.40787 0.27089 3.3932
H       -3.13521 -1.40781 0.49091
H       -1.20383 -0.6083  -0.59429
```
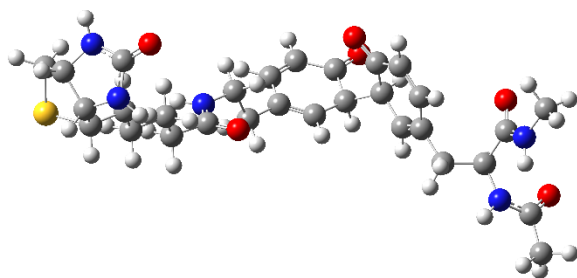

**ketone-peptide_plus_biotin-
tyramide_ketone_b3lyp_6311gplus2d2p_h2o_mfgeom_unfreeze1to54_optfreqtight_2**
Zero-point correction=   0.668668 (Hartree/Particle)
Thermal correction to Energy=   0.711865
Thermal correction to Enthalpy=   0.712809
Thermal correction to Gibbs Free Energy=   0.581343
Sum of electronic and zero-point Energies=   -2290.018346
Sum of electronic and thermal Energies=   -2289.975149
Sum of electronic and thermal Enthalpies=   -2289.974205
Sum of electronic and thermal Free Energies= -2290.105671

```
C        5.09364 -0.37611 0.08508
C        4.49307 -0.80632 1.33976
C        3.85685 0.03282 2.18423
C        3.69801 1.44313 1.86329
C        4.49816 1.97327 0.67702
```

```
C      5.05722  0.9277  -0.23415
H      4.53472 -1.86037  1.58359
H      5.49149  1.27321 -1.16485
O      2.97203  2.18826  2.51613
H      3.37204 -0.32892  3.08032
C      5.70597 -1.40331 -0.83846
C      7.20027 -1.72344 -0.58787
H      5.63403 -1.04122 -1.86373
H      5.13256 -2.33123 -0.78555
H      7.77495 -0.80115 -0.65065
C      8.96751 -2.73947 -1.97747
C      9.27563 -3.61789 -3.16758
H      9.99977 -4.37369 -2.86773
C      7.45368 -2.25922  0.83214
N      7.48165 -3.59251  0.98149
H      7.43915 -4.16534  0.15579
O      7.58008 -1.4733   1.77217
N      7.65638 -2.62666 -1.6361
H      6.96864 -3.06117 -2.22932
O      9.8505  -2.1617  -1.34661
H      8.39649 -4.10811 -3.57926
H      9.73634 -3.00561 -3.9422
C      7.7027  -4.2312   2.27016
H      6.95258 -3.90972  2.99059
H      7.63072 -5.30666  2.13947
H      8.68847 -3.98623  2.66564
C      3.76822  3.12545 -0.05873
C      2.43937  2.73196 -0.62725
C      3.78184  4.41766  0.75834
C      1.36006  3.52845 -0.58597
H      2.38905  1.77254 -1.12854
C      2.58437  5.24437  0.70768
C      1.46643  4.81869  0.0844
H      2.62049  6.19843  1.21505
H      0.59289  5.45997  0.08146
O      4.79141  4.76072  1.36842
C      0.03582  3.13714 -1.19385
C     -1.00636  2.74027 -0.1313
H      0.17572  2.30112 -1.8778
H     -0.36031  3.97151 -1.77762
H     -0.65916  1.86608  0.41447
H     -1.14659  3.54809  0.58596
C     -2.67237  1.17859 -1.08779
C     -4.06363  1.04621 -1.68159
C     -4.98301  0.17741 -0.8106
H     -3.94811  0.58307 -2.6637
H     -4.5141   2.0275  -1.83645
```

```
C        -6.36489 -0.02282 -1.43678
H        -4.50669 -0.79094 -0.64822
H        -5.09271  0.64292  0.17256
C        -7.28588 -0.88349 -0.56909
H        -6.83093  0.94938 -1.61102
H        -6.25155 -0.49368 -2.41807
H        -6.80722 -1.85301 -0.40982
H        -7.39419 -0.42992  0.41853
N        -2.30459  2.4238  -0.70781
H        -2.94434  3.18092 -0.87887
O        -1.93408  0.20008 -0.94841
C       -10.30347  0.18878  0.41011
C       -10.39316 -1.32325  0.67399
C        -8.66258 -1.13072 -1.19179
C        -9.59536 -2.10379 -0.41949
C        -8.99266 -2.8993   1.71321
S        -9.70844  0.38678 -1.31884
H       -10.28285 -2.54103 -1.13941
H       -11.43626 -1.63888  0.66623
N        -8.95391 -3.14347  0.36734
H        -8.28793 -3.79592 -0.00832
N        -9.73662 -1.75466  1.90736
H       -10.20013 -1.64854  2.79489
O        -8.45932 -3.57245  2.59076
H        -8.53571 -1.48981 -2.21253
H       -11.26496  0.68635  0.49539
H        -9.60412  0.65575  1.09881
H         5.36891  2.45391  1.15278
H         4.40589  3.37405 -0.92006
```
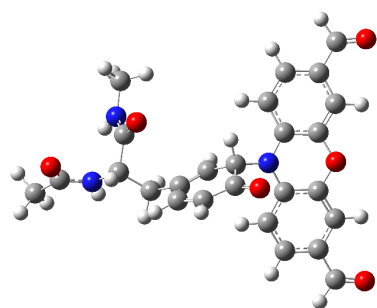

keton-peptide_plus_flavin_b3lyp_6311gplus2d2p_H2O_noH
Zero-point correction=   0.448413 (Hartree/Particle)
Thermal correction to Energy=   0.480787
Thermal correction to Enthalpy=   0.481731
Thermal correction to Gibbs Free Energy=   0.379557
Sum of electronic and zero-point Energies=   -1620.289523
Sum of electronic and thermal Energies=   -1620.257150

Sum of electronic and thermal Enthalpies=   -1620.256205
Sum of electronic and thermal Free Energies=   -1620.358380

```
C      -1.87196 -1.51225  0.72318
C      -0.67001 -0.98697  0.26386
C       0.40582 -0.78051  1.12547
C       0.29237 -1.10278  2.47994
C      -0.90547 -1.64199  2.94971
C      -1.96436 -1.84313  2.08053
H      -0.55104 -0.72799 -0.77982
H      -2.8814  -2.26866  2.46662
O       1.30676 -0.9225   3.36859
H      -0.98692 -1.90094  3.99569
C      -3.03448 -1.73875 -0.2131
C      -4.21579 -0.75115 -0.04821
H      -3.4392  -2.73883 -0.04714
H      -2.68553 -1.70324 -1.24592
H      -4.55849 -0.76544  0.98477
C      -6.59604 -0.81325 -0.69542
C      -7.63498 -1.44166 -1.59484
H      -8.1427  -0.6524  -2.14789
C      -3.78804  0.70478 -0.30894
N      -3.9362   1.16193 -1.56319
H      -4.41534  0.58031 -2.22923
O      -3.30116  1.37855  0.59912
N      -5.30847 -1.19428 -0.90435
H      -5.12716 -1.91932 -1.579
O      -6.89395  0.00644  0.17144
H      -7.21787 -2.15768 -2.29908
H      -8.37724 -1.94168 -0.97421
C      -3.572   2.51631 -1.95046
H      -2.52419  2.70929 -1.72798
H      -3.7329   2.62533 -3.01872
H      -4.1781   3.2531  -1.42286
C       1.78443  1.14705  0.46622
C       2.60626 -1.09411  0.07558
C       0.78749  2.05054  0.83812
C       2.98163  1.65314 -0.07845
C       3.78616 -0.54078 -0.4609
C       2.44734 -2.48065  0.04508
C       0.97994  3.41494  0.67244
H      -0.13631  1.68272  1.2553
C       3.17031  3.00245 -0.25201
C       4.75976 -1.33776 -1.01164
H       1.55146 -2.92263  0.45112
C       3.43408 -3.28864 -0.50221
C       2.16567  3.90602  0.12757
```

221

H   0.19905 4.10194 0.96883
H   4.098   3.3607 -0.674
C   4.59524 -2.73142 -1.03605
H   5.65228 -0.88476 -1.41814
H   3.29702 -4.36135 -0.515
N   1.64475 -0.23889 0.63421
O   4.01909 0.81665 -0.42849
C   2.33932 5.35018 -0.03642
H   1.48013 5.95803 0.29629
C   5.61599 -3.60842 -1.61185
H   5.37173 -4.68427 -1.57647
O   6.6681 -3.23469 -2.10484
O   3.33114 5.89189 -0.49751
H   0.05162 0.2087 1.32772
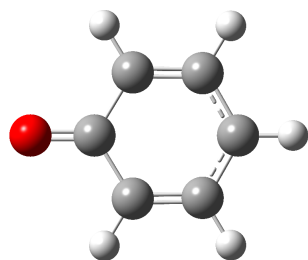
PHENOL_RADICAL_H2O_B3LYP_6-311GPLUS2D2P_OPT_FREQ

Zero-point correction=   0.091396 (Hartree/Particle)
Thermal correction to Energy=   0.096693
Thermal correction to Enthalpy=   0.097637
Thermal correction to Gibbs Free Energy=   0.061834
Sum of electronic and zero-point Energies=   -306.841002
Sum of electronic and thermal Energies=   -306.835705
Sum of electronic and thermal Enthalpies=   -306.834761
Sum of electronic and thermal Free Energies=   -306.870564

C   1.77851 0.   0.
C   1.08335 1.22195 0.00007
C   -0.2887 1.23714 -0.00004
C   -1.04432 0.   -0.00005
C   -0.2887 -1.23714 0.00004
C   1.08335 -1.22195 -0.00003
H   2.8597 0.   -0.00004
H   1.63897 2.14978 -0.00002
H   -0.85322 2.15885 -0.00006
H   -0.85322 -2.15885 0.00004
H   1.63897 -2.14978 -0.00002
O   -2.29652   0.00002
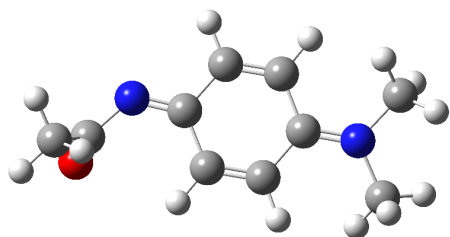
dimethyl_amine_probe_H2O_b3lyp_6311gplus2d2p
Zero-point correction=   0.216245 (Hartree/Particle)
Thermal correction to Energy=   0.229696
Thermal correction to Enthalpy=   0.230640
Thermal correction to Gibbs Free Energy=   0.175143
Sum of electronic and zero-point Energies=   -573.388264
Sum of electronic and thermal Energies=   -573.374813
Sum of electronic and thermal Enthalpies=   -573.373869
Sum of electronic and thermal Free Energies=   -573.429366

C	-0.12332	1.5895	-0.18984
C	-1.08688	0.50077	-0.05923
C	-0.54479	-0.84352	0.14669
C	0.78192	-1.05989	0.18076
C	1.72711	0.03358	0.03231
C	1.20358	1.37472	-0.13948
H	-0.52642	2.57947	-0.34864
H	-1.23297	-1.66689	0.2649
H	1.14808	-2.05828	0.35346
H	1.88064	2.20177	-0.27206
N	3.02831	-0.19028	0.05475
N	-2.33353	0.79723	-0.14114
C	4.0248	0.89692	0.06247
H	4.92461	0.52413	0.54141
H	4.266	1.19534	-0.95795
H	3.66634	1.75051	0.62572
C	3.60955	-1.54564	0.06562
H	3.73383	-1.89525	1.09068
H	2.99363	-2.23944	-0.49395
H	4.58469	-1.49566	-0.40876
C	-3.36406	-0.1833	-0.15395
O	-3.37519	-1.0315	-1.01326
C	-4.42997	0.03583	0.87762
H	-5.0982	-0.82004	0.89179
H	-3.99674	0.19903	1.86509
H	-4.99297	0.93489	0.62132
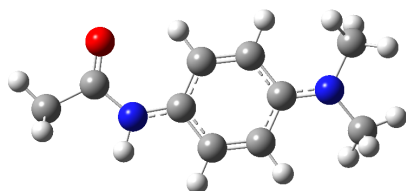
radical_dimethyl_amine_probe_H2O_b3lyp_6311gplus2d2p
Zero-point correction=   0.228320 (Hartree/Particle)
Thermal correction to Energy=   0.241974
Thermal correction to Enthalpy=   0.242918
Thermal correction to Gibbs Free Energy=   0.186307
Sum of electronic and zero-point Energies=   -574.017702
Sum of electronic and thermal Energies=   -574.004048
Sum of electronic and thermal Enthalpies=   -574.003104
Sum of electronic and thermal Free Energies=   -574.059715

C	-0.12193	1.51459	-0.01975
C	-1.00383	0.39411	-0.00398
C	-0.44045	-0.91483	0.01609
C	0.92434	-1.07946	0.01622
C	1.81919	0.03956	0.00045
C	1.2398	1.35163	-0.01575
H	-0.53562	2.52044	-0.0384
H	-1.09616	-1.77539	0.03343
H	1.316	-2.0895	0.03886
H	1.87002	2.23264	-0.03564
N	3.16351	-0.13406	0.00061
N	-2.35423	0.64268	-0.00895
C	4.07731	1.01725	0.04659
H	5.0978	0.65375	0.16002
H	4.01372	1.60011	-0.88024
H	3.84253	1.66243	0.89911
C	3.7543	-1.4805	-0.0464
H	3.54726	-2.02746	0.88133
H	3.35928	-2.04527	-0.89664
H	4.83321	-1.3882	-0.16389
C	-3.43769	-0.28185	0.00316
O	-3.2496	-1.4758	0.01959
C	-4.79386	0.38119	-0.00549
H	-5.56002	-0.39512	-0.00709
H	-4.92341	1.01459	0.88117
H	-4.91565	1.01191	-0.89504
H	-2.62015	1.62106	-0.02235
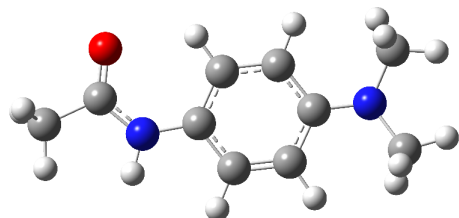
reduced_dimethyl_amine_probe_H2O_b3lyp_6311gplus2d2p
Zero-point correction=   0.227380 (Hartree/Particle)
Thermal correction to Energy=   0.240929
Thermal correction to Enthalpy=   0.241873
Thermal correction to Gibbs Free Energy=   0.185889
Sum of electronic and zero-point Energies=   -574.198955
Sum of electronic and thermal Energies=   -574.185406
Sum of electronic and thermal Enthalpies=   -574.184462
Sum of electronic and thermal Free Energies=   -574.240446

C	-0.13224	1.48379	0.02681
C	-0.99802	0.38108	0.02434
C	-0.43375	-0.9025	0.04469
C	0.95188	-1.06247	0.07315
C	1.83719	0.03852	0.09367
C	1.25053	1.32467	0.05461
H	-0.54096	2.49367	-0.00017
H	-1.0796	-1.77124	0.03304
H	1.33752	-2.0757	0.0815
H	1.86724	2.21622	0.04844
N	3.22253	-0.13252	0.16882
N	-2.39254	0.63554	-0.00789
C	4.08077	1.00647	-0.11721
H	5.12373	0.70781	0.01551
H	3.95841	1.39374	-1.14477
H	3.88648	1.82795	0.58227
C	3.7769	-1.45017	-0.10449
H	3.39023	-2.19155	0.60409
H	3.55937	-1.80625	-1.12716
H	4.86168	-1.41227	0.0241
C	-3.43953	-0.25448	-0.02385
O	-3.30335	-1.47129	-0.01168
C	-4.82088	0.38549	-0.05915
H	-5.38713	0.03787	0.81147
H	-4.80942	1.48089	-0.06252
H	-5.34468	0.03217	-0.95378
H	-2.64312	1.61354	-0.02045
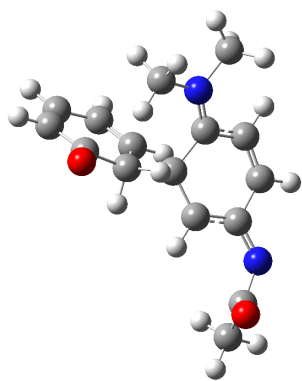
dimethyl_amine_probe_addn_phenoxyl_radical_C-C_H2O_b3lyp_6311gplus2d2p
Zero-point correction=   0.309928 (Hartree/Particle)
Thermal correction to Energy=   0.329529
Thermal correction to Enthalpy=   0.330473
Thermal correction to Gibbs Free Energy=   0.259287
Sum of electronic and zero-point Energies=   -880.198254
Sum of electronic and thermal Energies=   -880.178653
Sum of electronic and thermal Enthalpies=   -880.177708
Sum of electronic and thermal Free Energies=   -880.248894

C   -0.28842 -0.81414 -1.00233
C   1.11672 -0.39814 -0.71806
C   -0.90499 -1.7594 0.03124
C   1.9017 -0.99785 0.2739
C   -0.04845 -2.31348 1.05109
C   1.2537 -1.98318 1.14088
H   -0.44725 -3.04612 1.73177
H   1.87474 -2.44636 1.89409
H   -0.24041 -1.39836 -1.93254
H   1.52188 0.35671 -1.37493
N   3.1656 -0.72452 0.52301
N   -2.15615 -2.10994 -0.06695
C   -3.02872 -1.76672 -1.20443
H   -3.63771 -2.64156 -1.41316
H   -3.675 -0.93624 -0.92887
H   -2.45117 -1.50602 -2.07956
C   -2.82527 -2.95038 0.94773
H   -3.88581 -2.7282 0.90813
H   -2.66819 -4.00139 0.71216
H   -2.45676 -2.72344 1.94014
C   3.94076 0.13024 -0.26278
O   4.29902 -0.19725 -1.38043
C   4.38229 1.38844 0.43129
H   3.51957 1.92964 0.82075
H   5.0146 1.13161 1.28183
H   4.93643 2.01415 -0.26219

```
C       -1.17952  0.38309 -1.38205
C       -1.29197  0.77327 -2.71681
C       -1.87428  1.07731 -0.39164
C       -2.09849  1.85787 -3.06091
C       -2.68186  2.16164 -0.73579
H       -1.7859   0.7698   0.66039
C       -2.79396  2.55209 -2.07015
H       -2.18668  2.16587 -4.11289
H       -3.22985  2.70856  0.04527
H       -3.42985  3.40718 -2.34171
O       -0.57874  0.0619  -3.73177
H       -0.34583  1.04251 -1.25948
```
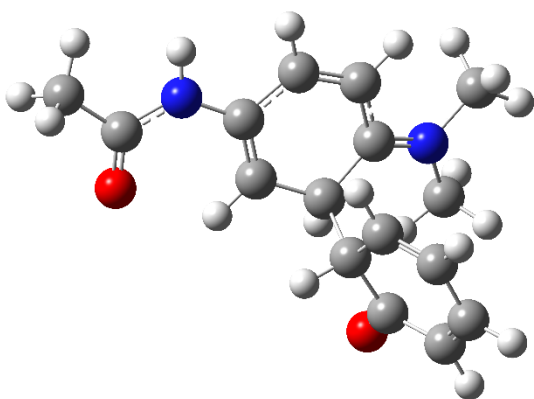

radical_dimethyl_amine_probe_addn_phenoxyl_radical_C-C_H2O_b3lyp_6311gplus2d2p
Zero-point correction=   0.324298 (Hartree/Particle)
Thermal correction to Energy=   0.343908
Thermal correction to Enthalpy=   0.344852
Thermal correction to Gibbs Free Energy=   0.274481
Sum of electronic and zero-point Energies=   -880.848227
Sum of electronic and thermal Energies=   -880.828617
Sum of electronic and thermal Enthalpies=   -880.827673
Sum of electronic and thermal Free Energies=   -880.898044

```
C       -0.28381 -0.76814 -1.02962
C        1.10351 -0.26032 -0.78961
C       -0.81841 -1.7719  -0.01098
C        1.90163 -0.78303  0.15964
C        0.08509 -2.23786  0.99873
C        1.35989 -1.79015  1.05139
H       -0.2371  -2.9736   1.7151
H        2.01018 -2.19701  1.81496
H       -0.22746 -1.33219 -1.97059
H        1.44835  0.50043 -1.46745
N        3.23532 -0.42963  0.40068
N       -2.03449 -2.24304 -0.11526
```

```
C       -2.94314 -1.9431  -1.23355
H       -3.48525 -2.85535 -1.46435
H       -3.64945 -1.1702  -0.93716
H       -2.39468 -1.61391 -2.10548
C       -2.58959 -3.18717  0.87433
H       -3.66921 -3.16755  0.78371
H       -2.22876 -4.19377  0.66923
H       -2.31849 -2.88935  1.88094
C        3.99489  0.49933 -0.26831
O        3.55181  1.17343 -1.18805
C        5.42265  0.62418  0.20692
H        5.63933  0.03202  1.09255
H        6.08415  0.30888 -0.59969
H        5.62936  1.6723   0.41544
H        3.69476 -0.92914  1.14448
C       -1.26674  0.36739 -1.37023
C       -1.399    0.80333 -2.68892
C       -2.02486  0.96   -0.36047
C       -2.2887   1.8321  -2.99758
C       -2.9156   1.98842 -0.66921
H       -1.92087  0.61642  0.67889
C       -3.04754  2.42463 -1.98748
H       -2.39255  2.17619 -4.03687
H       -3.51352  2.4552   0.12709
H       -3.74902  3.23572 -2.2311
H       -0.49108  1.08686 -1.21014
O       -0.62084  0.1962  -3.7237
```
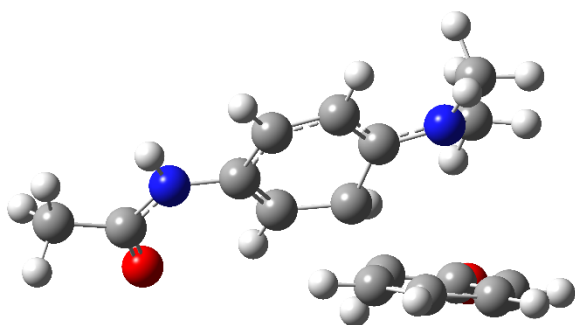
reduced_dimethyl_amine_probe_addn_phenoxyl_radical_C-C_H2O_b3lyp_6311gplus2d2p
Zero-point correction=   0.320709 (Hartree/Particle)
Thermal correction to Energy=   0.340605
Thermal correction to Enthalpy=   0.341550
Thermal correction to Gibbs Free Energy=   0.270017
Sum of electronic and zero-point Energies=   -880.993727
Sum of electronic and thermal Energies=   -880.973830
Sum of electronic and thermal Enthalpies=   -880.972886
Sum of electronic and thermal Free Energies=   -881.044418

```
C      -0.57394 -0.93854 -1.0376
C       0.8916  -0.89066 -0.82622
C      -1.37284 -1.40135  0.14643
C       1.43986 -0.98046  0.41672
C      -0.74962 -1.47324  1.39407
C       0.60954 -1.24182  1.54893
H      -1.32046 -1.73815  2.26998
H       1.05285 -1.30616  2.53309
H      -0.80229 -1.53022 -1.92092
H       1.50834 -0.72559 -1.69139
N       2.82163 -0.87072  0.69726
N      -2.70036 -1.67777 -0.02539
C      -3.28742 -1.85917 -1.35103
H      -3.08707 -2.85931 -1.74881
H      -4.36403 -1.73258 -1.27532
H      -2.91047 -1.11556 -2.04444
C      -3.48178 -2.17721  1.09903
H      -4.51866 -2.27165  0.79336
H      -3.12768 -3.15532  1.43821
H      -3.43712 -1.48461  1.93878
C       3.86416 -0.613   -0.14318
O       3.73679 -0.43503 -1.35217
C       5.22495 -0.558    0.51904
H       5.19897 -0.74802  1.58962
H       5.87366 -1.29273  0.04378
H       5.6573   0.42665  0.34444
H       3.06481 -1.00258  1.66514
C      -1.09755  0.41886 -1.54247
C      -1.28957  0.6281  -2.90842
C      -1.37995  1.43908 -0.63419
C      -1.76324  1.85754 -3.36596
C      -1.85471  2.66862 -1.09163
H      -1.22884  1.27428  0.44244
C      -2.04625  2.87804 -2.45728
H      -1.91402  2.02275 -4.44265
H      -2.07767  3.47269 -0.37523
H      -2.41977  3.8473  -2.81826
H      -0.09211  0.77444 -1.62929
O      -0.99899 -0.41777 -3.83934
```
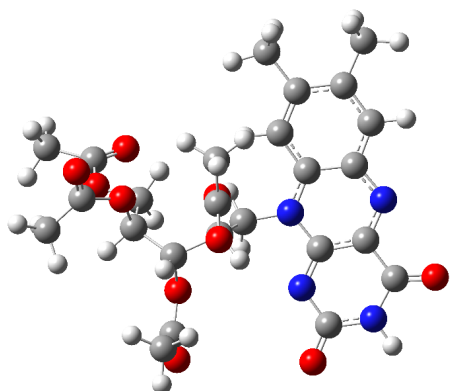
RTA_ox_neut_triplet_b3lyp_6311gplus2d2p_H2O_4_opttight
Zero-point correction=   0.517924 (Hartree/Particle)
Thermal correction to Energy=   0.557588
Thermal correction to Enthalpy=   0.558533
Thermal correction to Gibbs Free Energy=   0.437539
Sum of electronic and zero-point Energies=   -1940.919348
Sum of electronic and thermal Energies=   -1940.879684
Sum of electronic and thermal Enthalpies=   -1940.878739
Sum of electronic and thermal Free Energies=   -1940.999733

C	4.94233	-1.98595	-0.3802
C	4.05665	-0.82576	-0.36142
C	2.67086	-1.08086	-0.49746
C	2.93143	-3.38965	-0.66881
C	2.27889	1.28242	-0.30743
C	3.71685	1.43928	-0.20141
C	4.21223	2.7368	-0.06851
H	5.28439	2.8504	0.00171
C	3.39082	3.85958	-0.02427
C	1.97124	3.69589	-0.10953
C	1.45621	2.4248	-0.24474
H	4.87184	-4.03087	-0.5524
H	0.38665	2.3162	-0.28257
N	1.77455	0.0115	-0.47625
N	4.5956	0.40277	-0.22588
N	2.12222	-2.26654	-0.64577
N	4.29141	-3.20388	-0.53465
C	1.05562	4.88462	-0.04937
H	1.18617	5.43949	0.88162
H	1.25924	5.58228	-0.86407
H	0.01459	4.57863	-0.11858
C	3.99123	5.22106	0.11695
H	3.70441	5.86125	-0.72047
H	3.62492	5.71507	1.01995

```
H      5.0758  5.17492  0.16291
O      2.4581  -4.51395 -0.80386
O      6.16462 -1.94401 -0.27413
C      0.3418  -0.25789 -0.68736
C     -0.37066 -0.66977  0.60395
O     -0.44753  0.48955  1.45084
C     -0.43289  0.29371  2.79489
O     -0.39419 -0.80469  3.29609
H      0.23544 -1.42365  1.1007
H      0.26567 -1.0734  -1.39534
H     -0.09991  0.62272 -1.13405
C     -0.47369  1.59881  3.53017
H      0.36325  2.22448  3.22301
H     -1.39148  2.1294   3.27881
H     -0.43236  1.41825  4.59887
C     -1.7723  -1.30578  0.42551
H     -2.03927 -1.71637  1.39391
O     -1.63925 -2.34668 -0.55641
C     -1.78882 -3.67608 -0.28152
O     -1.67143 -4.43742 -1.20857
C     -2.08444 -4.10886  1.12809
H     -1.31244 -3.77268  1.81911
H     -3.03956 -3.70975  1.46913
H     -2.12889 -5.19218  1.14253
C     -2.98316 -0.44773 -0.00596
H     -3.78476 -1.15778 -0.18701
C     -2.80597  0.38412 -1.26049
H     -2.36417 -0.21088 -2.05735
H     -2.1945   1.26304 -1.07448
O     -3.32539  0.42387  1.08795
O     -4.12485  0.80871 -1.65579
C     -4.19832  1.60483 -2.74517
C     -4.55118  0.4459   1.6768
C     -5.61269 -0.51829  1.2214
H     -6.50191 -0.34401  1.81697
H     -5.84759 -0.37036  0.1685
H     -5.2907  -1.55083  1.35466
C     -5.61793  1.98242 -3.05236
H     -6.05817  2.4951  -2.19789
H     -5.6446   2.62673 -3.9245
H     -6.20731  1.0848  -3.23663
O     -4.71892  1.2558   2.55708
O     -3.22189  1.94851 -3.37069
```

RTA_ox_neut_singlet_b3lyp_6311gplus2d2p_H2O_6_readwrite_freqonly
Zero-point correction=　　　　0.520942 (Hartree/Particle)
Thermal correction to Energy=　　　0.560161
Thermal correction to Enthalpy=　　　0.561105
Thermal correction to Gibbs Free Energy=　0.442534
Sum of electronic and zero-point Energies=　-1940.987745
Sum of electronic and thermal Energies=　　-1940.948526
Sum of electronic and thermal Enthalpies=　　-1940.947582
Sum of electronic and thermal Free Energies=　-1941.066153

```
C        4.93056 -2.01608 -0.3805
C        4.01624 -0.8417  -0.35642
C        2.60132 -1.10436 -0.49745
C        2.88645 -3.39314 -0.68361
C        2.28148  1.26811 -0.3157
C        3.68923  1.41428 -0.19749
C        4.24435  2.70187 -0.05123
H        5.32016  2.7659  0.03298
C        3.46363  3.83205 -0.01651
C        2.05092  3.67956 -0.12368
C        1.48872  2.42087 -0.26516
H        4.83817 -4.04571 -0.57391
H        0.41616  2.35131 -0.31248
N        1.76862 -0.01324 -0.47761
N        4.52492  0.34531 -0.21985
N        2.07186 -2.29835 -0.64626
N        4.27315 -3.20801 -0.5439
C        1.15583  4.88521 -0.0772
H        1.28904  5.43546  0.85602
H        1.39343  5.57822 -0.88644
H        0.10894  4.60549 -0.16345
C        4.08438  5.19378  0.13742
H        3.83708  5.84033 -0.7063
H        3.72392  5.69494  1.03744
H        5.16755  5.12037  0.20168
```

```
O        2.46672 -4.53505 -0.83065
O        6.14319 -1.94727 -0.26925
C        0.32703 -0.25472 -0.69174
C       -0.38113 -0.67241  0.59722
O       -0.44218  0.48191  1.45357
C       -0.42488  0.27495  2.79538
O       -0.39668 -0.82782  3.28806
H        0.2205  -1.43614  1.08406
H        0.24492 -1.06222 -1.40965
H       -0.09966  0.63983 -1.12409
C       -0.44827  1.57447  3.54153
H        0.39566  2.19231  3.23762
H       -1.35993  2.11844  3.2966
H       -0.40679  1.38471  4.60863
C       -1.78932 -1.29381  0.42185
H       -2.05732 -1.70494  1.38967
O       -1.67136 -2.33249 -0.56429
C       -1.8195  -3.66186 -0.2901
O       -1.71188 -4.42218 -1.21928
C       -2.10335 -4.09621  1.1215
H       -1.32449 -3.7628   1.80614
H       -3.05443 -3.69504  1.47143
H       -2.1503  -5.17943  1.13482
C       -2.99298 -0.42288 -0.0034
H       -3.80247 -1.12479 -0.18121
C       -2.81316  0.40749 -1.25848
H       -2.38024 -0.19151 -2.0572
H       -2.19276  1.28069 -1.07516
O       -3.32161  0.45222  1.09189
O       -4.12985  0.84433 -1.64798
C       -4.20113  1.63826 -2.73899
C       -4.54184  0.4805   1.69167
C       -5.61143 -0.47995  1.24744
H       -6.49424 -0.30168  1.85129
H       -5.85602 -0.33205  0.19671
H       -5.29206 -1.51356  1.37858
C       -5.61835  2.03069 -3.03863
H       -6.04524  2.55609 -2.18507
H       -5.64381  2.66825 -3.91576
H       -6.22052  1.13919 -3.2106
O       -4.69835  1.29249  2.57213
O       -3.22477  1.96993 -3.37112
```
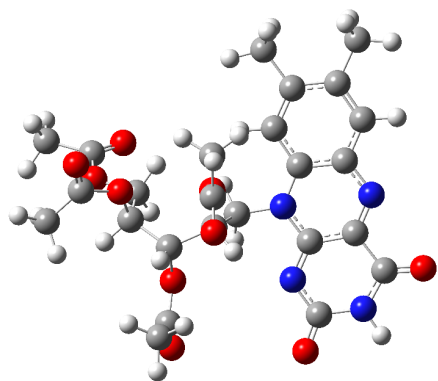
233
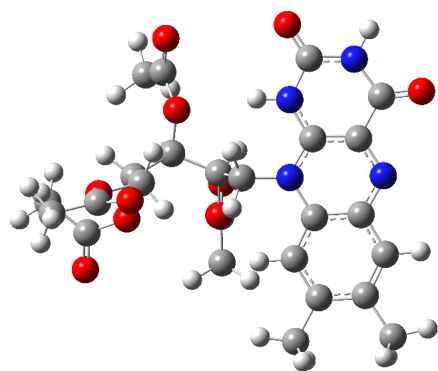
RTA-H_1ered_rad_neut_b3lyp_6311gplus2d2p_H2O_4_opttight
Zero-point correction=   0.531717 (Hartree/Particle)
Thermal correction to Energy=   0.571402
Thermal correction to Enthalpy=   0.572347
Thermal correction to Gibbs Free Energy=   0.452629
Sum of electronic and zero-point Energies=   -1941.566106
Sum of electronic and thermal Energies=   -1941.526421
Sum of electronic and thermal Enthalpies=   -1941.525477
Sum of electronic and thermal Free Energies=   -1941.645194

C   4.50827 2.58672 0.49005
C   3.81462 1.3034 0.45078
C   2.42192 1.29802 0.41155
C   2.31204 3.73507 0.44759
C   2.47059 -1.09331 0.36851
C   3.88676 -1.00554 0.42793
C   4.61903 -2.2102 0.44349
H   5.69621 -2.12567 0.49457
C   4.01764 -3.45436 0.39772
C   2.60823 -3.52414 0.32333
C   1.86453 -2.34406 0.30646
H   4.13929 4.61193 0.51458
H   0.79434 -2.43074 0.22009
N   1.72972 0.11939 0.38128
N   4.56356 0.17326 0.46963
N   1.72354 2.48271 0.40803
N   3.67956 3.71295 0.48501
C   1.9013 -4.8514 0.25464
H   2.2156 -5.42566 -0.61958
H   2.12298 -5.46628 1.12955
H   0.82264 -4.72024 0.20092
C   4.85397 -4.70693 0.42144
H   4.603 -5.3365 1.27742
H   4.69119 -5.31172 -0.4728
H   5.91364 -4.4671 0.47822
O   1.64979 4.76012 0.44695

```
O      5.72294  2.73612  0.53107
C      0.26426  0.10881  0.46599
C     -0.43338  0.2582  -0.8924
O     -0.42996 -1.0274  -1.53046
C     -0.36643 -1.05561 -2.88826
O     -0.3442  -0.05387 -3.56294
H      0.1364   0.9444  -1.51675
H     -0.04802  0.90566  1.13469
H     -0.03052 -0.81508  0.94716
C     -0.33382 -2.46469 -3.39626
H      0.51522 -2.99395 -2.96579
H     -1.23867 -2.98615 -3.08545
H     -0.26207 -2.46156 -4.47847
C     -1.86123  0.85129 -0.85121
H     -2.18686  0.90681 -1.88519
O     -1.70997  2.16966 -0.28928
C     -2.13207  3.3175  -0.91642
O     -2.03951  4.3382  -0.28673
C     -2.64798  3.23511 -2.32502
H     -1.90076  2.80668 -2.99228
H     -3.54579  2.62157 -2.38605
H     -2.88622  4.24114 -2.65195
C     -3.00191  0.15114 -0.07645
H     -3.8736   0.78787 -0.20443
C     -2.78567 -0.0407   1.41396
H     -2.42022  0.87566  1.87237
H     -2.09542 -0.85401  1.62016
O     -3.2236  -1.13082 -0.68847
O     -4.07347 -0.37215  1.96846
C     -4.10822 -0.62909  3.29513
C     -4.43265 -1.55376 -1.14807
C     -5.61923 -0.63169 -1.07958
H     -6.47572 -1.15678 -1.48769
H     -5.82754 -0.34068 -0.05153
H     -5.44821  0.27413 -1.66043
C     -5.49587 -0.97641  3.74876
H     -5.83683 -1.87431  3.23404
H     -5.49934 -1.14306  4.82054
H     -6.1833  -0.17064  3.49467
O     -4.48132 -2.67267 -1.59967
O     -3.12453 -0.5776   3.99658
H      0.71634  2.50915  0.36581
```
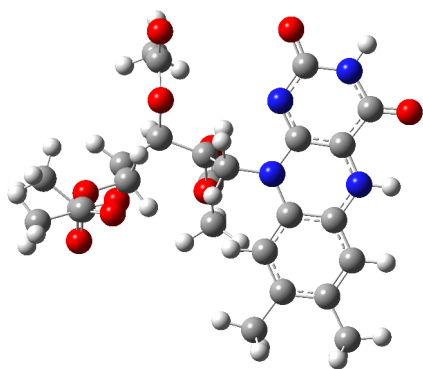
RTA-H_1ered_rad_other-n_neut_b3lyp_6311gplus2d2p_H2O_opttight
Zero-point correction=   0.532256 (Hartree/Particle)
Thermal correction to Energy=   0.571931
Thermal correction to Enthalpy=   0.572875
Thermal correction to Gibbs Free Energy=   0.452587
Sum of electronic and zero-point Energies=   -1941.579373
Sum of electronic and thermal Energies=   -1941.539698
Sum of electronic and thermal Enthalpies=   -1941.538754
Sum of electronic and thermal Free Energies=   -1941.659042

C	4.50828	2.58669	0.49001
C	3.81462	1.30338	0.45075
C	2.42192	1.29802	0.41153
C	2.31207	3.73506	0.44756
C	2.47056	-1.09332	0.36851
C	3.88673	-1.00556	0.42792
C	4.61899	-2.21023	0.44348
H	5.69618	-2.12571	0.49455
C	4.01759	-3.45437	0.39772
C	2.60818	-3.52414	0.32334
C	1.86449	-2.34406	0.30647
H	4.13932	4.61191	0.51453
H	0.7943	-2.43073	0.22011
N	1.72971	0.11939	0.38128
N	4.56355	0.17323	0.46961
N	1.72355	2.48272	0.40801
N	3.67959	3.71294	0.48497
C	1.90124	-4.8514	0.25466
H	2.21553	-5.42567	-0.61955
H	2.12291	-5.46628	1.12958
H	0.82258	-4.72023	0.20094
C	4.85391	-4.70696	0.42145
H	4.60294	-5.33652	1.27743
H	4.69113	-5.31175	-0.47279
H	5.91359	-4.46713	0.47822
O	1.64983	4.76013	0.44693

```
O        5.72295  2.73609  0.53103
C        0.26424  0.10883  0.46599
C       -0.43339  0.25823 -0.89239
O       -0.42995 -1.02735 -1.53048
C       -0.36635 -1.05555 -2.88827
O       -0.34413 -0.05379 -3.56294
H        0.13637  0.94445 -1.51673
H       -0.04802  0.90568  1.1347
H       -0.03054 -0.81506  0.94717
C       -0.33355 -2.46462 -3.39629
H        0.51619 -2.9934  -2.96658
H       -1.23781 -2.98657 -3.08464
H       -0.26272 -2.46147 -4.47856
C       -1.86125  0.8513  -0.8512
H       -2.18688  0.90682 -1.88518
O       -1.71001  2.16967 -0.28928
C       -2.13209  3.31752 -0.91642
O       -2.0395   4.33822 -0.28675
C       -2.64802  3.23512 -2.32502
H       -1.90079  2.80672 -2.99229
H       -3.5458   2.62154 -2.38605
H       -2.8863   4.24114 -2.65194
C       -3.00193  0.15114 -0.07645
H       -3.87363  0.78786 -0.20443
C       -2.7857  -0.04068  1.41397
H       -2.42025  0.87568  1.87237
H       -2.09543 -0.85399  1.62018
O       -3.2236  -1.13083 -0.68846
O       -4.07349 -0.37214  1.96847
C       -4.10823 -0.62912  3.29514
C       -4.43265 -1.55381 -1.14801
C       -5.61924 -0.63175 -1.07956
H       -6.47571 -1.15685 -1.4877
H       -5.82759 -0.34075 -0.05152
H       -5.44821  0.27408 -1.66041
C       -5.49589 -0.97637  3.74878
H       -5.83708 -1.87401  3.23376
H       -5.49928 -1.1434   4.8205
H       -6.18319 -0.17037  3.49506
O       -4.48132 -2.67275 -1.59955
O       -3.12453 -0.57766  3.99657
H        5.56214  0.20491  0.51199
```

237
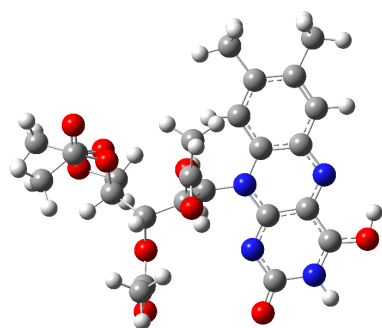
RTA-H_1ered_rad-OH_neut_b3lyp_6311gplus2d2p_H2O_6_readwrite_freqonly
Zero-point correction=   0.531465 (Hartree/Particle)
Thermal correction to Energy=   0.571136
Thermal correction to Enthalpy=   0.572080
Thermal correction to Gibbs Free Energy=   0.451744
Sum of electronic and zero-point Energies=   -1941.559531
Sum of electronic and thermal Energies=   -1941.519860
Sum of electronic and thermal Enthalpies=   -1941.518916
Sum of electronic and thermal Free Energies=   -1941.639252

C	4.70701	-2.02103	-0.57539
C	3.90614	-0.88589	-0.49969
C	2.49964	-1.12331	-0.54643
C	2.74532	-3.42743	-0.73787
C	2.24572	1.26525	-0.35051
C	3.66516	1.39321	-0.33106
C	4.21806	2.68675	-0.22912
H	5.29746	2.75727	-0.22118
C	3.44295	3.82564	-0.14178
C	2.03428	3.68694	-0.14639
C	1.4688	2.41738	-0.24554
H	4.72696	-4.05844	-0.74297
H	0.39442	2.34706	-0.21593
N	1.68252	-0.02603	-0.47615
N	4.50062	0.3249	-0.40358
N	1.95448	-2.32539	-0.65772
N	4.14307	-3.23597	-0.68563
C	1.14099	4.89337	-0.03787
H	1.33038	5.44729	0.88406
H	1.31195	5.5894	-0.86192
H	0.09116	4.6085	-0.05046
C	4.08722	5.18308	-0.03695
H	3.78771	5.83108	-0.86301
H	3.79663	5.69216	0.88414
H	5.17206	5.10101	-0.04889
O	2.32374	-4.57719	-0.84983
O	6.03083	-1.95805	-0.54818

```
C        0.23359 -0.23097 -0.61395
C       -0.42901 -0.62893  0.70384
O       -0.38211  0.50425  1.59117
C       -0.24867  0.25983  2.91753
O       -0.20609 -0.85651  3.38116
H        0.15495 -1.43351  1.14472
H        0.08566 -1.03768 -1.32443
H       -0.19361  0.67299 -1.02695
C       -0.16824  1.53799  3.6973
H        0.67161  2.13476  3.34367
H       -1.07502  2.12105  3.53968
H       -0.04977  1.31678  4.75253
C       -1.87284 -1.17499  0.61209
H       -2.16146 -1.4217   1.62925
O       -1.83226 -2.35659 -0.20805
C       -1.8929  -3.6242   0.29372
O       -1.85047 -4.52743 -0.50406
C       -2.01548 -3.82033  1.77953
H       -1.22574 -3.3035   2.32301
H       -2.97307 -3.44066  2.13734
H       -1.96044 -4.88386  1.98357
C       -3.03264 -0.32262  0.05035
H       -3.90192 -0.97321  0.08725
C       -2.884    0.16675 -1.3775
H       -2.52101 -0.62953 -2.02309
H       -2.21828  1.02257 -1.4415
O       -3.21881  0.81522  0.91135
O       -4.20144  0.56882 -1.80452
C       -4.29905  1.08051 -3.05059
C       -4.37469  1.07833  1.57546
C       -5.53154  0.12254  1.46384
H       -6.34904  0.51491  2.05846
H       -5.85469  0.01888  0.42913
H       -5.26316 -0.866    1.83577
C       -5.71219  1.4698  -3.37363
H       -6.05438  2.23017 -2.67223
H       -5.76354  1.85366 -4.38682
H       -6.36864  0.60686 -3.26898
O       -4.40676  2.08891  2.2369
O       -3.34646  1.19702 -3.78715
H        6.26484 -1.01462 -0.46909
```
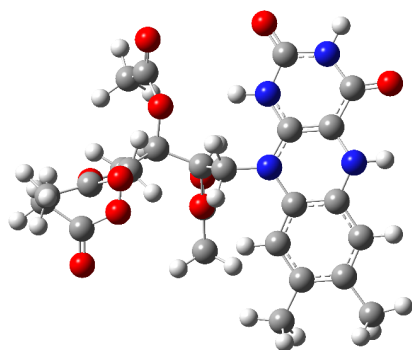
RTA-H2_b3lyp_6311gplus2d2p_H2O
Zero-point correction=   0.543754 (Hartree/Particle)
Thermal correction to Energy=   0.584021
Thermal correction to Enthalpy=   0.584965
Thermal correction to Gibbs Free Energy=   0.463381
Sum of electronic and zero-point Energies=   -1942.169533
Sum of electronic and thermal Energies=   -1942.129265
Sum of electronic and thermal Enthalpies=   -1942.128321
Sum of electronic and thermal Free Energies=   -1942.249905

```
C       4.50828  2.58669  0.49001
C       3.81462  1.30338  0.45075
C       2.42192  1.29802  0.41153
C       2.31207  3.73506  0.44756
C       2.47056 -1.09332  0.36851
C       3.88673 -1.00556  0.42792
C       4.61899 -2.21023  0.44348
H       5.69618 -2.12571  0.49455
C       4.01759 -3.45437  0.39772
C       2.60818 -3.52414  0.32334
C       1.86449 -2.34406  0.30647
H       4.13932  4.61191  0.51453
H       0.7943  -2.43073  0.22011
N       1.72971  0.11939  0.38128
N       4.56355  0.17323  0.46961
N       1.72355  2.48272  0.40801
N       3.67959  3.71294  0.48497
C       1.90124 -4.8514   0.25466
H       2.21553 -5.42567 -0.61955
H       2.12291 -5.46628  1.12958
H       0.82258 -4.72023  0.20094
C       4.85391 -4.70696  0.42145
H       4.60294 -5.33652  1.27743
H       4.69113 -5.31175 -0.47279
H       5.91359 -4.46713  0.47822
O       1.64983  4.76013  0.44693
```

```
O        5.72295  2.73609  0.53103
C        0.26424  0.10883  0.46599
C       -0.43339  0.25823 -0.89239
O       -0.42995 -1.02735 -1.53048
C       -0.36635 -1.05555 -2.88827
O       -0.34413 -0.05379 -3.56294
H        0.13637  0.94445 -1.51673
H       -0.04802  0.90568  1.1347
H       -0.03054 -0.81506  0.94717
C       -0.33355 -2.46462 -3.39629
H        0.51619 -2.9934  -2.96658
H       -1.23781 -2.98657 -3.08464
H       -0.26272 -2.46147 -4.47856
C       -1.86125  0.8513  -0.8512
H       -2.18688  0.90682 -1.88518
O       -1.71001  2.16967 -0.28928
C       -2.13209  3.31752 -0.91642
O       -2.0395   4.33822 -0.28675
C       -2.64802  3.23512 -2.32502
H       -1.90079  2.80672 -2.99229
H       -3.5458   2.62154 -2.38605
H       -2.8863   4.24114 -2.65194
C       -3.00193  0.15114 -0.07645
H       -3.87363  0.78786 -0.20443
C       -2.7857  -0.04068  1.41397
H       -2.42025  0.87568  1.87237
H       -2.09543 -0.85399  1.62018
O       -3.2236  -1.13083 -0.68846
O       -4.07349 -0.37214  1.96847
C       -4.10823 -0.62912  3.29514
C       -4.43265 -1.55381 -1.14801
C       -5.61924 -0.63175 -1.07956
H       -6.47571 -1.15685 -1.4877
H       -5.82759 -0.34075 -0.05152
H       -5.44821  0.27408 -1.66041
C       -5.49589 -0.97637  3.74878
H       -5.83708 -1.87401  3.23376
H       -5.49928 -1.1434   4.8205
H       -6.18319 -0.17037  3.49506
O       -4.48132 -2.67275 -1.59955
O       -3.12453 -0.57766  3.99657
H        0.71635  2.50916  0.36581
H        5.56214  0.20491  0.51199
```

HOOH_B3LYP_6311GPLUS2D2P_H2O4_
Zero-point correction=　　　　　0.026497 (Hartree/Particle)
Thermal correction to Energy=　　　0.029713
Thermal correction to Enthalpy=　　0.030657
Thermal correction to Gibbs Free Energy=　0.004208
Sum of electronic and zero-point Energies=　-151.589764
Sum of electronic and thermal Energies=　-151.586549
Sum of electronic and thermal Enthalpies=　-151.585604
Sum of electronic and thermal Free Energies=　-151.612054

O　　　0.00112 -0.73247　0.
O　　　0.00112　0.72917　0.
H　　　-0.6196　-1.25904　0.52085
H　　　0.6064　1.28547　0.50789
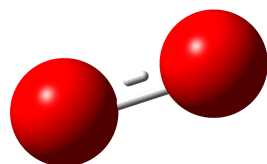
O2_triplet_b3lyp_6311gplus2d2p_H2O
Zero-point correction=　　　　　0.003710 (Hartree/Particle)
Thermal correction to Energy=　　　0.006074
Thermal correction to Enthalpy=　　0.007018
Thermal correction to Gibbs Free Energy=　-0.016259
Sum of electronic and zero-point Energies=　-150.371057
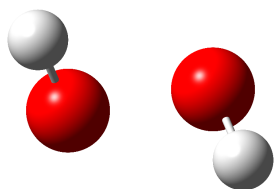Sum of electronic and thermal Energies=　-150.368693
Sum of electronic and thermal Enthalpies=　-150.367749
Sum of electronic and thermal Free Energies=　-150.391025

O　　　0.02182 -2.04714 0.
O　　　-1.13978 -2.04714 0.

O2_SINGLET_B3LYP_6311GPLUS2D2P_H2O
Zero-point correction=　　　　　0.003686 (Hartree/Particle)

Thermal correction to Energy=   0.006049
Thermal correction to Enthalpy=   0.006994
Thermal correction to Gibbs Free Energy=   -0.015245
Sum of electronic and zero-point Energies=   -150.310385
Sum of electronic and thermal Energies=   -150.308022
Sum of electronic and thermal Enthalpies=   -150.307078
Sum of electronic and thermal Free Energies=   -150.329316

O   0.   0.   0.60402
O   0.   0.   -0.60402
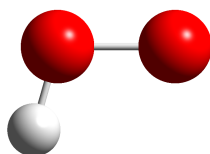
HOO_rad_b3lyp_6311gplus2d2p_H2O
Zero-point correction=   0.014213 (Hartree/Particle)
Thermal correction to Energy=   0.017070
Thermal correction to Enthalpy=   0.018014
Thermal correction to Gibbs Free Energy=   -0.007961
Sum of electronic and zero-point Energies=   -150.955767
Sum of electronic and thermal Energies=   -150.952911
Sum of electronic and thermal Enthalpies=   -150.951967
Sum of electronic and thermal Free Energies=   -150.977941

O   0.02182 -2.04714 0.
O   -1.06471 -1.63635 0.
H   0.76482 -1.43924 0.

H_b3lyp_6311gplus2d2p_H2O
Zero-point correction=   0.000000 (Hartree/Particle)
Thermal correction to Energy=   0.001416
Thermal correction to Enthalpy=   0.002360
Thermal correction to Gibbs Free Energy=   -0.010654
Sum of electronic and zero-point Energies=   -0.502177
Sum of electronic and thermal Energies=   -0.500761
Sum of electronic and thermal Enthalpies=   -0.499817
Sum of electronic and thermal Free Energies=   -0.512831

H   -0.83147 0.52088 0.05876
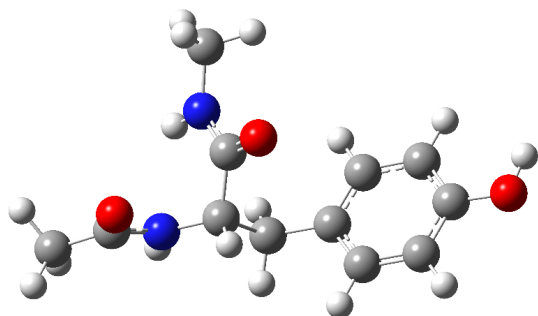
ωB97XD

phenol-peptide_wb97xd_6311gplus2d2p_H2O
Zero-point correction=   0.273741 (Hartree/Particle)
Thermal correction to Energy=   0.291537
Thermal correction to Enthalpy=   0.292481
Thermal correction to Gibbs Free Energy=   0.225311
Sum of electronic and zero-point Energies=   -801.871738
Sum of electronic and thermal Energies=   -801.853942
Sum of electronic and thermal Enthalpies=   -801.852998
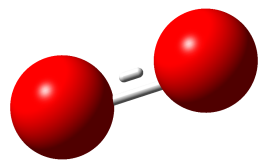Sum of electronic and thermal Free Energies=   -801.920168

C	1.41079	-0.60027	-0.64588
C	2.17179	0.47641	-1.09933
C	3.49282	0.65316	-0.6972
C	4.07548	-0.26028	0.17674
C	3.33579	-1.34908	0.6358
C	2.02086	-1.5111	0.22235
H	1.73302	1.19394	-1.78037
H	1.46259	-2.3662	0.58181
O	5.36979	-0.14474	0.61321
H	4.06545	1.49568	-1.06375
H	3.79822	-2.05998	1.30626
C	-0.01961	-0.79253	-1.09042
C	-1.09475	-0.45707	-0.0274
H	-0.17465	-1.83703	-1.36825
H	-0.21021	-0.19439	-1.98291
H	-0.89974	-1.02754	0.87879
C	-3.47634	-1.0454	0.24797
C	-4.72464	-1.5683	-0.42454
H	-5.5525	-0.8989	-0.19651
C	-1.03472	1.01921	0.4043
N	-1.77241	1.88518	-0.31091
H	-2.40351	1.5176	-1.00247
O	-0.30737	1.36684	1.3346
N	-2.39756	-0.84668	-0.55323

H	-2.45935	-1.12645	-1.51843
O	-3.43733	-0.80774	1.45412
H	5.77427	0.64362	0.23517
H	-4.62617	-1.66078	-1.50361
H	-4.96281	-2.54531	-0.00498
C	-1.8074	3.30999	-0.01871
H	-0.80383	3.73061	-0.04671
H	-2.4187	3.80212	-0.76924
H	-2.23339	3.50013	0.96676
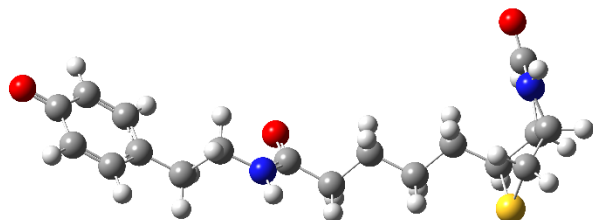
biotin-tyramide_rad_wb97xd_6311gplus2d2p_h2o_optfreqtight_geom2
Zero-point correction=   0.411593 (Hartree/Particle)
Thermal correction to Energy=   0.435802
Thermal correction to Enthalpy=   0.436746
Thermal correction to Gibbs Free Energy=   0.350463
Sum of electronic and zero-point Energies=   -1488.130167
Sum of electronic and thermal Energies=   -1488.105958
Sum of electronic and thermal Enthalpies=   -1488.105014
Sum of electronic and thermal Free Energies=   -1488.191297

C	-7.78691	1.4423	-0.40783
C	-6.58055	0.87756	-0.72336
C	-8.68546	0.80066	0.52896
C	-6.17148	-0.34907	-0.14943
H	-5.9238	1.36922	-1.42911
C	-8.24605	-0.45351	1.10381
C	-7.03357	-0.99346	0.76812
H	-8.90991	-0.94513	1.8012
H	-6.72366	-1.9342	1.20408
O	-9.79691	1.30766	0.82726
C	-4.8308	-0.93498	-0.47838
C	-3.72446	-0.41416	0.47283
H	-4.55054	-0.67867	-1.49986
H	-4.86961	-2.02194	-0.40282
H	-3.66043	0.66914	0.40584
H	-3.96571	-0.67706	1.50121
C	-1.55832	-0.39332	-0.71787
C	-0.24584	-1.12438	-0.93724
C	0.968	-0.25724	-0.57545
H	-0.20227	-1.38793	-1.99652

```
H       -0.22309 -2.05668 -0.37155
C        2.29651 -0.96322 -0.85498
H        0.9174  0.67495 -1.14026
H        0.91512  0.01318  0.4826
C        3.509  -0.09426 -0.51337
H        2.34199 -1.89427 -0.28572
H        2.34187 -1.24253 -1.9121
H        3.45662  0.82303 -1.10512
H        3.46134  0.21413  0.53325
N       -2.41771 -0.96437  0.15915
H       -2.16374 -1.84679  0.56946
O       -1.81683  0.66359 -1.29748
C        5.90442 -1.08304  1.6017
C        6.58475  0.08005  0.86098
C        4.85018 -0.7734  -0.80395
C        6.11588  0.11004 -0.62899
C        5.94632  2.26985  0.29268
S        5.21857 -2.19951  0.31077
H        6.89256 -0.298  -1.27114
H        7.6675  -0.03571  0.90581
N        5.96043  1.5359  -0.86237
H        5.58726  1.92388 -1.7114
N        6.19087  1.40495  1.33833
H        6.60454  1.79036  2.17149
O        5.74793  3.47805  0.38506
H        4.835  -1.18146 -1.81398
H        6.59867 -1.65577  2.2093
H        5.10305 -0.71466  2.23703
H       -8.10567  2.37687 -0.84794
```
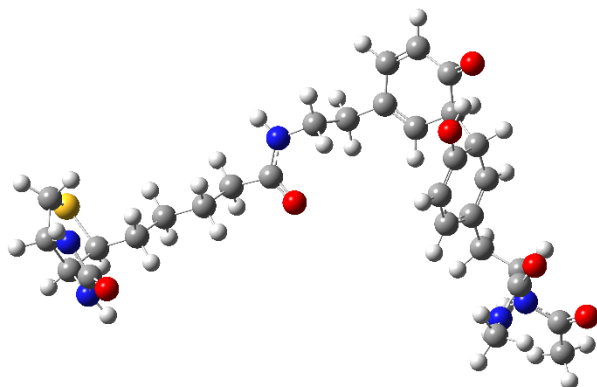
**peptide-OH-rad_plus_biotin-
tyramide_ketone_wb97xd_6311gplus2d2p_h2o_mfgeom_unfreeze1to54_optfreqtight_2**
Zero-point correction=   0.687492 (Hartree/Particle)
Thermal correction to Energy=   0.730392
Thermal correction to Enthalpy=   0.731336
Thermal correction to Gibbs Free Energy=   0.600042
Sum of electronic and zero-point Energies=   -2289.972983
Sum of electronic and thermal Energies=   -2289.930083
Sum of electronic and thermal Enthalpies=   -2289.929139
Sum of electronic and thermal Free Energies=   -2290.060433

C   4.79112 -0.29122 0.20796
C   4.10186 -0.48319 1.43347
C   3.90906 0.59164 2.32418
C   4.32783 1.85097 2.00536
C   4.92486 2.18901 0.66872
C   5.198   0.96071 -0.15074
H   3.75394 -1.4691 1.70653
H   5.72086 1.11524 -1.08693
O   4.20505 2.85175 2.91765
H   3.45037 0.4239 3.28975
C   5.06741 -1.47645 -0.69228
C   6.49344 -2.06894 -0.58926
H   4.92872 -1.1809 -1.73311
H   4.34351 -2.26637 -0.48475
H   7.22241 -1.29092 -0.80782
C   7.82566 -3.58448 -2.01314
C   7.79799 -4.59507 -3.13645
H   8.32684 -5.49116 -2.81525
C   6.82968 -2.54479 0.83592
N   6.48085 -3.80492 1.14622
H   6.1308 -4.39807 0.4133
O   7.35705 -1.77764 1.64118
N   6.62095 -3.1252 -1.5869

```
H        5.79515 -3.41748 -2.08319
O        8.87936 -3.20167 -1.50703
H        6.79143 -4.86629 -3.44637
H        8.33375 -4.18187 -3.99038
C        6.73571 -4.38736  2.45484
H        6.26701 -3.792    3.23648
H        6.31818 -5.38963  2.47472
H        7.80509 -4.44399  2.65945
C        4.05518  3.21816 -0.16244
C        2.75775  2.68679 -0.68103
C        3.97511  4.61394  0.43657
C        1.69937  3.47764 -0.932
H        2.72316  1.63129 -0.91677
C        2.8804   5.44822 -0.02068
C        1.80822  4.89674 -0.63373
H        2.90457  6.49558  0.24555
H        0.97217  5.53446 -0.89516
O        4.81098  5.01801  1.25338
C        0.40633  2.9507  -1.50366
C       -0.71447  2.86859 -0.44995
H        0.56618  1.95877 -1.92415
H        0.07471  3.59879 -2.31827
H       -0.42607  2.17813  0.33916
H       -0.88324  3.84427  0.00433
C       -2.35166  1.11035 -1.04807
C       -3.69589  0.8233  -1.69391
C       -4.68161  0.16493 -0.71839
H       -3.50761  0.14798 -2.53158
H       -4.13025  1.7352  -2.10571
C       -6.01231 -0.19146 -1.3847
H       -4.2227  -0.73375 -0.30309
H       -4.8642   0.84145  0.12089
C       -6.99922 -0.85064 -0.41864
H       -6.46195  0.70998 -1.80676
H       -5.82548 -0.86793 -2.22438
H       -6.53903 -1.75612 -0.01506
H       -7.17849 -0.1924   0.43425
N       -1.97783  2.41007 -1.0078
H       -2.58166  3.09129 -1.43563
O       -1.65338  0.20738 -0.58052
C      -10.07942  0.36253  0.08855
C      -10.19207 -1.06075  0.65909
C       -8.32673 -1.24307 -1.07296
C       -9.31702 -2.04357 -0.18336
C       -8.87777 -2.36465  2.10743
S       -9.35633  0.19918 -1.59471
H       -9.95005 -2.63143 -0.84347
```

```
H        -11.23248 -1.38491  0.64187
N        -8.73913 -2.88588  0.85
H        -8.05178 -3.59707  0.67074
N        -9.6298  -1.21366  2.00037
H        -10.15792 -0.92952  2.80915
O        -8.41434 -2.83138  3.14431
H        -8.12519 -1.80824 -1.98231
H        -11.04337  0.85376 -0.00457
H        -9.43252  0.97412  0.71218
H         5.86631  2.7232   0.84544
H         4.66229  3.40513 -1.06577
H         4.57408  3.67377  2.54684
```

REFERENCES

Al-Nu'airat, J., Dlugogorski, B.Z., Gao, X., Zeinali, N., Skut, J., Westmoreland, P.R., Oluwoye, I. and Altarawneh, M. (2019). Reaction of phenol with singlet oxygen. *Physical Chemistry Chemical Physics*, *21*(1), 171-183.

Bachmann, W. E., & Wiselogle, F. Y. (1936). The relative stability of pentaarylethanes. III. 1 The reversible dissociation of pentaarylethanes. *The Journal of Organic Chemistry*, *1*(4), 354-382.

Barone, V., & Cossi, M. (1998). Quantum calculation of molecular energies and energy gradients in solution by a conductor solvent model. *The Journal of Physical Chemistry A*, *102*(11), 1995-2001.

Barton, D. H. R., Boivin, J., Gaudin, D., & Jankowski, K. (1989). On the gif oxidaton of alicyclic tertiary amines. *Tetrahedron letters*, *30*(11), 1381-1382.

Barton, D. H., & Doller, D. (1992). The selective functionalization of saturated hydrocarbons: Gif chemistry. *Accounts of chemical research*, *25*(11), 504-512

Becke, A. D. (1992). Density-functional thermochemistry. I. The effect of the exchange-only gradient correction. *The Journal of chemical physics*, *96*(3), 2155-2160.

Becke, A. D. (1993) Density-functional thermochemistry. III. The role of exact exchange. *The Journal of Chemical Physics*, *98(7)*, 5648-5652.

Boess, E., Schmitz, C., & Klussmann, M. (2012). A comparative mechanistic study of Cu-catalyzed oxidative coupling reactions with N-phenyltetrahydroisoquinoline. *Journal of the American Chemical Society*, *134*(11), 5317-5325.

Boivin, J., Gaudin, D., Labrecque, D., & Jankowski, K. (1990). Gif oxidation of some alicyclic amines. *Tetrahedron letters*, *31*(16), 2281-2282.

Boutadla, Y., Davies, D. L., Macgregor, S. A., & Poblador-Bahamonde, A. I. (2009). Mechanisms of C–H bond activation: rich synergy between computation and experiment. *Dalton Transactions*, (30), 5820-5831.

Bravo, A., Bjørsvik, H. R., Fontana, F., Liguori, L., & Minisci, F. (1997). Ingold− Fischer "Persistent Radical Effect", Solvent Effect, and Metal Salt Oxidation of Carbon-Centered Radicals in the Synthesis of Mixed Peroxides from tert-Butyl Hydroperoxide. *The Journal of Organic Chemistry*, *62*(12), 3849-3857.

Brimioulle, R., & Bach, T. (2013). Enantioselective Lewis acid catalysis of intramolecular enone [2+ 2] photocycloaddition reactions. *Science*, *342*(6160), 840-843.

Buksh, B. F., Knutson, S. D., Oakley, J. V., Bissonnette, N. B., Oblinsky, D. G., Schwoerer, M. P., Seath, C. P.; Geri, J. B.; Rodriguez-Rivera, F. P.; Parker, D. L.; Scholes, G. D; Ploss, A., & MacMillan, D. W. (2022). μMap-Red: Proximity Labeling by Red Light Photocatalysis. *Journal of the American Chemical Society*, *144*(14), 6154-6162.

Bünzli, J. C. G. (2013). Lighting up cells with lanthanide self-assembled helicates. *Interface focus*, *3*(5), 20130032.

Burton, G. W., & Ingold, K. U. (1986). Vitamin E: application of the principles of physical organic chemistry to the exploration of its structure and function. *Accounts of chemical research*, *19*(7), 194-201.

Buzzetti, L., Crisenza, G. E., & Melchiorre, P. (2019). Mechanistic studies in photocatalysis. *Angewandte Chemie International Edition*, *58*(12), 3730-3747.

Catino, A. J., Nichols, J. M., Nettles, B. J., & Doyle, M. P. (2006). The oxidative mannich reaction catalyzed by dirhodium caprolactamate. *Journal of the American Chemical Society*, *128*(17), 5648-5649

Cerón-Carrasco, J. P., Jacquemin, D., Laurence, C., Planchat, A., Reichardt, C., & Sraïdi, K. (2014). Solvent polarity scales: determination of new ET (30) values for 84 organic solvents. *Journal of Physical Organic Chemistry*, *27*(6), 512-518.

Chai, J. D., & Head-Gordon, M. (2008). Long-range corrected hybrid density functionals with damped atom–atom dispersion corrections. *Physical Chemistry Chemical Physics*, *10*(44), 6615-6620.

Check, C. E., Faust, T. O., Bailey, J. M., Wright, B. J., Gilbert, T. M., & Sunderlin, L. S. (2001). Addition of polarization and diffuse functions to the LANL2DZ basis set for p-block elements. *The Journal of Physical Chemistry A*, *105*(34), 8111-8116.

Chen, K., & Baran, P. S. (2009). Total synthesis of eudesmane terpenes by site-selective C–H oxidations. *Nature*, *459*(7248), 824-828.

Chen, K., & Que, L. (2001). Stereospecific alkane hydroxylation by non-heme iron catalysts: mechanistic evidence for an FeV O active species. *Journal of the American Chemical Society*, *123*(26), 6327-6337.

Chen, W., Chen, J. J., Lu, R., Qian, C., Li, W. W., & Yu, H. Q. (2014). Redox reaction characteristics of riboflavin: a fluorescence spectroelectrochemical analysis and density functional theory calculation. *Bioelectrochemistry*, *98*, 103-108.

Cheng, W. M., Shang, R., Fu, M. C., & Fu, Y. (2017). Photoredox-Catalysed Decarboxylative Alkylation of N-Heteroarenes with N-(Acyloxy) phthalimides. *Chemistry–A European Journal*, *23*(11), 2537-2541.

Chiavarino, B., Cipollini, R., Crestoni, M. E., Fornarini, S., Lanucara, F., & Lapi, A. (2008). Probing the compound I-like reactivity of a bare high-valent oxo iron porphyrin complex: the oxidation of tertiary amines. *Journal of the American Chemical Society*, *130*(10), 3208-3217.

Close, D. M., & Wardman, P. (2018). Calculation of standard reduction potentials of amino acid radicals and the effects of water and incorporation into peptides. *The Journal of Physical Chemistry A*, *122*(1), 439-445.

Davies, D. L., Donald, S. M., & Macgregor, S. A. (2005). Computational study of the mechanism of cyclometalation by palladium acetate. *Journal of the American Chemical Society*, *127*(40), 13754-13755.

De Melo, J. S., & Fernandes, P. F. (2001). Spectroscopy and photophysics of 4-and 7-hydroxycoumarins and their thione analogs. *Journal of Molecular Structure*, *565*, 69-78.

DeRosa, M. C., & Crutchley, R. J. (2002). Photosensitized singlet oxygen and its applications. *Coordination Chemistry Reviews*, *233*, 351-371.

DiRocco, D. (2014). Electrochemical Series of Photocatalysts and Common Organic Compounds. (https://macmillan.princeton.edu/photoredox-3/)

DiRocco, D. A., Dykstra, K., Krska, S., Vachal, P., Conway, D. V., & Tudge, M. (2014). Late-stage functionalization of biologically active heterocycles through photoredox catalysis. *Angewandte Chemie International Edition*, *53*(19), 4802-4806.

Etheridge, F. S., Fernando, R., Golen, J. A., Rheingold, A. L., & Sauve, G. (2015). Tuning the optoelectronic properties of core-substituted naphthalene diimides by the selective conversion of imides to monothioimides. *RSC Advances*, *5*(58), 46534-46539.

Fancy, D. A., & Kodadek, T. (1999). Chemistry for the analysis of protein–protein interactions: rapid and efficient cross-linking triggered by long wavelength light. *Proceedings of the National Academy of Sciences*, *96*(11), 6020-6024.

Feit Electricity. (2022). *Blue LED sources*. Retrieved from https://www.feit.com/

Fischer, H. (1986). Unusual selectivities of radical reactions by internal suppression of fast modes. *Journal of the American Chemical Society*, *108*(14), 3925-3927.

Fischer, H. (2001). The persistent radical effect: a principle for selective radical reactions and living radical polymerizations. *Chemical reviews*, *101*(12), 3581-3610.

Focsaneanu, K. S., & Scaiano, J. C. (2006). The persistent radical effect: From mechanistic curiosity to synthetic tool. *Helvetica chimica acta*, *89*(10), 2473-2482.

Focsaneanu, K. S., Aliaga, C., & Scaiano, J. C. (2005). Clean Photochemical Synthesis Mediated by Radical− Radical Reactions: Radical Buffer or the Persistent Free Radical Effect?. *Organic Letters*, *7*(22), 4979-4982.

Gardner, K. A., & Mayer, J. M. (1995). Understanding CH Bond Oxidations: H· and H-Transfer in the Oxidation of Toluene by Permanganate. *Science*, *269*(5232), 1849-1851.

Garza-Sanchez, R. A., Tlahuext-Aca, A., Tavakoli, G., & Glorius, F. (2017). Visible light-mediated direct decarboxylative C–H functionalization of heteroarenes. *ACS Catalysis*, *7*(6), 4057-4061.

Gaussian 09, Revision C.01, M. J. Frisch, G. W. Trucks, H. B. Schlegel, G. E. Scuseria, M. A. Robb, J. R. Cheeseman, G. Scalmani, V. Barone, G. A. Petersson, H. Nakatsuji, X. Li, M. Caricato, A.

Marenich, J. Bloino, B. G. Janesko, R. Gomperts, B. Mennucci, H. P. Hratchian, J. V. Ortiz, A. F. Izmaylov, J. L. Sonnenberg, D. Williams-Young, F. Ding, F. Lipparini, F. Egidi, J. Goings, B. Peng, A. Petrone, T. Henderson, D. Ranasinghe, V. G. Zakrzewski, J. Gao, N. Rega, G. Zheng, W. Liang, M. Hada, M. Ehara, K. Toyota, R. Fukuda, J. Hasegawa, M. Ishida , T. Nakajima, Y. Honda, O. Kitao, H. Nakai, T. Vreven, K. Throssell, J. A. Montgomery, Jr., J. E. Peralta, F. Ogliaro, M. Bearpark, J. J. Heyd, E. Brothers, K. N. Kudin, V. N. Staroverov, T. Keith, R. Kobayashi, J. Normand, K. Raghavachari, A. Rendell, J. C. Burant, S. S. Iyengar, J. Tomasi, M. Cossi, J. M. Millam, M. Klene, C. Adamo, R. Cammi, J. W. Ochterski, R. L. Martin, K. Morokuma, O. Farkas, J. B. Foresman, and D. J. Fox, Gaussian, Inc., Wallingford CT, 2016.

Gaussian 16, Revision C.01, M. J. Frisch, G. W. Trucks, H. B. Schlegel, G. E. Scuseria, M. A. Robb, J. R. Cheeseman, G. Scalmani, V. Barone, G. A. Petersson, H. Nakatsuji, X. Li, M. Caricato, A. V. Marenich, J. Bloino, B. G. Janesko, R. Gomperts, B. Mennucci, H. P. Hratchian, J. V. Ortiz, A. F. Izmaylov, J. L. Sonnenberg, D. Williams-Young, F. Ding, F. Lipparini, F. Egidi, J. Goings, B. Peng, A. Petrone, T. Henderson, D. Ranasinghe, V. G. Zakrzewski, J. Gao, N. Rega, G. Zheng, W. Liang, M. Hada, M. Ehara, K. Toyota, R. Fukuda, J. Hasegawa, M. Ishida, T. Nakajima, Y. Honda, O. Kitao, H. Nakai, T. Vreven, K. Throssell, J. A. Montgomery, Jr., J. E. Peralta, F. Ogliaro, M. J. Bearpark, J. J. Heyd, E. N. Brothers, K. N. Kudin, V. N. Staroverov, T. A. Keith, R. Kobayashi, J. Normand, K. Raghavachari, A. P. Rendell, J. C. Burant, S. S. Iyengar, J. Tomasi, M. Cossi, J. M. Millam, M. Klene, C. Adamo, R. Cammi, J. W. Ochterski, R. L. Martin, K. Morokuma, O. Farkas, J. B. Foresman, and D. J. Fox, Gaussian, Inc., Wallingford CT, 2016

Genovino, J., Sames, D., Hamann, L. G., & Toure, B. B. (2016). Accessing Drug Metabolites via Transition-Metal Catalyzed C− H Oxidation: The Liver as Synthetic Inspiration. *Angewandte Chemie International Edition*, *55*(46), 14218-14238.

Geri, J.B., Oakley, J.V., Reyes-Robles, T., Wang, T., McCarver, S.J., White, C.H., Rodriguez-Rivera, F.P., Parker Jr, D.L., Hett, E.C., Fadeyi, O.O., Oslund, R.C.& MacMillan, D. W. (2020). Microenvironment mapping via Dexter energy transfer on immune cells. *Science*, *367*(6482), 1091-1097.

Glaser, F., & Wenger, O. S. (2020). Recent progress in the development of transition-metal based photoredox catalysts. *Coordination chemistry reviews*, *405*, 213129.

Goldstein, S., & Meyerstein, D. (1999). Comments on the mechanism of the "Fenton-like" reaction. *Accounts of Chemical Research*, *32*(7), 547-550.

Griffin, J. D., Zeller, M. A., & Nicewicz, D. A. (2015). Hydrodecarboxylation of carboxylic and malonic acid derivatives via organic photoredox catalysis: substrate scope and mechanistic insight. *Journal of the American Chemical Society*, *137*(35), 11340-11348.

Grosheva, D. and Hyster, T.K. Light-driven flavin-based biocatalysis. *Flavin-Based Catalysis: Principles and Applications*, Radek Cibulka and Marco Fraaije; Wiley-VCH Verlag GmbH & Co. KGaA., **2021**, 291-313, https://doi.org/10.1002/9783527830138.ch12.

Groves, J. T. (2014). Using push to get pull. *Nature chemistry*, *6*(2), 89-91.

Hernandez-Perez, A. C., & Collins, S. K. (2016). Heteroleptic Cu-based sensitizers in photoredox catalysis. *Accounts of Chemical Research*, *49*(8), 1557-1565.

Horiba Scientific. (2022) *PTI Quantamaster Series*. Retrieved from https://www.horiba.com/fileadmin/uploads/Scientific/Fluorescence/Downloads/QuantaMaster_New.pdf

Huang, X., & Groves, J. T. (2017). Beyond ferryl-mediated hydroxylation: 40 years of the rebound mechanism and C–H activation. *JBIC Journal of Biological Inorganic Chemistry*, *22*(2), 185-207

Huff, C. A., Cohen, R. D., Dykstra, K. D., Streckfuss, E., DiRocco, D. A., & Krska, S. W. (2016). Photoredox-catalyzed hydroxymethylation of heteroaromatic bases. *The Journal of Organic Chemistry*, *81*(16), 6980-6987.

Hung, V., Udeshi, N. D., Lam, S. S., Loh, K. H., Cox, K. J., Pedram, K., Carr, S. A., & Ting, A. Y. (2016). Spatially resolved proteomic mapping in living cells with the engineered peroxidase APEX2. *Nature protocols*, *11*(3), 456-475.

Ie, Y., Jinnai, S., Nitani, M., & Aso, Y. (2013). Arenedithiocarboxyimide-containing extended π-conjugated systems with high electron affinity. *Journal of Materials Chemistry C*, *1*(34), 5373-5380.

Ischay, M. A., Anzovino, M. E., Du, J., & Yoon, T. P. (2008). Efficient visible light photocatalysis of [2+2] enone cycloadditions. *Journal of the American Chemical Society*, *130*(39), 12886-12887.

Juneau, A., Hope, T. O., Malenfant, J., Mesko, M., McNeill, J., & Frenette, M. (2022). Methods to Predict Potential Reagents in Iridium-Based Photoredox Catalysis Calibrated with Stern–Volmer Quenching Rate Constants. *ACS Catalysis*, *12*(4), 2348-2356.

Kasha, M. (1950). Characterization of electronic transitions in complex molecules. *Discussions of the Faraday society*, *9*, 14-19.

Khusnutdinova, J. R., Ben-David, Y., & Milstein, D. (2014). Oxidant-free conversion of cyclic amines to lactams and H2 using water as the oxygen atom source. *Journal of the American Chemical Society*, *136*(8), 2998-3001.

Kiani, S., Tapper, A., Staples, R. J., & Stavropoulos, P. (2000). Functional aspects of gif-type oxidation of hydrocarbons mediated by iron picolinate H2O2-dependent systems: Evidence for the generation of carbon-and oxygen-centered radicals. *Journal of the American Chemical Society*, *122*(31), 7503-7517.

Kim, J. W., Yamaguchi, K., & Mizuno, N. (2008). Heterogeneously catalyzed efficient oxygenation of primary amines to amides by a supported ruthenium hydroxide catalyst. *Angewandte Chemie International Edition*, *47*(48), 9249-9251.

Kothe, T., Martschke, R., & Fischer, H. (1998). Photoreactions of the decatungstate anion W10O324–with organic substrates in solution studied by EPR and kinetic absorption spectroscopy: an example for the persistent radical effect. *Journal of the Chemical Society, Perkin Transactions 2*, (3), 503-508.

Kozycz, L. M., Guo, C., Manion, J. G., Tilley, A. J., Lough, A. J., Li, Y., & Seferos, D. S. (2015). Enhanced electron mobility in crystalline thionated naphthalene diimides. *Journal of Materials Chemistry C*, *3*(43), 11505-11515.

Lee, C., Yang, W., & Parr, R. G. (1988). Development of the Colle-Salvetti correlation-energy formula into a functional of the electron density. *Physical review B*, *37*(2), 785.

Legacy, C. J., Wang, A., O'Day, B. J., & Emmert, M. H. (2015). Iron-Catalyzed Cα-H Oxidation of Tertiary, Aliphatic Amines to Amides under Mild Conditions. *Angewandte Chemie*, *127*(49), 15120-15123.

Lévesque, S., Gendron, D., Berube, N., Grenier, F., Leclerc, M., & Cote, M. (2014). Thiocarbonyl Substitution in 1, 4-Dithioketopyrrolopyrrole and Thienopyrroledithione Derivatives: An Experimental and Theoretical Study. *The Journal of Physical Chemistry C*, *118*(8), 3953-3959.

Li, B. X., Kim, D. K., Bloom, S., Huang, R. Y. C., Qiao, J. X., Ewing, W. R., Oblinsky, D. G., Scholes, G. D., & MacMillan, D. W. (2021). Site-selective tyrosine bioconjugation via photoredox catalysis for native-to-bioorthogonal protein transformation. *Nature chemistry*, *13*(9), 902-908.

Li, G. X., Morales-Rivera, C. A., Wang, Y., Gao, F., He, G., Liu, P., & Chen, G. (2016). Photoredox-mediated Minisci C–H alkylation of N-heteroarenes using boronic acids and hypervalent iodine. *Chemical science*, *7*(10), 6407-6412.

Li, Z., Bohle, D. S., & Li, C. J. (2006). Cu-catalyzed cross-dehydrogenative coupling: A versatile strategy for C–C bond formations via the oxidative activation of sp3 C–H bonds. *Proceedings of the National Academy of Sciences*, *103*(24), 8928-8933

Lind, J., Shen, X., Eriksen, T. E., & Merenyi, G. (1990). The one-electron reduction potential of 4-substituted phenoxyl radicals in water. *Journal of the American Chemical Society*, *112*(2), 479-482.

Liu, F., Zhang, Y., Wang, H., & Zhang, S. (2018). Novel Conjugated Polymers Prepared by Direct (Hetero) arylation: An Eco-Friendly Tool for Organic Electronics. *Molecules*, *23*(2), 408.

MacFaul, P. A., Wayner, D. D. M., & Ingold, K. U. (1998). A radical account of "oxygenated Fenton chemistry". *Accounts of Chemical Research*, *31*(4), 159-162.

Maciejewski, A., & Steer, R. P. (1993). The photophysics, physical photochemistry, and related spectroscopy of thiocarbonyls. *Chemical reviews*, *93*(1), 67-98.

Matsui, J. K., Primer, D. N., & Molander, G. A. (2017). Metal-free C–H alkylation of heteroarenes with alkyltrifluoroborates: a general protocol for 1°, 2° and 3° alkylation. *Chemical science*, *8*(5), 3512-3522.

McCallum, T., & Barriault, L. (2016). Direct alkylation of heteroarenes with unactivated bromoalkanes using photoredox gold catalysis. *Chemical science*, *7*(7), 4754-4758.

McTiernan, C. D., Morin, M., McCallum, T., Scaiano, J. C., & Barriault, L. (2016). Polynuclear gold (i) complexes in photoredox catalysis: understanding their reactivity through characterization and kinetic analysis. *Catalysis Science & Technology*, *6*(1), 201-207.

Merck & Co. Inc Image , Accessed August 2022 (https://cen.acs.org/articles/93/i29/Chemists-100-Organic-2015-NOS.html)

Meunier, B. (Ed.). (2003). *Metal-oxo and metal-peroxo species in catalytic oxidations* (Vol. 97). Springer.

Michon, T., Chenu, M., Kellershon, N., Desmadril, M., & Guéguen, J. (1997). Horseradish peroxidase oxidation of tyrosine-containing peptides and their subsequent polymerization: a kinetic study. *Biochemistry*, *36*(28), 8504-8513.

Minisci, F., Bernardi, R., Bertini, F., Galli, R., & Perchinummo, M. (1971). Nucleophilic character of alkyl radicals—VI: A new convenient selective alkylation of heteroaromatic bases. *Tetrahedron*, *27*(15), 3575-3579.

Müller, M., Gräbnitz, F., Barandun, N., Shen, Y., Wendt, F., Steiner, S. N., Severin, Y., Vetterli, S. U., Mondal, M., Prudent, J. R., Hofmann, R., van Oostrum, M., Sarott, R. C., Nesvizhskii, A. I., Carreira, E. M., Bode, J. W., Snijder, B., Robinson, J. A., Loessner, M. J., Oxenius, A., & Wollscheid, B. (2021). Light-mediated discovery of surfaceome nanoscale organization and intercellular receptor interaction networks. *Nature communications*, *12*(1), 1-17.

Nam, W. (2007). High-valent iron (IV)–oxo complexes of heme and non-heme ligands in oxygenation reactions. *Accounts of Chemical Research*, *40*(7), 522-531.

Narayanam, J. M., Tucker, J. W., & Stephenson, C. R. (2009). Electron-transfer photoredox catalysis: development of a tin-free reductive dehalogenation reaction. *Journal of the American Chemical Society*, *131*(25), 8756-8757.

Nicewicz, D. A., & MacMillan, D. W. (2008). Merging photoredox catalysis with organocatalysis: the direct asymmetric alkylation of aldehydes. *Science*, *322*(5898), 77-80.

Niederer, K. A., Gilmartin, P. H., & Kozlowski, M. C. (2020). Oxidative Photocatalytic Homo-and Cross-Coupling of Phenols: Nonenzymatic, Catalytic Method for Coupling Tyrosine. *ACS catalysis*, *10*(24), 14615-14623.

Nuhant, P., Oderinde, M. S., Genovino, J., Juneau, A., Gagné, Y., Allais, C., Chinigo, G. M., Choi, C., Sach, N. W., Bernier, L., Fobian, Y. M., Bundesmann, M., Khunte, B., Frenette, M., & Fadeyi, O. O. (2017). Visible-Light-Initiated Manganese Catalysis for C− H Alkylation of Heteroarenes: Applications and Mechanistic Studies. *Angewandte Chemie International Edition*, *56*(48), 15309-15313.

Oakley, J.V., Buksh, B.F., Fernández, D.F., Oblinsky, D.G., Seath, C.P., Geri, J.B., Scholes, G.D. and MacMillan, D.W. (2022). Radius measurement via super-resolution microscopy enables the development of a variable radii proximity labeling platform. *Proceedings of the National Academy of Sciences*, *119*(32). https://doi.org/10.1073/pnas.2203027119

Oscarson, M. (2001). Genetic polymorphisms in the cytochrome P450 2A6 (CYP2A6) gene: implications for interindividual differences in nicotine metabolism. *Drug Metabolism and Disposition*, *29*(2), 91-95.

Oslund, R. C., Reyes-Robles, T., White, C. H., Tomlinson, J. H., Crotty, K. A., Bowman, E. P., Chang, D., Peterson, V.M., Li, L., Frutos, S., Vila-Perelló, M., Vlerick D., Cromie, K., Perlman D.H., Ingale, S., O'Hara, D.D., Roberts, L.R., Piizzi, G., Hett, E.C., Hazuda, D.J., & Fadeyi, O. O. (2022). Detection of cell–cell interactions via photocatalytic cell tagging. *Nature Chemical Biology*, 1-9.

Perkin Elmer. (2022). *Determination of Relative Fluorescence Quantum Yields using the FL6500 Fluorescence Spectrometer*. Retrieved from https://www.perkinelmer.com/lab-solutions/resources/docs/APP_Determination_of_Relative_FluorescenceQuantum_Yields_using_FL6500_Fluorescence_Spect.pdf

Perkins, M. J. (1964). 1145. The thermal decomposition of phenylazotriphenylmethane in p-xylene. *Journal of the Chemical Society (Resumed)*, 5932-5935.

Perkins, M. J. (1996). A radical reappraisal of Gif reactions. *Chemical Society Reviews*, *25*(4), 229-236.

Pitre, S. P., McTiernan, C. D., Vine, W., DiPucchio, R., Grenier, M., & Scaiano, J. C. (2015). Visible-light actinometry and intermittent illumination as convenient tools to study Ru (bpy) 3Cl2 mediated photoredox transformations. *Scientific reports*, *5*(1), 1-10.

Pitre, S. P., McTiernan, C. D., Vine, W., DiPucchio, R., Grenier, M., & Scaiano, J. C. (2015). Visible-light actinometry and intermittent illumination as convenient tools to study Ru (bpy) 3Cl2 mediated photoredox transformations. *Scientific reports*, *5*(1), 1-10.

Pitre, S. P.; McTiernan, C. D.; Ismaili, H.; Scaiano, J. C. Mechanistic insights and kinetic analysis for the oxidative hydroxylation of arylboronic acids by visible-light photoredox catalysis: A metal-free alternative. J. Am. Chem. Soc. 2013, 135, 13286-13289.

Preedasuriyachai, P., Chavasiri, W., & Sakurai, H. (2011). Aerobic oxidation of cyclic amines to lactams catalyzed by PVP-stabilized nanogold. *Synlett*, *2011*(08), 1121-1124.

Psutka, K. M., & Maly, K. E. (2016). Synthesis and characterization of novel dibenz [a, c] anthracenedicarboxythioimides: The effect of thionation on self-assembly. *RSC advances*, *6*(82), 78784-78790.

Psutka, K. M., Bozek, K. J., & Maly, K. E. (2014). Synthesis and mesomorphic properties of novel dibenz [a, c] anthracenedicarboximides. *Organic letters*, *16*(20), 5442-5445.

Psutka, K. M., LeDrew, J., Taing, H., Eichhorn, S. H., & Maly, K. E. (2019). Synthesis and self-assembly of liquid crystalline triphenylenedicarboxythioimides. *The Journal of Organic Chemistry*, *84*(17), 10796-10804.

Ramnath, N., Ramesh, V., & Ramamurthy, V. (1983). Photochemical oxidation of thio ketones: steric and electronic aspects. *The Journal of Organic Chemistry*, *48*(2), 214-222.

Ratnikov, M. O., & Doyle, M. P. (2013). Mechanistic investigation of oxidative Mannich reaction with tert-butyl hydroperoxide. The role of transition metal salt. *Journal of the American Chemical Society*, *135*(4), 1549-1557.

Rehm, D., & Weller, A. (1970). Kinetics of fluorescence quenching by electron and H-atom transfer. *Israel Journal of Chemistry*, *8*(2), 259-271.

Reichardt, C. (1979). Empirical parameters of solvent polarity as linear free-energy relationships. *Angewandte chemie international edition in English*, *18*(2), 98-110.

Revol, G., McCallum, T., Morin, M., Gagosz, F., & Barriault, L. (2013). Photoredox transformations with dimeric gold complexes. *Angewandte Chemie International Edition*, *52*(50), 13342-13345.

Ryu, K. A., Kaszuba, C. M., Bissonnette, N. B., Oslund, R. C., & Fadeyi, O. O. (2021). Interrogating biological systems using visible-light-powered catalysis. *Nature Reviews Chemistry*, *5*(5), 322-337.

Sato, S., & Nakamura, H. (2013). Ligand-Directed Selective Protein Modification Based on Local Single-Electron-Transfer Catalysis. *Angewandte Chemie*, *125*(33), 8843-8846.

Sawyer, D. T., Sobkowiak, A., & Matsushita, T. (1996). Metal [ML x; M= Fe, Cu, Co, Mn]/hydroperoxide-induced activation of dioxygen for the oxygenation of hydrocarbons: oxygenated Fenton chemistry. *Accounts of chemical research*, *29*(9), 409-416.

Schlichting, I., Berendzen, J., Chu, K., Stock, A. M., Maves, S. A., Benson, D. E., ... & Sligar, S. G. (2000). The catalytic pathway of cytochrome P450cam at atomic resolution. *Science*, *287*(5458), 1615-1622.

Scully Jr, F. E., & Hoigné, J. (1987). Rate constants for reactions of singlet oxygen with phenols and other compounds in water. *Chemosphere*, *16*(4), 681-694.

Sjöback, R., Nygren, J., & Kubista, M. (1995). Absorption and fluorescence properties of fluorescein. *Spectrochimica Acta Part A: Molecular and Biomolecular Spectroscopy*, *51*(6), L7-L21

Stephanopoulos, N., & Francis, M. B. (2011). Choosing an effective protein bioconjugation strategy. *Nature chemical biology*, *7*(12), 876-884.

Studer, A. (2001). The persistent radical effect in organic synthesis. *Chemistry–A European Journal*, *7*(6), 1159-1164.

Tamura, T., Takato, M., Shiono, K., & Hamachi, I. (2020). Development of a photoactivatable proximity labeling method for the identification of nuclear proteins. *Chemistry Letters*, *49*(2), 145-148.

Tay, N., Ryu, K.A., Weber, J., Olow, A., Reichman, D., Oslund, R., Fadeyi, O. and Rovis, T. (2021). Targeted activation in localized protein environments via deep red photoredox catalysis. . https://doi.org/10.26434/chemrxiv-2021-x9bjv (accessed 2022-07-28).

Thomas, M. J., & Foote, C. S. (1978). Chemistry of singlet oxygen—XXVI. Photooxygenation of phenolsy. *Photochemistry and Photobiology*, *27*(6), 683-693.

Tilley, A. J., Guo, C., Miltenburg, M. B., Schon, T. B., Yan, H., Li, Y., & Seferos, D. S. (2015). Thionation Enhances the Electron Mobility of Perylene Diimide for High Performance n-Channel Organic Field Effect Transistors. *Advanced Functional Materials*, *25*(22), 3321-3329.

Trowbridge, A. D., Seath, C. P., Rodriguez-Rivera, F. P., Li, B. X., Dul, B. E., Schwaid, A. G., Buksh, B. F., Geri, J. B., Oakley, J. V., Fadeyi, O. O., Oslund, R. C., Ryu, K. A., White, C., Reyes-Robles, T., Tawa, P., Parker Jr, D. L., MacMillan, D. W. C. (2022). Small molecule photocatalysis enables drug target identification via energy transfer. *Proceedings of the National Academy of Sciences*, *119*(34), e2208077119. https://doi.org/10.1073/pnas.2208077119

Tsushima, M., Sato, S., & Nakamura, H. (2017). Selective purification and chemical labeling of a target protein on ruthenium photocatalyst-functionalized affinity beads. *Chemical Communications*, *53*(35), 4838-4841.

Walsh, A. A., Szklarz, G. D., & Scott, E. E. (2013). Human cytochrome P450 1A1 structure and utility in understanding drug and xenobiotic metabolism. *Journal of Biological Chemistry*, *288*(18), 12932-12943.

Wang, H., Zhang, Y., Zeng, K., Qiang, J., Cao, Y., Li, Y., Fand, Y., Zhang, Y., & Chen, Y. (2021). Selective mitochondrial protein labeling enabled by biocompatible photocatalytic reactions inside live cells. *Jacs Au*, *1*(7), 1066-1075.

Welford, A., Maniam, S., Gann, E., Thomsen, L., Langford, S. J., & McNeill, C. R. (2018). Thionation of naphthalene diimide molecules: Thin-film microstructure and transistor performance. *Organic Electronics*, *53*, 287-295.

Wilkinson, F., Helman, W. P., & Ross, A. B. (1995). Rate constants for the decay and reactions of the lowest electronically excited singlet state of molecular oxygen in solution. An expanded and revised compilation. *Journal of Physical and Chemical Reference Data*, *24*(2), 663-677.

Würthner, F., Saha-Möller, C. R., Fimmel, B., Ogi, S., Leowanawat, P., & Schmidt, D. (2016). Perylene bisimide dye assemblies as archetype functional supramolecular materials. *Chemical reviews*, *116*(3), 962-1052.

Xu, W., Jiang, Y., & Fu, H. (2012). Copper-catalyzed aerobic oxidative synthesis of primary amides from (aryl) methanamines. *Synlett*, *23*(05), 801-804.

Yang, T.F., Huang, S.H., Chiu, Y.P., Chen, B.H., Shih, Y.W., Chang, Y.C., Yao, J.Y., Lee, Y.J. and Kuo, M.Y. (2015). Pyromellitic dithioimides: thionation improves air-stability and electron mobility of N-type organic field-effect transistors. *Chemical Communications*, *51*(72), 13772-13775.

Yilmaz, O., Oderinde, M. S., & Emmert, M. H. (2018). Photoredox-Catalyzed Cα–H Cyanation of Unactivated Secondary and Tertiary Aliphatic Amines: Late-Stage Functionalization and Mechanistic Studies. *The Journal of organic chemistry*, *83*(18), 11089-11100.

Zhan, X., Facchetti, A., Barlow, S., Marks, T. J., Ratner, M. A., Wasielewski, M. R., & Marder, S. R. (2011). Rylene and related diimides for organic electronics. *Advanced Materials*, *23*(2), 268-284.

Zhao, Y., & Truhlar, D. G. (2008). The M06 suite of density functionals for main group thermochemistry, thermochemical kinetics, noncovalent interactions, excited states, and transition elements: two new functionals and systematic testing of four M06-class functionals and 12 other functionals. *Theoretical chemistry accounts*, *120*(1), 215-241.

Zhuang, B., Liebl, U., & Vos, M. H. (2022). Flavoprotein Photochemistry: Fundamental Processes and Photocatalytic Perspectives. *The Journal of Physical Chemistry B*, *126*(17), 3199-3207.

Zou, Y.-Q.; Chen, J.-R.; Liu, X.-P.; Lu, L.-Q.; Davis, R. L.; Jørgensen, K. A.; Xiao, W.-J. Highly efficient aerobic oxidative hydroxylation of arylboronic acids: photoredox catalysis using visible light. Angew. Chem., Int. Ed. 2012, 51, 784-788.

Zuo, Z., Ahneman, D. T., Chu, L., Terrett, J. A., Doyle, A. G., & MacMillan, D. W. (2014). Merging photoredox with nickel catalysis: Coupling of α-carboxyl sp3-carbons with aryl halides. *Science*, *345*(6195), 437-440.